

OFFICE OF CIVILIAN RADIOACTIVE WASTE MANAGEMENT
ANALYSIS/MODEL COVER SHEET

1. QA: QA
Page: 1 of 176

Complete Only Applicable Items

<p>2. <input checked="" type="checkbox"/> Analysis Check all that apply</p> <table border="1" style="width:100%; border-collapse: collapse;"> <tr> <td style="width:20%;">Type of Analysis</td> <td> <input type="checkbox"/> Engineering <input type="checkbox"/> Performance Assessment <input checked="" type="checkbox"/> Scientific </td> </tr> <tr> <td>Intended Use of Analysis</td> <td> <input type="checkbox"/> Input to Calculation <input type="checkbox"/> Input to another Analysis or Model <input checked="" type="checkbox"/> Input to Technical Document </td> </tr> <tr> <td colspan="2">Describe use:</td> </tr> <tr> <td colspan="2">Provides simulations for comparison with geochemistry data and estimate of ground water travel time.</td> </tr> </table>	Type of Analysis	<input type="checkbox"/> Engineering <input type="checkbox"/> Performance Assessment <input checked="" type="checkbox"/> Scientific	Intended Use of Analysis	<input type="checkbox"/> Input to Calculation <input type="checkbox"/> Input to another Analysis or Model <input checked="" type="checkbox"/> Input to Technical Document	Describe use:		Provides simulations for comparison with geochemistry data and estimate of ground water travel time.		<p>3. <input checked="" type="checkbox"/> Model Check all that apply</p> <table border="1" style="width:100%; border-collapse: collapse;"> <tr> <td style="width:20%;">Type of Model</td> <td> <input type="checkbox"/> Conceptual Model <input type="checkbox"/> Mathematical Model <input checked="" type="checkbox"/> Process Model </td> <td style="width:20%;"> <input type="checkbox"/> Abstraction Model <input type="checkbox"/> System Model </td> </tr> <tr> <td>Intended Use of Model</td> <td colspan="2"> <input type="checkbox"/> Input to Calculation <input checked="" type="checkbox"/> Input to another Model or Analysis <input checked="" type="checkbox"/> Input to Technical Document </td> </tr> <tr> <td colspan="3">Describe use:</td> </tr> <tr> <td colspan="3">Provides 3-D flow fields for TSPA and the UZ PMR.</td> </tr> </table>	Type of Model	<input type="checkbox"/> Conceptual Model <input type="checkbox"/> Mathematical Model <input checked="" type="checkbox"/> Process Model	<input type="checkbox"/> Abstraction Model <input type="checkbox"/> System Model	Intended Use of Model	<input type="checkbox"/> Input to Calculation <input checked="" type="checkbox"/> Input to another Model or Analysis <input checked="" type="checkbox"/> Input to Technical Document		Describe use:			Provides 3-D flow fields for TSPA and the UZ PMR.		
Type of Analysis	<input type="checkbox"/> Engineering <input type="checkbox"/> Performance Assessment <input checked="" type="checkbox"/> Scientific																				
Intended Use of Analysis	<input type="checkbox"/> Input to Calculation <input type="checkbox"/> Input to another Analysis or Model <input checked="" type="checkbox"/> Input to Technical Document																				
Describe use:																					
Provides simulations for comparison with geochemistry data and estimate of ground water travel time.																					
Type of Model	<input type="checkbox"/> Conceptual Model <input type="checkbox"/> Mathematical Model <input checked="" type="checkbox"/> Process Model	<input type="checkbox"/> Abstraction Model <input type="checkbox"/> System Model																			
Intended Use of Model	<input type="checkbox"/> Input to Calculation <input checked="" type="checkbox"/> Input to another Model or Analysis <input checked="" type="checkbox"/> Input to Technical Document																				
Describe use:																					
Provides 3-D flow fields for TSPA and the UZ PMR.																					

4. Title:
UZ Flow Models and Submodels

5. Document Identifier (including Rev. No. and Change No., if applicable):
MDL-NBS-HS-000006 REV00

<p>6. Total Attachments: 3</p>	<p>7. Attachment Numbers - No. of Pages in Each: Attachment I-38 Attachment II-11 Attachment III-86</p>
------------------------------------	---

	Printed Name	Signature	Date
8. Originator	Y.S. Wu	SIGNATURE ON FILE	3/13/00
9. Checker	T.M. Bandurraga	SIGNATURE ON FILE	3/13/00
	R.C. Stover	SIGNATURE ON FILE	3/13/00
10. Lead/Supervisor	G.S. Bodvarsson	SIGNATURE ON FILE	3/14/00
11. Responsible Manager	G.S. Bodvarsson	SIGNATURE ON FILE	3/14/00

12. Remarks:

Initial Issue

Block 8: The AMR report was prepared by Y.S. Wu, J. Liu, T. Xu, C. Haukwa, W. Zhang, H.H. Liu, and C.F. Ahlers.

Block 9: Backcheck was performed by Richard Stover

Editorial correction to page 4, Table of Contents JSH 4/11/00
Editorial correction to page 7, List of Figures JSH 4/11/00
Editorial correction to page 12, Table caption JSH 4/11/00
Editorial correction to Attachment I - added "N/A" to "Change" box throughout JSH 4/11/00
Editorial correction to Attachment III - pagination throughout JSH 4/11/00

**OFFICE OF CIVILIAN RADIOACTIVE WASTE MANAGEMENT
ANALYSIS/MODEL REVISION RECORD**

Complete Only Applicable Items

1. Page: 2 of 176

2. Analysis or Model Title:

UZ Flow Models and Submodels

3. Document Identifier (including Rev. No. and Change No., if applicable):

MDL-NBS-HS-000006 REV00

4. Revision/Change No.

5. Description of Revision/Change

00

Initial Issue

CONTENTS

	Page
ACRONYMS.....	15
1. PURPOSE	17
2. QUALITY ASSURANCE	19
3. COMPUTER SOFTWARE AND MODEL USAGE	21
4. INPUTS	23
4.1 PARAMETERS	23
4.2 CRITERIA	29
4.3 CODES AND STANDARDS	29
5. ASSUMPTIONS	31
6. ANALYSIS/MODEL	33
6.1 MODEL DESCRIPTION	35
6.1.1 Geological Model and Numerical Grids	35
6.1.2 Numerical Codes and Modeling Approach	40
6.1.3 Model Boundary Conditions	42
6.1.4 Infiltration Scenarios	42
6.1.5 Model Parameters and Rock Properties.....	47
6.2 3-D UZ FLOW MODEL CALIBRATION	47
6.2.1 Calibration Data	47
6.2.2 Perched Water Conceptual Models	48
6.2.3 Calibrated Parameters for Perched Water Zones	51
6.2.4 Numerical Treatment and Solution Convergence	52
6.2.5 Simulation Scenarios, Results and Analyses	53
6.3 TEMPERATURE CALIBRATION	68
6.3.1 Top Boundary Temperature	68
6.3.2 Bottom Boundary Temperature	68
6.3.3 Calibration of Ambient Temperature	68
6.4 ANALYSIS AND MODELING OF PORE-WATER CHEMICAL DATA	72
6.4.1 Available Data	73
6.4.2 Modeling Approaches	73
6.4.3 Modeling Results and Analyses	75
6.5 CALCITE ANALYSIS	86
6.5.1 Introduction	86
6.5.2 Model Description	87
6.5.3 Hydrogeochemical Data	87
6.5.4 NRG-7A Simulations	90

CONTENTS (Continued)

	Page
6.5.5 WT-24 Simulations	92
6.5.6 Discussion and Conclusions	99
6.6 SIMULATIONS OF TSPA 3-D FLOW FIELDS	101
6.6.1 Simulation Scenarios	101
6.6.2 Simulation Results	105
6.6.3 Result Analyses and Flow Fields	106
6.7 GROUNDWATER TRAVEL TIMES AND TRACER TRANSPORT	122
6.7.1 Methodology and Transport Parameters	123
6.7.2 Simulation Scenarios	124
6.7.3 Simulation Results and Analyses	129
6.8 MODEL VALIDATION	142
6.8.1 Alcove 1 Test Results	142
6.8.2 ECRB Results	149
6.8.3 SD-6 and WT-24 Modeling Results	151
6.8.4 3-D Pneumatic Prediction	153
7. CONCLUSIONS	157
7.1 UZ FLOW MODEL CALIBRATION	157
7.2 GEOTHERMAL MODEL CALIBRATION	158
7.3 CHLORIDE SUBMODEL	158
7.4 CALCITE SUBMODEL	158
7.5 TSPA FLOW FIELDS	159
7.6 GROUNDWATER TRAVEL TIMES AND TRACER TRANSPORT	160
7.7 MODEL VALIDATION	160
7.8 LIMITATIONS AND UNCERTAINTIES	161
8. REFERENCES	163
8.1 DOCUMENTS CITED	163
8.2 CODES, STANDARDS, REGULATIONS, AND PROCEDURES	166
8.3 SOURCE DATA, LISTED BY DATA TRACKING NUMBER	167
8.4 OUTPUT DATA, LISTED BY DATA TRACKING NUMBER	170
9. ATTACHMENTS	175
ATTACHMENT I - DOCUMENT INPUT REFERENCE SYSTEM SHEET <i>JEH 4/7/00</i>	
ATTACHMENT II - CALIBRATED PARAMETER SETS, COMBINING FROM ONE-DIMENSIONAL INVERSIONS AND THREE-DIMENSIONAL PERCHED WATER MODELING, USED IN GENERATING THE 18 FLOW FIELDS, GROUNDWATER TRAVEL AND TRACER TRANSPORT TIMES	
ATTACHMENT III - SOFTWARE ROUTINES	

FIGURES

		Page
6-1.	Plan View of the 3-D UZ Calibration Model Grid, Showing the Model Domain, Faults Incorporated, ESF and ECRB, and Several Borehole Locations.	38
6-2.	Plan View of the 3-D UZ TSPA Model Grid, Showing the Model Domain, Faults Incorporated and Several Borehole Locations.	39
6-3.	Plan View of Net Infiltration Distributed Over the 3-D UZ TSPA Model Grid for the Base-Case, or Present-day, Mean Infiltration Scenario.	44
6-4.	Plan View of Net Infiltration Distributed Over the 3-D UZ TSPA Model Grid for the Monsoon, Mean Infiltration Scenario.	45
6-5.	Plan View of Net Infiltration Distributed Over the 3-D UZ TSPA Model Grid for the Glacial Transition, Mean Infiltration Scenario.	46
6-6.	Comparison to the Simulated and Observed Matrix Liquid Saturations and Perched-Water Elevations for Borehole UZ-14, using the Results of pch1_m2 and pch2_m2 with Present-Day, Mean Infiltration Rate.	56
6-7.	Comparison to the Simulated and Observed Matrix Liquid Saturations and Perched-Water Elevations for Borehole SD-12, Using the Results of pch1_m2 and pch2_m2 with Present-Day, Mean Infiltration Rate.	57
6-8.	Comparison to the Simulated and Observed Matrix Water Potentials and Perched-Water Elevations for Borehole SD-12, Using the Results of pch1_m2 and pch2_m2 with Present-Day, Mean Infiltration Rate.	57
6-9.	Simulated Perspective View of 3-D Perched Bodies Along the Base of the TSw, Using the Results of Simulation pch1_m2 of Conceptual Model #1 (Flow-Through) with Present-Day, Mean Infiltration Rate.	59
6-10.	Simulated Perspective View of 3-D Perched Bodies Along the Top of the CHn, Using the Results of Simulation pch1_m2 of Conceptual Model #2 (By-Passing) with Present-Day, Mean Infiltration Rate.	60
6-11.	Simulated Percolation Fluxes at the Potential Repository Horizon Under Present-Day, Lower-Bound Infiltration Using the Results of Simulation pch1_L2.	62
6-12.	Simulated Percolation Fluxes at the Potential Repository Horizon Under Present-Day, Mean Infiltration Using the Results of Simulation pch1_m2.	63
6-13.	Simulated Percolation Fluxes at the Potential Repository Horizon Under Present-Day, Upper-Bound Infiltration Using the Results of Simulation pch1_u2.	64

FIGURES (Continued)

6-14.	Comparisons between Simulated Vertical Percolation Fluxes at the Location of SD-6	
6-15.	Comparisons between Simulated Vertical Percolation Fluxes at the Location of UZ-14 using Different Perched-Water Conceptual Models.	67
6-16.	Measured and Modeled Ambient Temperature Profiles for the Q-Boreholes, with the Present-Day Mean Infiltration.	70
6-17.	Model Ambient Temperature Distribution at the Water Table, with the Present-Day, Mean Infiltration.	71
6-18.	Present-Day, Mean Infiltration Map	75
6-19.	ESF Cl Concentrations by 3-D Simulation with the Present-Day, Mean Infiltration.	78
6-20.	ECRB Cl Concentrations by 3-D Simulation with the Present-Day, Mean Infiltration. ..	78
6-21.	Borehole UZ#16 Cl Concentrations by 3-D Simulation with the Present-Day, Mean Infiltration.	79
6-22.	Infiltration at ECRB Stations and Cl 3-D Simulation Results using the Infiltration.	79
6-23.	Cross Drift Cl Infiltration Concentration Based on the ECRB Infiltration.	80
6-24.	Calibrated Infiltration Map	81
6-25.	ESF Cl Concentrations by 3-D Simulation with Calibrated Infiltration.	82
6-26.	ECRB Cl Concentrations by 3-D Simulation with Calibrated Infiltration.	82
6-27.	Borehole UZ#16 Cl Concentrations by 3-D Simulation with Calibrated Infiltration.....	83
6-28.	ESF Cl Concentrations by Analytical Method and 3-D Simulation.	83
6-29.	Analytical Results of Cl Transient Distributions at ESF Stations.	84
6-30.	Analytical Results of Cl Transient Distributions at ECRB Stations.	84
6-31.	Analytical Results of ³⁶ Cl/Cl Transient Analyses at ESF Stations.	85
6-32.	Pore-water Cl, SO ₄ Concentrations and SO ₄ /Cl Ratios by Hydrogeologic Units.	85

FIGURES (Continued)

6-33. Change of Calcite Volume Fraction with Infiltration Rate after 10 Million Years in the NRG-7A Column Using the Type 1 Water for the Top Boundary of Chemical Transport 91

6-34. Change of Calcite Volume Fraction with Reactive Surface Area after 10 Million Years in Borehole NRG-7A Column Obtained Using the Average TSw Water for the Top Boundary of Chemical Transport92

6-35. Simulated Changes of Calcite Volume Fraction (Lines) Using Simple Mineralogy with Infiltration Rate after 10 Million Years in Borehole WT-24 Column Together with Measured Calcite Deposition Data (In Diamond Symbols) that are Taken from the Analysis of Geochemical Data for the Unsaturated Zone (CRWMS M&O, 2000a, Figure 53).....94

6-36. Change of Calcite Volume Fraction after IO Million Years in the WT-24 Column under Different Mineralogy Conditions. The values of changes of calcite volume fraction under complex mineralogy in the PTn layers are much smaller than 2, and they are increased to a value of 2 for display purposes.95

6-37. Change of Calcite Volume Fraction With Water Type after 10 Million Years in the WT-24 Column96

6-38. Simulated Changes of Calcite Volume Fraction (Lines) Using Complex Mineralogy with Infiltration Rate after 10 Million Years in the WT-24 Column, Together with Measured Calcite Deposition Data (Diamond Symbols) that are Taken from the Analysis of Geochemical Data for the Unsaturated Zone (CRWMS M&O, 2000a, Figure 53).....97

6-39. Change of Calcite Volume Fraction in Fracture (Calculated by Fracture Calcite Volume Divided by Total Fracture and Matrix Solid Volume) and in Total (Same as the Previous Figures, or Calculated by Fracture and Matrix Calcite Volume Divided by Total Fracture and Matrix Solid Volume) under Complex Mineralogy Conditions (Using a Infiltration Rate of 5.92 mm/yr).....98

6-40. Change of Calcite Volume Fraction in Fracture and in Total under Simple Mineralogy Conditions (Using an Infiltration Rate of 5.92 mm/yr).....98

6-41. Comparison to the Simulated and Observed Matrix Liquid Saturations and Perched Water Elevations for Borehole UZ-14, Using the Results of pa_pchml, pa-momnl and pa_glaml Simulations for Three Mean Infiltration Scenarios of Three Climates.107

6-42. Simulated Percolation Fluxes at the Potential Repository Horizon Under Present-Day, Mean Infiltration Using the Results of Simulation pa_pchml. 108

6-43. Simulated Percolation Fluxes at the Potential Repository Horizon Under Monsoon, Mean Infiltration Using the Results of Simulation pa-momnl.....109

FIGURES (Continued)

6-44.	Simulated Percolation Fluxes at the Potential Repository Horizon Under Glacial Transition, Mean Infiltration Using the Results of Simulation pa_glam1.	110
6-45.	Simulated Percolation Fluxes at the Water Table under Present-Day, Mean Infiltration Using the Results of Simulation pa_pchm1– Conceptual Model #1.	112
6-46.	Simulated Percolation Fluxes at the Water Table Under Present-Day, Mean Infiltration Using the Results of Simulation pa_pchm2 – Conceptual Model #2.	113
6-47.	Simulated Percolation Fluxes at the Water Table Under Present-Day, Mean Infiltration Using the Results of Simulation pa99_m – Conceptual Model #3.	114
6-48.	Simulated Percolation Fluxes at the Water Table Under Monsoon, Mean Infiltration Using the Results of Simulation pa_monm1 – Conceptual Model #1.	115
6-49.	Simulated Percolation Fluxes at the Water Table Under Monsoon, Mean Infiltration Using the Results of Simulation pa_monm2 – Conceptual Model #2.	116
6-50.	Simulated Percolation Fluxes at the Water Table Under Monsoon, Mean Infiltration Using the Results of Simulation mon99_m – Conceptual Model #3.	117
6-51.	Simulated Percolation Fluxes at the Water Table Under Glacial Transition, Mean Infiltration Using the Results of Simulation pa_glam1 – Conceptual Model #1.	118
6-52.	Simulated Percolation Fluxes at the Water Table Under Glacial Transition, Mean Infiltration Using the Results of Simulation pa_glam2 – Conceptual Model #2.	119
6-53.	Simulated Percolation Fluxes at the Water Table Under Glacial Transition, Mean Infiltration Using the Results of Simulation gla99_m – Conceptual Model #3.	120
6-54.	Simulated Breakthrough Curves of Cumulative Tracer Mass Arriving at the Water Table, Since Release from the Potential Repository, Using the Three Present-Day Infiltration Scenarios and Three Conceptual Models for Nonadsorbing and Adsorbing Transport .	130
6-55.	Simulated Breakthrough Curves of Cumulative Tracer Mass Arriving at the Water Table, Since Release from the Potential Repository, Using the Three Monsoon Infiltration Scenarios and Three Conceptual Models for Nonadsorbing and Adsorbing Transport.	130

FIGURES (Continued)

6-56. Simulated Breakthrough Curves of Cumulative Tracer Mass Arriving at the Water Table, Since Release from the Potential Repository, Using the Three Glacial Transition Infiltration Scenarios and Three Conceptual Models for Nonadsorbing and Adsorbing Transport.131

6-57. Correlations of Average Infiltration Rates and Groundwater Travel or Tracer Transport Times at 50% Mass Breakthrough for the 42 Simulation Scenarios.132

6-58. (a) Simulated Mass Fraction Contours of a Conservative Tracer at the Water Table after 1,000 Years, Indicating Potential Breakthrough Locations at the Time, Using the Present-Day, Mean Infiltration with Conceptual Model #1135

6-58 (b) Simulated Mass Fraction Contours of a Conservative Tracer at the Water Table after 1,000 Years, Indicating Potential Breakthrough Locations at the Time, Using the Present-Day, Mean Infiltration with Conceptual Model #2136

6-59. (a) Simulated Mass Fraction Contours of a Conservative Tracer at the Water Table after 1,000 Years, Indicating Potential Breakthrough Locations at the Time, Using the Present-Day, Mean Infiltration and Conceptual Model #2 (By-Passing) with Conceptual Model #1.137

6-59 (b) Simulated Mass Fraction Contours of a Conservative Tracer at the Water Table after 1,000 Years, Indicating Potential Breakthrough Locations at the Time, Using the Present-Day, Mean Infiltration and Conceptual Model #2 (By-Passing) with Conceptual Model #2.138

6-60. Simulated Breakthrough Curves of Cumulative Tracer (³⁶Cl) Mass Arriving at the Potential Repository Level, Since Release from the Ground Surface, Using the Present-Day, Mean Infiltration and Four Simulation Scenarios140

6-61. Simulated Spatial Distribution of Tracer (³⁶Cl) in the US System at 50 Years since Release from the Ground Surface, Simulated Normalized Mass Fraction Contours at the Potential Repository Level (Note X3 denotes tracer mass fraction normalized to mass fraction values at source).....141

6-62. Numerical Grid for the Model of the Infiltration Test.143

6-63. Model Calibration Using the Seepage Rate Data of the Phase I of the Test and Prediction for Phase II of the Test.145

6-64. Model Calibration Using Seepage Rate Data from Phases I and II Test.147

FIGURES (Continued)

6-65. Comparison between Simulation Results of Tracer Transport and Observations. (Note that alpha-l, alpha-t, phi refer to longitudinal dispersivity, transverse dispersivity and fracture porosity, respectively.) 148

6-66. Predicted Water Potential along ECRB using the Present-Day Mean Infiltration Rate and Perched Water Conceptual Model #1 150

6-67. Predicted Matrix Saturation for Borehole SD-6 using the Present-Day Mean Infiltration Rate and Perched Water Model #1 151

6-68. Predicted Matrix Saturation for Borehole WT-24 using the Present-Day Mean Infiltration Rate and Perched Water Model #1 152

6-69. Comparison of 3-D Pneumatic Prediction to Data (Observation) from Borehole USW SD-12 and 1-D Calibrated Simulation. 154

6-70. Comparison of 3-D Pneumatic Prediction to Data (Observation) from Borehole USW UZ-7a and 2-D Calibrated Simulation. 155

TABLES

3-1.	Computer Software	21
4-1.	Input Data Source and Data Tracking Numbers	24
6-1.	Model Development Documentation Scientific Notebooks	35
6-2.	GFM3.1 Lithostratigraphy, UZ Model Layer, and Hydrogeologic Unit Correlation Used in the UZ Flow Model and Submodels	36
6-3.	Infiltration Rates (mm/year) Averaged over the Model Domain	43
6-4.	Data Used for 3-D Flow Model Calibration	48
6-5.	Conceptual Flow Scenarios	49
6-6.	Calibrated Parameters for Perched Water Conceptual Model #1 (Flow-Through Model) for the Base-Case Present-Day Infiltration Scenario	51
6-7.	Calibrated Parameters for Perched Water Conceptual Model #1 (Flow-Through Model) for the Upper-Bound Present-Day Infiltration Scenario	52
6-8.	Calibrated Parameters for Perched Water Conceptual Model #1 (Flow-Through Model) for the Lower-Bound Present-Day Infiltration Scenario	52
6-9.	Seven UZ Flow Simulation Scenarios: Data Files, Conceptual Models/Grids, Parameter Sets, Infiltration Maps for the UZ Model Calibrations	54
6-10.	Mass Balance Results for Flow Simulations Using the Calibration Grid	55
6-11.	Comparison of the Water Flux Through Matrix and Fractures as a Percentage of the Total Flux at Two Different Horizons (1) at the Potential Repository and (2) at the Water Table.	65
6-12.	Boreholes with Qualified Data Used in Calibration of UZ Ambient Temperature Distribution	69
6-13.	Infiltration Data by Region	81
6-14.	Aqueous and Gaseous Chemical Concentrations (mg/L) Used for Initial and Boundary Conditions of Hydrochemical Transport Simulations.	89
6-15.	List of Simulations Performed for Borehole WT-24 Column using Different Combinations of Infiltration Rate, Boundary Water Chemical Composition, Initial Mineralogy, and Reactive Surface Areas.	93

TABLES (Continued)

	Page
6-16. Seven TSPA Simulation Scenarios: Data Files, Conceptual Models/Grids, and Parameter Sets for Three Present-Day Infiltration Maps.	102
6-17. Seven TSPA Simulation Scenarios: Data Files, Conceptual Models/Grids, and Parameter Sets for Three Monsoon Climatic Infiltration Maps.	103
6-18. Seven TSPA Simulation Scenarios: Data Files, Conceptual Models/Grids, Parameter Sets for Three Glacial Transition Infiltration Rates.	104
6-19. Mass-Balance Results for TSPA Simulations using the Present-Day Infiltration Rates.	105
6-20. Mass-Balance Results for TSPA Simulations using the Monsoon Infiltration Rates.	105
6-21. Mass-Balance Results for TSPA Simulations using the Glacial Transition Infiltration Rates.	106
6-22. Comparison of the Water Flux through Matrix and Fractures as a Percentage of the Total Flux at Two Different Horizons (1) at the Potential Repository and (2) at the Water Table, using the Three Present-Day Infiltration Scenarios.	121
6-23. Comparison of the Water Flux through Matrix and Fractures as a Percentage of the Total Flux at Two Different Horizons (1) at the Potential Repository and (2) at the Water Table, using the Three Monsoon Infiltration Scenarios.	122
6-24. Comparison of the Water Flux through Matrix and Fractures as a Percentage of the Total Flux at Two Different Horizons (1) at the Potential Repository and (2) at the Water Table, using the Three Glacial Transition Infiltration Scenarios.	122
6-25. K_d Values Used for a Reactive Tracer Transport in Different Hydrogeologic Units.	123
6-26. Transport Simulation Scenarios: Data Files, Conceptual Models/Grids, Corresponding TSPA Flow Fields with Three Present-Day Infiltration Rates.	125
6-27. Transport Simulation Scenarios: Data Files, Conceptual Models/Grids, Corresponding TSPA Flow Fields with Three Monsoon Infiltration Rates.	127
6-28. Transport Simulation Scenarios: Data Files, Conceptual Models/Grids, Corresponding TSPA Flow Fields with Three Glacial Transition Infiltration Rates.	128
6-29. Groundwater Travel/Tracer Transport Times at 10% and 50% Mass Breakthrough Times for 14 Transport Simulation Scenarios, Corresponding to TSPA Flow Fields With Three Present-Day Infiltration Rates.	132

TABLES (Continued)

	Page
6-30. Groundwater Travel/Tracer Transport Times at 10% and 50% Mass Breakthrough for 14 Transport Simulation Scenarios, Corresponding to TSPA Flow Fields with Three Monsoon Infiltration Rates.	133
6-31. Groundwater Travel/Tracer Transport Times at 10% and 50% Mass Breakthrough for 14 Transport Simulation Scenarios, Corresponding to TSPA Flow Fields with Three Glacial Transition Infiltration Rates.	133
6-32. Initial Estimated Hydrologic Properties for Infiltration Test Model	144
6-33. Calibrated Hydrologic Properties for Infiltration Test Model Based on the Phase I Seepage Rate Data	146
6-34. Calibrated Hydrologic Properties for Infiltration Test Model Based on the Phases I and II Seepage Rate Data	147
6-35. Pneumatic Data Used for Inversion (First Thirty Days) and Validation (Last Thirty Days).	153

INTENTIONALLY LEFT BLANK

ACRONYMS

1-D	one-dimensional
2-D	two-dimensional
3-D	three-dimensional
ACC	Accession Number
AFM	Active Fracture Model
AMR	Analysis/Model Report
AP	Administrative Procedure (DOE)
CFu	Crater Flat undifferentiated hydrogeologic unit
CH	Calico Hills
CHn	Calico Hills non-welded hydrogeologic unit
CRWMS	Civilian Radioactive Waste Management System
DOE	Department of Energy
DTN	Data Tracking Number
ECM	Effective Continuum Method
ECRB	Enhanced Characterization of Repository Block
ESF	Exploratory Studies Facility
FY	Fiscal Year
GFM	Geologic Framework Model
HGU	Hydrogeologic Unit
ISM	Integrated Site Model
ITN	Input Transmittal Number
LA	License Application
LBNL	Lawrence Berkeley National Laboratory
masl	Meters above sea level
MINC	Multiple Interacting Continua
M&O	Management and Operating Contractor
non-Q	non-Qualified
NSP	Nevada State Planar
OCRWM	Office of Civilian Radioactive Waste Management
PA	Performance Assessment
PMR	Process Model Report
PTn	Paintbrush non-welded hydrogeologic unit

ACRONYMS (Continued)

Q	Qualified
QA	Quality Assurance
QAP	Administrative Procedure (M&O)
QARD	Quality Assurance Requirements and Description
QIP	Quality Implementing Procedure
RIB	Reference Information Base
RIP	Performance assessment model used by TSPA
RIS	Records Information System
SR	Site Recommendation
STN	Software Tracking Number
TBD	To Be Determined
TBV	To Be Verified
TCw	Tiva Canyon welded hydrogeologic unit
TDMS	Technical Data Management System
TSPA	Total System Performance Assessment
TSw	Topopah Spring welded hydrogeologic unit
USGS	United States Geological Survey
UZ	Unsaturated Zone
UZ Model	Unsaturated Zone Flow and Transport Model
YMP	Yucca Mountain Site Characterization Project

1. PURPOSE

The purpose of this Analysis/Model Report (AMR) is to document the unsaturated zone (UZ) fluid flow and solute transport models and submodels as well as the flow fields generated utilizing the UZ Flow and Transport Model of Yucca Mountain, Nevada (UZ Model). This is in accordance with the AMR *Development Plan for U0050 UZ Flow Models and Submodels* (CRWMS M&O 1999a). The flow fields are used directly by Performance Assessment (PA). The model and submodels evaluate important hydrogeologic processes in the unsaturated zone as well as geochemistry. These provide the necessary framework to test conceptual hypotheses of flow and transport at different scales and predict flow and transport behavior under a variety of climatic conditions. The AMR supports the UZ Flow and Transport Process Model Report (PMR); PA activities including abstractions, particle tracking transport simulations, and conversion of flow fields for use in the RIP model; and the UZ Radionuclide Transport Model.

The UZ Model is an important process model for the YMP's Repository Safety Strategy and for support of the License Application (LA). The Total System Performance Assessment for Site Recommendation (TSPA-SR) will use the unsaturated-zone flow simulation to provide input to other models such as ambient and thermal drift-scale models, and the mountain-scale thermohydrological model.

The base case flow fields are generated using the UZ Model, with input parameters based on the calibrated property sets documented in the AMR *Calibrated Properties Model* (CRWMS M&O 2000b) and in this AMR. The flow fields are developed for spatially varying maps representing the mean, lower, and upper bounds of estimated net infiltration for the current climate and two projected future climates (Monsoon and Glacial Transition). Each net infiltration case is evaluated using two different perched water models, providing a total of 18 flow fields. These flow fields have been submitted to the Technical Data Management System (TDMS) for use by PA and for Total System Performance Assessment (TSPA) activities.

The process submodels documented in this AMR include the temperature, geochemistry, and groundwater travel and tracer transport submodels. The temperature submodel characterizes ambient geothermal conditions with temperature data for use in the UZ Model. The geochemical submodel includes two specific constituents (chloride and calcite). The chloride submodel represents the conceptual model for the spatial and temporal variations in chloride chemistry and is compared with pore-water concentrations measured in samples from boreholes and the Exploratory Studies Facility (ESF). The strontium submodel incorporates the effects of rate-limited dissolution and precipitation on the concentration of a solute, in addition to dispersion, radioactive decay, and linear equilibrium adsorption.

The caveats for use of the modeling results and flow fields documented in this AMR are that the model development and calibrated properties on which these modeling results and flow fields were based are limited by the available site data, and the flow fields reflect only the conceptual models and quantitative approaches utilized in the models and submodels, as discussed in the AMR *Conceptual and Numerical Models for UZ Flow and Transport* (CRWMS M&O 2000c).

INTENTIONALLY LEFT BLANK

2. QUALITY ASSURANCE

This AMR was developed in accordance with AP-3.10Q, *Analyses and Models*. Other applicable Department of Energy (DOE) Office of Civilian Radioactive Waste Management (OCRWM) Administrative Procedures (APs) and YMP-LBNL Quality Implementing Procedures (QIPs) are identified in the *AMR Development Plan for U0050 UZ Flow Models and Submodels, Rev 00* (CRWMS M&O 1999a).

The activities documented in this Analysis/Model Report (AMR) were evaluated with other related activities in accordance with QAP-2-0, *Conduct of Activities*, and were determined to be subject to the requirements of the U.S. DOE Office of Civilian Radioactive Waste Management (OCRWM) *Quality Assurance Requirements and Description* (QARD) (DOE 1999). This evaluation is documented in CRWMS M&O (1999b, 1999c) and Wemheuer (1999, *Activity Evaluation for Work Package WP 1401213UM1*).

INTENTIONALLY LEFT BLANK

3. COMPUTER SOFTWARE AND MODEL USAGE

The software and routines used in this study are listed in Table 3-1. These are appropriate for the intended application, were used only within the range of validation. These codes were submitted and obtained from software configuration management in accordance with AP-SI.1Q, *Software Management*. The codes were obtained after these simulations were completed and an impact review per AP-3.17Q, *Impact Reviews*, is being conducted, but no impact is expected. The qualification status of this software is given in Attachment I.

Table 3-1. Computer Software

Software Name, Codes	Version	Software Tracking Number (STN)	Computer Type, Operational System
TOUGH2	1.4	10007-1.4-01	Win95/98, SUN and DEC w/ Unix OS
T2R3D	1.4	10006-1.4-00	Win95/98, SUN and DEC w/ Unix OS
ITOUGH2	3.2	10054-3.2-00	SUN and DEC w/ Unix OS
TOUGHREACTE9	1.0	10153-1.0-00	SUN w/ Unix OS
TOUGHREACT	2.2	10154-2.2-00	SUN and DEC w/ Unix OS
Infil2grid	1.6	10077-1.6-00	Win95/98 PC,SUN and DEC w/ Unix OS
EARTHVISION	4.0	30035-2 V4.0	UNIX
EXT	1.0_MEOS9	10227-1.0MEOS9-00	UNIX
Software Routines:			
Read- TDB	1.0	MOL.19990903.0031	Win95/98 or DOS
Frac_Calc	1.1	MOL.19990903.0032	Win95/98 or DOS
TBgas3D	1.0	MOL.19991012.0222	SUN and DEC w/ Unix OS
ECRB-XYZ	.03	30093 V.03	PC

The codes listed in Table 3-1 were qualified under AP-SI.1Q. The software code TOUGH2 V1.4 was used to generate flow fields (Section 6.6), conduct model calibrations (Sections 6.2 and 6.3). T2R3D V1.4 was used for tracer transport simulations and groundwater travel-time estimates (Section 6.7) and modeling pore-water chemistry (Section 6.4). ITOUGH2 V3.2, TOUGHREACTE9 (TOUGH Code for Multiphase multi-species reactive transport with EOS9 flow module) V1.0 and were TOUGHREACT V2.2 used for modeling of calcite geochemistry (Section 6.5). ITOUGH2 V3.2 was used for Alcove 1 tests. Infil2grid V1.6 was used to apply infiltration maps onto the grids used for simulating flow and transport (Sections 6.1, 6.2, 6.3, 6.4, 6.6 and 6.7). The routines in Table 3-1 were qualified per Section 5.1 of AP-SI.1Q.

Standard spreadsheet (Excel 97.SR-1) and plotting programs (Tecplot v 7) were also used but are not subject to software quality assurance requirements.

INTENTIONALLY LEFT BLANK

4. INPUTS

Inputs to the modeling activities described in this AMR are obtained from TDMS include the following:

- Matrix property data from the ESF (Exploratory Studies Facility) and boreholes
- Stratigraphy data from borehole logs
- Infiltration maps
- Calibrated fracture and matrix properties
- Hydrologic property data for CHn (Calico Hills non-welded hydrogeologic unit)
- Geochemistry data from the ESF and boreholes
- UZ Model grids
- Temperature data for boreholes
- Pneumatic pressure data
- Locations and elevations of perched water in boreholes
- Uncalibrated fracture and matrix properties
- Water-potential data
- Matrix liquid-saturation data

4.1 PARAMETERS

The key input data used in the UZ Model and its submodel development include the following:

- Fracture properties (frequency, permeability, van Genuchten α and m parameters, aperture, porosity, and interface area per unit volume rock) for each UZ Model layer
- Matrix properties (porosity, permeability, and the van Genuchten α and m parameters) for each UZ Model layer
- Thermal properties (grain density, wet and dry thermal conductivity, grain specific heat, and tortuosity coefficients) for each UZ Model layer
- Fault properties (matrix and fracture parameters) for each major hydrogeologic unit as defined by [Table 6-2](#).

The calibrated parameter sets also include an estimate of the active-fracture parameter, γ , (Liu et al. 1998) for each model layer that accounts for the reduction in interaction between matrix and fracture flow resulting from flow fingering and channelization. Specific input data sets, associated Data Tracking Numbers (DTNs) and Accession Numbers (ACC) are tabulated below. Quality assurance status is provided in [Attachment 1](#).

Table 4-1. Input Data Source and Data Tracking Numbers

Data Description	Section Used In	DTN or Reference
SO4 infiltration flux	6.4.4.3	GS910908315214.003
SO4 infiltration flux	6.4.4.3	GS931008315214.032
NRG-6 and NRG-7a pneumatic pressure and temperature	6.3 6.8.4	GS951108312232.008 GS950208312232.003
NRG#5 pneumatic pressure	6.8.4	GS960208312261.001
SD-12, UZ-7a, NRG-6, and NRG-7a pneumatic pressure and temperature	6.2 6.3 6.6 6.8.4	GS960308312232.001
Perched water elevation UZ-14	6.2 6.6	GS960308312312.005
NRG-6 and NRG-7a pneumatic pressure and temperature	6.4 6.8.4	GS960808312232.004
Matrix hydrologic property data	6.2 6.3 6.6 6.7 6.8.1, 6.8.2 6.8.3	GS960908312231.004
In situ gas pressure - SD-7	6.8.4	GS960908312261.004
Chemical composition of pore water samples	6.4.2.1	GS961108312261.006
In situ borehole instrumentation and monitoring for NRG-7a, NRG-6, UZ#4, UZ#5, UZ-7a and SD-12-temperature, pressure, and water potential	6.3	GS970108312232.002
Perched water elevation - G-2	6.2 6.6	GS970208312312.003
In situ borehole instrumentation and monitoring for NRG-7a, UZ#4, UZ#5, UZ-7a and SD-12 -temperature, pressure, and water potential	6.3	GS970808312232.005
In situ borehole instrumentation and monitoring for NRG-7a, UZ#4, UZ#5, UZ-7a and SD-12-temperature, pressure, and water potential	6.3	GS971108312232.007

Table 4-1. Input Data Source and Data Tracking Numbers

Data Description	Section Used In	DTN or Reference
Detailed line survey data from ESF station 0+60m to 0+80m	6.8.1	GS971108314224.020
In situ borehole instrumentation and monitoring for NRG-7a, NRG-6, UZ#4, UZ#5, UZ-7a and SD-12-temperature, pressure, and water potential	6.3	GS980408312232.001
WT-24 perched water observations	6.2 6.6 6.8.3	GS980508312313.001
WT-24 saturation data	6.2 6.6 6.8.3	GS980708312242.010
SD-6 saturation data	6.2 6.6 6.8.3	GS980808312242.014
Water potential data along ECRB tunnel	6.8.2	GS980908312242.036
Perched water elevation G-2	6.2 6.6	GS981008312313.003
Matrix diffusion coefficients for Tc and ²³⁷ Np	6.7	LAIT831341AQ96.001
Mineral abundance in fractures	6.5	LASL831151AQ98.001
Chemical composition of pore water samples	6.4.2.1	LASL831222AQ98.002
Model input and output files for Mineralogic Model (borehole SD-9 XRD data)	6.5	LA9908JC831321.001
Flow fields and calibrated hydrologic properties	6.2 6.3 6.6 6.7 6.8.1, 6.8.2 6.8.3	LB971212001254.006
Air-injection, tracer test, and fracture porosity data	6.2 6.3 6.6 6.7 6.8	LB980912332245.002

Table 4-1. Input Data Source and Data Tracking Numbers

Data Description	Section Used In	DTN or Reference
Uncalibrated hydrologic property data	6.2 6.3 6.6 6.7 6.8	LB990501233129.001
1-D grid for flow property calibration	6.5	LB990501233129.002
3-D UZ Model calibration grid	6.1 6.2 6.3 6.8.2 6.8.3	LB990501233129.004
3-D UZ Model TSPA grid	6.1 6.6 6.7 6.8.4	LB990701233129.001
3-D UZ Model calibration grid for non water-perching model	6.1 6.2 6.3 6.8.2 6.8.3	LB990701233129.002
Calibrated fault property	6.2 6.3 6.6 6.7 6.8	LB991091233129.003
Calibrated fault property	6.8.4	LB991091233129.004
Kinetic Data	6.5	LB991200DSTTHC.001
Calibrated parameters for the base case infiltration scenario - flow through perched water conceptual model	6.2 6.3 6.4 6.6 6.7 6.8.2 6.8.3 6.8.4	LB991121233129.001

Table 4-1. Input Data Source and Data Tracking Numbers

Data Description	Section Used In	DTN or Reference
Calibrated parameters for the base case infiltration scenario - by-passing perched water conceptual model	6.2 6.3 6.4 6.6 6.7 6.8.4	LB991121233129.002
Calibrated parameters for the upper bound infiltration scenario - flow through perched water conceptual model	6.2 6.6 6.7	LB991121233129.003
Calibrated parameters for the upper bound infiltration scenario - by-passing perched water conceptual model	6.2 6.6 6.7	LB991121233129.004
Calibrated parameters for the lower bound infiltration scenario - flow through perched water conceptual model	6.2 6.6 6.7	LB991121233129.005
Calibrated parameters for the lower bound infiltration scenario - by-passing perched water conceptual model	6.2 6.6 6.7	LB991121233129.006
Calibrated parameters for the base case infiltration scenario - non-perching perched water conceptual model	6.2 6.6 6.7	LB991121233129.007
Calibrated flow and thermal parameters base case	6.2 6.3 6.4 6.6 6.7 6.8.2, 6.8.3 6.8.4	LB997141233129.001
Calibrated flow and thermal parameters upper-bound	6.2 6.6 6.7 6.8.4	LB997141233129.002
Calibrated flow and thermal parameters lower-bound	6.2 6.6 6.7 6.8.4	LB997141233129.003

Table 4-1. Input Data Source and Data Tracking Numbers

Data Description	Section Used In	DTN or Reference
Saturation data from cores for boreholes USW SD-7, USW SD-9, USW SD-12, USW UZ-14, UE-25, UZ#16 & USW UZ-7a	6.1 6.2 6.6	DTN: GS000399991221.004., ACC: MOL.19991027.0149
Mean, lower-bound, and upper-bound infiltration rates for present-day, future monsoon, and future glacial transition climates	6.1 6.2 6.3 6.6 6.7 6.8.2, 6.8.3	DTN: GS000399991221.002., ACCN: MOL.1991014.0102
Alcove 1 infiltration and tracer test data	6.8.1	DTN: GS000399991221.003., ACCN: MOL.20000118.0092
Perched water elevation for well SD-12	6.2 6.6	DTN: GS960908312232.006., ACCN: MOL.19991213.0041

This AMR documents the flow models and submodels in the UZ Flow and Transport Model. It utilizes properties from the Calibrated Properties Model. The input and output files for the model runs presented in this AMR are listed in [Tables 6-9, 6-16, 6-17, 6-18, 6-26, 6-27, and 6-28](#), and some of the model input fracture and matrix parameters are given in [Attachment II](#).

4.2 CRITERIA

This AMR complies with the DOE interim guidance (Dyer 1999). Subparts of the interim guidance that apply to this analysis or modeling activity are those pertaining to the characterization of the Yucca Mountain site (Subpart B, Section 15). The compilation of information regarding geology of the site is in support of the License Application (Subpart B, Section 21(c)(1)(ii)), and the definition of geologic parameters and conceptual models used in performance assessment, (Subpart E, Section 114(a)). The compilation of information regarding hydrology of the site is in support of the License Application (Subpart B, Section 21(c)(1)(ii)) and the definition of hydrologic parameters and conceptual models used in performance assessment (Subpart E, Section 114(a)). The compilation of information regarding geochemistry and mineral stability of the site is in support of the License Application (Subpart B, Section 21(c)(1)(ii)), and the definition of geochemical parameters and conceptual models used in performance assessment (Subpart E, Section 114(a)).

4.3 CODES AND STANDARDS

No specific formally established standards have been identified as applying to this analysis and modeling activity.

INTENTIONALLY LEFT BLANK

5. ASSUMPTIONS

The assumptions documented below are required to develop the UZ flow models and submodels. This section presents these assumptions and the rationale which are used throughout the development of the UZ models.

1. The water table is used as the bottom model boundary which is subject to constant water pressure (equal to the atmospherical pressure). *Rationale:* The water table is a surface where the water pressure is a fixed single value. Within the numerical models, only one single set of model primary variables for solving Richards' equations is specified for the bottom boundary and this is equivalent to specifying a constant saturation.
2. The bottom model boundary representing the water table is subject to fixed gas pressure. *Rationale:* Due to limitations in the way boundaries may be specified in the numerical models used, a constant gas pressure must be specified when a constant water pressure (saturation) is specified. The impact of this assumption on all but simulations of barometric pumping is insignificant (see assumption 4 below for an alternate assumption used for simulations of barometric pumping).
3. The bottom model boundary representing the water table is subject to spatially varying but constant temperature conditions. *Rationale:* This assumption is corroborated by data reported by Sass et al. (1988) and the actual temperature distribution along the water table and further confirmed by matching qualified temperature profiles from a number of boreholes.
4. For simulations of barometric pumping, the bottom model boundary representing the water table is assumed to be a no-flow boundary. *Rationale:* At the water table, a connected gas phase does not exist, so gas phase flow does not occur across this boundary. Due to the limitations of the code used for simulation, this boundary must also be no-flow for the liquid phase (heat flow is not considered in these simulations). Liquid flow across the boundary over the time span of the simulation (360 days) is not large enough to significantly change the gas flow in the TSw (Topopah Spring welded hydrogeologic unit) and above where data is available.
5. The lateral boundaries of the model domain are subject to no-flow boundary conditions. *Rationale:* The boundaries of the northern and southern model domain are located so far away from the potential repository area that lateral flow effects along these boundaries on flow at the potential repository should be small. The eastern boundary is for most parts along the Bow Ridge fault, and no lateral flow crossing the fault is reasoned. The western boundary is separated from the potential repository by the Solitario Canyon fault, therefore this boundary condition effects are expected to be insignificant.
6. Perched water occurrence results from permeability barrier effects. *Rationale:* Consistent with the conceptual model that ambient conditions reflect long-term, steady-state or transient flow through the unsaturated zone, perched water under steady-state flow conditions may only be due to a permeability barrier.

7. Under steady-state flow conditions, moisture flow and tracer transport processes can be decoupled. *Rationale:* Steady-state flow conditions result in an unchanging flow field, and as long as the concentrations of tracers and/or radionuclides are such that they do not significantly change the properties of the fluid, which is the case for simulations documented in this AMR, then the flow field does not have to be coupled to transport.
8. Water flow through the UZ is assumed to occur under steady-state conditions. Transient, “fast-pathway” flow, such as conveyed ^{36}Cl to the ESF horizon, is assumed not to contribute significantly to the total flow through the UZ.
9. The dual-permeability formulation is assumed to be appropriate for simulating flow and transport through fractured tuffs.
10. The time required for moisture conditions within the UZ to adjust to changes in the spatial and temporal distribution of net infiltration at land surface induced by climatic change is assumed to be short compared to the time over which climatic conditions change so that simulated conditions within the UZ reflect the present-day and estimated future net-infiltration rates imposed on the upper land-surface boundary of the UZ model.
11. Regarding calcite deposition in the unsaturated zone, the following assumptions are made: (a) the gas phase is at a constant (atmospheric) pressure, and air flow is neglected for the purpose of solving water flow; (b) a constant infiltration rate and water chemistry over the entire simulation period is applied to the top boundary; (c) steady-state water flow condition remains during chemical transport and fluid-rock interactions.

All the assumptions made are justifiable based on the rationales stated and the scientific principles and practices used in conducting modeling studies of flow and transport in porous media.

The methodological premises used for specific modeling studies are more appropriately discussed in the context of the modeling methodologies in Section 6.

6. ANALYSIS/MODEL

As outlined in Section 1, this AMR documents the development and results of the unsaturated zone (UZ) flow and the temperature and geochemistry submodels. This section consists of the following:

- Model description
- 3-D (three-dimensional) UZ flow calibrations
- Geothermal model
- Geochemical model for chloride
- Calcite analysis
- 3-D flow fields for performance analyses
- Groundwater travel and tracer transport

The UZ flow and temperature model and submodels of geochemistry have been developed to simulate past, present, and future hydrologic, geothermal and geochemical conditions in the UZ of Yucca Mountain. Yucca Mountain has been studied extensively, and many types of data have been collected. These data have been used in developing conceptual and numerical models for the hydrological, geothermal and geochemical behavior of the site. These models simulate ambient conditions and perform predictive studies of changes in the mountain caused by climatic, thermal, and geochemical perturbations. The comprehensive model that integrates all pertinent data from the UZ at Yucca Mountain is the 3-D site-scale UZ flow and transport model, developed over the past decade at the Lawrence Berkeley National Laboratory (LBNL) by Bodvarsson et al. (1999) and Wu et al. (1999a), among others. Model development described in this AMR results from the continued modeling investigations on flow and transport behavior in the UZ system of Yucca Mountain.

The primary objectives of developing the UZ flow model and its submodels are:

- To integrate the available data from the UZ system into a single, comprehensive, and calibrated 3-D model for simulating the ambient hydrological, thermal, and geochemical conditions and predicting system response to future climate conditions
- To quantify the flow of moisture, heat, and gas through the UZ, under Present-Day and hypothesized future climate scenarios
- To evaluate the effects of potential repository thermal loading on moisture, gas, and heat flow within the mountain
- To perform detailed studies of perched water, percolation through the Paintbrush non-welded (PTn) unit flow, through Calico Hills non-welded (CHn) zeolitic units, and the pore-water chemical and calcite analyses.
- To predict the migration of potential radionuclide releases after waste emplacement
- To contribute model parameters and boundary conditions for drift seepage studies

- To provide Performance Assessment and Repository Design with a scientifically defensible and credible model of all relevant UZ processes

The UZ Model is a process model whose results directly address Principal Factors within the YMP Repository Safety Strategy (CRWMS M&O 2000e) and for support of the License Application (LA). The Total System Performance Assessment for Site Recommendation (TSPA-SR) will use the unsaturated-zone flow simulation to provide input to other models such as ambient and thermal drift-scale models, the mountain-scale thermohydrological model, and the radionuclide transport model. The UZ Model and its submodels evaluate processes that are important to the performance of the potential repository, all of which contribute to the TSPA-SR and TSPA-LA, such as:

- The spatially distributed values of the percolation flux at the potential repository horizon
- The components of fracture and matrix flow within and below the potential repository horizon
- The perched water zones and associated flow barriers
- The probable flow paths from the potential repository to the water table
- Groundwater travel/tracer transport times and radionuclide migration paths from the potential repository to the water table, and breakthrough curves and areas at the water table for tracers and radionuclides.

In developing the UZ Model, much emphasis has been placed on preparing a defensible and credible UZ Model for Yucca Mountain to evaluate its potential as an underground radioactive waste potential repository. Major activities, as reported in this AMR, include updated model calibration studies of 3-D UZ flow, perched water, geochemistry, geothermal conditions, estimates of groundwater travel time and radionuclide transport, and model validation efforts.

The other activities involving generating 28 3-D flow fields (Sections 6.2 and 6.6) to evaluate the uncertainty and sensitivity of the UZ Model relative to fracture-matrix parameters and infiltration rates over the mountain by using three sets of model parameters and nine infiltration scenarios. Eighteen of the 28 flow fields are submitted for use in TSPA calculations of radionuclide transport through the UZ system and other activities such as drift seepage abstraction.

Key scientific notebooks (with relevant page numbers) used for modeling and validation activities described in this AMR are listed in [Table 6-1](#).

Table 6-1. Model Development Documentation Scientific Notebooks

LBNL Scientific Notebook	Page #/Related Contents	Accession Number (ACC)
YMP-LBNL-GSB-YSW-2	p. 132-188/ UZ Model calibrations, TSPA flow fields and groundwater travel times and tracer transport	MOL.20000308.129
YMP-LBNL-UZJL-1.0	P.1 - 104 / Chloride modeling studies and analyses	MOL.20000308.130
YMP-LBNL-YSW-WZ-1	p. 73-93, 122-127/Post-processing and analyses of results for calibrations, flow fields and transport	MOL.20000308.131
YMP-LBNL-GSB-1.6.3	p. 74-104/Geothermal calibrations	MOL.20000308.132
YMP-LBNL-GBS-TX-1	p. 17-59/Calcite calibrations	MOL.20000308.133
YMP-LBNL-JSW-CFA-6.1	p. 1-26, 39-48, 72-88/Alcove 1 simulations	MOL.20000308.134
YMP-LBNL-GBS-1.1.2	p. 153-157-D pneumatic & Alcove 1 simulations	MOL.20000308.135
YMP-LBNL-GSB-LHH-2	p. 67-73/Alcove1 modeling	MOL.20000308.136
YMP-LBNL-YWT-ELS-1	p. 37-42, p. 49-52 / Reactive surface areas	MOL.20000308.137

6.1 MODEL DESCRIPTION

The conceptual and numerical models used for the modeling studies documented in this AMR are fully documented in the AMR: *Conceptual and Numerical Models for Flow & Transport* (CRWMS M&O 2000c). Elements of the conceptual and numerical models are included in this section so that a complete discussion of the model is presented.

6.1.1 Geological Model and Numerical Grids

The geological model used in this AMR for developing the UZ Model and its submodels is based on the Geological Framework Model (GFM) 3.1 and Integrated Site Model (ISM) 3.0, and the development and features of the two 3-D model grids with the geological model are documented in the AMR entitled, *Development of Numerical Grids for UZ Flow and Transport Modeling* (CRWMS M&O 1999d). [Table 6-2](#) lists the geological units/layers for different hydrogeologic units and the associated UZ Model numerical grid-layer information. These geologic formations have been reorganized into layered hydrogeologic units based primarily on the degree of welding (Montazer and Wilson. 1984). These are the Tiva Canyon welded (TCw) hydrogeologic unit, the Paintbrush nonwelded unit (PTn), the Topopah Spring welded (TSw) unit, the Calico Hills nonwelded (CHn), and the Crater Flat undifferentiated (CFu) units.

Table 6-2. GFM3.1 (CRWMS M&O 1999d) Lithostratigraphy, UZ Model Layer, and Hydrogeologic Unit Correlation Used in the UZ Flow Model and Submodels

Major Unit	GFM3.1* Lithostratigraphic Nomenclature	FY 99 UZ Model Layer	Hydrogeologic Unit
Tiva Canyon welded (TCw)	Tiva_Rainier	tcw11	CCR, CUC
	Tpcp	tcw12	CUL, CW
	TpcLD		
	Tpcpv3	tcw13	CMW
	Tpcpv2		
Paintbrush nonwelded (PTn)	Tpcpv1	ptn21	CNW
	Tpbt4	ptn22	BT4
	Tpy (Yucca)		
		ptn23	TPY
		ptn24	BT3
	Tpbt3		
	Tpp (Pah)	ptn25	TPP
	Tpbt2	ptn26	BT2
	Tptrv3		
	Tptrv2		
Topopah Spring welded (TSw)	Tptrv1	tsw31	TC
	Tptrn	tsw32	TR
	Tptrl, Tptf	tsw33	TUL
	Tptpul		
	Tptpmn	tsw34	TMN
	Tptpll	tsw35	TLL
	Tptpln	tsw36	TM2 (upper 2/3 of Tptpln)
		tsw37	TM1 (lower 1/3 of Tptpln)
	Tptpv3	tsw38	PV3
	Tptpv2	tsw39	PV2
Calico Hills nonwelded (CHn)	Tptpv1	ch1 (vit, zeo)	BT1 or BT1a (altered)
	Tpbt1		

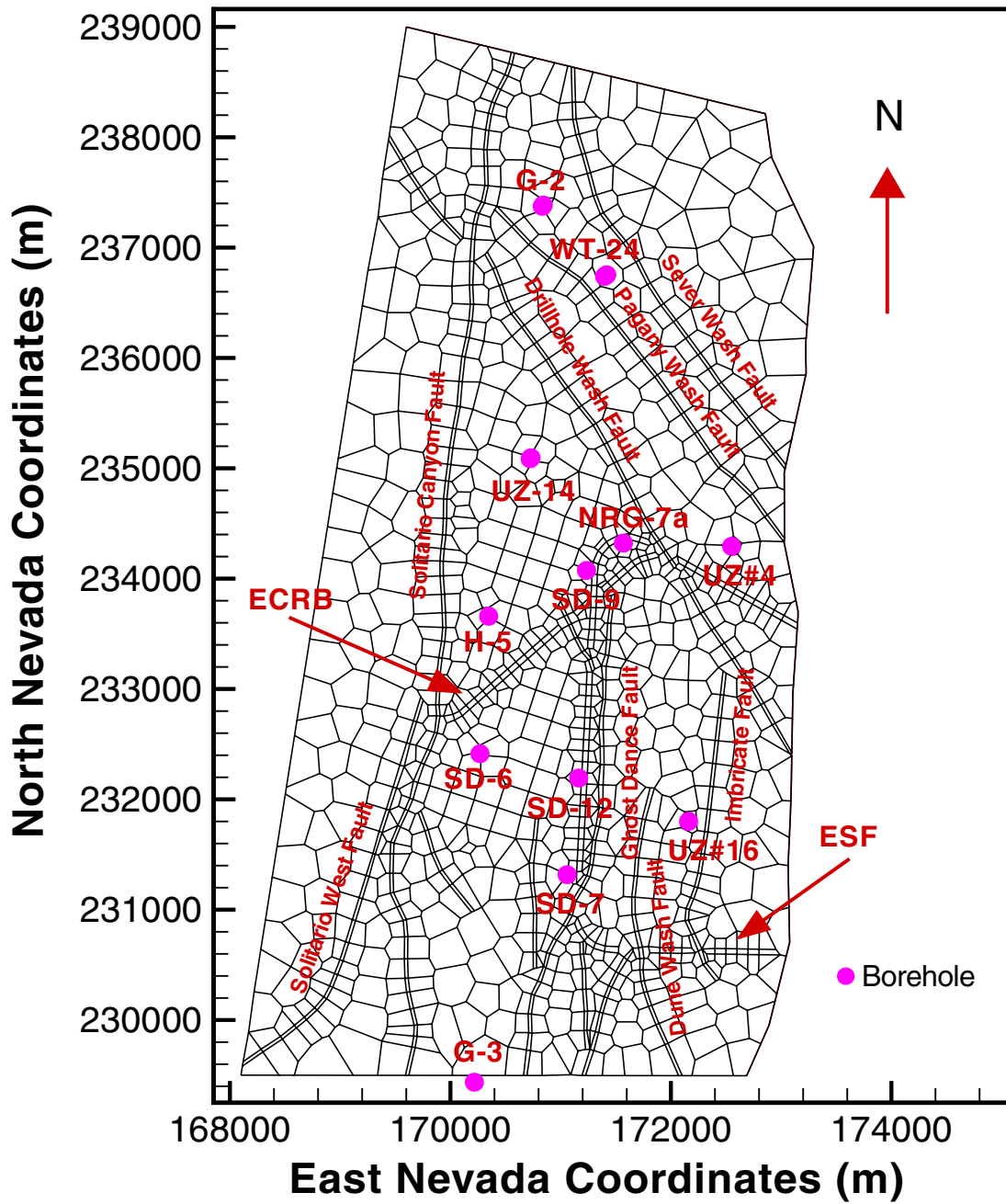
NOTE: * GFM3.1 (CRWMS M&O 1999d) refers to the Geologic Framework Model Version 3.1.

Table 6-2. GFM3.1 (CRWMS M&O 1999d) Lithostratigraphy, UZ Model Layer, and Hydrogeologic Unit Correlation Used in the UZ Flow Model and Submodels (Cont.)

Major Unit	GFM3.1* Lithostratigraphic Nomenclature	FY 99 UZ Model Layer	Hydrogeologic Unit
	Tac (Calico)	ch2 (vit, zeo)	CHV (vitric) or CHZ (zeolitic)
		ch3 (vit, zeo)	
		ch4 (vit, zeo)	
		ch5 (vit, zeo)	
	Tacbt (Calicobt)	ch6	BT
	Tcpuv (Prowuv)	pp4	PP4 (zeolitic)
	Tcpuc (Prowuc)	pp3	PP3 (devitrified)
	Tcpm (Prowmd)	pp2	PP2 (devitrified)
	Tcplc (Prowlc)		
	Tcplv (Prowlv)	pp1	PP1 (zeolitic)
	Tcpbt (Prowbt)		
	Tcbuv (Bullfroguv)		
Crater Flat undifferentiated (CFu)	Tcbuc (Bullfroguc)	bf3	BF3 (welded)
	Tcbm (Bullfrogmd)		
	Tcblc (Bullfroglc)		
	Tcblv (Bullfroglv)	bf2	BF2 (nonwelded)
	Tcbbt (Bullfrogbt)		
	Tctuv (Tramuv)		
	Tctuc (Tramuc)	tr3	Not Available
	Tctm (Trammd)		
	Tctlc (Tramlc)		
	Tctlv (Tramlv)	tr2	Not Available
	Tctbt (Trambt)		

NOTE: * GFM3.1 (CRWMS M&O 1999d) refers to the Geologic Framework Model Version 3.1.

The 3-D model domain and the two 3-D numerical grids for this study are shown in plan view in Figures 6-1 and 6-2 respectively. The first model grid, shown in Figure 6-1, is referred to as the 3-D calibration grid. It includes refined gridding along the Enhanced Characterization of Repository Block (ECRB) and ESF tunnels and is primarily used for the purpose of model calibration. The second grid (Figure 6-2), the TSPA grid, is designed for simulations of 3-D flow fields delivered for use in TSPA calculations. This TSPA grid uses a refined mesh in the vicinity of the potential repository, located near the center of the model domain. Also, shown in Figures 6-1 and 6-2 are the locations of several boreholes used in model calibrations and analyses. The model domain is selected to focus on the study area of the potential repository area and to investigate the effects of different infiltration scenarios and major faults on moisture flow around and below the potential repository. Faults are represented in the model by vertical or inclined 30-meter thick zones.



DTN: LB990501233129.004

Figure 6-1. Plan View of the 3-D UZ Calibration Model Grid, Showing the Model Domain, Faults Incorporated, ESF and ECRB, and Several Borehole Locations.

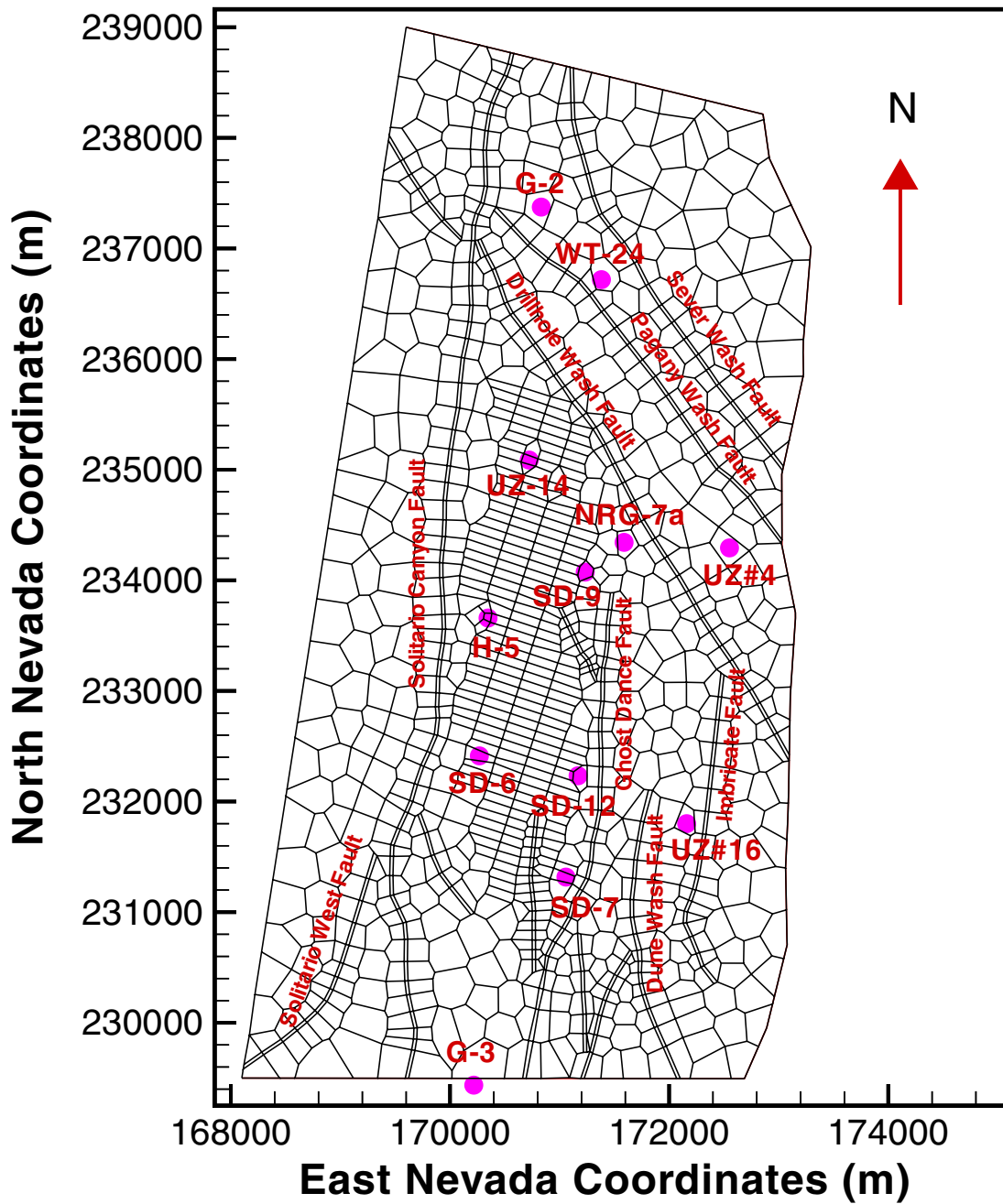


Figure 6-2. Plan View of the 3-D UZ TSPA Model Grid, Showing the Model Domain, Faults Incorporated and Several Borehole Locations.

The calibration grid, as shown in Figure 6-1, has 1,434 mesh columns of both fracture and matrix continua and a maximum of 37 computational grid layers in the vertical direction, resulting in 104,156 gridblocks and 421,134 connections in a dual-permeability grid. The TSPA grid (Figure 6-2) has 1,324 mesh columns for the TSPA grid, a maximum of 37 computational grid layers in the vertical direction, with 97,976 gridblocks and 396,770 connections in a dual-permeability grid.

6.1.2 Numerical Codes and Modeling Approach

The simulation results presented in this AMR were carried out using TOUGH2 V1.4 (STN: 10007-1.4-0.1, Version 1.4); T2R3D V1.4 (STN: 10006-1.4-00, Version 1-4), TOUGHREACT9 V1.0 (STN: 10153-1.0-00), and TOUGHREACT V2.2 (STN: 10154-2.2-00, Version 2.2), as summarized in Section 3. The single active liquid phase flow module (EOS9) (Wu et al. 1996) was used to calibrate the UZ Model and several submodels and to generate 3-D TSPA flow fields. For temperature simulation, the TOUGH2 V1.4 EOS3 module (Pruess 1991) was used. Tracer transport and chloride studies were performed using the decoupled module of T2R3D V1.4 and flow fields from the EOS9 module. The TOUGHREACT9 V1.0 code was used for calcite calibration.

To model the flow and transport processes occurring in the UZ at Yucca Mountain, mathematical models or governing equations are needed to describe the physical processes quantitatively to model the flow and transport processes occurring in the unsaturated zone. The physical processes associated with flow and transport in porous media are governed by the fundamental conservation laws, i.e., conservation of mass, momentum, and energy governs the behavior of fluid flow, chemical transport, and heat transfer through fractured porous media. The macroscopic continuum approach has been most commonly used in practical applications. In this approach the physical laws governing flow of several fluids, transport of multicomponents, and heat transfer in porous media are often represented mathematically on the macroscopic level by a set of partial differential or integral equations. Fluid and heat flow and chemical transport processes in fracture and matrix systems in the UZ are described using a macroscopic continuum approach.

In addition to the conservation or continuity equations of mass and thermal energy in fracture and matrix systems, specific relationships or *mechanisms* are needed that describe why and how fluid flow, solute transport, and heat transfer occur in porous and fractured media. The following specific laws act as such mechanisms by governing local fluid flow, component transport, and heat transfer processes in porous and fractured media:

1. Darcy's law is applied to describe the two-phase flow of gas and water in both fractures and matrix. In particular, Richards' equation is used in describing isothermal, unsaturated liquid flow through the UZ at Yucca Mountain. Relative permeability and capillary functions of both fractures and matrix follow the van Genuchten model (van Genuchten, 1980).
2. The migration of dissolved mass components or chemical species within a fluid in the two-phase fractured-porous media system is governed by advective, diffusive, and dispersive processes. It is also subject to other processes such as radioactive decay, adsorption, dissolution and precipitation, mass exchange or partition between phases,

and other chemical reactions under local thermodynamic equilibration or kinetic reactions.

3. The generalized Fick's law, including hydrodynamic dispersion effects in a multiphase system, is used to evaluate diffusive and dispersive flux of chemical transport.

The multiphase extension of Darcy's law, Richards' equation, and the generalized Fick's law have been used as fundamental laws that govern flow and transport processes within porous medium rocks in both research and application. These fundamental laws or correlations, mainly based on experimental and field studies, reflect our current understanding of porous-medium physics.

A key issue for simulating fluid and heat flow and chemical transport in the fractured-porous rock of Yucca Mountain is how to handle fracture and matrix flow and interactions under multiphase, multicomponent, and isothermal or nonisothermal conditions. The available methods for treating fluid flow in fractures and the rock matrix using a numerical approach include: (1) an explicit discrete-fracture and matrix representation; (2) the dual-continua method, including double- and multi-porosity, dual-permeability, or the more general "multiple interacting continua" (MINC) method (Pruess and Narasimhan 1985); and (3) the generalized effective continuum method (ECM). For the work documented in this AMR, the dual-permeability conceptual model is applied to evaluate fluid and heat flow and transport in the fracture-matrix system of the UZ system of Yucca Mountain and the active fracture model is adopted to modify fracture-matrix interface areas for flow and transport between fracture and matrix systems.

The dual-continua method provides an appropriate representation of flow and transport processes within the UZ at Yucca Mountain (Doughty 1999; CRWMS M&O 2000c) and is computationally much less demanding than the discrete-fracture-modeling approach and therefore has become the main approach used in the modeling studies of the Yucca Mountain Site Characterization Project. The dual-permeability methodology for handling fluid flow, tracer transport, and heat transfer through fractured rocks treats fracture and rock matrix flow and interactions with a multi-continua numerical approach. It considers global flow occurring not only between fractures but also between matrix grid blocks. In this approach, fracture and matrix are each represented by one gridblock, connected to each other. Because of the one-block representation of fracture or matrix, the interflow between fractures and matrix has to be handled using some quasi-steady-state flow assumption, and this may limit its application in estimating effects of gradients of pressures, temperatures, and concentrations within the matrix. Under steady-state flow conditions, however, the gradients near the matrix surfaces become minimal, and the model is expected to produce accurate solutions (Doughty 1999). When applied as documented in this AMR, the traditional dual-permeability concept is further modified using an active fracture model (Liu et al. 1998) to represent fingering effects of flow through fractures and to limit flow into the matrix system. As an alternative, use of the discrete fracture or weeps type model will face extremely high uncertainties in fracture distribution data within the mountain and extensive computational burden that cannot be solved in the near future. On the other hand, the ECM approach, although the most computationally efficient, may not capture important, rapid transient interactions in flow and transport between fractures and matrix. For temperature calibration, the ECM modeling approach is used instead of the dual-permeability formulation because at ambient geothermal conditions, fractures and matrix are in thermal equilibrium and the ECM provides a good approximation.

Ambient variably saturated flow in the UZ underlying Yucca Mountain is approximated as an isothermal, steady-state flow system. This is considered to be a good approximation within the UZ below the PTn unit because the relatively unfractured nonwelded PTn unit is expected to damp and homogenize downward moving transient pulses arising from episodic surface infiltration events.

6.1.3 Model Boundary Conditions

The ground surface of the mountain (or the tuff-alluvium contact in areas of significant alluvial cover) is taken as the top model boundary; the water table is treated as the bottom model boundary. Both the top and bottom boundaries of the model are treated as Dirichlet-type conditions with specified constant but spatially distributed temperature, gas pressure, and constant liquid saturation values along these surfaces. For flow simulations using the EOS9 module, only pressure or saturation values are needed along the top and bottom model boundaries. Surface infiltration, as discussed below in Section 6.1.4, is applied using a source term in the gridblocks within the second grid layer from the top. This method was adopted because the first layer is treated as a Dirichlet-type boundary with constant pressure, saturation, and temperature to represent average atmospheric conditions.

All lateral boundaries, as shown in Figures 6-1 and 6-2, are treated as no-flow (closed) boundaries, which allow flow only within the faults. This treatment should be reasonable for the eastern boundary, which is along the Bow Ridge fault, because high vertical permeability and lower capillary forces are expected for the faults (see fault properties estimated in the AMR, (CRWMS M&O 1999d). For the southern, western, and northern lateral boundaries, no lateral flow boundaries would have little effect on moisture flow within and near the potential repository areas because these boundaries are far away from the potential repository.

The spatially distributed values of temperatures along the top and bottom boundaries are based on field observation. The pressure conditions at the bottom boundary of the model are based on observed gas-pressure values. The water table, which is the bottom boundary of the UZ Model, is assumed to be a flat, stable surface (CRWMS M&O 1999d). The flat water table specification has little effect on the flow simulation results because flow is essentially determined by upstream, not downstream conditions. In the eastern part of the site to the Solitario Canyon fault, the water table elevation is about 730 meters above sea level (masl); however, the water table elevation increases by 46 meters west of the Solitario Canyon fault. The gas pressures are estimated using a pressure value of 0.92 bars at an elevation of 730 m. Surface gas pressures are determined by running the TOUGH2 code, EOS3 module to steady-state under given temperature, bottom pressure, and surface-infiltration conditions. This is necessary to generate a steady-state, equilibrated gas-pressure boundary to avoid artificial air flow or circulation, which may occur when nonequilibrated pressures are imposed on the ground surface boundaries.

6.1.4 Infiltration Scenarios

Water entering the UZ as net infiltration from precipitation at land surface is the major control on overall hydrologic and thermohydrologic conditions within the UZ at Yucca Mountain. Net infiltration is the ultimate source of percolation through the UZ, and water percolating downward

through the UZ will be the principal means by which radionuclides may be transported from the potential repository to the water table.

A total of nine net infiltration maps are implemented with the UZ Model and its submodels. These infiltration maps are documented in the two AMRs (*Climate Model; Infiltration Model*) for infiltration and climate models. They include present-day, Monsoon, and Glacial Transition – three climatic scenarios, each of which consists of lower-bound, mean and upper-bound rates. The nine infiltration rates are summarized in [Table 6-3](#) for average values over the model domain.

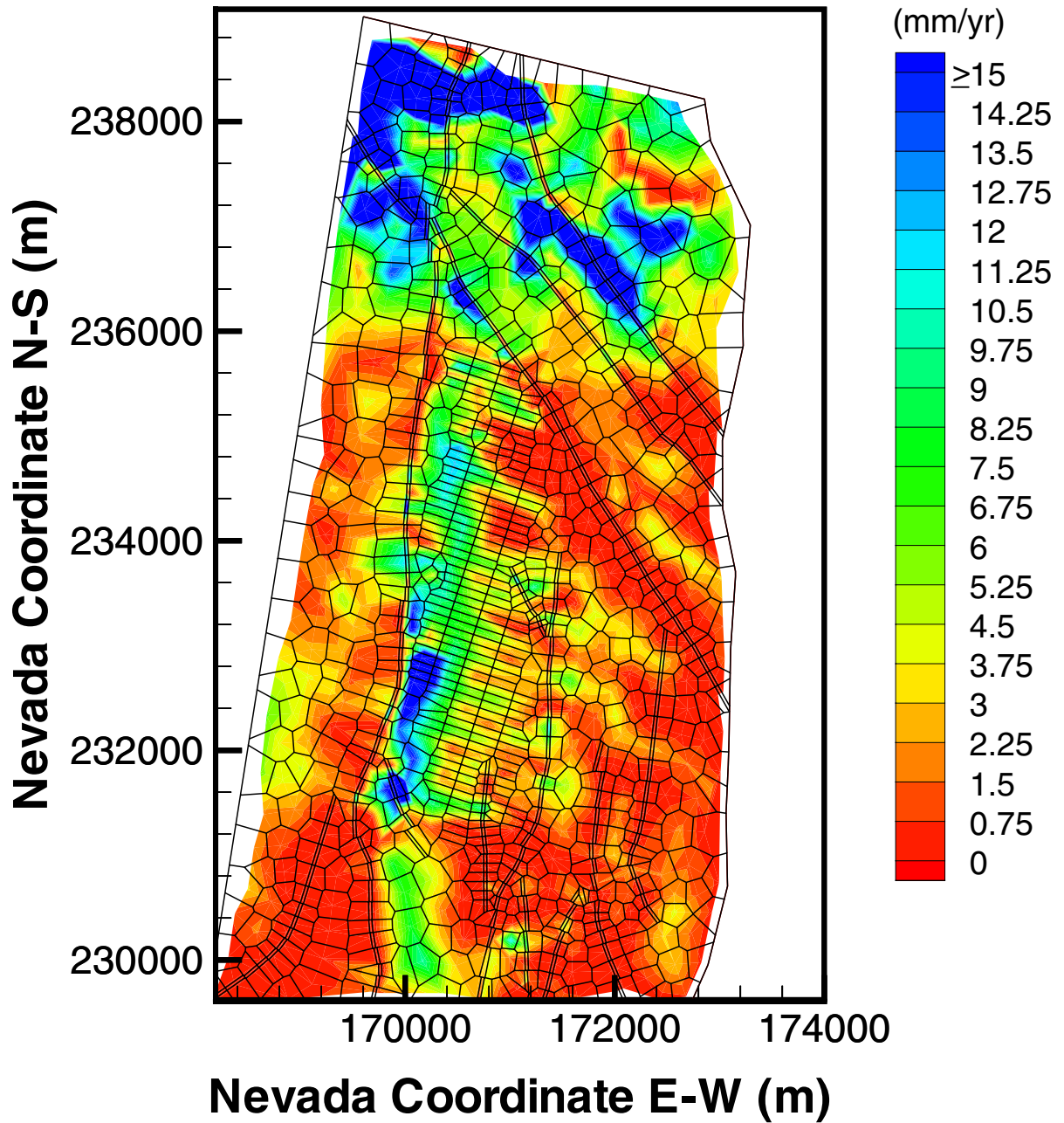
Table 6-3. Infiltration Rates (mm/year) Averaged over the Model Domain

Scenario	Lower Bound Infiltration	Mean Infiltration	Upper Bound Infiltration
Present-Day	1.20	4.56	11.24
Monsoon	4.60	12.36	20.12
Glacial Transition	2.40	17.96	33.52

ACC and DTNs: MOL.19991014.0102.; LB990501233129.004, LB990701233129.001

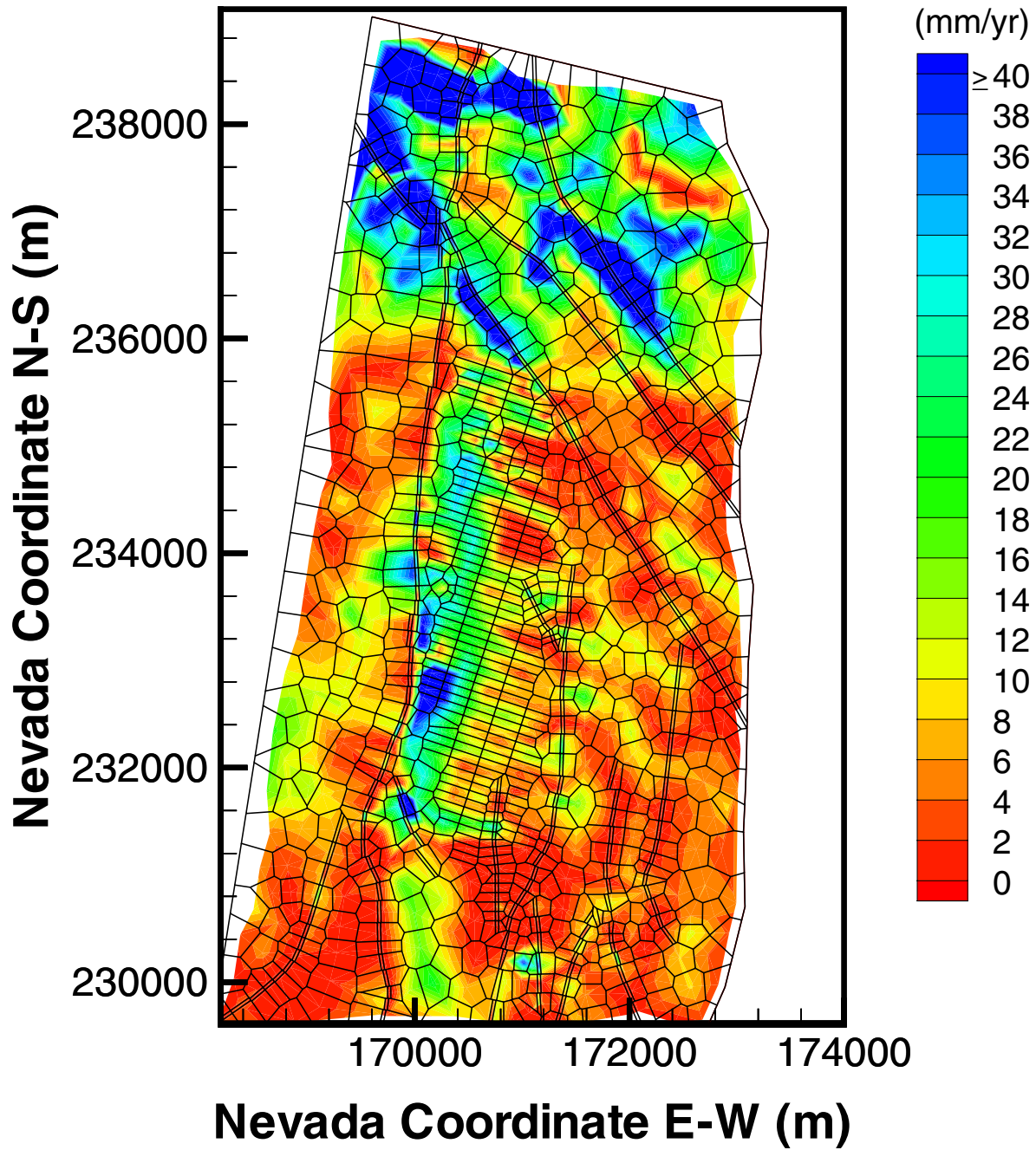
As shown in [Table 6-3](#), the average rate for the present-day mean infiltration with the calibration grid is 4.56 mm/yr distributed over the model domain, which is considered as a base-case scenario. The lower- and upper-bound infiltration values are intended to cover the uncertainties in the infiltration models of possible higher or lower rates. The two future climatic scenarios, the Monsoon and Glacial Transition periods, are used to account for possible higher precipitation and infiltration conditions in the future at Yucca Mountain. Note that the Glacial Transition has higher infiltration rates except for the lower-bound use. The average values in [Table 6-3](#) are based on the TSPA grid shown in [Figure 6-2](#).

A plan view of the spatial distribution of the three mean infiltration maps, as interpolated onto the TSPA grid, is shown in [Figures 6-3, 6-4 and 6-5](#) respectively, for the present-day, Monsoon, and Glacial Transition mean infiltration scenarios. The figures show similar flux distributions of the three infiltration rates, with higher infiltration rates in the northern part of the model domain and along the mountain ridge east of the Solitario Canyon fault from south to north.



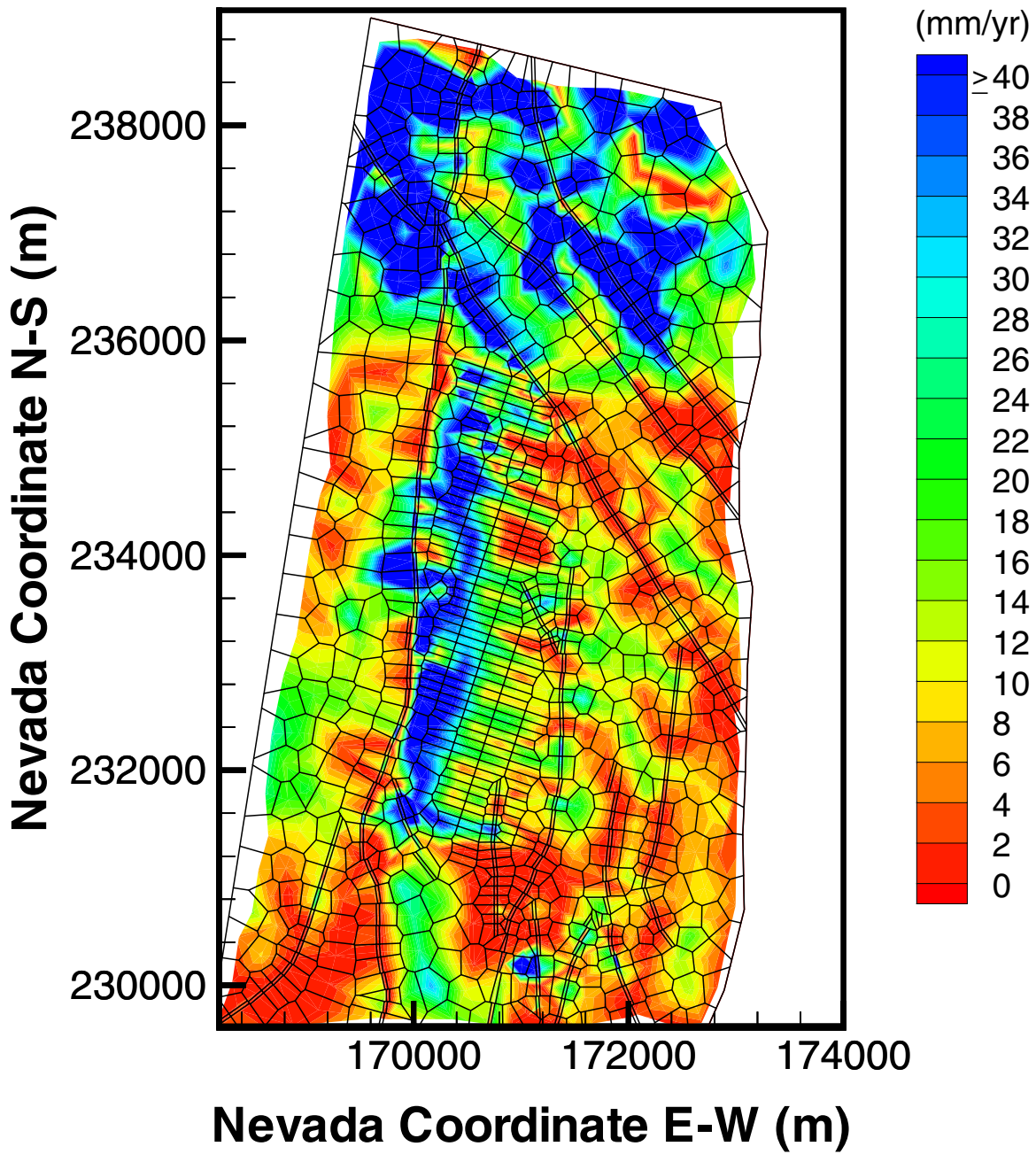
DTN: GS000399991221.002

Figure 6-3. Plan View of Net Infiltration Distributed Over the 3-D UZ TSPA Model Grid for the Base-Case, or Present-Day, Mean Infiltration Scenario.



DTN: GS000399991221.002

Figure 6-4. Plan View of Net Infiltration Distributed Over the 3-D UZ TSPA Model Grid for the Monsoon, Mean Infiltration Scenario.



DTN: GS000399991221.002

Figure 6-5. Plan View of Net Infiltration Distributed Over the 3-D UZ TSPA Model Grid for the Glacial Transition, Mean Infiltration Scenario.

6.1.5 Model Parameters and Rock Properties

The key input rock and fluid-flow parameters used in UZ Model development are summarized in Section 4. They include (1) fracture properties (frequency, permeability, van Genuchten α and m parameters, aperture, porosity, interface area, and residual and saturated saturations) for each UZ Model layer; (2) matrix properties (porosity, permeability, the van Genuchten a and m parameters, and residual and saturated saturations) for each UZ Model layer; (3) thermal and transport properties (grain density, wet and dry thermal conductivity, grain specific heat, and tortuosity coefficients) for each UZ Model layer; and (4) fault properties (matrix and fracture parameters) for each of the major hydrogeologic units (Table 6-1). The development and estimation of these parameters are presented in the AMR: *Calibrated Properties Model* (CRWMS M&O 2000b) and DTN: GS000399991221.004.

The rock parameter specification in the 3-D UZ Model and its submodels is, in general, layer by layer, but certain portions of grid layers representing the CHn unit are altered. In these layers, zeolitic tuff properties are specified for altered zones. We treat all of the geological units, including those representing fault zones, as fracture-matrix systems using a dual-permeability approach. The van Genuchten relative permeability and capillary pressure functions (van Genuchten 1980) are used to describe flow in both fractures and matrix.

6.2 3-D UZ FLOW MODEL CALIBRATION

A critical step in developing the 3-D UZ flow model was to use field-measured liquid saturation, water potential, and perched water data for calibrations of the 3-D model. This is part of the important iterative processes of model calibration and verification which increases confidence in model predictions for the site conditions. A detailed modeling investigation is reported in the AMR (CRWMS M&O 2000b) using one-dimensional (1-D) models for estimating model parameters with water potential, saturation and other types of data. However, these 1-D models do not predict perched water occurrence in several hydrogeological units below the potential repository level. This section documents a further model calibration effort, focusing on the 3-D perched water calibrations using the 3-D calibration grid (Figure 6-1).

The calibration was conducted using the three sets of parameters (CRWMS M&O 2000b), three present-day infiltration rates (See Table 6-3), and the geological model and numerical grid for calibration (CRWMS M&O 1999d). Two water perching models were investigated in which rock properties were locally modified in several gridlayers of the lower basal vitrophyre in the TSw unit and upper zeolites in the CHn unit. The objective of using these different water-perching models was (1) to match occurrences as observed at the site with different conceptual models for perched water and (2) to investigate effects on groundwater travel and radionuclide transport by varying the percentage of “flow-through” and “by-passing” flow of the perched bodies.

6.2.1 Calibration Data

Calibration data used in the 3-D UZ flow model calibration are matrix liquid saturations, matrix water potentials and perched water elevations, as observed from boreholes and the ECRB.

Table 6-4 shows the types of data from boreholes and the ECRB used in the calibration, and Figure 6-1 shows the locations of the boreholes and the tunnel at Yucca Mountain.

Table 6-4. Data Used for 3-D Flow Model Calibration

Borehole/ECRB	Matrix Liquid Saturation (core)	Matrix Liquid Water Potential (in situ)	Perched Water Elevation (masl)
USW NRG-7a		✓	✓
USW SD-6	✓		
USW SD-7	✓		✓
USW SD-9	✓		✓
USW SD-12	✓	✓	✓
USW UZ-14	✓		✓
UE-25 UZ#16	✓		
USW WT-24	✓		✓
USW G-2			✓
ECRB		✓	

6.2.2 Perched Water Conceptual Models

Conceptual models involving perched water in the unsaturated zone below the potential repository horizon are of particular interest in assessing the system performance of the potential repository. Waste-isolation strategies at the potential repository depend in part on sorption within the zeolitic portions of the CHn and on groundwater travel times between the potential repository horizon and the water table. The genesis of perched water at Yucca Mountain is much debated among Yucca Mountain project scientists, and several conceptual models have been discussed (e.g., Wu et al. 1999b).

Perched water may occur where percolation flux exceeds the capacity of the geologic media to transmit vertical flux in the unsaturated zone. Perched water has been encountered in a number of boreholes at Yucca Mountain, including UZ-14, SD-7, SD-9, SD-12, NRG-7a, G-2, and WT-24. These perched water occurrences are found to be associated with low-permeability zeolites in the CHn or the densely welded basal vitrophyre (Ttpv3, Table 6-2) of the TSw unit. Possible mechanisms of water-perching in the unsaturated zone of Yucca Mountain may be permeability or capillary barrier effects at faults, or a combination of both.

A permeability-barrier conceptual model (Conceptual Model #1) for perched water occurrence has been used in the UZ flow-modeling studies since 1996, as summarized in Wu et al. (1999b). In this model, perched water bodies in the vicinity of the ESF North Ramp (near boreholes UZ-14, SD-9, NRG-7a, G-2 and WT-24) are observed to occur above the base of the TSw, underlain by a zone of low-permeability zeolitized rock. The perched bodies in this northern area of the potential repository may be interconnected. However, the perched water zones at boreholes SD-7 and SD-12 are considered here as local, isolated bodies. In this conceptual model, both vertical and lateral water movement in the vicinity of the perched zones is considered to be controlled mainly by the fracture and matrix permeability distribution in these areas. The major aspects of the permeability-barrier conceptual model are: (1) no large-scale vertically connected potentially

fluid-conducting fractures transect the underlying low-permeability units, (2) both vertical and horizontal permeabilities within and below the perched water zone are small compared with permeabilities outside perching zones, and (3) sufficient percolation flux (>1 mm/yr) exists due to the lower permeability of the matrix rock. Previous modeling studies (Wu et al. 1999b) concluded that this conceptual water-perching model is able to match the observation data of perched water in the unsaturated zone of Yucca Mountain.

Another perched water conceptual model (Conceptual Model #2) is the unfractured zeolite model. Similar to the permeability barrier model discussed above, this model presumes that the occurrence of perched water at Yucca Mountain results mainly from the lack of globally connected, fluid conducting fractures within zeolitic units. This model can be considered a special case of the permeability-barrier model, in which a water-perching mechanism is controlled by the low-permeability zeolitic matrix only, i.e., it is assumed that fractures are not present in perching layers. The concept of an unfractured zeolite model is partially supported by the fracture data presented in an AMR for the analysis of hydrologic properties data (DTN: LB990501233129.001), which suggests a very small fracture frequency within zeolitic units.

In the present numerical studies, the occurrence of perched water is assumed to follow either of the two conceptual models, i.e., permeability-barrier and unfractured-zeolite models. In other words, perched water bodies are formed as a result of permeability-barrier effects. There are three conceptual flow scenarios investigated in this AMR, as described in Table 6-5. In addition to the two conceptual water-perching models, Table 6-5 also lists a third scenario called the non-water-perching model. This scenario cannot predict perched water in the UZ, and therefore provides an extreme case in which maximum flow through the zeolites occurs. This non-perching model is used for sensitivity analyses and comparative studies with the two water-perching models.

Table 6-5. Conceptual Flow Scenarios

Conceptual Model	Description
#1 Flow-through Model	Conceptual Model #1 (flow-through model) is the permeability-barrier model, using the calibrated, perched water parameters for fractures and matrix in the northern part of model domain. Properties are modified property layers in the tsw38, tsw39, ch1z, and ch2z, where the lower basal vitrophyre of the TSw is above the perching zeolites of the CHn. For local regions near boreholes SD-7 and SD-12 in the southern part of the model domain, properties are modified only for the gridblocks to which the borehole grid columns are directly connected, as well as the gridblocks along the two boreholes, for blocks representing ch5z, ch6z and pp4z for SD-7 and tsw38 and tsw39 for SD-12, respectively.

Table 6-5. Conceptual Flow Scenarios

#2 By-passing Model	Conceptual Model #2 is the unfractured zeolite model, excluding all fractures in the zeolitic units of the CHn and using the permeability values of 1-D calibration results directly for matrix rocks in the zeolitic and transitional units of the CHn. For a local region near Borehole SD-12, properties are modified of the direct neighboring blocks as well as the borehole gridblocks, for representing tsw38 and tsw39.
#3 Non-perching Model	Conceptual Model #3 is a non-perched-water model, in which the property sets from the 1-D inversion are directly used.

The simulations with respect to the three water-perching modeling scenarios are realized and carried out by modifying the two grid files. For Conceptual Model #1 (flow-through model), a dual-permeability mesh for the UZ calibration grid is modified by the following:

- Replace property cards of grid layers of tsw38 (tswF8/tswM8), tsw39 (tswF9/tswM9), ch1z (ch1Fz/ch1Mz) and ch2z (ch2Fz/ch2Mz) by (pcF38/pcM38), (pcF39/ pcM39), (pcF1z/pcM1z), and (pcF2z/pcM2z), respectively, where the basal vitrophyre of the TSW is underlain by zeolitic units.
- Near Borehole SD-7, properties are modified for the gridblocks in grid columns, i62, k88, l43, l44, and k90, over grid layers of ch5z (ch5Fz/ch5Mz), ch6z (ch6Fz/ch6Mz) and pp4 (pp4Fz/pp4Mz) by (pcF5z/pcM5z), (pcF6z/pcM6z), and (pcF4p/pcM4p), respectively.
- Near borehole SD-12, properties are modified for the gridblocks in grid columns, k64, b93, b99, k61, k62 and k67, over grid layers of tsw38 (tswF8/tswM8) and tsw39 (tswF9/tswM9) by (pcF38/pcM38) and (pcF39/pcM39), respectively.

For Conceptual Model #2 (unfractured zeolite or by-passing model), the dual-permeability mesh is modified by reassigning rock properties only at SD-12 over two gridlayers:

- Near gridblocks in grid columns, k64, b93, b99, k61, k62 and k67, over grid layers of tsw38 (tswF8/tswM8) and tsw39 (tswF9/tswM9) by (pcF38/pcM38) and (pcF39/pcM39), were modified respectively.
- Assigning the fracture blocks in the zeolitic CHn layers of model to matrix parameters, effectively removing the fractures.

The two perched models and the non-perched model are represented using three sets of 3-D, dual-permeability calibration model grids:

- “3d2kcalib_pc1.mesh” for perched water Conceptual Model #1 (DTN: LB990501233129.004).
- “3d2kcalib_pc2.mesh” for perched water Conceptual Model #2 (DTN: LB990501233129.004).

- “MESH_CAL.V1” for non-perched water or Conceptual Model #3 of this AMR (DTN: LB990701233129.002).

6.2.3 Calibrated Parameters for Perched Water Zones

As discussed above, to calibrate the 3-D UZ flow model against observed perched water conditions at Yucca Mountain, some local modification of rock properties is necessary. In general, permeability was adjusted only within the model layers associated with the perched water occurrence. At Yucca Mountain, a common example of water-perching caused by a permeability barrier is the case in which the highly fractured basal vitrophyre of the TSw unit overlies bedded units of low permeability. In addition to a permeability barrier, two other conditions are required for perched water to exist: a certain lateral flow resistance and sufficient percolation flux.

For perched water Conceptual Model #1, calibrated parameters of fracture and matrix permeabilities within perched zones are results from a series of modeling studies of 3-D simulations. Matrix permeabilities of potential perched layers/zones, as identified in the model grid layers of Section 6.2.2, are based on average values of the measured matrix permeabilities, while fracture permeabilities used for the northern perched zones are 10 times higher than matrix permeabilities under the mean and upper-bound infiltration scenarios. In the lower infiltration case, the same permeability values exist for both fractures and matrix for perched zones near SD-7 or SD-12 effectively removing fractures and making this into a special case of Conceptual Model #2. Other than intrinsic permeabilities, van Genuchten’s α and m parameters, as well as residual saturations for matrix blocks within perched zones, are identical to parameters estimated from the 1-D inversions (CRWMS M&O 2000b). The active-fracture parameter, γ , is set to zero for all the perched zones, causing the fracture-matrix interface area factor to be equivalent to liquid saturation (Liu et al. 1998). Tables 6-6, Table 6-7 and 6-8 present the final three sets of calibrated rock properties at zones with perched water using Conceptual Model #1, with base-case (mean), upper-bound, and lower-bound present-day infiltration scenarios, respectively.

Table 6-6. Calibrated Parameters for Perched Water Conceptual Model #1 (Flow-Through Model) for the Base-Case Present-Day Infiltration Scenario

Model Layer	k_M (m ²)	α_M (1/Pa)	m_M (-)	k_F (m ²)	α_F (1/Pa)	m_F (-)	γ (-)
Tsw38/pcM38/ pcF38	3.00E-19	6.94E-6	0.324	3.00E-18	6.94E-6	0.324	0.00
Tsw39/pcM39/ pcF39	6.20E-18	2.29E-5	0.381	6.20E-17	2.29E-5	0.381	0.00
ch1z/pcM1z/pcF1z	9.30E-20	2.68E-7	0.316	9.30E-19	2.68E-7	0.316	0.00
ch2z/pcM2z/pcF2z	2.40E-18	3.47E-6	0.245	2.40E-17	3.47E-6	0.245	0.00
ch5z/pcM5z/pcF5z	2.40E-18	3.47E-6	0.245	2.40E-18	3.47E-6	0.245	0.00
ch6/pcM6z/pcF6z	1.10E-19	3.38E-7	0.510	1.10E-19	3.38E-7	0.510	0.00
pp4/pcM4p/pcF4p	7.70E-19	1.51E-7	0.676	7.70E-19	1.51E-7	0.676	0.00

DTN: LB991121233129.001

Table 6-7. Calibrated Parameters for Perched Water Conceptual Model #1 (Flow-Through Model) for the Upper-Bound Present-Day Infiltration Scenario

Model Layer	k_M (m2)	α_M (1/Pa)	m_M (-)	k_F (m2)	α_F (1/Pa)	m_F (-)	γ (-)
tsw38/pcM38/pcF38	3.00E-19	5.56E-7	0.314	3.00E-18	5.56E-7	0.314	0.00
tsw39/ pcM39/ pcF39	6.20E-18	1.82E-5	0.377	6.20E-17	1.82E-5	0.377	0.00
ch1z/pcM1z/pcF1z	9.30E-20	4.23E-7	0.336	9.30E-19	4.23E-7	0.336	0.00
ch2z/pcM2z/pcF2z	2.40E-18	1.13E-6	0.229	2.40E-17	1.13E-6	0.229	0.00
ch5z/pcM5z/pcF5z	2.40E-18	1.13E-6	0.229	2.40E-18	1.13E-6	0.229	0.00
ch6/pcM6z/pcF6z	1.10E-19	3.57E-7	0.502	1.10E-19	3.57E-7	0.502	0.00
pp4/pcM4p/pcF4p	7.70E-19	1.83E-7	0.683	7.70E-19	1.83E-7	0.683	0.00

DTN: LB991121233129.003

Table 6-8. Calibrated Parameters for Perched Water Conceptual Model #1 (Flow-Through Model) for the Lower-Bound Present-Day Infiltration Scenario

Model Layer	k_M (m2)	α_M (1/Pa)	m_M (-)	k_F (m2)	α_F (1/Pa)	m_F (-)	γ (-)
tsw38/pcM38/pcF38	3.00E-19	3.72E-6	0.291	3.00E-19	3.72E-6	0.291	0.00
tsw39/ pcM39/ pcF39	6.20E-18	2.37E-5	0.321	6.20E-18	2.37E-5	0.321	0.00
ch1z/pcM1z/pcF1z	9.30E-20	7.26E-7	0.304	9.30E-20	7.26E-7	0.304	0.00
ch2z/pcM2z/pcF2z	2.40E-18	2.44E-6	0.135	2.40E-18	2.44E-6	0.135	0.00
ch5z/pcM5z/pcF5z	2.40E-18	2.44E-6	0.135	2.40E-18	2.44E-6	0.135	0.00
ch6/pcM6z/pcF6z	1.10E-19	5.06E-7	0.445	1.10E-19	5.06E-7	0.445	0.00
pp4/pcM4p/pcF4p	7.70E-19	1.83E-7	0.653	7.70E-19	1.83E-7	0.653	0.00

DTN: LB991121233129.005

The modified “fracture” properties in the three tables are more close to those of matrix, in other words, fractures in water perching layers are effectively removed. For perched water Conceptual Model #2 of the unfractured zeolite or by-passing model, rock properties of all the fractures within the potential perched layers/zones are replaced by the corresponding matrix properties from the 1-D inversions (CRWMS M&O 2000b). In addition, properties of the blocks adjacent to SD-12 and the borehole column itself were adjusted. The actual perched water parameters are given in Tables 6-6, 6-7, and 6-8 under layer names tsw38/pcM38/pcF38 and tsw38/pcM38/pcF38.

6.2.4 Numerical Treatment and Solution Convergence

Numerical modeling of large-scale 3-D flow and transport in the UZ beneath Yucca Mountain is mathematically challenging. The difficulty mainly stems from the highly nonlinear coupling of

the flow system. First, the hydrogeologic system is distinctly heterogeneous on all model scales, and there are orders-of-magnitude contrasts in permeabilities across geological layers and between fracture and matrix rock. Secondly, the two-phase flow functions of relative permeability and capillary pressure for Yucca Mountain tuffs are extremely nonlinear for both fractures and matrix systems. The mathematical difficulties become even more severe when using the dual-permeability modeling approach for handling fracture-matrix interactions. In this case, flows through fractures and matrix are on very different time scales, with fracture flow being orders of magnitude faster than matrix flow. In addition, fracture elements have a much smaller storage space than matrix elements. In general, it takes simulation times of thousands to millions of years for the system to equilibrate. Rapid flow through fractures, plus the slow response in the matrix, makes it very difficult to obtain steady-state solutions numerically.

For all flow simulations (this section and Section 6.6), the EOS9 module of TOUGH2 VI.4 is used to solve Richards' equation in the unsaturated flow calculations. In this method, air/gas flow dynamics are ignored by using a constant gas-phase pressure in an isothermal system. The reason for using this simplified two-phase flow solution for the 3-D model calibrations and TSPA flow field simulations is that it is the most computationally efficient approach and at the same time provides accurate results for isothermal two-phase flow. We solve two-phase flow problems with one equation per gridblock instead of solving two or three equations as required by the EOS3 module. Secondly, numerical tests conclude that for moisture flow and distributions at steady state, the EOS9 solutions always provide almost identical answers to EOS3, "true two-phase" flow solutions ((LBNL Scientific Notebook: YMP-LBNL-YSW-2, p. 152).

Model calibrations and flow-field simulations are based on steady-state solutions using the EOS9 module. In each simulation, fracture, fault, and zeolitic element volumes are increased by a factor of 10,000 to overcome convergence difficulties associated with these nodes while keeping all other mesh geometric information unchanged. This approach does not affect the final solution as long as a "true" steady-state solution is obtained for a given run. The initial condition for a new scenario run is estimated using a default (uniform) initial condition or results of a previous, different run with a similar modeling condition. Each simulation is usually subdivided into stages. For the first-stage runs, a large convergence tolerance on the order of 10,000 or more is used to keep simulation progressing with a large time step size. It has been found that at this stage using large residual tolerance has no effects on final, steady-state solutions as long as no oscillations or unphysical solutions occur. After running the solution to 10^9 years or more with a large tolerance, the convergence tolerance is reduced to 10^{-4} , and the model is run until a steady-state solution is reached. The final steady-state solutions are confirmed using a global mass-balance check, as discussed in the next section.

6.2.5 Simulation Scenarios, Results and Analyses

This section summarizes the seven flow model calibration scenarios performed for this AMR, including simulation results and analyses. The seven model calibrations are performed using (1) the calibration grid (Figure 6-1), and three present-day infiltration maps, as discussed in Section 6.1.4; (2) the seven parameter sets in Attachment II of this AMR; and (3) the three conceptual models and the calibrated perched water parameters of Section 6.2.3.

Simulation Scenarios: Table 6-9 summarizes these seven simulation scenarios, associated conceptual models/grids, parameter sets, and infiltration rates used.

Table 6-9. Seven UZ Flow Simulation Scenarios: Data Files, Conceptual Models/Grids, Parameter Sets, Infiltration Maps for the UZ Model Calibrations

Designation/ Simulation	Conceptual Model/Grid (Table 6-5)	Parameter Set/ Calibration	Infiltration Map
uz99_m	#3 Non-perching model/ MESH_CAL.V1 DTN:LB990701233129.002	Parameter set from Table II-7, base-case/present-day, mean infiltration (AMR: CRWMS M&O 2000b) without 3-D calibration (DTN: LB991121233129.007)	Present-day, mean infiltration (Figure 6-3)
pch1_L2	#1 Flow-through perched water model/ 3d2kcalib_pc1.mesh DTN:LB990501233129.004	Parameter set from Table II-1, lower-bound/present-day infiltration (DTN: LB991121233129.005)	Present-day, lower-bound infiltration
pch2_L2	#2 By-passing perched water model/ 3d2kcalib_pc2.mesh DTN:LB990501233129.004	Parameter set from Table II-2, lower-bound/present-day infiltration (DTN: LB991121233129.006)	Present-day, lower-bound infiltration
pch1_m2	#1 Flow-through perched water model/ 3d2kcalib_pc1.mesh DTN:LB990501233129.004	Parameter set from Table II-3, base-case/mean/present-day infiltration (DTN: LB991121233129.001)	Present-day, mean infiltration (Figure 6-3)
pch2_m2	#2 By-passing perched water model/ 3d2kcalib_pc2.mesh DTN:LB990501233129.004	Parameter set from Table II-4, base-case/mean /present-day infiltration (DTN: LB991121233129.002)	Present-day, mean infiltration (Figure 6-3)
pch1_u2	#1 Flow-through perched water model/ 3d2kcalib_pc1.mesh DTN:LB990501233129.004	Parameter set from Table II-5, upper-bound/present-day infiltration (DTN: LB991121233129.003)	Present-day, upper-bound infiltration
pch2_u2	#2 By-passing perched water model/ 3d2kcalib_pc2.mesh DTN:LB990501233129.004	Parameter set from Table II-6, upper-bound/present-day infiltration (DTN: LB991121233129.004)	Present-day, upper-bound infiltration

As shown in Table 6-9, only one simulation is conducted for the non-perching model, which uses the present-day mean infiltration map. For perched water Conceptual Models #1 or #2, simulations are carried out for all the three infiltration scenarios.

Mass Balance and Solution Convergence: Table 6-10 shows the mass-balance results for the seven simulation scenarios. In Table 6-10, “Inflow” is the total infiltration rate over the entire model top boundary, representing a net water recharge rate into the system for the infiltration scenario simulated. “Outflow” is the cumulative total-flow rate out of the model and into the lower boundary representing the water table. Global mass-balance errors of inflow and outflow out of the system, as shown in Table 6-10, are less than 0.001% for the seven simulations leading to the conclusions that steady-state solutions are obtained.

Table 6-10. Mass Balance Results for Flow Simulations Using the Calibration Grid

Simulation Scenarios	Inflow from infiltration (kg/s)	Outflow to water table (kg/s)	Relative error (%)
uz99_m	5.6190232	5.6190755	0.00093
pch1_L2	1.4704485	1.4704460	0.00017
pch2_L2	1.4704485	1.4704472	0.00009
pch1_m2	5.6190232	5.6190643	0.00073
pch2_m2	5.6190232	5.6190252	0.00004
pch1_u2	13.842166	13.842181	0.00011
pch2_u2	13.842166	13.842169	0.00002

Model Results - DTNs: LB990801233129.022, LB990801233129.023, LB990801233129.024, LB990801233129.025, LB990801233129.026, LB990801233129.027, LB990801233129.028, respectively.

Model Calibrations and Results: As listed in Table 6-9, there are seven scenarios for model calibrations, consisting of one non-perching simulation (uz99_m) and the rest – six water perching simulations with the two perched water conceptual models and three infiltration rates. Six out of the seven simulations, except the non-perching one, have been calibrated against the field-observed data of perched water. The observed matrix liquid saturations and water potentials (when available), are used to examine modeling results. A perched water body is defined as fully liquid saturated gridblocks with zero capillary pressure or possible waterbend for calibration. The data source used in the calibrations are listed in Section 4-1. Only in-situ measurement water potentials are used. In this section, the simulation results are presented and discussed in terms of (1) comparisons with matrix liquid saturation, water potential, and perched water data, (2) examination of simulated perched water bodies, and (3) examination of simulated percolation flux and fracture-matrix flow components.

All the seven simulations are checked against observed saturation, water potential and perched water data. However, only a few of these comparisons are shown in the report and boreholes UZ-14 and SD-12 are selected to show the match between observed and modeled vertical-saturation profiles and perched water locations for six simulations with perched water occurrence. Matches to other borehole data are similar.

Comparisons with Liquid Saturation, Water Potential and Perched-Water Data: Measured matrix liquid saturation, water-potential data and perched water elevations are compared against 3-D model results from the seven simulations. Matrix liquid saturation, water potential, and perched water data used for comparisons are taken from nine boreholes (NRG-7a, SD-6, SD-7, SD-9, SD-12, UZ-14, UZ#16, WT-24 and G-2). The locations of these boreholes are shown in Figure 6-1.

The comparisons of simulated and observed matrix liquid saturations along the vertical column representing boreholes UZ-14 and SD-12 are shown in Figures 6-6 and 6-7 for the two perched water conceptual models under the present-day, mean infiltration scenario. Figure 6-8 shows comparison with water potentials for SD-12. In general, the modeled results from all the six simulations with perched water Conceptual Models #1 and #2 are in reasonable agreement with the measured saturation and water potential profiles, as shown in Figures 6-6, 6-7 and 6-8.

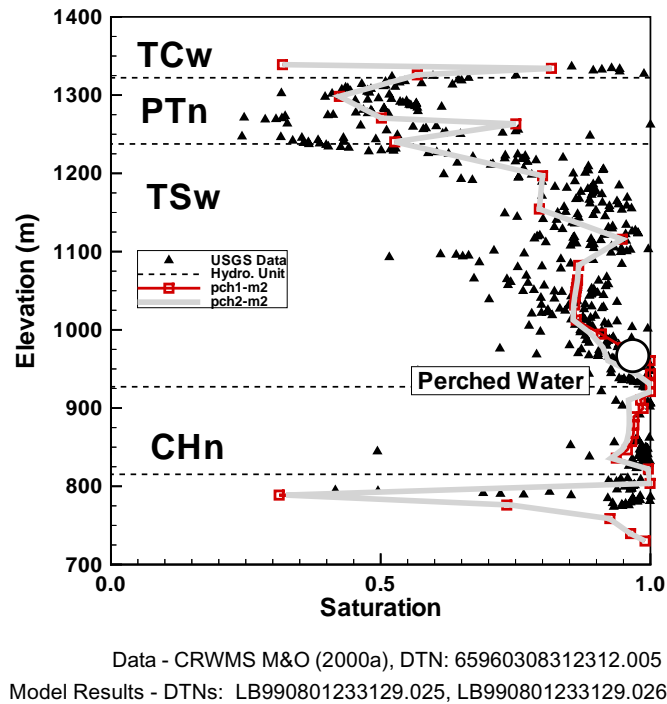


Figure 6-6. Comparison to the Simulated and Observed Matrix Liquid Saturations and Perched-Water Elevations for Borehole UZ-14, Using the Results of pch1_m2 and pch2_m2 with Present-Day, Mean Infiltration Rate.

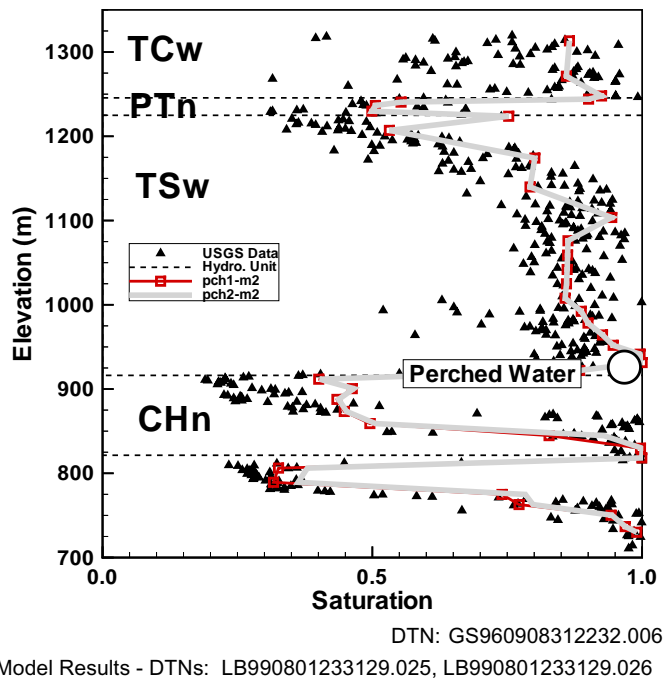


Figure 6-7. Comparison to the Simulated and Observed Matrix Liquid Saturations and Perched-Water Elevations for Borehole SD-12, Using the Results of pch1_m2 and pch2_m2 with Present-Day, Mean Infiltration Rate.

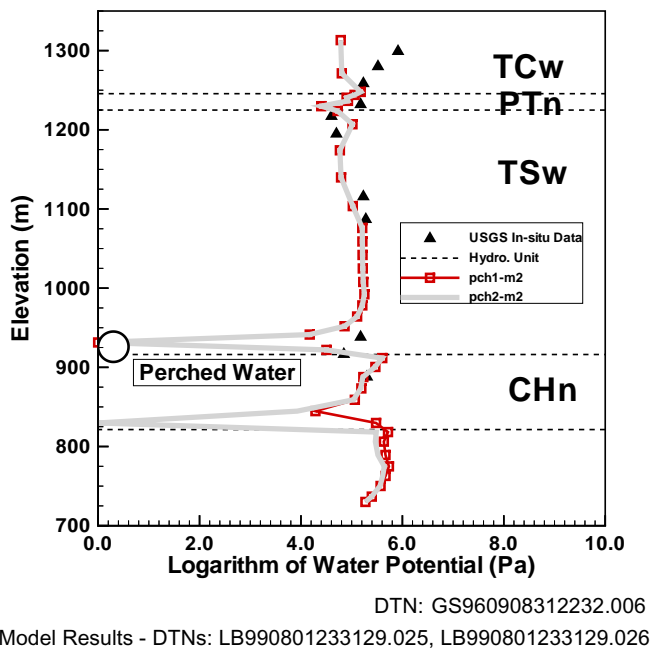


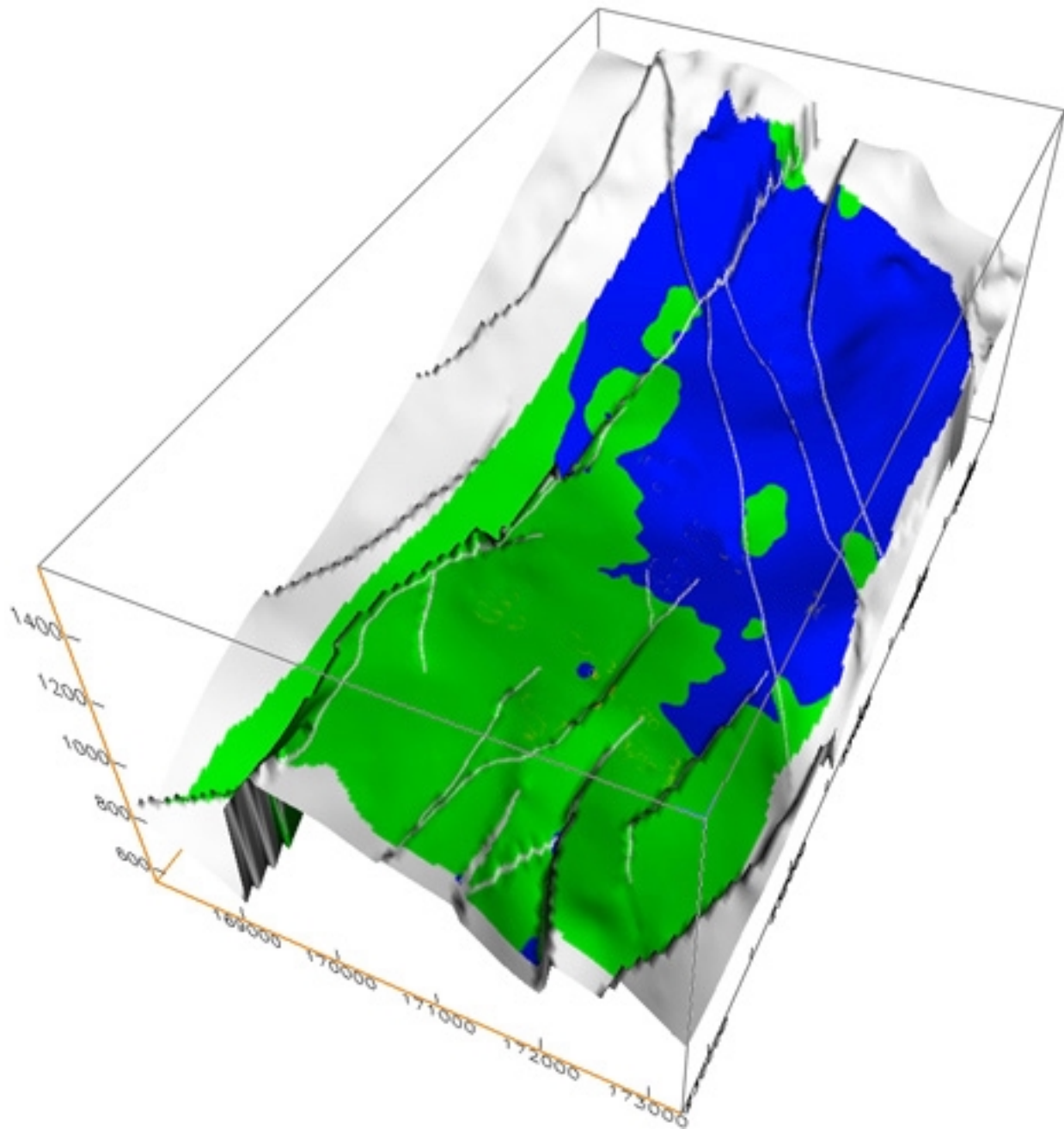
Figure 6-8. Comparison to the Simulated and Observed Matrix Water Potentials and Perched-Water Elevations for Borehole SD-12, Using the Results of pch1_m2 and pch2_m2 with Present-Day, Mean Infiltration Rate.

Also shown in Figures 6-6, 6-7 and 6-8 are the perched water elevations at the two boreholes, indicating a good agreement between observed and simulated data. For borehole UZ-14 under Conceptual Model #2, Figure 6-6 shows that the modeled perched water elevation is a little lower than the observed elevation. In addition, each of the six simulations has been compared to perched water data as observed from the seven perched water boreholes of Table 6-4 (See Appendix A of YMP-LBNL-GSB-YSW-2 for detailed comparisons), and the results are as follows:

- Under the present-day, mean infiltration scenario (pch1_m2 and pch2_m2, Table 6-9), both perched water conceptual models generally match water perching conditions in the UZ Model domain.
- Under the present-day, upper-bound infiltration scenario (pch1_u2 and pch2_u2, Table 6-9), the two perched water conceptual models generally reproduce water perching conditions in the UZ Model domain.
- Under the present-day, lower-bound infiltration scenario (pch1_L2 and pch2_L2, Table 6-9), the perched water conceptual models generally reproduce water-perching conditions at G-2, NRG-7a, SD-12, and WT-24 only. The models do not match the perched water data very well in SD-7, SD-9 and UZ-14 because of the low percolation fluxes at these borehole locations (0.01, 0.01 and 0.005 mm/year, respectively).

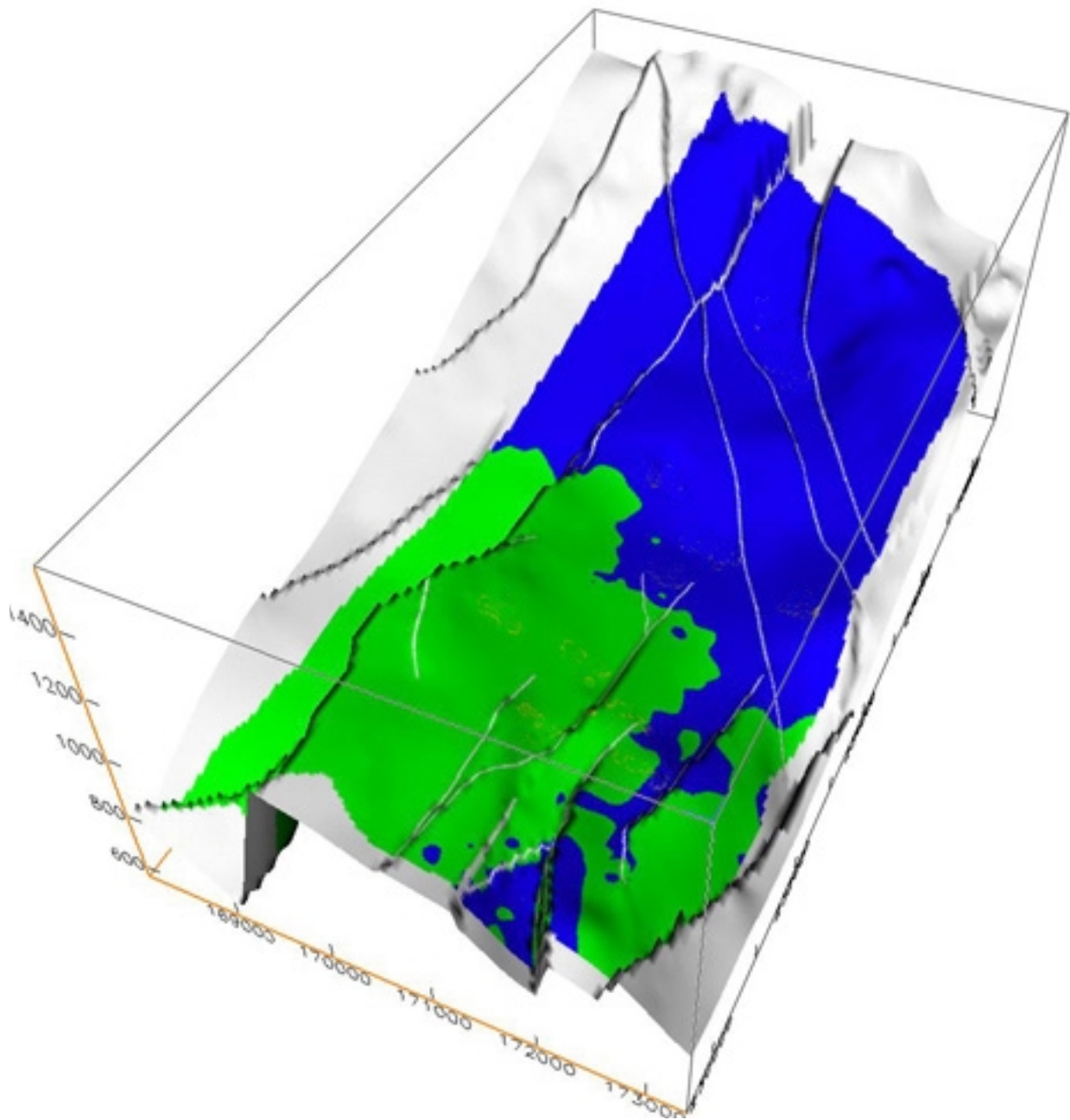
Examination of Simulated Perched Water Bodies: Figures 6-9 and 6-10 present examples of a simulated perspective view of 3-D perched water bodies and their volumetric extensions. Figure 6-9 shows a perspective view of fracture-water saturation contours along the bottom of the TSw or the low basal vitrophyre layer for perched water Conceptual Model #1. The blue isosurfaces on the figure reflect the regions of 100% liquid saturations, or perched water zones, within fractures along the model layer, while the green isosurface represents a portion of the model layer with fracture liquid saturations less than 100%. Figure 6-9 shows clearly several extensive perched water bodies predicted in the northern part of the model domain, located near the basal vitrophyre of the TSw, and separated by faults. Figure 6-9 also indicates that boreholes G-2, WT-24, UZ-14, NRG-7a, SD-9, as well as SD-12, intersect perched water bodies at this layer.

Figure 6-10 shows perched water bodies simulated using perched water Conceptual Model #2, along the top, zeolitic layer of the CHn. The perched water zone (Blue) on Figure 6-10 is similar to that of Figure 6-9 (Conceptual Model #1), but slightly larger.



Based on - DTN: LB990801233129.025

Figure 6-9. Simulated Perspective View of 3-D Perched Bodies Along the Base of the TSw, Using the Results of Simulation pch1_m2 of Conceptual Model #1 (Flow-Through) with Present-Day, Mean Infiltration Rate.(Blue 100% Saturation, Green < 100%)



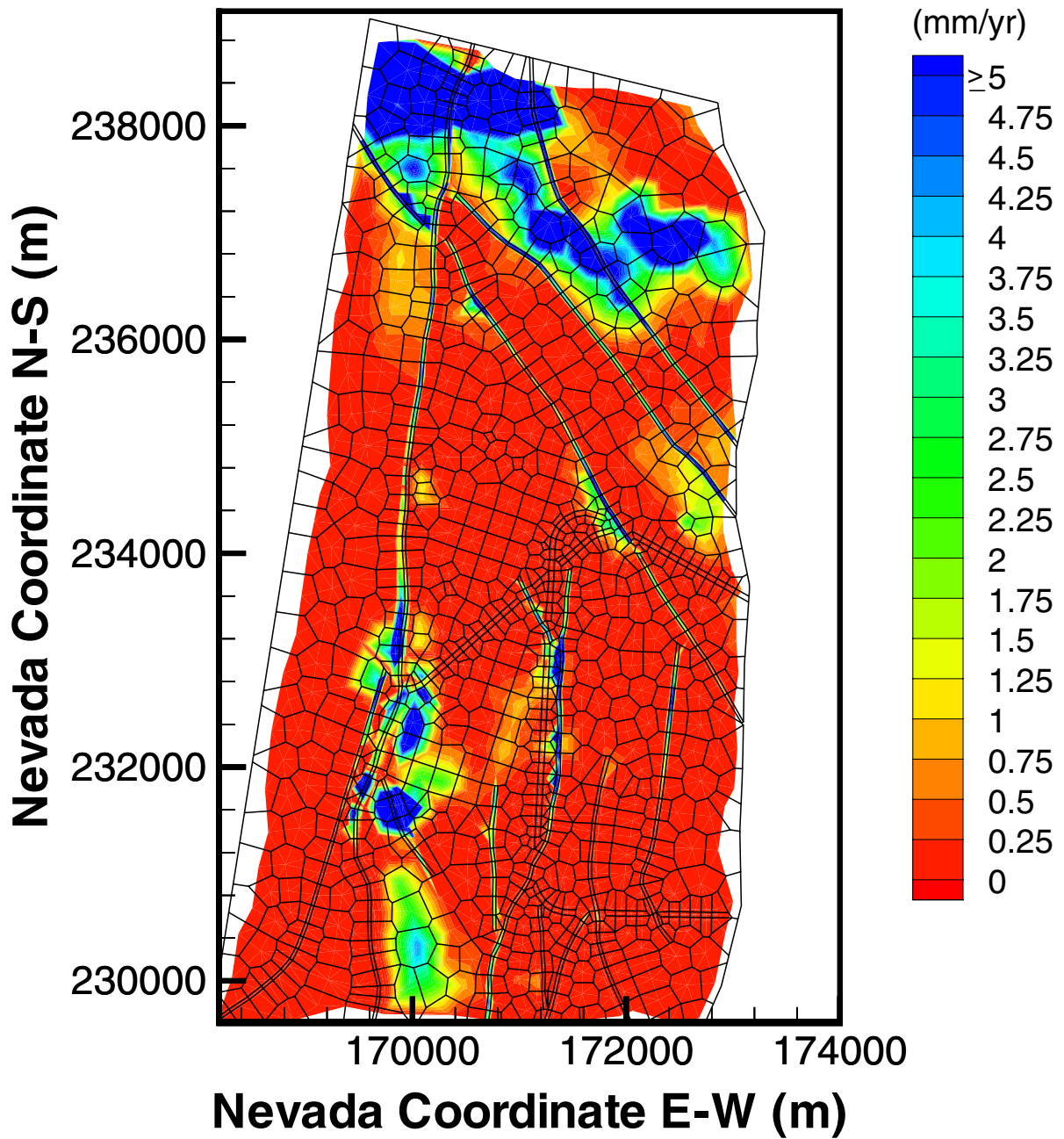
Based on - DTN: LB990801233129.026

Figure 6-10. Simulated Perspective View of 3-D Perched Bodies Along the Top of the CHn, Using the Results of Simulation pch1_m2 of Conceptual Model #2 (By-Passing) with Present-Day, Mean Infiltration Rate. (Blue 100% Saturation, Green < 100%)

Percolation Fluxes and Fracture-Matrix Flow Components: Percolation flux through the unsaturated zone is one of the most critical factors affecting potential repository performance for TSPA calculations. The quantity and spatial and temporal variations in percolation flux directly affect: (1) the amount of water flowing into potential waste-emplacement drifts; (2) moisture conditions and the corrosion environment of waste packages within the drifts; (3) waste mobilization from the potential repository; and (4) radionuclide migration from the UZ to the saturated zone. However, because percolation fluxes of unsaturated flow cannot be readily measured in the field, indirect data and model results are used to estimate these fluxes.

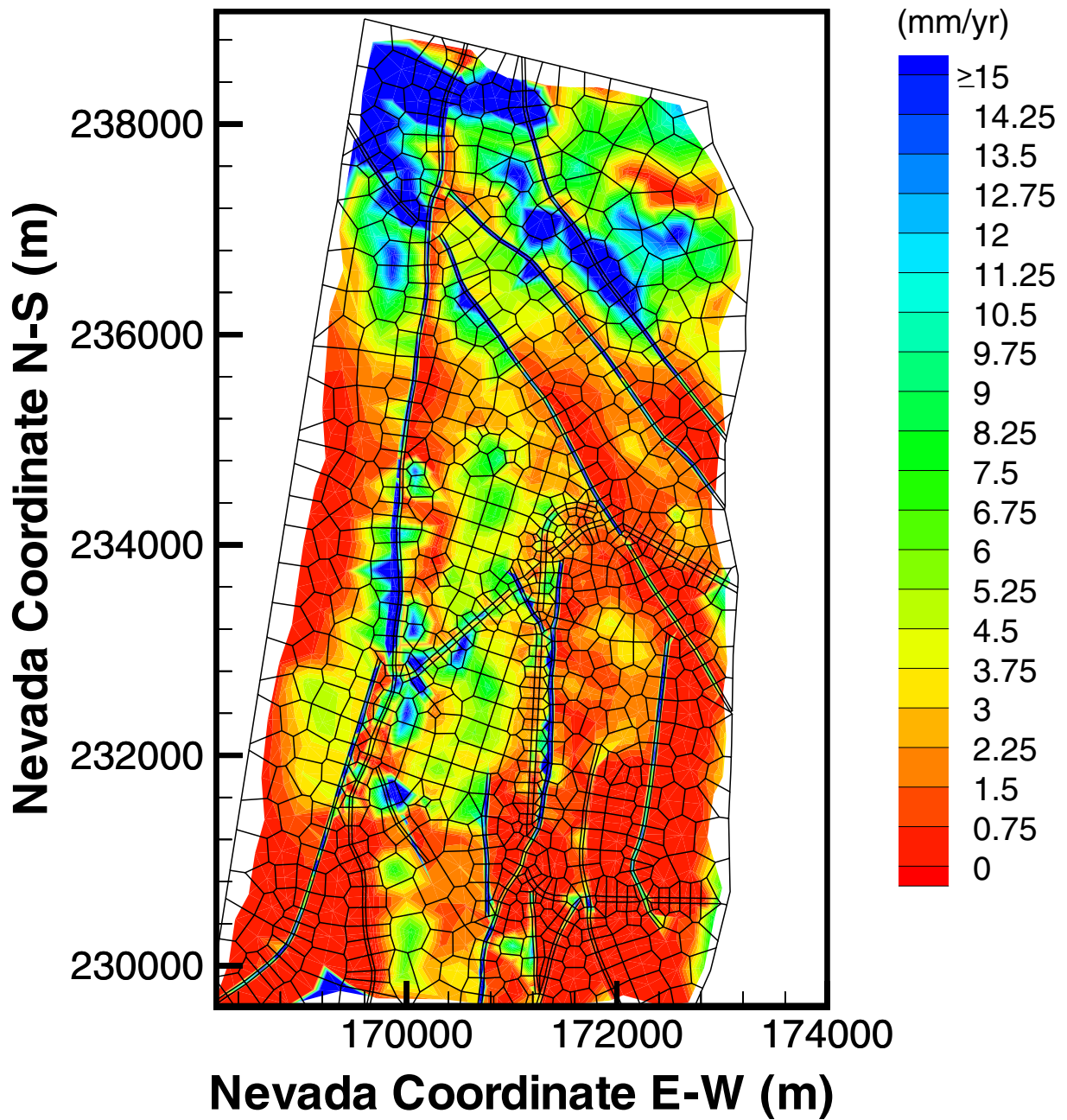
Model studies (Wu et al. 1999a, 1999b) indicate that accuracy of model predictions of percolation fluxes at Yucca Mountain depend on many factors. The most important factors are (1) net infiltration rates over the surface boundary; (2) representative geological and conceptual models; (3) reliable distributed rock-property values of fractures and matrix blocks; and (4) treatment of fracture-matrix flow and interactions. In this section, percolation fluxes at the potential repository horizon are analyzed using the seven simulation results of [Table 6-9](#). The percolation flux is defined as total vertical liquid mass flux through both fractures and matrix, and is converted to mm/yr per unit area using a constant water density.

[Figures 6-11, 6-12, and 6-13](#) show percolation fluxes at the potential repository level for the three present-day infiltration scenarios with perched water Conceptual Model #1. Percolation fluxes at the potential repository are nearly the same if the same infiltration map is used, regardless of the perched water conceptual model. This occurs because the perched water models are different in the rock properties only in the bottom layers of the TSw and zeolitic units in the CHn, which have little effect on flow at and above the potential repository level. [Figures 6-11, 6-12 and 6-13](#) display a nonuniform pattern of flux distributions (the darker blue spots on the figure indicate the higher modeled percolation fluxes). The high percolation fluxes are located primarily north of the potential repository, but also along the Solitario Canyon fault in the middle portion of the model domain. A comparison of the present-day surface infiltration maps (e.g., [Figure 6-3](#)) and the modeled, corresponding flux maps shown in [Figures 6-11, 6-12 and 6-13](#) indicate similar flux patterns. Especially for the lower-bound and upper-bound infiltration cases, the simulation results show little lateral diversion occurring during flow from surface to potential repository level. For the mean infiltration, the simulated percolation fluxes at the potential repository level show that small lateral movement occurs in the middle of the model domain, and higher fluxes are seen to move down the faults in these areas.



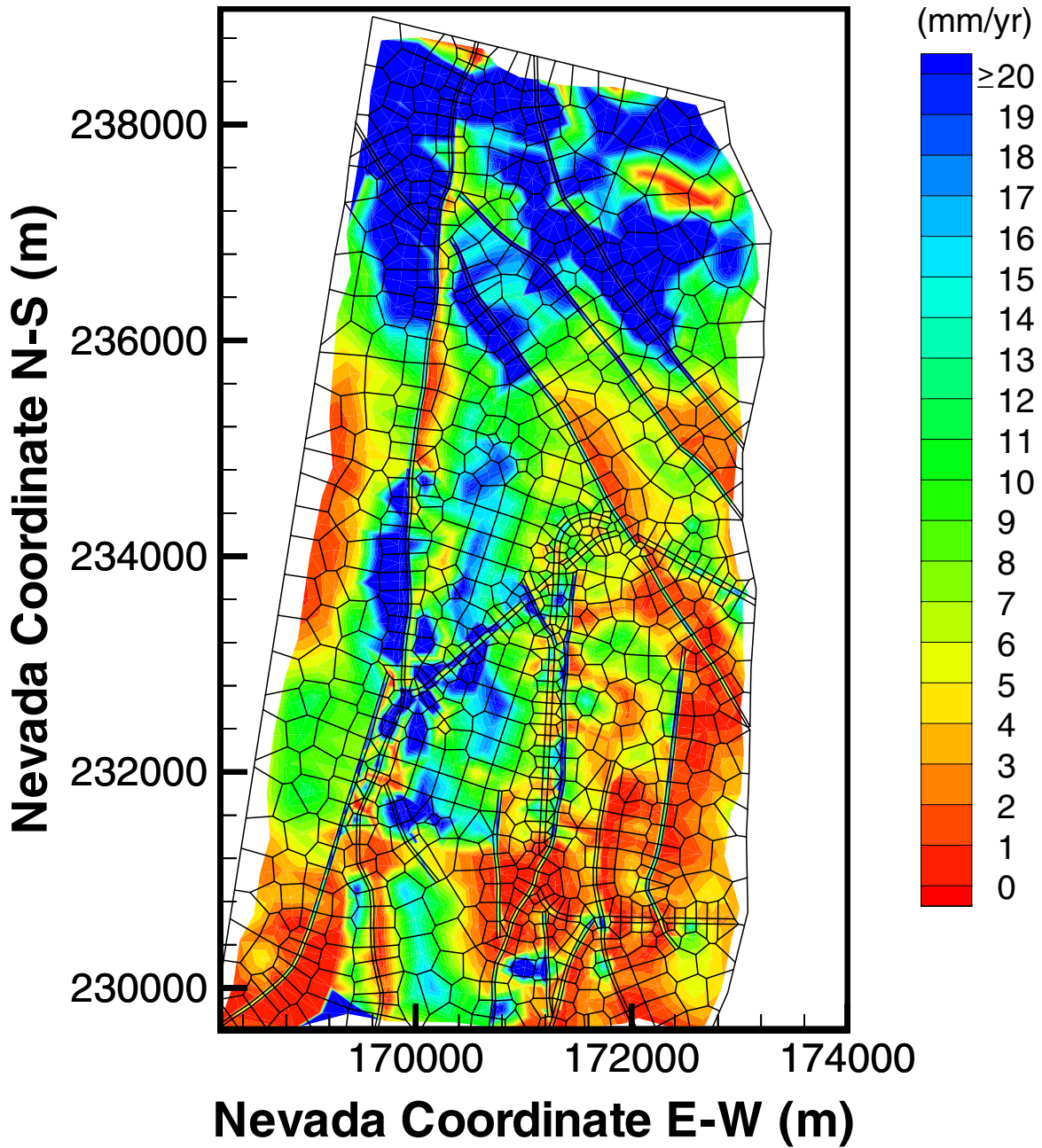
Based on model results from this AMR submitted under DTN: LB990801233129.023

Figure 6-11. Simulated Percolation Fluxes at the Potential Repository Horizon Under Present-Day, Lower-Bound Infiltration Using the Results of Simulation pch1_L2.



Based on DTN: LB990801233129.025

Figure 6-12. Simulated Percolation Fluxes at the Potential Repository Horizon Under Present-Day, Mean Infiltration Using the Results of Simulation pch1_m2.



Based on DTN: LB990801233129.027

Figure 6-13. Simulated Percolation Fluxes at the Potential Repository Horizon Under Present-Day, Upper-Bound Infiltration Using the Results of Simulation pch1_u2.

Table 6-11 lists fracture-matrix flow components at the potential repository horizon and the water table within the model domain, calculated based on vertical flow along each grid column. These statistics indicate that fracture flow is dominant both at the potential repository horizon and at the water table. At the potential repository level, fracture flow consists of more than 80% of the total percolation fluxes. Fracture flow at the water table takes 70-90% of the total flow, whereas the second perched water conceptual model predicts consistently lower fracture-flow components at the water table for all three infiltration scenarios.

Table 6-11. Comparison of the Water Flux Through Matrix and Fractures as a Percentage of the Total Flux at Two Different Horizons (1) at the Potential Repository and (2) at the Water Table.

Simulation Designation	Flux at Potential Repository Horizon (%)		Flux at Water Table (%)	
	Fracture	Matrix	Fracture	Matrix
uz99_m			80.80	19.20
pch1_L2	86.13	13.87	84.23	15.77
pch2_L2	86.00	14.00	70.04	29.96
pch1_m2	82.44	17.56	87.28	12.72
pch2_m2	82.44	17.56	72.70	27.30
pch1_u2	94.06	5.94	95.46	4.54
pch2_u2	93.97	6.03	82.67	17.33

Model Results - DTNs: LB990801233129.022, LB990801233129.023, LB990801233129.024, LB990801233129.025, LB990801233129.026, LB990801233129.027, LB990801233129.028, respectively.

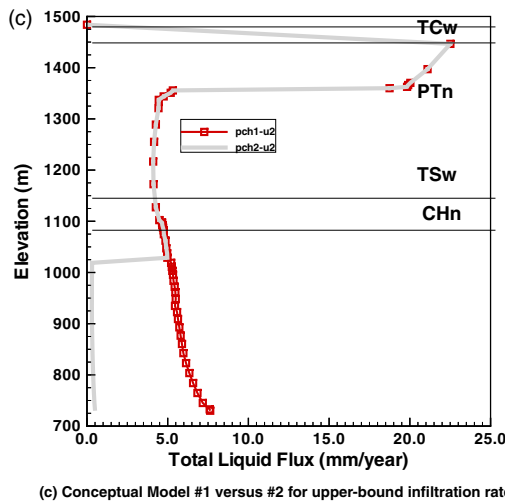
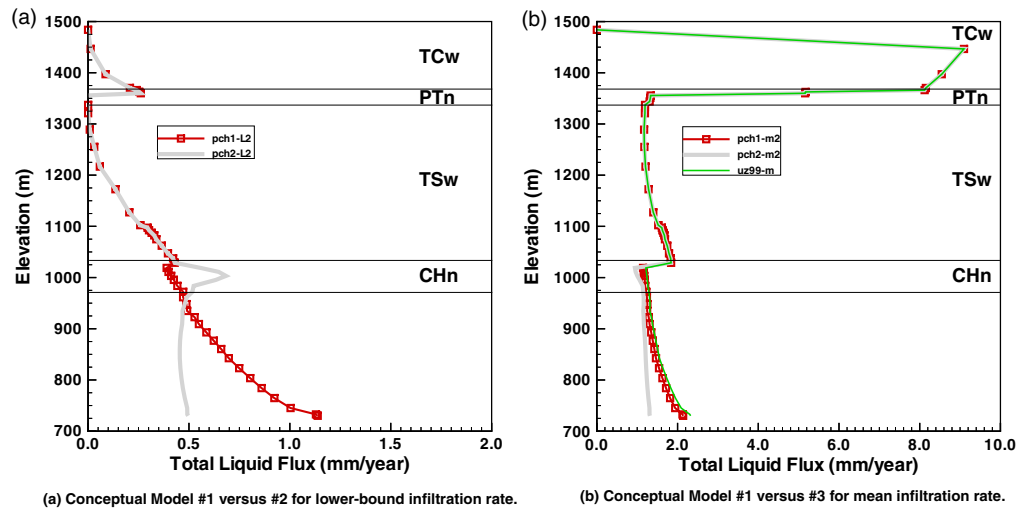
Flow-Through and By-Passing Perched Water Zones: The percentage of water flowing through or by-passing perched water bodies below the potential repository may have an effect on groundwater flow paths and travel times. This may in turn affect the adsorption of radionuclides onto zeolitic and vitric rocks, directly impacting potential repository performance. The percentage of flow-through or by-passing perched bodies can be further analyzed using the 3-D model calibration results. Figures 6-14 and 6-15 show vertical flow at locations near SD-6 and UZ-14 from the seven calibration simulations. The locations of the two boreholes are shown in Figure 6-1, with SD-6 and UZ-14 located in the southern and northern parts of the potential repository, respectively.

Figure 6-14 shows that at SD-6, perched water Conceptual Model #1 permits much larger (almost complete) flow through the CHn unit than Conceptual Model #2. For the location near UZ-14, Conceptual Model #1 also predicts more percentage (50%) of flow through perched water layers with the mean infiltration rate than Conceptual Model #2. In both cases, the non-water-perching, Conceptual Model #3 predicts the highest, most complete flow through for the mean infiltration scenario (Figures 6-14b and 6-15b). Figures 6-14 and 6-15, as well as the analyses of the seven calibration runs, indicate the following:

- Perched water zones may only partially block vertical water flow; a certain percentage of water is always flowing through perched bodies.
- The higher the infiltration rates, the higher the by-passing percentages predicted by Conceptual Model #2.

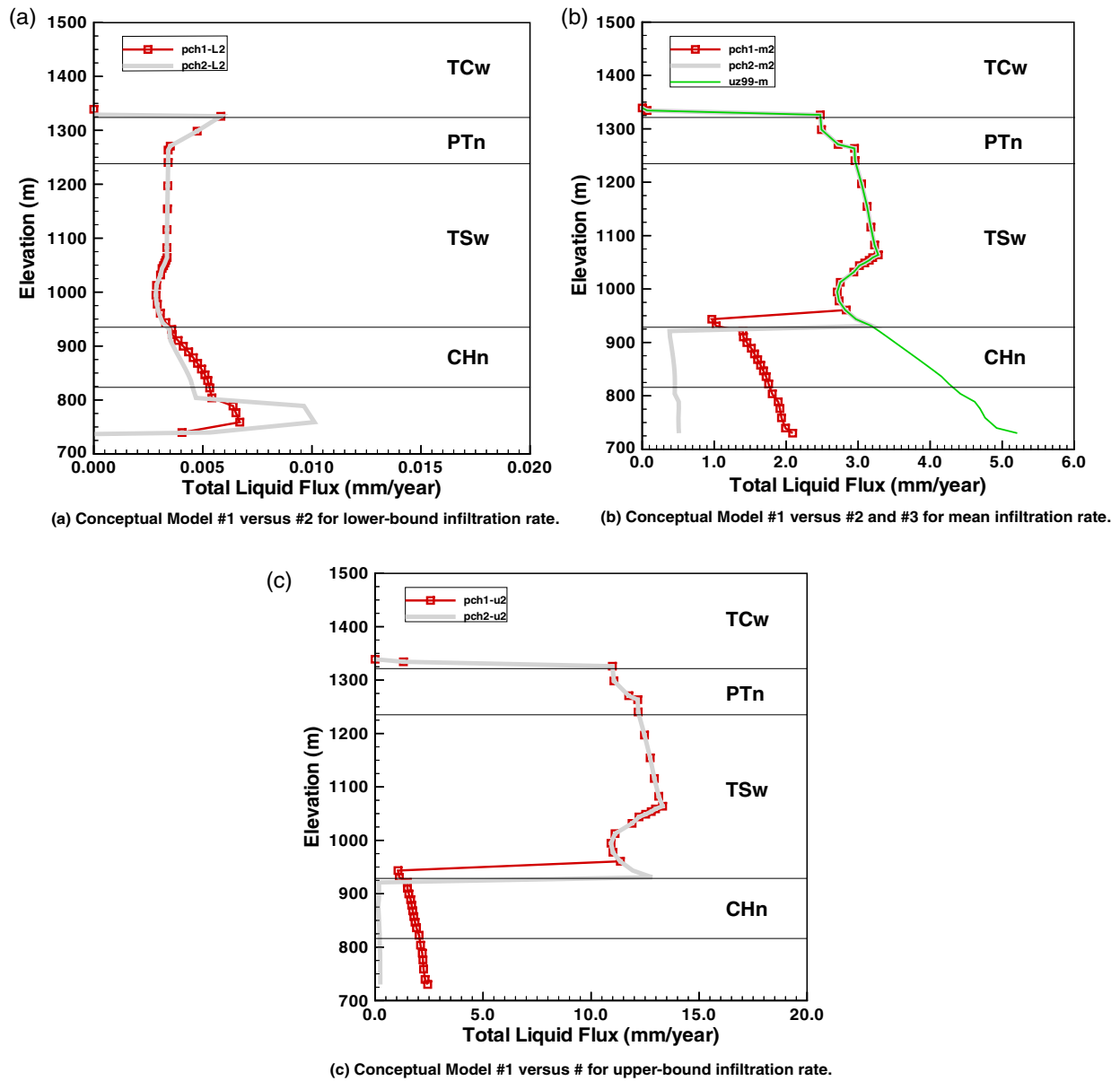
- Conceptual Model #1 results in consistently higher flow-through rates than Conceptual Model #2.
- Non-water-perching model (#3) predicts nearly complete flow through the zeolites in the CHn.

As a result, perched water Conceptual Model #1 is defined as the “flow-through” model, even though it is only partially “flow-through,” and Conceptual Model #2 is called the “by-passing” model. These results are consistent with the conceptual models used to develop the modeling scenarios.



Model Results - DTNs: LB990801233129.022, LB990801233129.023, LB990801233129.024, LB990801233129.025, LB990801233129.026, LB990801233129.027, LB990801233129.028

Figure 6-14. Comparisons between Simulated Vertical Percolation Fluxes at the Location of SD-6 using Different Perched-Water Conceptual Models.



Model Results - DTN: LB990801233129.022, LB990801233129.023, LB990801233129.024, LB990801233129.025, LB990801233129.026, LB990801233129.027, LB990801233129.028

Figure 6-15. Comparisons between Simulated Vertical Percolation Fluxes at the Location of UZ-14 using Different Perched-Water Conceptual Models.

6.3 TEMPERATURE CALIBRATION

For thermo-hydrological studies, the steady-state, ambient temperature and saturation distributions are needed to serve as initial conditions for the UZ model to evaluate various thermal-load and infiltration scenarios. Temperature data are required to describe the geothermal conditions of the UZ Model using measured field data. A steady-state, ambient temperature distribution for Yucca Mountain can be obtained using TOUGH2 simulation under fixed top and bottom temperature-boundary conditions.

6.3.1 Top Boundary Temperature

To account for differences in temperature in the mountain caused by variations in elevation, measured mean surface temperature and an equation that correlates surface temperature with elevation are used. The surface temperature was measured for mean surface temperature in boreholes NRG-6 and NRG-7a (DTN: GS950208312232.003), with several years of continuous temperature monitoring data. The surface temperature T_s at any elevation Z is computed and fixed according to the following equation (Driscoll, 1986, pp. 49–51; Wu et al. 1999a, p. 196):

$$T_s = T_{ref} - \lambda(Z - Z_{ref}) \quad (\text{Eq. 1})$$

where T_{ref} is mean surface temperature at reference elevation Z_{ref} and λ is the dry adiabatic atmospheric lapse rate in $^{\circ}\text{C}/\text{m}$. This lapse is $0.01^{\circ}\text{C}/\text{m}$ (Driscoll 1986, p. 50). In this model, the reference temperature used is 18.23°C , the mean value at an elevation of 1231.0 m measured in borehole NRG-6 (DTN: GS950208312232.003). The mean temperature at NRG-7a at an elevation 1282.2 m is 17.78°C . The calculated mean lapse rate, based on these field measurements, is $0.009^{\circ}\text{C}/\text{m}$.

6.3.2 Bottom Boundary Temperature

For the bottom boundary at the water table, temperatures were interpolated from unqualified borehole temperature profile data reported in Sass et al. (1988). Because several of these boreholes do not actually extend to the water table, temperatures at the water table were obtained by linear extrapolation of the measured profiles. The resulting temperature distribution was plotted and interpolated over the entire model domain. This interpolated temperature distribution was calibrated against recently acquired qualified temperature data in boreholes NRG-6, NRG-7a, SD-12 UZ#4, UZ#5 and UZ-7a.

To obtain accurate bottom-temperature boundary conditions for use in thermo-hydrological simulations, the initial distribution of boundary temperature was adjusted so that the computed steady-state temperature profiles matched measured temperature profiles in the six boreholes with Q-temperature data. Several non-Q measured temperature profiles (Sass et al. 1988) were used as corroborative data.

6.3.3 Calibration of Ambient Temperature

The temperature profiles are controlled by many factors, such as the formation thermal conductivity, the geothermal gradient, and the ambient infiltration. Because of the small range of

uncertainties associated with measured thermal conductivities, the temperature calibration may be conducted using either ambient infiltration or temperature gradient data or both. In this report, we fixed the ambient infiltration rate and only calibrated the temperature conditions along the bottom and top boundaries because there is insufficient temperature data collected along these boundaries. The ambient temperature condition was calibrated using the 3-D calibration grid (DTN: LB990501233129.002 and CRWMS M&O 1999d), an ECM mesh. The simulations were performed using TOUGH2 V1.4 with the EOS3 module. The rock properties of the ECM formulation were obtained from the 1-D inversion (DTN: LB997141233129.001), thermal properties (DTN: LB991091233129.001), and UZ fracture properties (DTN: LB990501233129.001). We use the definition of parameters in the ECM model to obtain an equivalent set of ECM properties directly from the dual-permeability property set (Table II-7). Thermal conductivities are treated as a linear function of liquid saturation between their dry and wet values. The infiltration was the base-case, present-day, mean infiltration scenario. Table 6-12 shows the boreholes and the corresponding column names used in the 3-D calibration of model ambient temperature. The last three columns give the x- and y-coordinates of grid columns, the absolute distance between the coordinates of the boreholes (in GFM 3.1) and the nearest gridblock center.

Table 6-12. Boreholes with Qualified Data Used in Calibration of UZ Ambient Temperature Distribution

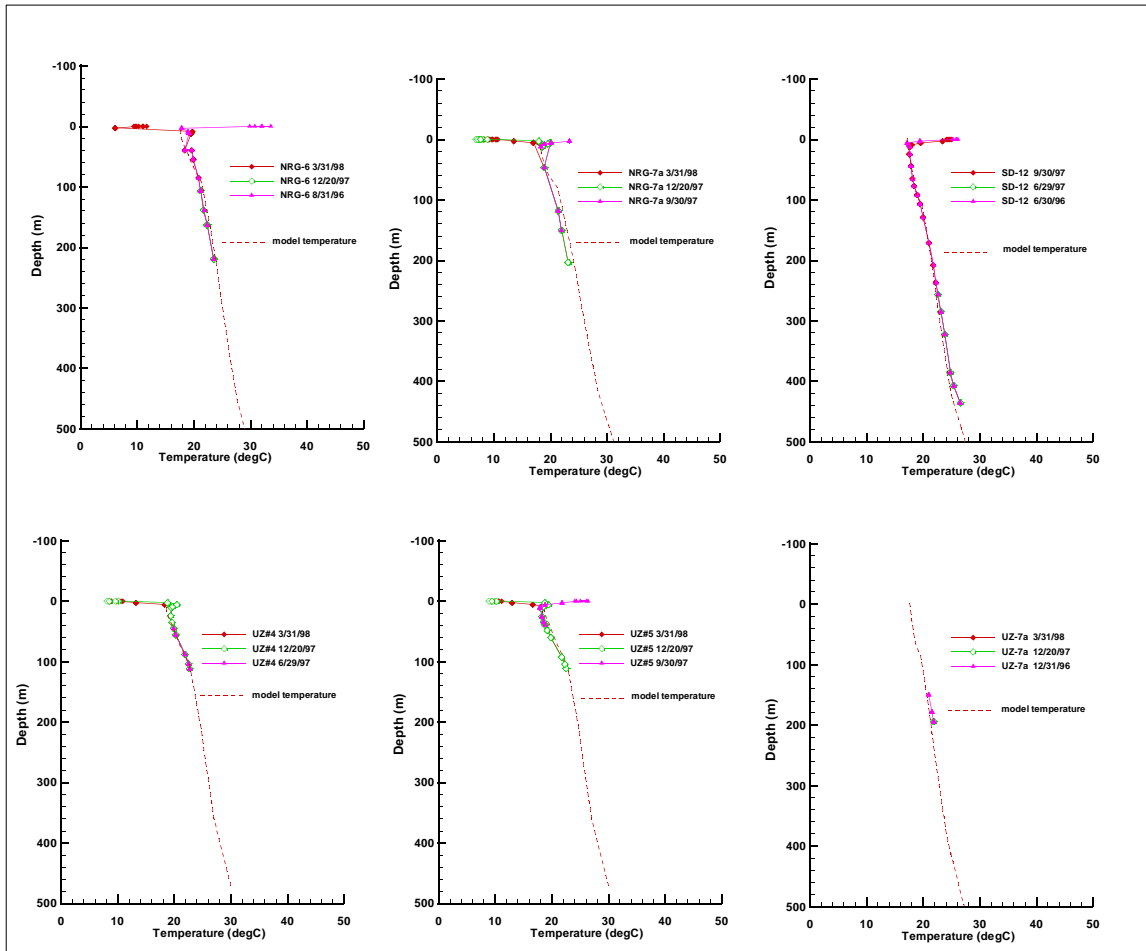
Borehole	Element Column	Nevada Coordinates of Element Columns		Distance to Boreholes (m)
		E-W (m)	N-S (m)	
NRG-6	I61	171956.0	233687.0	13.8
NRG-7A	k 3	171569.5	234372.4	33.2
SD-12	k61	171169.6	232292.8	49.0
UZ#4	i67	172551.0	234293.0	14.4
UZ#5	i67	172551.0	234293.0	26.9
UZ-7	e37	171379.7	231799.8	59.4

DTN: LB990501233129.004

NOTES: 1. XXXXq = boreholes with Q-temperature data used in model calibration

2. dist (m) is the absolute distance between the nearest grid column coordinates (x_ele, y_ele) and the borehole location (in GFM 3.1).

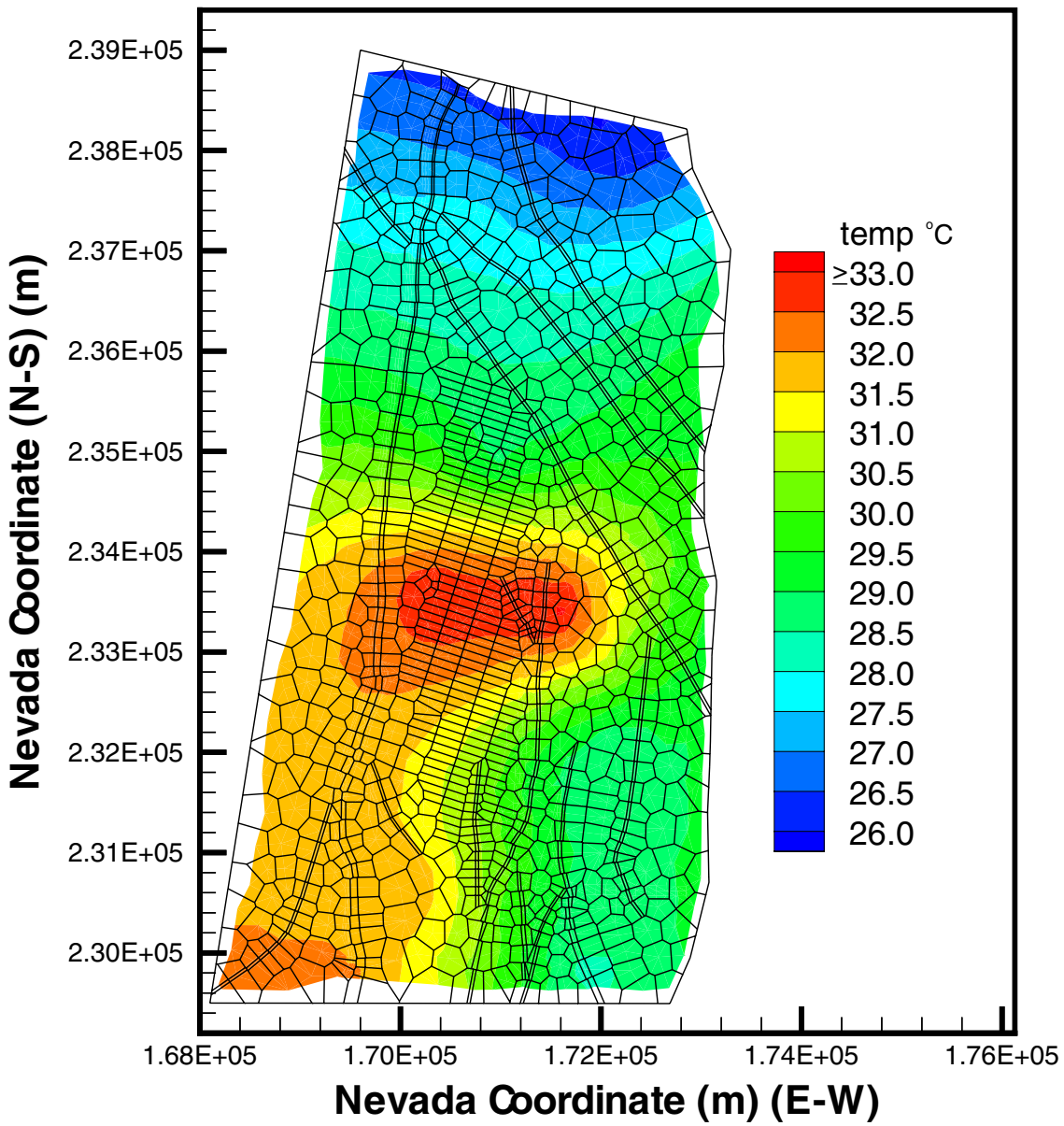
The corresponding simulated temperature profiles for the boreholes were extracted from the TOUGH2 output. Figure 6-16 shows the calibrated and measured temperature profiles in the Q-temperature boreholes. The figures show a reasonable match between measured and simulated temperature using the specified boundary conditions and the infiltration rate. However, near the ground surface in five of the boreholes, observed temperature show significant seasonal variations. However, these seasonal changes in surface temperature have little impact on steady-state heat flow in the deeper (more than 20 meters) UZ.



Data - See Table 4.1

Model Results - DTN: LB991131233129.004, GS970808312232.005

Figure 6-16. Measured and Modeled Ambient Temperature Profiles for the Q-boreholes, with the Present-Day Mean Infiltration.



Based on DTN: LB991131233129.004

Figure 6-17. Model Ambient Temperature Distribution at the Water Table with the Present-Day, Mean Infiltration.

Figure 6-17 shows the contour plot of calibrated temperature distribution at the water table. This temperature distribution can be used for simulations in which the model boundary temperature needs to be fixed at the water table. The average temperature at the water table (730 masl) ranges from 28–33°C over the model domain.

Based on calibration results, the simulated ambient temperature distribution in the UZ Model can be used to specify steady-state, mountain-scale temperature conditions. The distribution was computed using an ECM formulation of the calibration grid and using present-day, mean infiltration, and base-case properties. Although this temperature distribution is strictly calibrated only under these ECM model conditions, it should be applicable with different model formulations such as the dual-permeability approach. This is because the ambient heat flow is controlled by the steady-state heat conduction process, in which case the ECM model predicts similar results to those from dual-permeability model (Doughty 1999).

6.4 ANALYSIS AND MODELING OF PORE-WATER CHEMICAL DATA

This study is part of continuing efforts to analyze and model the geochemical data in the unsaturated zone at Yucca Mountain. The studies use the geochemical model to evaluate the hydrologic system, and assess the magnitude and spatial distribution of surface net infiltration over time (Sonnenthal and Bodvarsson 1999).

The UZ system of Yucca Mountain has been the subject of intensive geological, hydrologic, and subsurface engineering studies. One of the main issues is the percolation flux at the potential nuclear waste potential repository. Percolation flux strongly depends on the infiltration rates and their spatial distribution. Much work has been done to estimate the infiltration flux based on various evapotranspiration models (Hevesi et al. 1992; Flint and Flint 1994), and the present mean infiltration rate across the study area has been estimated as low as one millimeter per year to as high as several tens of millimeters per year. The climate change over the past 100,000 years has been used to estimate the possible range in infiltration rates over the next 10,000 years (Sonnenthal and Bodvarsson 1999).

Geochemical data provide additional information to analyze the UZ system. Pore-water chemical concentration data have been used to calibrate the UZ model to bound the infiltration flux, flow pathways, and transport time. Distribution of chemical constituents in both liquid and solid phases of the UZ system depends on many factors, such as hydrological and geochemical processes of surface precipitation, evapotranspiration, the fracture-matrix interactions of flow and transport, large-scale mixing via lateral transport, and history of climate changes and recharge. A dual-permeability transient model is necessary to investigate fluid flow and chemical transport phenomena and represent the large spatial and temporal chemical variations.

In this study, pore-water chemical concentration data are analyzed and modeled by 3-D chemical transport simulations and analytical methods. Water infiltration-rate calibrations are performed using the pore-water chloride concentrations. Model results of chloride distributions were improved in matching the observed data when the calibrated infiltration rates were used. In addition, an analytical method was applied to analyze transient transport of chemicals. This method was verified by 3-D simulations as able to capture major chloride and chlorine-36 transient behavior and trends. The combined data of chloride and chlorine-36 distributions in the UZ groundwater furnish important information for the UZ Model calibrations.

6.4.1 Available Data

6.4.1.1 Pore-water Chemical Concentration Data

Geochemical data available and applied to this study were pore-water concentrations of chloride (Cl), sulfate (SO₄), strontium (Sr), and bromine (Br), and the ratio of chloride-36 (³⁶Cl) to chloride (³⁶Cl/Cl). Pore-water samples were mainly collected from eight boreholes: NRG-6, NRG-7A, SD-7, SD-9, SD-12, UZ#4, UZ#14, and UZ#16 (Data Sources: DTN: LA9910JF12213U.007), the ECRB tunnel, the ESF tunnel, including South Ramp, North Ramp, and Main Drift (Data Sources: DTN: LASL831222AQ98.002, DTN: LA9910JF12213U.013). The detailed description of these data was given in several reports (e.g. Yang et al. 1998).

6.4.1.2 Infiltration Flux Data

The net infiltration flux in the base-case study was from the present-day, mean or modern infiltration map (Table 6-3 and Figure 6-18). Based on studies of Cl chemistry presented in Sonnenthal and Bodvarsson (1999, p. 148, Figure 23), the glacial maximum infiltration rate was about 28 mm/year and the modern mean infiltration was approximately 5 mm/year. As an approximation, a glacial infiltration scenario in this section was obtained by multiplying the present-day mean infiltration rate by a factor of 5 with the same distribution pattern.

Surface chloride flux includes dissolved material in rain, particulate in snow, and a contribution from windblown dusts (Tyler et al. 1996). Either chloride concentration in infiltrating water or total surface chloride flux can be input into the model. Combining the mean annual precipitation of about 170 mm/year with a present day chloride surface flux of 106 mg/m² year yields a mean chloride concentration of about 0.62 mg/l (Fabryka-Martin et al., 1997, Sonnenthal and Bodvarsson 1999). Surface chloride flux of this study was obtained applying the mean chloride concentration of precipitated water (which combines infiltrating water in the form of precipitation, run on, and runoff). The same mean chloride concentration was applied to glacial total water precipitation to derive a glacial chloride flux. The ³⁶Cl/Cl ratio in infiltrated water was assumed to be 500 x 10⁻¹⁵ during modern times and 1000 x 10⁻¹⁵ during glacial times (Sonnenthal and Bodvarsson 1999).

6.4.2 Modeling Approaches

6.4.2.1 Three-Dimensional Simulations

The system was assumed to be under two-phase isothermal flow conditions of water and air. A three-dimensional dual-permeability model and the T2R3D V1.4 (Section 4) of the TOUGH2 code, which takes into account tracer diffusion, dispersion, radioactive decay, and linear first-order adsorption (Sonnenthal and Bodvarsson, Section 5.1, 1999), were employed for the simulations. The steady-state liquid-flow fields were obtained using the EOS9 module of T2R3D, as discussed in Section 6.1. Chemical distributions were then computed from transport equations using the decoupled T2R3D module. The flow boundary conditions, simulation grids, basic hydrologic properties of rock matrix and fractures are the same as those used in the 3-D UZ non-perched water model flow simulations described in Section 6.1. Boundary conditions for

chemical components were treated similarly to those for flow simulations, with mass fluxes described at the top boundary, and no-flow and water table conditions at the lateral and bottom boundaries, respectively. The dispersivities for both fracture and matrix continua in the simulation were assumed to be zero (Sonnenthal and Bodvarsson 1999). Diffusion coefficients used were those for chemical ions at 25°C and infinite dilution in water (Lasaga 1998). The tortuosity was set to 0.7 for fracture and 0.2 for matrix (Section 6.8.1), respectively.

6.4.2.2 Analytical Method

For transport dominated by vertical flow and porous media of ECM type, the analytical method provides an alternative interpretation of chemical transient transport, which could be difficult by 3-D simulations. It is also efficient in conducting flow parameter sensitivity studies qualitatively. Transient transport modeling in this section was analyzed using an analytical solution for a one-dimensional semi-infinite chemical-transport system (Javandel et al. 1984, p.14-18):

$$C(t, z) = C_0 + \frac{1}{2}(C_1 - C_0) \left[\exp\left(\frac{v - \sqrt{v^2 + 4\lambda D}}{2D} z\right) \operatorname{erfc}\left(\frac{z - vt}{2\sqrt{Dt}}\right) + \exp\left(\frac{v + \sqrt{v^2 + 4\lambda D}}{2D} z\right) \operatorname{erfc}\left(\frac{z + vt}{2\sqrt{Dt}}\right) \right] \quad (\text{Eq. 2})$$

where C_0 [mg/l] is the system initial chemical concentration at $t=0$ [s], C_1 [mg/l] the concentration at the surface ($z=0$ [m]), v [m/s] the pore velocity, D [m²/s] the dispersion coefficient, and λ [1/s] the chemical decay constant. The dispersion coefficient is evaluated by

$$D = \alpha v + D_m \quad (\text{Eq. 3})$$

with the dispersivity α [m] and the molecular diffusion coefficient D_m [m²/s].

The solution becomes

$$C(t, z) = C_0 + \frac{1}{2}(C_1 - C_0) \left[\operatorname{erfc}\left(\frac{z - vt}{2\sqrt{Dt}}\right) + \exp\left(\frac{vz}{D}\right) \operatorname{erfc}\left(\frac{z + vt}{2\sqrt{Dt}}\right) \right] \quad (\text{Eq. 4})$$

in the case of no decay, and

$$C(z) = C_0 + (C_1 - C_0) \exp\left(\frac{v - \sqrt{v^2 + 4\lambda D}}{2D} z\right) \quad (\text{Eq. 5})$$

for steady state.

The analytical solution was applied to 1-D columns extracted from 3-D simulation model domain. Average column porosity was calculated by the total pore volume and bulk volume of the column, including both fracture and matrix volumes.

6.4.3 Modeling Results and Analyses

Pore-water chemical-concentration data were analyzed using 3-D transport simulations and analytical methods. Water infiltration rate calibrations were performed by calculating infiltration rates with measured pore-water Cl concentrations. As a result, modeled results of Cl and $^{36}\text{Cl}/\text{Cl}$ distributions were improved with the calibrated infiltration rates.

An analytical method was applied to the transient-transport analysis. This method, verified by the 3-D simulations under the same flow and transport conditions, was able to capture major Cl and ^{36}Cl transient transport behavior and trends.

6.4.3.1 Water Infiltration Calibration

A base-case simulation was conducted using the present-day (modern), mean infiltration rate (Table 6-3 and Figure 6-18) to compare the uncalibrated model with observed chloride data. Note that Figure 6-18 uses different scales of flux from Figure 6-3 for the same infiltrate map.

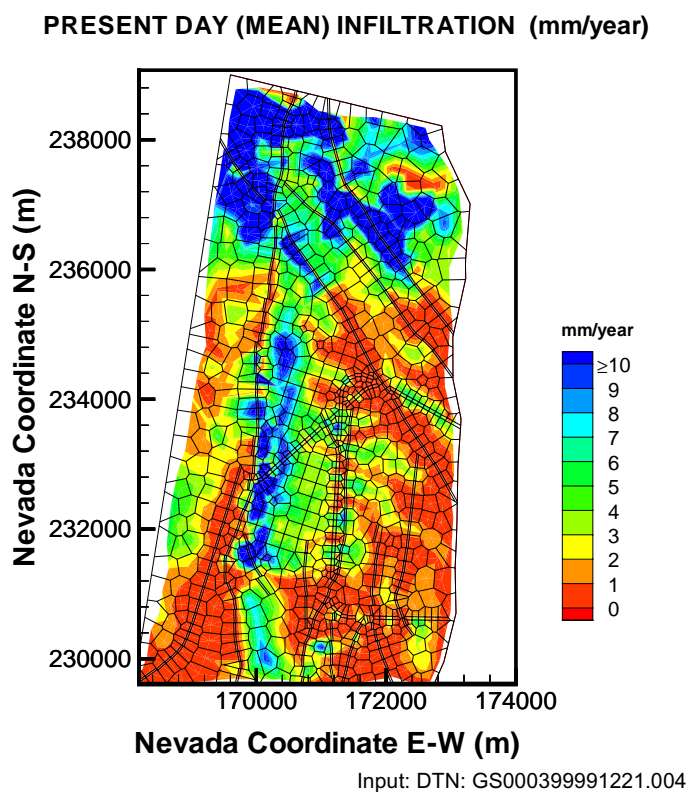


Figure 6-18. Present-Day, Mean Infiltration Map

Chloride concentrations predicted by the steady-state transport simulation were compared with measured pore-water chloride concentration data. The results of the simulated and measured concentrations along the stations in the ESF, ECRB, and borehole UZ#16 are shown in Figures 6-19 through 6-21, respectively. Compared to the measurements, the simulated Cl concentrations are higher at the North Ramp (0-2,000 m), South Ramp (6,400 m-8,000 m), the northeast side of

the ECRB (left side of the figure), and borehole UZ#16, and lower at the southwest end of the ECRB (right side of the figure). These differences may result from the infiltration variations, as demonstrated in [Figure 6-22](#), showing a plot of Cl infiltration along the ECRB. At the entrance of the ECRB, higher simulated Cl concentrations correspond to very low infiltration rates, while at the end of the ECRB, extreme higher infiltration leads to lower simulated values of Cl concentrations. The distribution of Cl concentration in infiltrated water shown in [Figure 6-23](#) confirms the significant effect infiltration rates have on Cl distributions and the need to calibrate infiltration.

The infiltration rate calibration proceeds from the relationship between water and Cl influxes, and Cl concentration at the surface (Sonnenthal and Bodvarsson 1999, p. 121).

$$J_I = \frac{J_{Cl}}{C_{Cl,I}} \quad (\text{Eq. 6})$$

where J_I [kg/s] is the water infiltration (mass) flux, J_{Cl} [kg/s] the chloride flux, $C_{Cl,I}$ [kg/kg] the mass fraction of Cl in the infiltrated water.

Applying Equation 6 with Cl concentration in infiltrated water estimated by the measured pore-water Cl concentration data, a modified water infiltration map can be developed, as shown in [Figure 6-24](#). The domain was divided into nine regions based on the observation of the measured Cl data range. The infiltration rate is approximated using an average value of the present-day, mean infiltration scenario ([Figure 6-18](#)) in regions where pore-water data is unavailable (Regions I, II and VIII). A comparison of infiltration rates in different regions of the model domain is given in [Table 6-13](#).

Simulation results using the calibrated water infiltration map are shown in [Figures 6-25](#) through [6-27](#). Improvements can be seen when these results are compared with the results in [Figures 6-19](#) through [6-21](#) using the original calibration rates.

6.4.3.2 Transient Transport

The $^{36}\text{Cl}/\text{Cl}$ ratios have been used to infer the ages of waters at depth and to locate rapid flow regions. Chloride and ^{36}Cl concentrations at ESF and ECRB stations were calculated using the 1-D analytical solution to each column of the 3-D calibration grid over the model domain. The assumed glacial infiltration rates, corresponding Cl and ^{36}Cl fluxes, and zero initial Cl and ^{36}Cl concentrations were first applied to estimate a glacial steady-state distribution of Cl and ^{36}Cl concentrations. Chloride concentrations and $^{36}\text{Cl}/\text{Cl}$ ratios at different modern times were then computed using the calibrated present-day infiltration rates and modern Cl and ^{36}Cl fluxes with the glacial steady-state Cl and ^{36}Cl results as initial concentrations.

Transport parameters and the radioactive-decay constant were the same as those used in the 3-D simulations. Porosity input was based on the simulation input rock data and converted from dual-continua type to effective-continuum type.

The analytical solutions were first verified by 3-D transport simulations, in which flow fields of both glacial and modern times were assumed at steady state, with all other input parameters the same as those used for the analytical solutions. Figure 6-28 shows good agreement in the comparisons of ESF Cl concentrations at 15,000 years by the two methods.

Chloride concentrations at ESF and ECRB stations, and ($^{36}\text{Cl}/\text{Cl}$ ratio at ESF stations at 10,000, 15,000 and 18,000 years modern times) were computed and plotted in Figures 6-29 through 6-31 against the observed pore-water concentration data. The model solutions are within the range of measured data and able to match major transient-transport behavior and trends.

6.4.3.3 Analysis of Sulfate Data

The sulfate analysis provides an alternative interpretation to estimate infiltration rates. The calibration results can be important at places where significant amount of pore-water chemical data are available. The sulfate discussion demonstrates an example of uncertainties in the interpretation of chemical data, and additional information on infiltration, flow mechanism, and climate-change effects is needed in further chemical transport investigations. To study the SO_4 distributions, pore-water SO_4 concentrations from all available boreholes (NRG-6, NRG-7A, SD-7, SD-9, SD-12, UZ-14, and UZ#16) and the ESF were averaged by each hydrologic unit, and the results were compared with the same Cl averages in Figure 6-32. The SO_4/Cl ratio indicates that SO_4 concentrations are higher than Cl concentrations in TCw and PTn, but lower than Cl concentrations in the TSw and CHn units. A preliminary 3-D simulation with SO_4 precipitated concentration and SO_4 molecular diffusion coefficient was unable to predict these vertical variations.

Additional information on infiltration, flow and transport mechanism, and climate-change effects may be needed in further investigations of the geochemistry at Yucca Mountain.

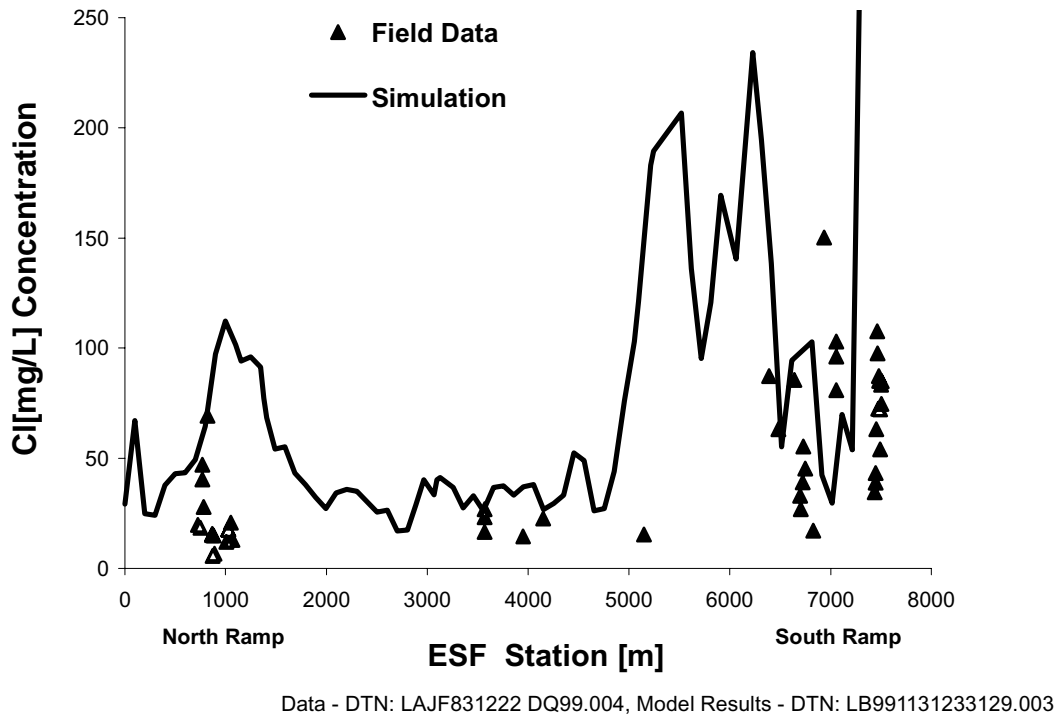


Figure 6-19. ESF CI Concentrations by 3-D Simulation with the Present-Day, Mean Infiltration.

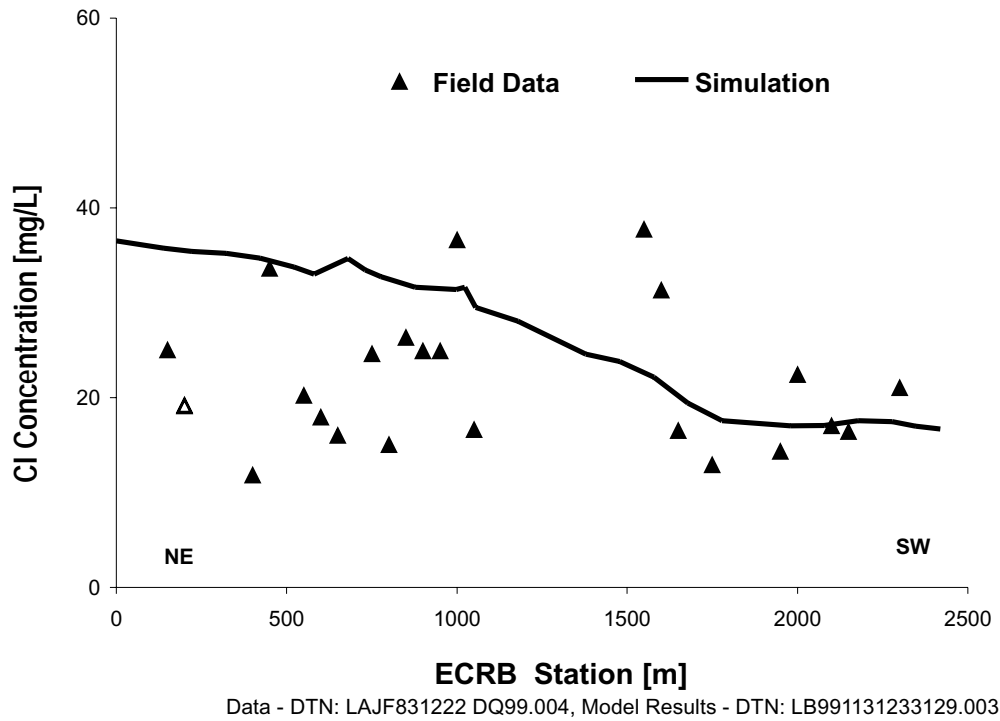
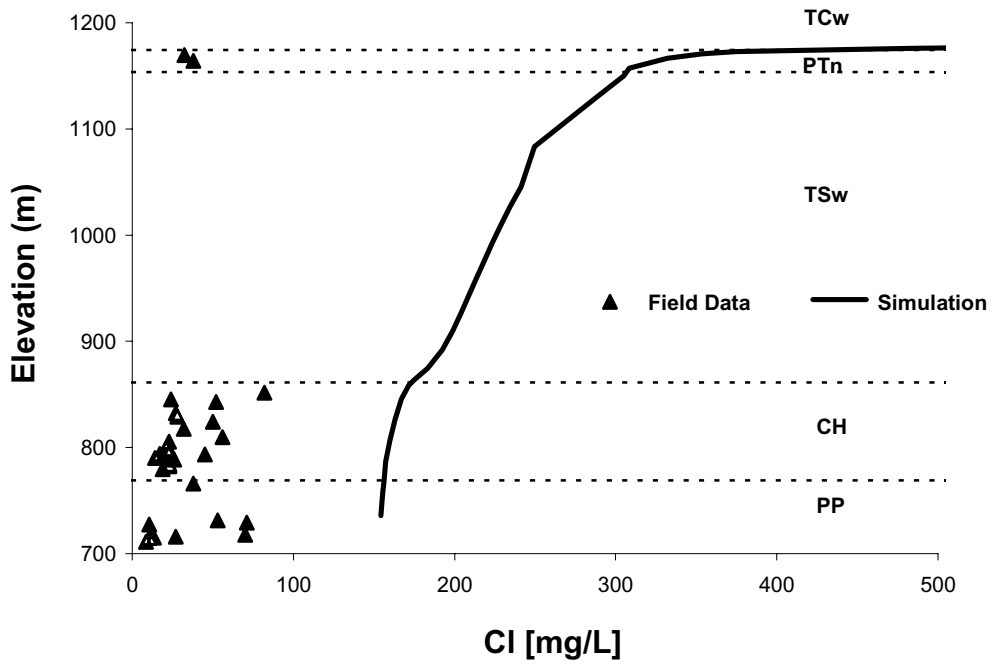
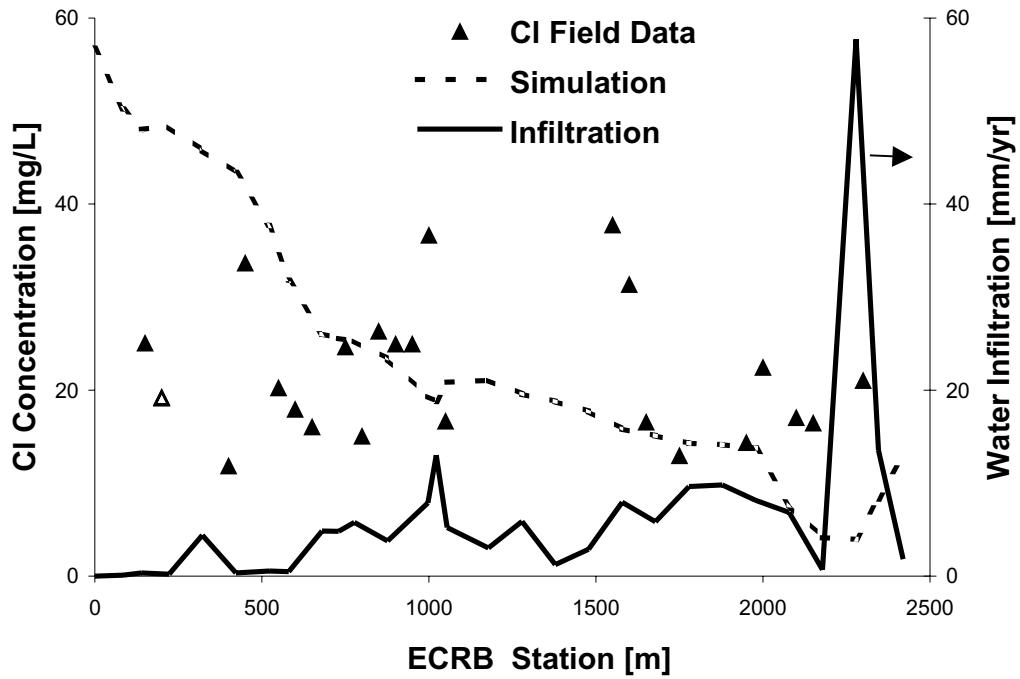


Figure 6-20. ECRB CI Concentrations by 3-D Simulation with the Present-Day Mean Infiltration.



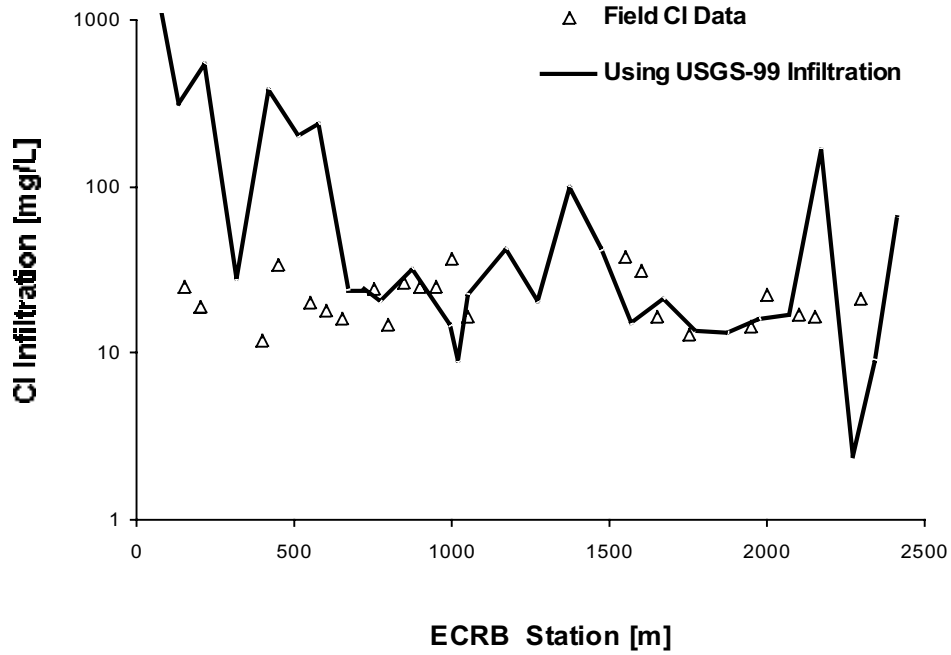
Data - DTN: LA9910JF12213U.0007 Model Results - DTN: LB991131233129.003

Figure 6-21. Borehole UZ#16 CI Concentrations by 3-D Simulation with the Present-Day, Mean Infiltration.



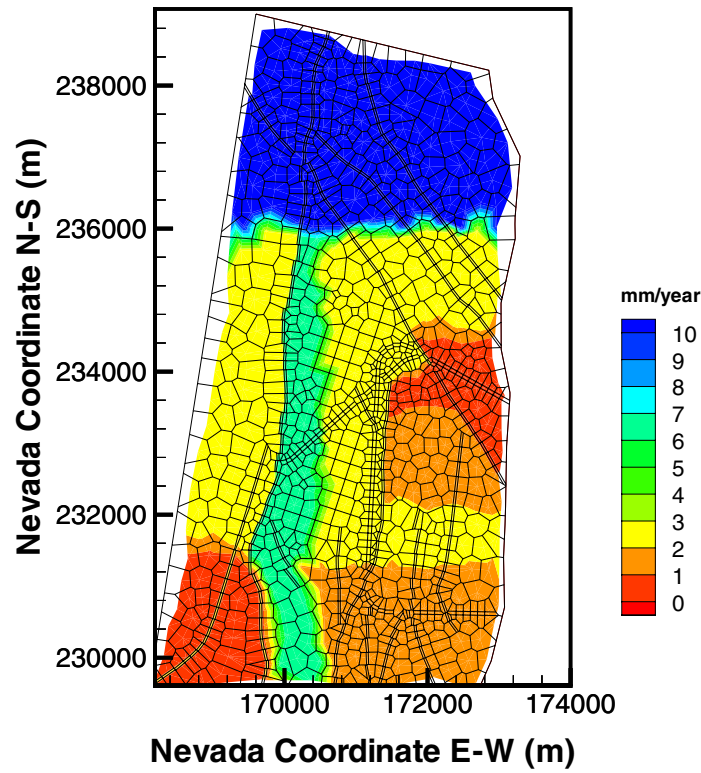
Data - DTN: LAJF831222 DQ99.004, Model Results - DTN: LB991131233129.003

Figure 6-22. Infiltration at ECRB Stations and CI 3-D Simulation Results Using the Infiltration.



Data - DTN: LAJF831222 DQ99.004, Model Results - DTN: LB991131233129.003

Figure 6-23. Cross Drift CI Infiltration Concentration Based on the ECRB Infiltration.



DTN: LB991131233129.003

Figure 6-24. Calibrated Infiltration Map

Table 6-13. Infiltration Data by Region

Region	Area		Infiltration Volume				Infiltration Rate	
			Present-Day Mean		Calibrated		Present-Day Mean	Calibrated
	km ²	%	m ³ /yr	%	m ³ /yr	%	mm/yr	mm/yr
I	9.9	25.5	104732	59	104708	58	10.60	10.60
II	5.3	13.8	12353	7	12262	7	2.32	2.30
III	3.7	9.6	26341	15	25910	14	7.12	7.00
IV	3.6	9.4	8844	5	8718	5	2.43	2.40
V	4.6	11.9	12545	7	13835	8	2.72	3.00
VI	2.2	5.6	2486	1	2168	1	1.15	1.00
VII	1.8	4.6	3355	2	2662	1	1.89	1.50
VIII	3.0	7.7	2162	1	2140	1	0.73	0.72
IX	4.7	12.0	5010	3	6993	4	1.07	1.50
Overall	38.7	100.0	177828	100	179396	100	4.6	4.6

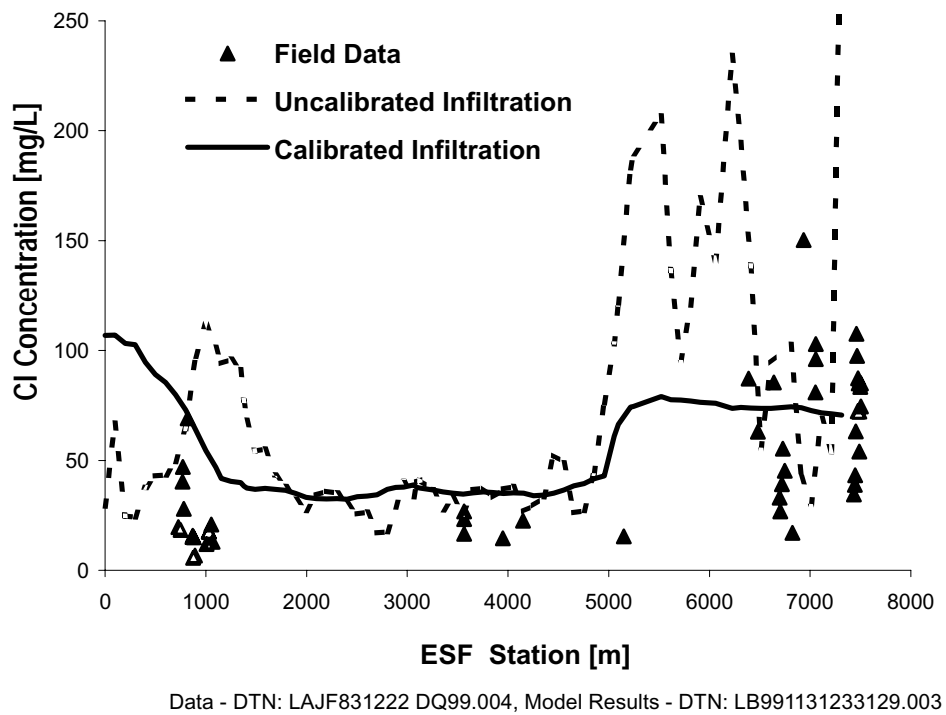


Figure 6-25. ESF CI Concentrations by 3-D Simulation with Calibrated Infiltration.

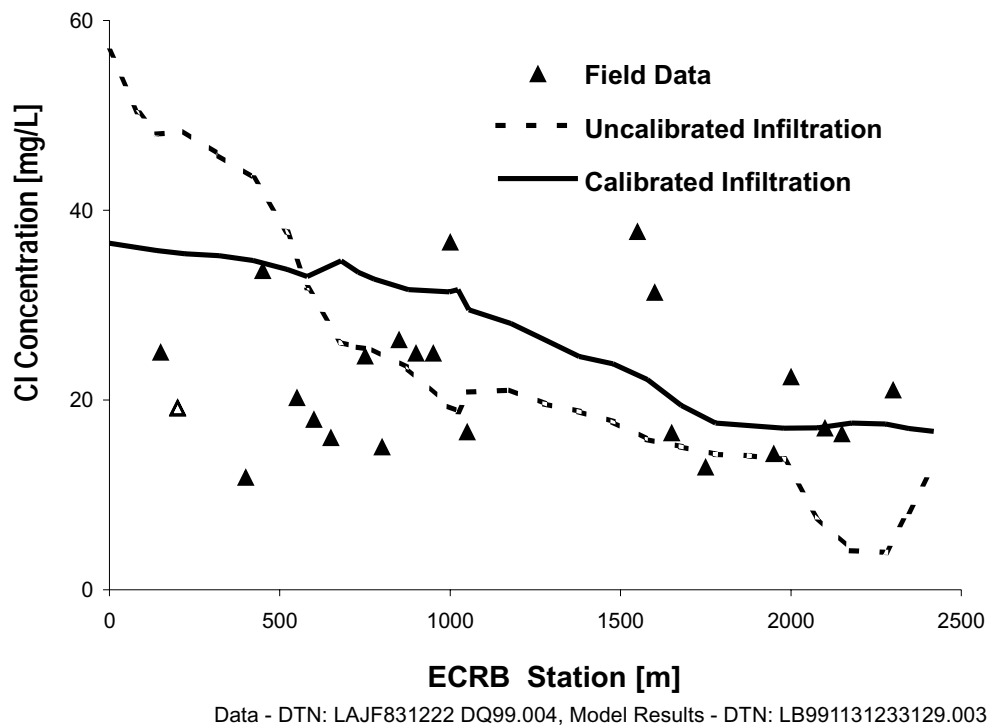
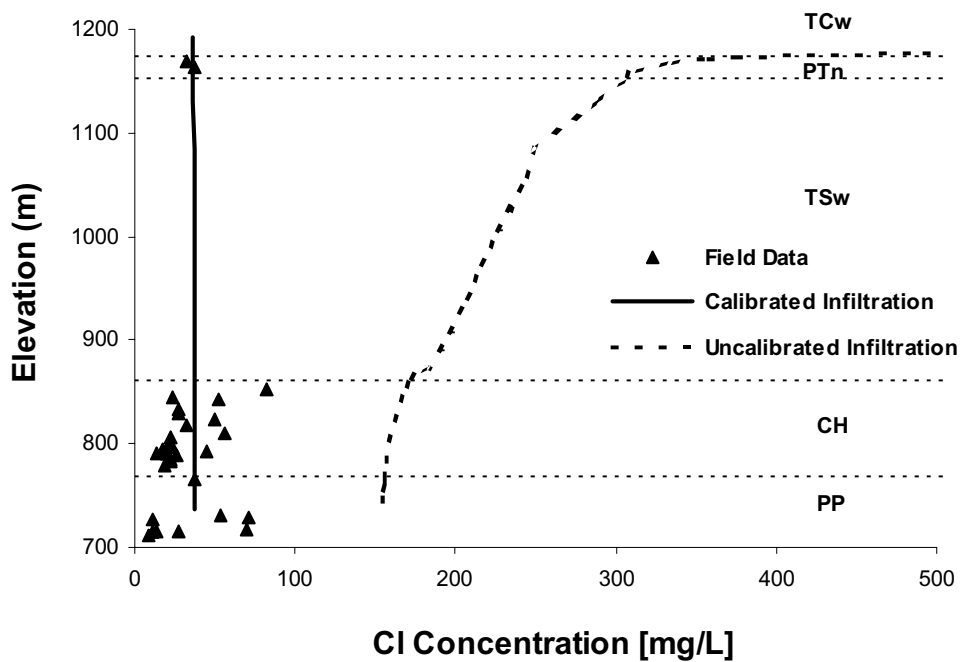
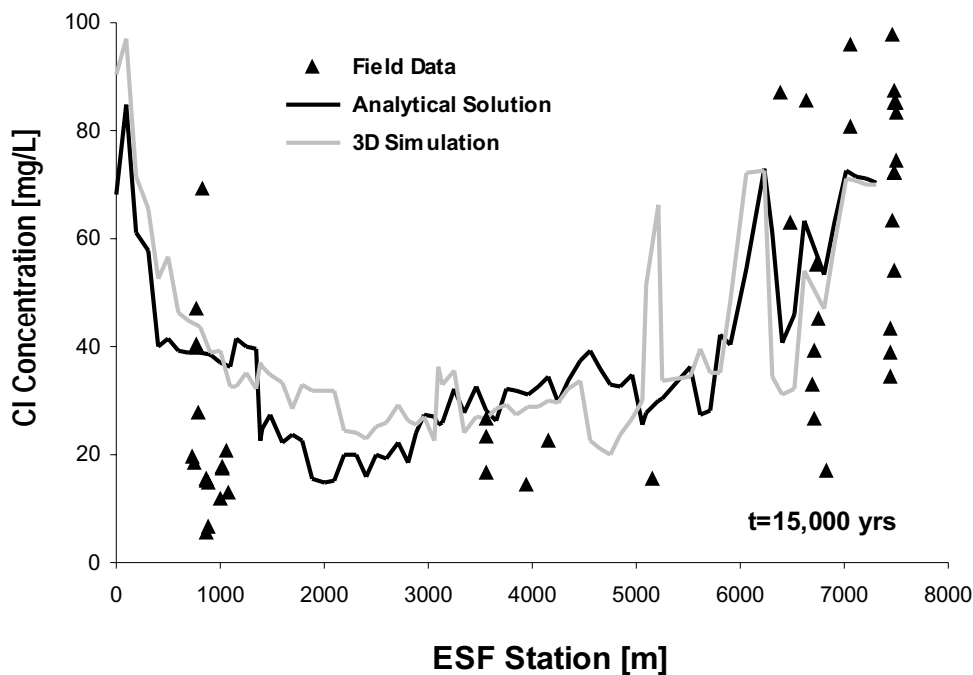


Figure 6-26. ECRB CI Concentrations by 3-D Simulation with Calibrated Infiltration.



Data - DTN: LA9910JF12213U.0007 Model Results - DTN: LB991131233129.003

Figure 6-27. Borehole UZ#16 CI Concentrations by 3-D Simulation with Calibrated Infiltration.



Data - DTN: LAJF831222 DQ99.004, Model Results - DTN: LB991131233129.003

Figure 6-28. ESF CI Concentrations by Analytical Method and 3-D Simulation.

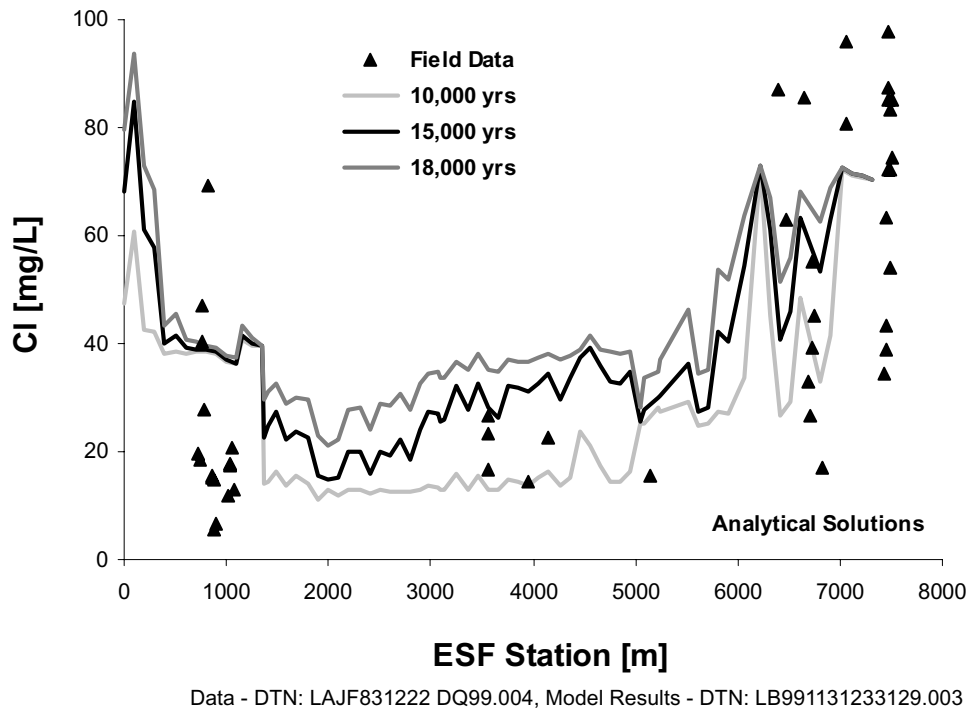


Figure 6-29. Analytical Results of Cl Transient Distributions at ESF Stations.

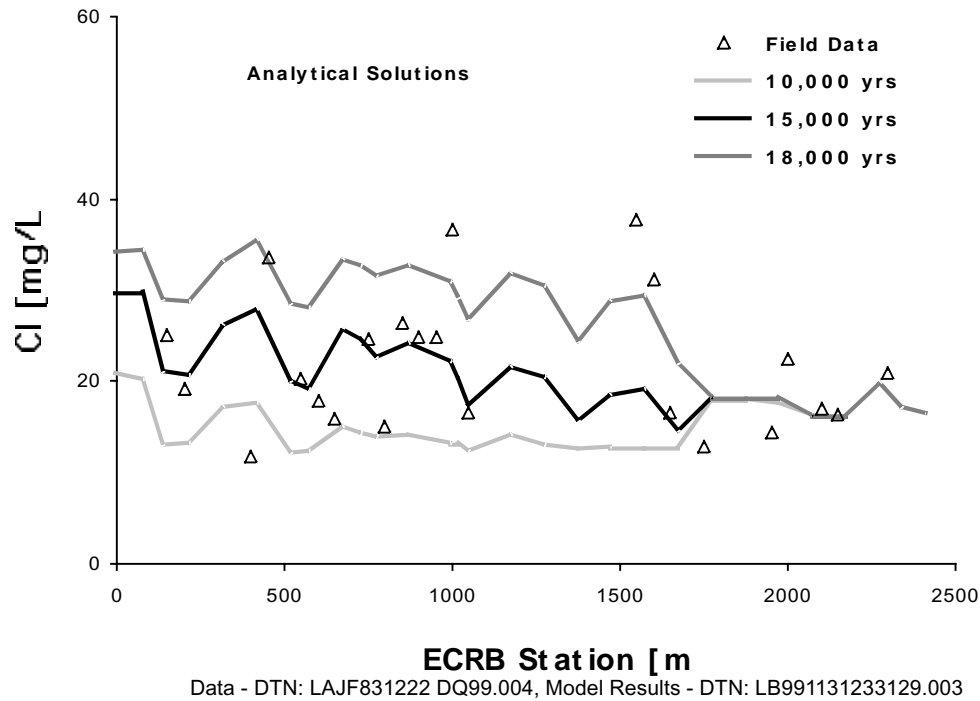
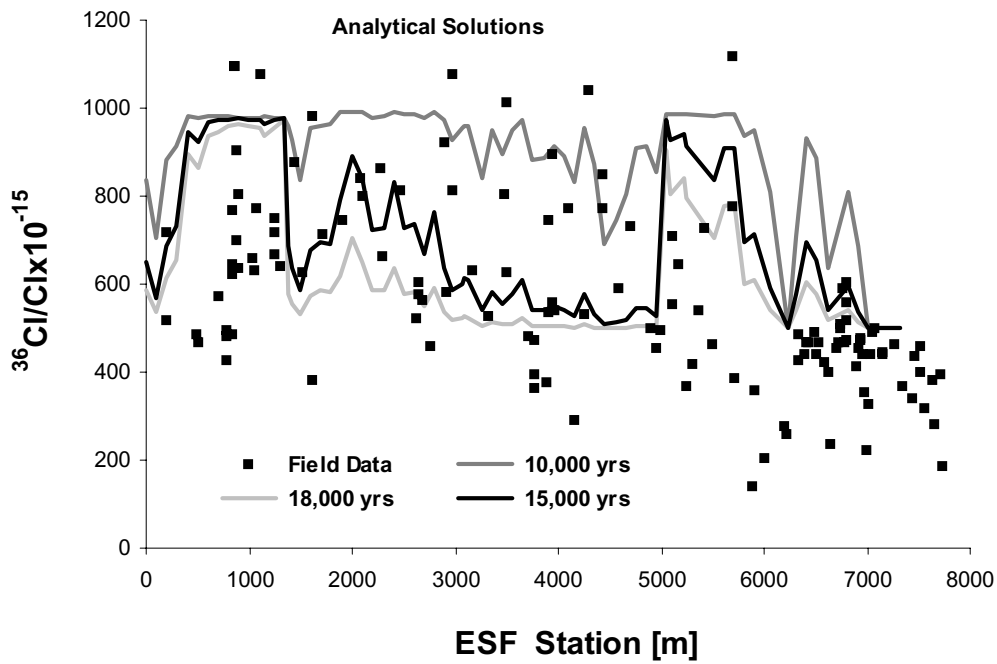
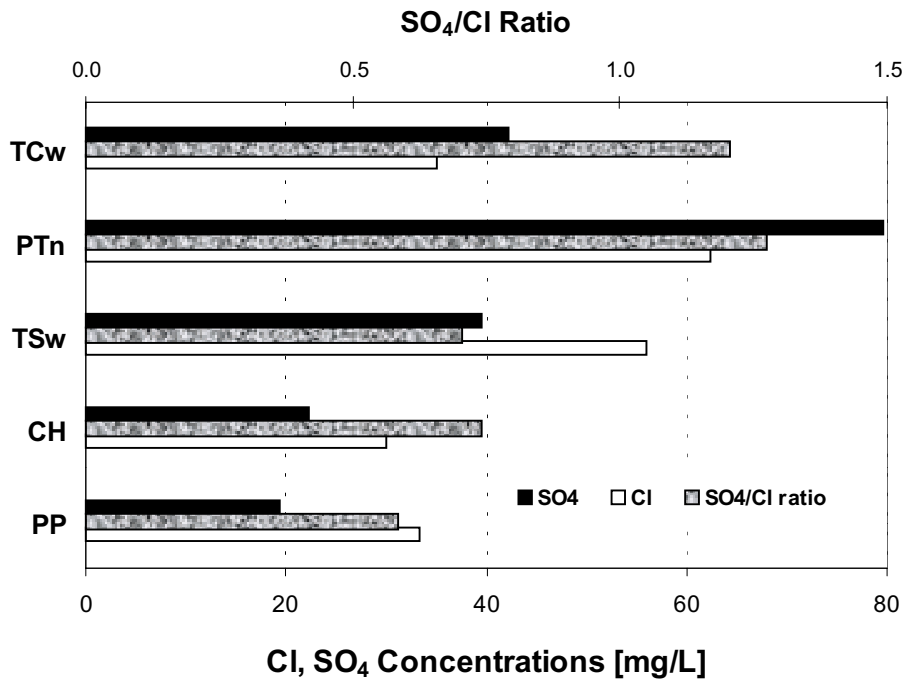


Figure 6-30. Analytical Results of Cl Transient Distributions at ECRB Stations.



Data - DTN:LASL831222AQ98.002 Model Results - DTN: LB991131233129.003

Figure 6-31. Analytical Results of $^{36}\text{Cl}/\text{Cl}$ Transient Analyses at ESF Stations.



DTN: LA9910JF122130.007

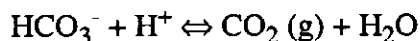
Figure 6-32. Pore-water Cl, SO₄ Concentrations and SO₄/Cl Ratios by Hydrogeologic Units.

6.5 CALCITE ANALYSIS

6.5.1 Introduction

The purpose of this study was to investigate the relationship between percolation flux and measured calcite abundances. Hydrogenic calcite deposits in fractures and cavities at Yucca Mountain (YM) have been studied to estimate past percolation fluxes (CRWMS M&O 2000a). These deposits may improve the understanding of the current and future UZ percolation (since direct measurements of infiltration fluxes over thousands of years are not possible). Here, we investigate several factors that influence calcite deposition using reaction-transport modeling. Calcite deposition in this unsaturated fractured rock system occurs through a complex interplay of fluid flow, chemical transport, and reaction processes. The present simulations consider the following essential processes: (1) fracture-matrix interaction (dual-permeability) for water flow and chemical constituents, (2) gaseous CO₂ diffusive transport and partitioning in liquid and gas phases, (3) ambient geothermal gradient for geochemical calculations, and (4) kinetics of fluid-rock chemical interaction.

The solubility of CO₂ gas in water decreases as temperature increases (with depth) as follows:



Then the gaseous CO₂ is removed by the gas-diffusive transport. The above process also increases the pH, which then contributes to calcite precipitation:



The elevated temperature also directly contributes to calcite precipitation because its solubility decreases as temperature increases. Therefore, the ambient geothermal gradient considered is a very important mechanism for calcite precipitation. An active fracture model, developed by Liu et al. (1998), was used to describe gravity-dominated and preferential liquid flow in fractures. Calcite in the preferential fast water flow path in fractures may not reach chemical equilibrium instantaneously. Evidence of calcite inhibition resulting from organic matter in the vadose zone has been described in the literature. Many UZ pore waters are oversaturated with calcite, possibly indicating kinetic inhibition or possibly measurement errors (CRWMS M&O 2000a). (Pore waters extracted from the YM rock matrix are generally oversaturated with calcite, and no water measurement is available from fractures.) Depending on water velocity, the kinetics of fluid-rock chemical interaction is likely to influence calcite distribution with depth in fractures .

A large number of simulations were performed using a range of infiltration rates, water and gas chemistries (at the top boundary), and reaction rates. Two sets of initial mineralogical conditions are considered. Validation of the calcite model for estimating percolation fluxes can only be done once significantly more data as a function of depth are available. The major uncertainty is the unknown effective reactive surface area for calcite, as well as uncertainties in the input thermodynamic and kinetic data, and the unknown water chemistry as a function of time for the several million years over which the calcite was precipitated. Thus, the parameters used to estimate calcite have been modified somewhat to match these data and are nonunique because of

the many parameters that could be modified simultaneously. Another complicating factor is that the development of the calcite abundances over time is unknown.

6.5.2 Model Description

The present analysis of calcite deposition in the Yucca Mountain UZ is performed by the reactive transport computer code TOUGHREACTE9 V1.0, (STN: 10153-1.0-00). The code was developed by introducing reactive chemistry into the framework of the existing multiphase fluid flow code TOUGH2 (Pruess 1991). The code uses a sequential iteration approach, which solves the transport and reaction equations separately.

Water flow is solved by the EOS9 flow module, which considers only saturated-unsaturated liquid phase water flow (Richards' equation). For the purpose of solving water flow, the gas phase is at a constant pressure (atmospheric). Under ambient steady-state conditions, the effects of heat and the gas phase on water flow are not significant. To test this, two flow simulations were performed, using a 1-D column model representing borehole WT-24 (later used for analysis of the calcite deposition). The first simulation (with the EOS9 flow module) only considered moisture flow using a constant temperature of 25°C for the entire column. The second simulation (using the EOS3 multiphase flow module) considered not only the liquid-phase water flow, but also the gas-phase flow and heat transfer using a (top) temperature of 15.60C at the land surface and a (bottom) temperature of 30°C at the water table (with the code TOUGHREACT V2.2, STN: 10154-2.2-00). A similar water saturation distribution was obtained from both simulations (Xu, Scientific Notebook, YMP-LBNL-GSB-TX-1, p. 40). Therefore, hydrochemical transport simulations presented later all were based on the single-phase water flow module EOS9.

Advective and diffusive transport of aqueous chemical species is considered in the liquid phase. Molecular diffusive transport of gaseous species (CO₂) is considered in the gas phase. The atmospheric pumping effects on CO₂ transport are not considered. These daily changes may not have significant influence on calcite deposition in the deep units because these changes are relatively small and are not likely to propagate to deep units. Aqueous chemical complexation and gas dissolution/exsolution are considered under the local equilibrium assumption. Mineral dissolution/precipitation proceed according to kinetic conditions. Temperature effects are considered for geochemical reaction calculations since equilibrium and kinetic data are functions of temperature. The depth dependent temperature distribution is read initially from the flow input file.

6.5.3 Hydrogeochemical Data

Flow condition: Two 1-D columns (representing boreholes NRG-7A and WT-24) were used for analysis of the calcite deposition in the Yucca Mountain UZ. These two columns were taken from the 1-D grid for flow property calibration model (DTN: LB990501233129.002, column numbers are a-8 for NRG-7A, and a-18 for WT-24). A dual-permeability model was employed for water flow and chemical transport. An active fracture model, developed by Liu et al. (1998), was used to describe gravity-dominated and preferential liquid flow in fractures. Full detailed investigations including fracture and matrix properties (frequency, permeability, van Genuchten a and m parameters, aperture, porosity, interface area, and residual and saturated saturations) are

reported in two AMRs: Calibrated Properties Model (CRWMS M&O 2000b), and Hydrologic Properties Data (CRWMS M&O 2000, U0090). The modeling mesh, hydrogeological parameters, and flow conditions (DTN: LB991131233129.001) were all adopted from this previous 1-D flow calibration. Initially, borehole NRG-7A was selected to analyze calcite deposition under ambient conditions. There is no calcite deposition data for NRG-7A, so that these runs cannot be compared with measured data. Later, borehole WT-24 was chosen because calcite deposition data for borehole WT-24 became available from CRWMS M&O (2000a, Figure 53). A constant infiltration rate over the entire simulation time was applied. The established steady-state water flow condition was used for chemical transport and fluid-rock interactions. Because a constant infiltration and steady-state water flow were considered, the term "percolation" through the entire column is equal to "infiltration." The temperature distribution (ambient geothermal gradient) obtained from TOUGHREACT V2.2 simulation (using the EOS3 flow module) was used for geochemical calculations. Details are given in Xu's Scientific Notebook (YMP-LBNL-GSB-TX-1, p. 36).

Mineralogical and kinetic data: Two sets of initial mineralogical conditions were evaluated so that the effect of uncertainties in thermodynamic and kinetic data for more complex minerals, such as zeolites and clay minerals, can be assessed. The first set considered only calcite, quartz, cristobalite- α (its solubility is similar to opal), and amorphous silica. The silica polymorphs were included for consistency with THC calculations done in AMR Drift-Scale Coupled Processes (DST and THC Seep-age) Models (CRWMS M&O 2000d), but are not essential for calcite reactions when aluminosilicates are not considered. Because the pH in this system is less than 10, calcium silicate minerals such as tobermorite or ettringite are not expected to form in this system (Steefel and Lichtner 1998, pp. 217-220), and therefore the silicate and carbonate systems are only very weakly coupled. For convenience of reporting, here we call this set "simple mineralogy". The second set considered more complex mineralogical constituents, including microcline, albite, anorthite, Ca-smectite, Na-smectite, Mg-smectite, K-smectite, illite, tridymite, cristobalite- α , amorphous silica, quartz, glass, hematite, calcite, stellerite, heulandite, mordenite, clinoptilolite, kaolinite, sepiolite, and fluorite. We called the second set "complex mineralogy". Each model layer is assigned two mineralogical compositions, one for the fracture block and the other for the rock matrix block. In the present study, mineralogical composition, kinetic data, and reactive surface areas were based on CRWMS M&O (2000d). The mineralogical data (Scientific Notebook, YMP-LBNL-YWT-ELS-1, p. 22-23, Table 4) were calculated based on the measurements presented in version 3.0 of the Mineralogic Model (DTN: LA9908JC831321.001). The kinetic rate law used is given in Section 6.1.4 of CRWMS M&O (2000d).

Kinetic data, including the reaction rate constants and activation energies, were taken directly from or were recalculated from published scientific literature. These data and their sources are listed in Table 4 of CRWMS M&O (2000d). Reactive surface areas of minerals on fracture walls were calculated from the fracture-matrix interface area/volume ratio, the fracture porosity, and the derived mineral volume fractions. These areas were based on the fracture densities, fracture porosities, and mean fracture diameter. Full details are given in Section 6.1.5.1 of CRWMS M&O (2000d). Mineral surface areas in the rock matrix were calculated using the geometric area of a cubic array of truncated spheres that make up the framework of the rock. Full details on mineral surface areas in the matrix are given in Section 6.1.5.2 of CRWMS M&O (2000d). Modifications were made to the rate constant for calcite that may have shifted it into the kinetic regime when it may be in local equilibrium. However, because the effective rate is a product of the surface area and the kinetic rate this effect becomes part of the sensitivity analysis.

The CHn unit (below the TSw) was not considered in the geochemical simulations because: (1) lateral flow may occur in the CHn and (2) the CHn has abundant zeolites and volcanic glass for which thermodynamic and kinetic data are more poorly known. The exclusion of the CHn unit doesn't affect the results on upper units because flow is predominantly gravity-driven, and backward diffusion is not important over the large vertical distance between the potential repository horizon and the CHn.

Boundary water and gas chemistry: Two types of chemical compositions were used for the top boundary of the hydrochemical transport simulations. The first water type (Table 6-14) was the average Topopah Spring Tuff water calculated from several observation samples (Scientific Notebook: YMP-LBNL-YWT-NS-1, pp. 78-79). The second water type was a measured TSw pore water extracted from a drill core from Alcove 5 in the Tptpmn (CRWMS M&O 2000d, Table 3), which has a higher Ca concentration. These two waters are slightly oversaturated with respect to calcite. These two water compositions merely provide some possible compositions that span a fairly wide range Ca concentration for the UZ pore waters that have been analyzed above the zeolitic units. Oxidizing conditions were considered for both waters. The boundary water type applied here is considered to be the water after transformation by soil zone processes. Finally, the initial water chemical composition used was uniform throughout the column for both the fracture and matrix blocks, and was adopted from the average TSw water (Type 1).

Table 6-14. Aqueous and Gaseous Chemical Concentrations (mg/L) Used for Initial and Boundary Conditions of Hydrochemical Transport Simulations.

Water type	1	2
Component	Average TSw water	Measured TSw water
Ca ²⁺	27	101
Mg ²⁺	5	17
Na ⁺	91	61.3
K ⁺	4	6
SiO ₂ (aq)	60	70.5
Al ³⁺	9.92×10 ⁻⁷ (5)	9.92×10 ⁻⁷ (1)
HCO ₃ ⁻ (3)	219	200
Cl	41	117
SO ₄ ²⁻	40	116
F ⁻	0.86	0.86
Water type	1	2
Fe ³⁺	6.46×10 ⁻⁸ (5)	6.46×10 ⁻⁸ (2)
pH	8.2	8.32

Table 6-14. Aqueous and Gaseous Chemical Concentrations (mg/L) Used for Initial and Boundary Conditions of Hydrochemical Transport Simulations. (Cont.)

PCO2 (bar) (4)	1.322x10 ⁻³	8.565x10 ⁻⁴
----------------	------------------------	------------------------

DTN: L6991131233129.001

NOTES:

- (1) Calculated by equilibrating with Ca-smactite at 25 °C
- (2) Calculated by equilibrating with hematite at 25 °C
- (3) Total aqueous carbonate as HCO₃, calculated from charge balance computed by speciation at 25 °C.
- (4) Calculated at equilibrium with the solution at 25 °C.
- (5) Total aqueous Al and Fe are set equal to those of Type 2 water.

In addition to aqueous species transport and reaction in water, we considered the diffusive transport of CO₂ in the gas phase and equilibration with pore water. The CO₂ gas partial pressures used for initial and top boundary conditions are in equilibrium with the corresponding aqueous chemical composition (the bottom row of Table 6-14). The elevated gas partial pressure (relative to atmospheric value 0.344×10^{-3} bar) at the upper boundary is uncertain, depending on soil-zone CO₂ production capability, which varies from location to location. The water chemical composition, especially pH, is controlled primarily by the CO₂ partial pressure.

Simulations: Two groups of simulations were performed. The first group of simulations were designed to analyze calcite deposition affected by infiltration (percolation) rate and reaction rate. These simulations were based on the NRG-IA borehole **column** with a simple mineralogy. For reporting purposes, this set of simulations is called “NRG-IA simulations”.

The second group of simulations was based on the borehole WT-24 column where measured **calcite** deposition data are available for comparison. Both sets of simple and complex mineralogy were used. The second group of simulations is called “WT-24 simulations”.

A **total simulation time** of 10 **million** years was carried out for all simulations. This simulation time was selected based on mineral growth having remained approximately constant over the past eight million years, as indicated by radiocarbon, ²³⁵U-VU, and U-Pb ages, and on all dated surfaces indicated by ages of outer mineral surfaces being young compared to the 12.7-million year age of the host tuffs (CRWMS M&O 2000a).

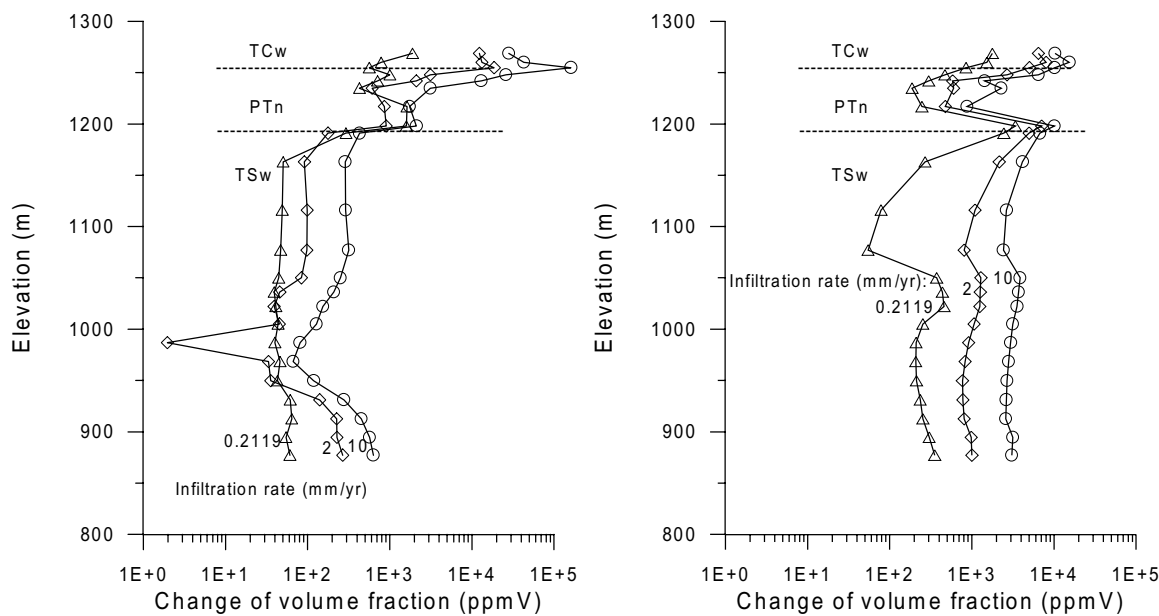
6.5.4 NRC-7A Simulations

In this section, the sensitivity analysis results of calcite deposition to infiltration (percolation) rate and reaction rate are reported.

Simulation setup: First, we used a base-case infiltration rate of 0.2119 mm/yr (DTN GSO00399991221.002.; ACC: MOL. 19991014.0102), then two additional infiltration rates of 2 and 10 mm/yr. Water Type 1 presented in Table 6-14 were used for the top boundary chemical transport conditions. Estimates of field mineral dissolution and precipitation rates

rates of 2 and 10 mm/yr. Water Type 1 presented in Table 6-14 were used for the top boundary chemical transport conditions. Estimates of field mineral dissolution and precipitation rates covered a wide range of values. We first used the reactive areas based on the initial estimated data. For the purpose of this analysis, we then reduced the areas by one order and two orders of magnitude. Scaling all rate constants (surface areas) by the same factor is justified for calcite precipitation in the simple mineralogy system because silica mineral dissolution and precipitation are not directly related to calcite precipitation. However, for the complex mineralogy system, scaling all rate constants (surface areas) by the same factor may not be sufficient. In the complex case, relative scaling of the reactive surface areas may be more appropriate, but there is no information on which to base such an approach at present. Simulations were performed using a different infiltration rate and reactive surface area (indicator of reaction rate). (Details are given in Xu's Scientific Notebook YMP-LBNL-GSB-TX-1, p. 30).

Results: We expressed the simulated changes of calcite volume fraction as the average among the matrix and the fractures (calculated by calcite volume in the matrix and fractures divided by the total matrix and fracture solid volume). The calcite precipitation generally increases as infiltration rate increases, especially in the TSw unit (Figure 6-33; more results are given in Xu's Scientific Notebook YMP-LBNL-GSB-TX-1, p. 33). An increase of infiltration results in a slight change in the amount of calcite at the bottom of the PTn unit.



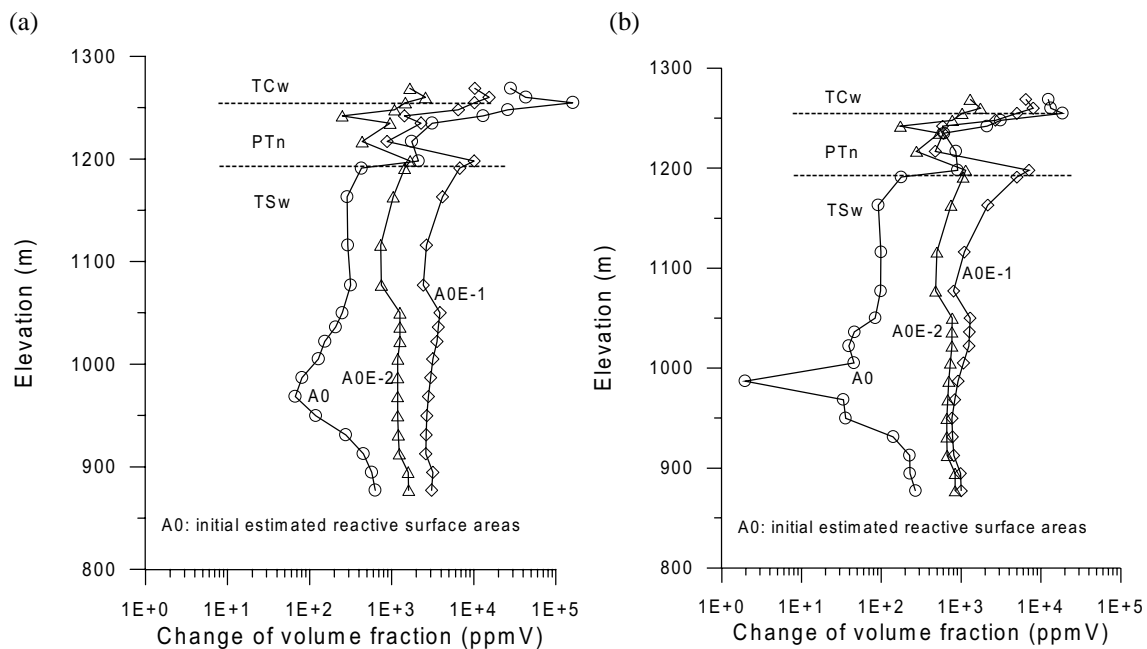
DTN: LB991131233129.001

NOTE: (a) Estimated reactive surface areas denoted by A_0 , (b) Use of reactive surface areas $A_0 \times 10^{-1}$

Figure 6-33. Change of Calcite Volume Fraction with Infiltration Rate after 10 Million Years in the NRG-7A Column Using the Type 1 Water for the Top Boundary of Chemical Transport

The calcite distribution is also dependent on reaction rate, which was achieved by changing the reactive surface area (Figure 6-34). For the welded TCw unit close to the land surface, the higher the reaction rate, the higher the calcite precipitation. For the deeper welded TSw unit, the highest surface areas (estimated) result in the lowest calcite precipitation. The shift of calcite precipitation

from the TCw to the TSw mainly results from the TCw being close to the top boundary, where percolation water and reactants of calcite are applied. Therefore, much more calcite precipitation occurs in the TCw than in the TSw. Increasing the areas by two orders of magnitude showed the same general trend as the initial estimated areas. The surface areas reduced by one order of magnitude from the initial estimated data give the most favorable conditions for calcite formation in the TSw unit.



Based on DTN: LB991131233129.001

NOTE: (a) 10 mm/yr infiltration rate, (b) 2 mm/yr infiltration rate

Figure 6-34. Change of Calcite Volume Fraction with Reactive Surface Area after 10 Million Years in Borehole NRG-7A Column Obtained Using the Average TSw Water for the Top Boundary of Chemical Transport

6.5.5 WT-24 Simulations

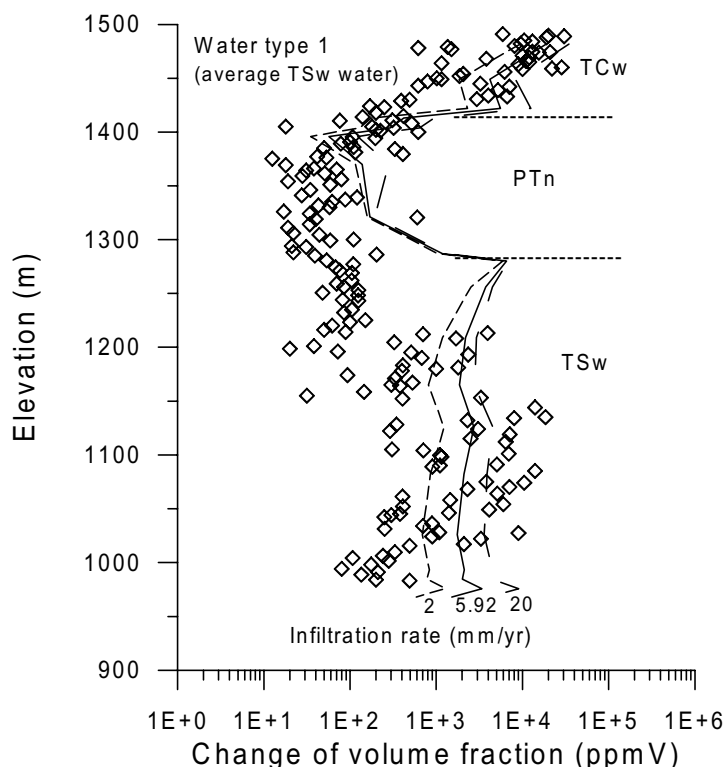
In this section, we report the WT-24 simulation results using two different sets of mineralogy (simple and complex) and water chemistry.

Simulation setup: We used three infiltration rates, a base-case rate of 5.92 mm/yr (DTN: GS000399991221.002.; ACCN: MOL. 19991014.0102), an additional lower rate of 2 mm/yr, and a higher rate of 20 mm/yr. An upper rate of 10 mm/yr was not chosen as it was for the previous NRG-7A simulations because the base-case rate is greater than that of the previous (5.92 over 0.2119 mm/yr). Two boundary types of water chemical compositions, average TSw water and measured TSw water (Table 6-14), were employed for the top boundary of the model. A total of nine simulations were performed using different infiltration rates, boundary water and gas chemistries, and reactive surface areas, which are summarized in Table 6-15.

Table 6-15. List of Simulations Performed for Borehole WT-24 Column Using Different Combinations of Infiltration Rate, Boundary Water Chemical Composition, Initial Mineralogy, and Reactive Surface Areas.

Simulation	Infiltration Rate (mm/yr)	Water and Gas Chemistry	Mineralogy	Surface Area (A_0 are referred areas of minerals)
1	5.92	Type 1 in Table 6-14	Simple	$A_0 \times 10^{-2}$ for PTn unit, $A_0 \times 10^{-1}$ for others
2	2	"	Simple	same as simulation 1
3	20	"	Simple	same as simulation 1
4	5.92	"	Complex	$A_0 \times 10^{-1}$
5	5.92	"	Complex	$A_0 \times 10^{-1}$ for calcite, $A_0 \times 10^{-3}$ for others
6	5.92	Type 2 in Table 6-14	Complex	same as simulation 5
7	2	"	Complex	same as simulation 5
8	20	"	Complex	same as simulation 5
9	5.92	"	Simple	same as simulation 1

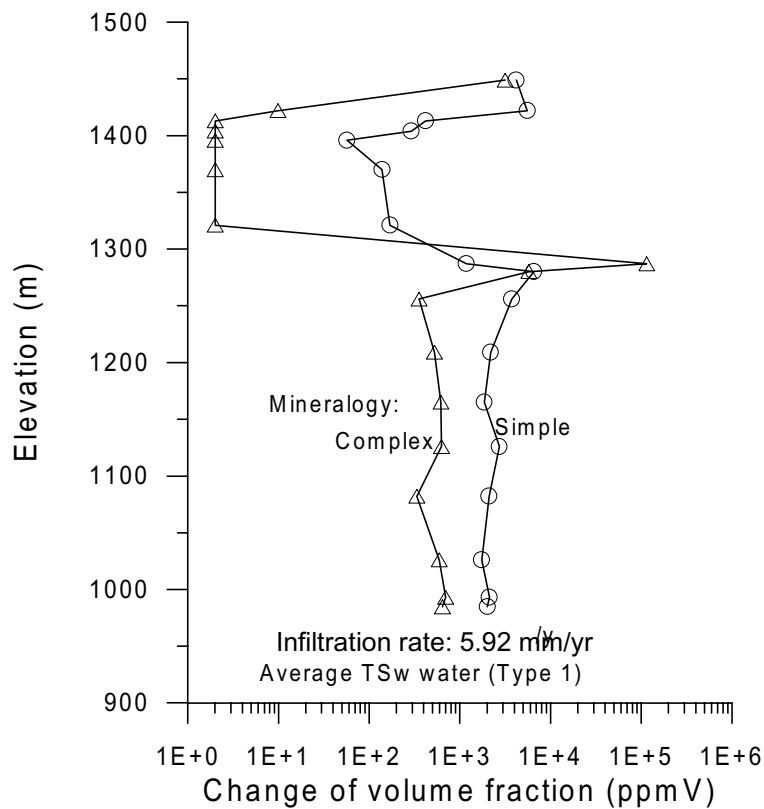
Results: Simulations 1, 2, and 3 use the same average TSw water (Type 1), simple mineralogy, and reactive surface areas. The reactive surface areas used for the welded TCw and TSw units were reduced by one order of magnitude from the initial estimated data, and those for the nonwelded PTn unit were reduced by two orders of magnitude. The surface-areas were reduced because at the field-scale multimineral system all mineral surfaces may not be in contact with the percolating waters. Reactive surface areas used in the simulations were modified somewhat to match measured calcite data. One order more surface-area reduction in the PTn was according to fewer fractures in this unit. A different infiltration rate was employed for each simulation. The changes of calcite volume fraction are presented in Figure 6-35 for Simulations 1-3, together with measured calcite deposition data in the WT-24 cuttings (the comparison with the measured data will be discussed in a later section). The resulting calcite precipitation in the nonwelded PTn was decreased because of the reduction of the reactive surface areas (compare Figure 6-35 with Figures 6-33 and 6-34).



Data - CRWMS M&O (2000a; Figure 53) Model Results - DTN: LB991131233129.001

Figure 6-35. Simulated Changes of Calcite Volume Fraction (Lines) Using Simple Mineralogy with Infiltration Rate after 10 Million Years in Borehole WT-24 Column Together with Measured Calcite Deposition Data (In Diamond Symbols) that are Taken from the Analysis of Geochemical Data for the Unsaturated Zone (CRWMS M&O 2000a, Figure 53).

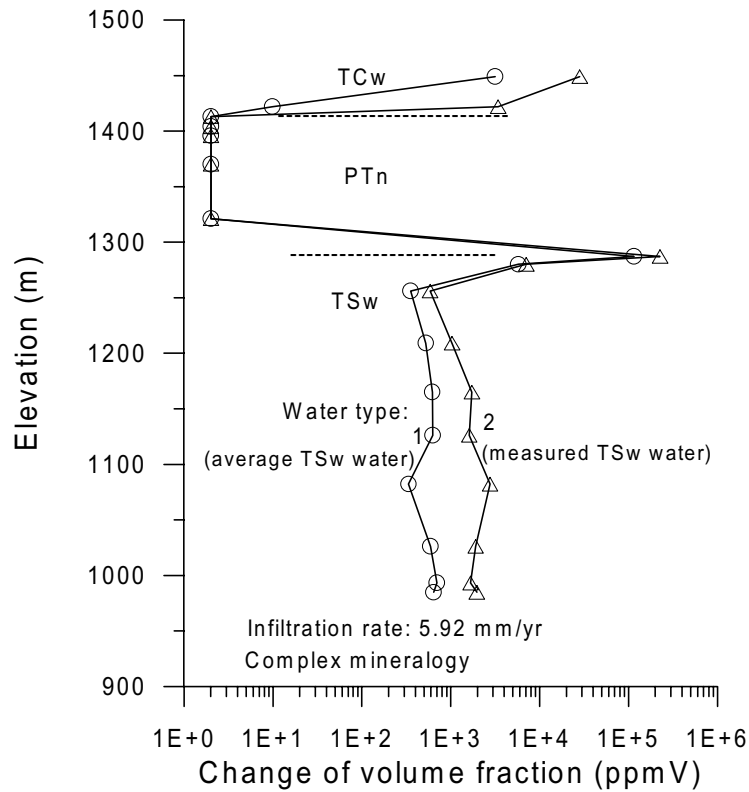
Unlike Simulation 1, Simulation 4 used complex mineralogy. Both simulations employ the same infiltration rate (5.92 mm/yr) and average TSw water-chemical composition (Type 1). The reactive surface areas used in Simulation 4 are reduced by one order of magnitude from the initial estimated data. No calcite precipitation was obtained from Simulation 4 because the other minerals (such as clay) were given very large reactive surface areas. Therefore, Ca was taken up by the Ca-bearing clay and zeolite minerals. (In a field-scale multiminer system, all the clay mineral physical surface areas may not effectively be in contact with the infiltration water). In Simulation 5, we reduced the surface areas by three orders of magnitude for all minerals except for calcite, whose area remained the same (reduced by one order of magnitude) to reflect the lesser water contact by the clays. Results for Simulations 1 and 5 are presented in Figure 6-36. Generally, calcite precipitation obtained with the complex mineralogy was much smaller than that with the simple mineralogy. Only one model layer at the bottom of the PTn unit was exceptional. This layer had a higher matrix water content (or higher water saturation and porosity) than that at the top layer of the TSw unit (Xu, Scientific Notebook, YMP-LBNL-GSB-TX-1, p. 41, Figure 14). Water can reside in the bottom of the PTn for a longer time, potentially precipitating more calcite.



Based on DTN: LB991131233129.001

Figure 6-36. Change of Calcite Volume Fraction after 10 Million Years in the WT-24 Column under Different Mineralogy Conditions. The values of changes of calcite volume fraction under complex mineralogy in the PTn layers are much smaller than 2, and they are increased to a value of 2 for display purposes.

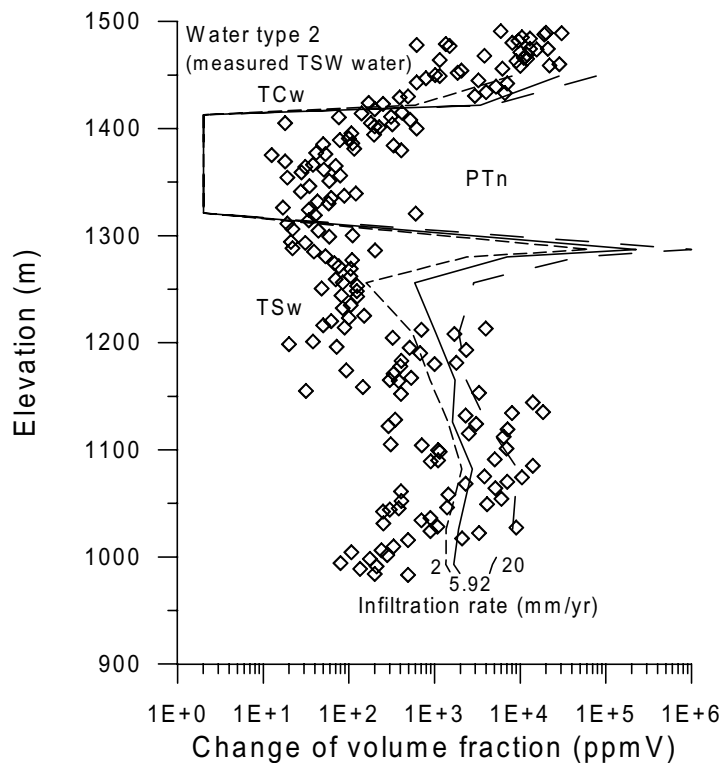
Simulation 6 employs the measured water-chemical composition (Type 4) with a much greater Ca concentration (Table 6-14) than the average TSw water (Type 1) used in Simulation 5. The results for Simulations 5 and 6 are presented in Figure 6-37. More calcite precipitation occurs in the welded TCw and TSw units using the greater Ca concentration water. In both simulations, again no calcite precipitation occurs in the nonwelded PTn unit except at the bottom layer.



Based on DTN: LB991131233129.001

Figure 6-37. Change of Calcite Volume Fraction with Water Type after 10 Million Years in the WT-24 Column.

Simulations 7 and 8 employ, respectively, 2 and 20 mm/yr infiltration rates to analyze the dependence of calcite deposition on infiltration rate under the complex mineralogy conditions (Figure 6-38). Calcite precipitation increases in the welded TCw and TSw units as infiltration rate increases. This is consistent with the result under the simple mineralogy condition (Figure 6-35).



Data - CRWMS M&O (2000a; Figure 53) Model Results - DTN: LB991131233129.001

Figure 6-38. Simulated Changes of Calcite Volume Fraction (Lines) Using Complex Mineralogy with Infiltration Rate after 10 Million Years in the WT-24 Column, Together with Measured Calcite Deposition Data (Diamond Symbols) that are Taken from the Analysis of Geochemical Data for the Unsaturated Zone (CRWMS M&O 2000a, Figure 53).

Under the complex mineralogy condition, most of the calcite precipitates in the rock matrix (Figure 6-39), especially in the TCw unit, whereas under the simple mineralogy condition (Figure 6-40), almost all calcite precipitation occurs in the fractures for the TCw and PTn units. Some calcite precipitation in the matrix can be observed in the TSw unit, but its density is much lower than that in the fractures. The results indicate that chemical interaction of fracture-matrix is more significant in the complex mineralogy condition than in the simple mineralogy condition for calcite deposition. In the simple mineralogy system, the reactant Ca for calcite precipitation comes only from percolation water. Therefore, calcite precipitation occurs mostly in the preferential water flow path in the fractures.

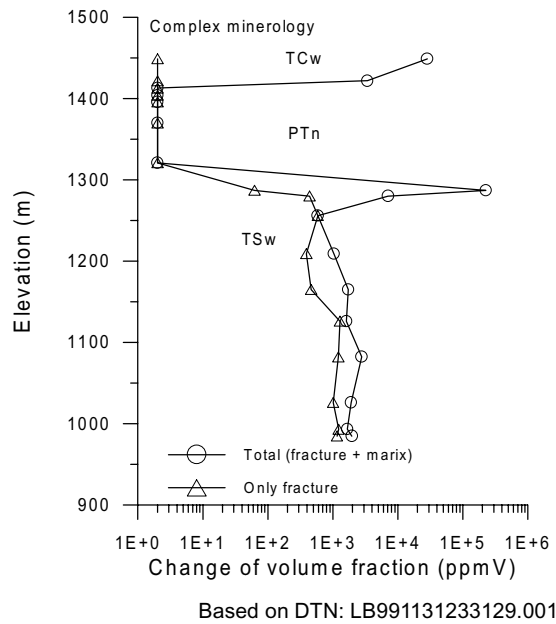


Figure 6-39. Change of Calcite Volume Fraction in Fracture (Calculated by Fracture Calcite Volume Divided by Total Fracture and Matrix Solid Volume) and in Total (Same as the Previous Figures, or Calculated by Fracture and Matrix Calcite Volume Divided by Total Fracture and Matrix Solid Volume) under Complex Mineralogy Conditions (Using an Infiltration Rate of 5.92 mm/yr).

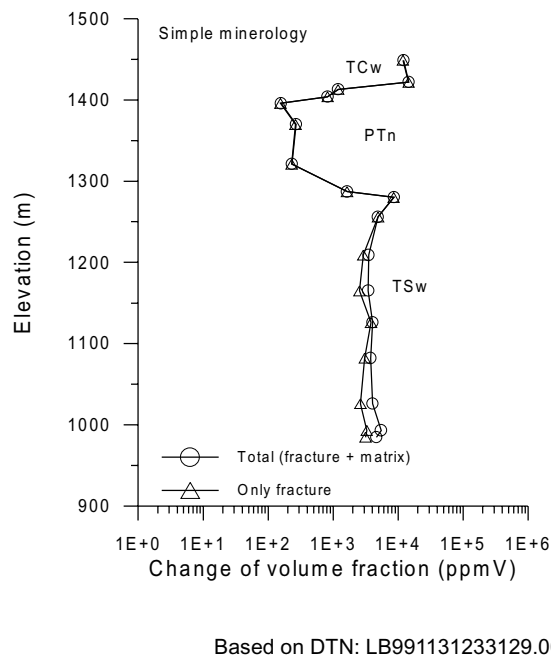


Figure 6-40. Change of Calcite Volume Fraction in Fracture and in Total under Simple Mineralogy Conditions (Using an Infiltration Rate of 5.92 mm/yr).

6.5.6 Discussion and Conclusions

Calcite precipitation values for the welded TCw unit obtained by using the simple mineralogy and the average TSw water (Type 1) are closer to the measured data than those obtained by using complex mineralogy and the measured TSw water (compare Figures 6-35 and 6-38). The simple mineralogy simulations also capture the calcite abundances in the nonwelded PTn unit more closely, except for the bottom layer. The improved agreement for the PTn unit is achieved by reducing the reactive surface area, which is consistent with the fact that fewer fractures occur in this unit. The simulated calcite precipitation values at the bottom of PTn unit may be overestimated for the WT-24 column, especially values from the complex-mineralogy simulation. However, according to measurements presented in the Mineralogic Model (DTN: LA9908JC831321.001) the high calcite concentrations at this layer have been observed at several other locations such as (USW G-2 Core).

According to Analysis of Geochemical Data for the Unsaturated Zone (CRWMS M&O 2000a, Section 6.10), calcite coatings are frequently found on fractures and lithophysal cavities in the welded TCw and TSw tuffs. This finding is better represented by simple mineralogy simulations such as presented in Figure 6-40, where calcite precipitation occurs primarily in the fractures. This is especially true for the TCw unit close to the land surface, in which reactants of calcite deposition come primarily from percolation water. The calcite precipitation occurs mostly in the preferential water flow paths in the fractures. Thus, the simple mineralogy simulations may be closer to calcite deposition condition. The effects of complex mineralogy on simulations may result from the uncertainty of thermodynamic and kinetic data for clay minerals, which are poorly known at present.

Measured calcite deposition varies significantly from location to location and depth to depth. Studies for the WT-24 column can give some general insight into calcite deposition conditions, but may not represent the whole picture at Yucca Mountain. For example, the peak values in the TSw observed in WT-24 cuttings are in contrast with calcite deposition in the Exploratory Studies Facility (ESF). According to the conclusion regarding calcite measurements in the ESF (CRWMS M&O 2000a, Section 6.10), calcite abundance decreases with depth in the TSw unit. The mean calcite abundance in the ESF is 0.034% which is close to the lower bound of calcite observed in WT-24 well cuttings. The mineral abundance in the ESF was determined for 30-m intervals. Thickness, length, and orientation of the mineral deposits were measured. The measured mineral in the ESF is calcite together with opal, with calcite the dominant phase.

The simulated results are sensitive to infiltration (percolation). Calcite deposition values obtained from the highest infiltration rate (20 mm/yr) are close to the high bound of the measurements (Figure 6-35). Those from the base-case (5.92 mm/yr) and lower infiltration rate (2 mm/yr) fall in the middle of the TSw measured data range. This may imply that the 20 mm/yr percolation rate is an upper bound for the WT-24 location, whereas the base infiltration (5.92 mm/yr) used in the flow model may be a moderate value. As pointed out in the previous "sensitivity simulation" section, the reactive surface area for calcite reduced by one order of magnitude from the initial estimation provides the most favorable condition for calcite formation in the deeper welded TSw unit. Therefore, the simulated values may be slightly overestimated.

The calcite data obtained from the sensitivity simulations for the NRG-7A column are generally in agreement with the wide range of the WT-24 measured data, except for the simulations with an infiltration equal to or less than 2 mm/yr and the initial estimated surface areas (Figure 6-33a and Figure 6-34b).

Calcite deposition data gives some constraints on infiltration-percolation flux, but cannot give a definite value or a narrow range of values. This is because calcite precipitation depends not only upon infiltration-percolation flux, but also water and gas chemistry, reaction rate, and mineralogy. The main reason for calcite precipitation with depth is its inverse solubility with temperature. However, the partial pressure of CO₂ and Ca concentration in percolating water controls the abundances of calcite and its stability. The reaction rate, and therefore the reactive surface area, influences its distribution with depth in the preferential fast water flow path in fractures.

A number of major uncertainties and approximations are involved in the numerical simulation results. The kinetics of heterogeneous reactions is scale and history-dependent, and cannot be reliably quantified. Reactive surface areas are uncertain and subject to poorly quantifiable phenomena such as armoring of mineral phases. Scaling all rate constants (surface areas) by the same factor is justified for calcite precipitation in the simple mineralogy system, but may not be sufficient in the complex mineralogy system. The effect of changing rate constants (surface areas) in the complex mineralogy system relative to one another may be more appropriate; however, there is no information at present on which to base such an analysis. Variations in water and gas chemistry data could considerably affect rock alteration and deposition patterns. The uncertainties associated with water and gas chemistry also needs to be addressed. In addition, uncertainties could arise from climate and infiltration variations over time, transient water flow condition, and possible lateral water recharge. An alternative conceptual model for calcite deposition would consider its formation as episodic, rather than as steady-state. Because of the kinetics of fracture calcite precipitation, an episodic fluid pulse would tend to change the distribution of calcite with depth. During more typical smaller infiltration events, more precipitation might take place near the surface and less at depth. This does not necessarily change the underlying conceptual model for calcite precipitation (kinetic rate law), but would change the parameters for matching measured abundances.

In summary, an analysis of calcite deposition using modeling tools can be used to build some constraints on hydrological parameters such as infiltration-percolation flux. Such an analysis also provides additional evidence for validation of flow and transport model. Over a range of 2-20 mm/yr infiltration rate, the simulated calcite distributions using simple mineralogy capture the measured data from the WT-24 well cuttings. The modeling results can provide useful insight into process mechanisms such as fracture-matrix interaction as well as conditions and parameters controlling calcite deposition. The modeled calcite abundances generally increased as infiltration rate increased. The simulated calcite abundances are also sensitive to water and gas chemistry, and reaction kinetics. However, it should be noted that similar calcite abundances could possibly be obtained by consideration of calcite precipitation under equilibrium conditions with different thermodynamic properties, water compositions, or under transient flow conditions. Hence the kinetic rates and infiltration rates are likely to be nonunique. To refine and improve the present simulations, we need additional studies on the major uncertainties and limitations as discussed above. Furthermore, the model presented here can be used to investigate processes for seepage in

cavities, which has been used as an analog for seepage into the potential repository waste emplacement drifts.

6.6 SIMULATIONS OF TSPA 3-D FLOW FIELDS

This section analyzes and summarizes the 21 simulation scenarios, 18 of which are based on perched water Conceptual Models #1 and #2 and are submitted to TSPA for performance analyses. The 21 model simulations are performed using (1) the TSPA grid ([Figure 6-2](#)), and nine infiltration maps, as discussed in Section 6.1; (2) the seven parameter sets in [Attachment II](#) of this AMR, and the two conceptual perched water models and a non-water perching model.

6.6.1 Simulation Scenarios

[Tables 6-16, 6-17 and 6-18](#) summarize the 21 simulation scenarios, associated conceptual models/grids, and parameter sets for the nine infiltration maps, respectively.

Table 6-16. Seven TSPA Simulation Scenarios: Data Files, Conceptual Models/Grids, and Parameter Sets for Three Present-Day Infiltration Maps.

Designation/ Simulation	Conceptual Model/Grid Name and DTN	Parameter Set/ Calibration	Infiltration Map (DTN: GS000399991221.002)
pa99_m	#3 Non-perching model/ 3d2kpa.mesh DTN:LB990701233129.001	Parameter set from Table II-7 , base-case/present-day, mean infiltration (AMR: CRWMS M&O 2000b) without 3-D calibration (DTN: LB991121233129.007)	Present-day, mean infiltration (Figure 6-3)
pa_pchL1	#1 Flow-through perched water model/ 3d2kpa_pc1.mesh DTN:LB990701233129.001	Parameter set from Table II-1 , lower-bound/present-day infiltration with 3-D calibration (Table 6-8) (DTN: LB991121233129.005)	Present-day, lower-bound infiltration
pa_pchL2	#2 By-passing perched water model/ 3d2kpa_pc2.mesh DTN:LB990701233129.001	Parameter set from Table II-2 , lower-bound/present-day infiltration with 3-D calibration (Table 6-8) (DTN: LB991121233129.006)	Present-day, lower-bound infiltration
pa_pchm1	#1 Flow-through perched water model/ 3d2kpa_pc1.mesh DTN:LB990701233129.001	Parameter set from Table II-3 , base-case/mean/present-day infiltration with 3-D calibration (Table 6-6) (DTN: LB991121233129.001)	Present-day, mean infiltration (Figure 6-3)
pa_pchm2	#2 By-passing perched water model/ 3d2kpa_pc2.mesh DTN:LB990701233129.001	Parameter set from Table II-4 , base-case/mean/present-day infiltration with 3-D calibration (Table 6-6) (DTN: LB991121233129.002)	Present-day, mean infiltration (Figure 6-3)
pa_pchu1	#1 Flow-through perched water model/ 3d2kpa_pc1.mesh DTN:LB990701233129.001	Parameter set from Table II-5 , upper-bound/present-day infiltration with 3-D calibration (Table 6-7) (DTN: LB991121233129.003)	Present-day, upper-bound infiltration
pa_pchu2	#2 By-passing perched water model/ 3d2kpa_pc2.mesh DTN:LB990701233129.001	Parameter set from Table II-6 , upper-bound/present-day infiltration with 3-D calibration (Table 6-7) (DTN: LB991121233129.004)	Present-day, upper-bound infiltration

Table 6-17. Seven TSPA Simulation Scenarios: Data Files, Conceptual Models/Grids, and Parameter Sets for Three Monsoon Climatic Infiltration Maps.

Designation/ Simulation	Conceptual Model/Grid Name and DTN	Parameter Set/ Calibration	Infiltration Map (DTN: GS000399991221.002)
mon99_m	#3 Non-perching model/ 3d2kpa.mesh DTN:LB990701233129.001	Parameter set from Table II-7 , base-case/present-day, mean infiltration (AMR: CRWMS M&O 2000b) without 3-D calibration (DTN: LB991121233129.007)	Monsoon, mean infiltration (Figure 6-3)
pa_monL1	#1 Flow-through perched water model/ 3d2kpa_pc1.mesh DTN:LB990701233129.001	Parameter set from Table II-1 , lower-bound/present-day infiltration with 3-D calibration (Table 6-8) (DTN: LB991121233129.005)	Monsoon, lower-bound infiltration
pa_monL2	#2 By-passing perched water model/ 3d2kpa_pc2.mesh DTN:LB990701233129.001	Parameter set from Table II-2 , lower-bound/present-day infiltration with 3-D calibration (Table 6-8) (DTN: LB991121233129.006)	Monsoon, lower-bound infiltration
pa_monm1	#1 Flow-through perched water model/ 3d2kpa_pc1.mesh DTN:LB990701233129.001	Parameter set from Table II-3 , base-case/mean/present-day infiltration with 3-D calibration (Table 6-6) (DTN: LB991121233129.001)	Present-day, mean infiltration (Figure 6-3)
pa_monm2	#2 By-passing perched water model/ 3d2kpa_pc2.mesh DTN:LB990701233129.001	Parameter set from Table II-4 , base-case/mean/present-day infiltration with 3-D calibration (Table 6-6) (DTN: LB991121233129.002)	Monsoon, mean infiltration (Figure 6-3)
pa_monu1	#1 Flow-through perched water model/ 3d2kpa_pc1.mesh DTN:LB990701233129.001	Parameter set from Table II-5 , upper-bound/present-day infiltration with 3-D calibration (Table 6-7) (DTN: LB991121233129.003)	Monsoon, upper-bound infiltration
pa_monu2	#2 By-passing perched water model/ 3d2kpa_pc2.mesh DTN:LB990701233129.001	Parameter set from Table II-6 , upper-bound/present-day infiltration with 3-D calibration (Table 6-7) (DTN: LB991121233129.004)	Monsoon, upper-bound infiltration

Table 6-18. Seven TSPA Simulation Scenarios: Data Files, Conceptual Models/Grids, Parameter Sets for Three Glacial Transition Infiltration Maps.

Designation/ Simulation	Conceptual Model/grid Name and DTN	Parameter Set/ Calibration	Infiltration Map (DTN: GS000399991221.002)
gla99_m	#3 Non-perching model/ 3d2kpa.mesh DTN:LB990701233129.001	Parameter set from Table II-7 , base-case/present-day, mean infiltration (AMR: CRWMS M&O 2000e) without 3-D calibration (DTN: LB991121233129.007)	Glacial Transition, mean infiltration (Figure 6.13)
pa_glaL1	#1 Flow-through perched water model/ 3d2kpa_pc1.mesh DTN:LB990701233129.001	Parameter set from Table II-1 , lower-bound/present-day infiltration with 3-D calibration (Table 6-8) (DTN: LB991121233129.005)	Glacial Transition, lower-bound infiltration
pa_glaL2	#2 By-passing perched water model/ 3d2kpa_pc2.mesh DTN:LB990701233129.001	Parameter set from Table II-2 , lower-bound/present-day infiltration with 3-D calibration (Table 6-8) (DTN: LB991121233129.006)	Glacial Transition, lower-bound infiltration
pa_glam1	#1 Flow-through perched water model/ 3d2kpa_pc1.mesh DTN:LB990701233129.001	Parameter set from Table II-3 , base-case/mean/present-day infiltration with 3-D calibration (Table 6-6) (DTN: LB991121233129.001)	Glacial Transition, mean infiltration (Figure 6-3)
pa_glam2	#2 By-passing perched water model/ 3d2kpa_pc2.mesh DTN:LB990701233129.001	Parameter set from Table II-4 , base-case/mean/present-day infiltration with 3-D calibration (Table 6-6) (DTN: LB991121233129.002)	Glacial Transition, mean infiltration (Figure 6-3 Figure 6-3)
pa_glau1	#1 Flow-through perched water model/ 3d2kpa_pc1.mesh DTN:LB990701233129.001	Parameter set from Table II-5 , upper-bound/present-day infiltration with 3-D calibration (Table 6-7) (DTN: LB991121233129.003)	Glacial Transition, upper-bound infiltration
pa_glau2	#2 By-passing perched water model/ 3d2kpa_pc2.mesh DTN:LB990701233129.001	Parameter set from Table II-6 , upper-bound/present-day infiltration with 3-D calibration (Table 6-7) (DTN: LB991121233129.004)	Glacial Transition, upper-bound infiltration

As shown in [Tables 6-16](#), [6-17](#) and [6-18](#), only one simulation is conducted for Conceptual Model #3 (non-perching model) using a mean infiltration map for each climatic scenario. For perched water Conceptual Models #1 and #2, calibrations are carried out for all three climatic scenarios

(i.e., present-day, Monsoon, and Glacial Transition), and mean, lower-bound and upper-bound infiltration scenarios.

6.6.2 Simulation Results

Similar to the calibration simulations, the mass-balance check has been conducted for the 21 simulations using the TSPA grid. Tables 6-19, 6-20 and 6-21 list the global mass balance results. Global mass-balance errors between inflow and outflow of the system for the 18 flow fields (Conceptual Models #1 and #2), as shown in Tables 6-19, 6-20 and 6-21, are about 0.01% or less, indicating that solutions approximate steady state for these cases.

Table 6-19. Mass-Balance Results for TSPA simulations using the Present-Day Infiltration Rates.

Simulation Scenarios	Inflow from infiltration (kg/s)	Outflow to water table (kg/s)	Relative error (%)
pa99_m	5.6404383	5.6350245	0.09598
pa_pchL1	1.4745351	1.4745216	0.00092
pa_pchL2	1.4745351	1.4745337	0.00009
pa_pchm1	5.6404383	5.6404290	0.00016
pa_pchm2	5.6404383	5.6404462	0.00014
pa_pchu1	13.796545	13.796548	0.00002
pa_pchu2	13.796545	13.796567	0.00016

Model Results - DTNs: LB990801233129.001, LB990801233129.002, LB990801233129.003, LB990801233129.004, LB990801233129.005, LB990801233129.006, LB990801233129.019

Table 6-20. Mass-Balance Results for TSPA Simulations using the Monsoon Infiltration Rates.

Simulation Scenarios	Inflow (kg/s)	Outflow (kg/s)	Relative Error (%)
mon99_m	15.168606	15.198690	0.19833
pa_monL1	5.6404075	5.6409797	0.01014
pa_monL2	5.6404075	5.6397595	0.01149
pa_monm1	15.168606	15.168599	0.00005
pa_monm2	15.168606	15.168625	0.00013
pa_monu1	24.696920	24.697014	0.00038
pa_monu2	24.696920	24.696911	0.00004

Model Results - DTNs: LB990801233129.013, LB990801233129.014, LB990801233129.015, LB990801233129.016, LB990801233129.017, LB990801233129.018, LB990801233129.020

Table 6-21. Mass-Balance Results for TSPA Simulations using the Glacial Transition Infiltration Rates.

Scenarios	Inflow (kg/s)	Outflow (kg/s)	Relative Error (%)
gla99_m	22.045112	22.045138	0.00012
pa_glaL1	2.9508085	2.9508075	0.00003
pa_glaL2	2.9508085	2.9507693	0.00133
pa_glam1	22.045112	22.045136	0.00011
pa_glam2	22.045112	22.044842	0.00122
pa_glau1	41.139432	41.139387	0.00011
pa_glau2	41.139432	41.139337	0.00023

Model Results - DTNs: LB990801233129.007, LB990801233129.008, LB990801233129.009, LB990801233129.010, LB990801233129.011, LB990801233129.012, LB990801233129.022

6.6.3 Result Analyses and Flow Fields

Model Examination: 18 out of the 21 3-D flow fields, as delivered for TSPA calculations, have been compared against the field-observed data of perched water. The observed matrix liquid saturations and water potentials (when available) are used for checking model results. The other three flow fields from the non-water perching model were used in sensitivity analyses. The available data used in the calibrations are listed in Table 6-4. One example of the simulation results is given in Figure 6-41, comparing the result for UZ-14 with the results using the three mean infiltration rates of the three climatic scenarios with perched water Conceptual Model #1. The figure shows a good match between simulated and observed saturation and perched water data at this location from the three simulations. Overall, we have the following calibration results:

- The simulation results, used for generating the 18 flow fields, matched the available saturation and water potential data from the nine boreholes (Table 6-4) reasonably well.
- For calibrations with perched water data, the six simulations with mean, lower-bound and upper-bound present-day infiltration rates and two conceptual perched water models (Models #1 and #2), are similar to the results of the corresponding six calibration simulations of Section 6.2, which match perched water data reasonably well.
- The 8 simulations with 4 infiltration scenarios having both mean and upper-bound infiltration rates of two future climates (Monsoon and Glacial Transition) and two perched water conceptual models can reproduce water-perching conditions well in all the observation boreholes. The four lower-bound infiltration simulations could also match perched water data for six of the seven perched water boreholes (at SD-7, the simulations do not match the observed perched water data well).

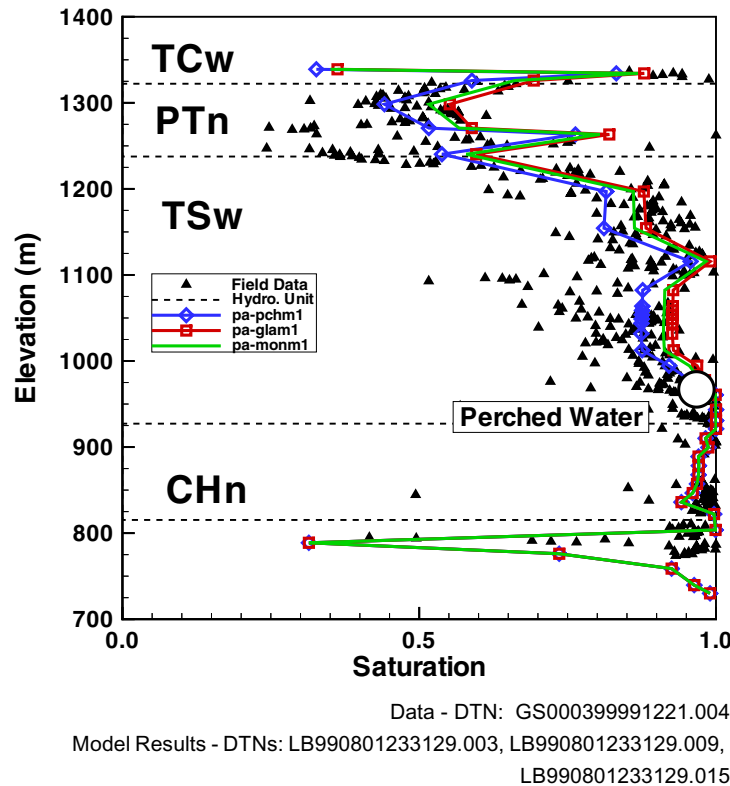
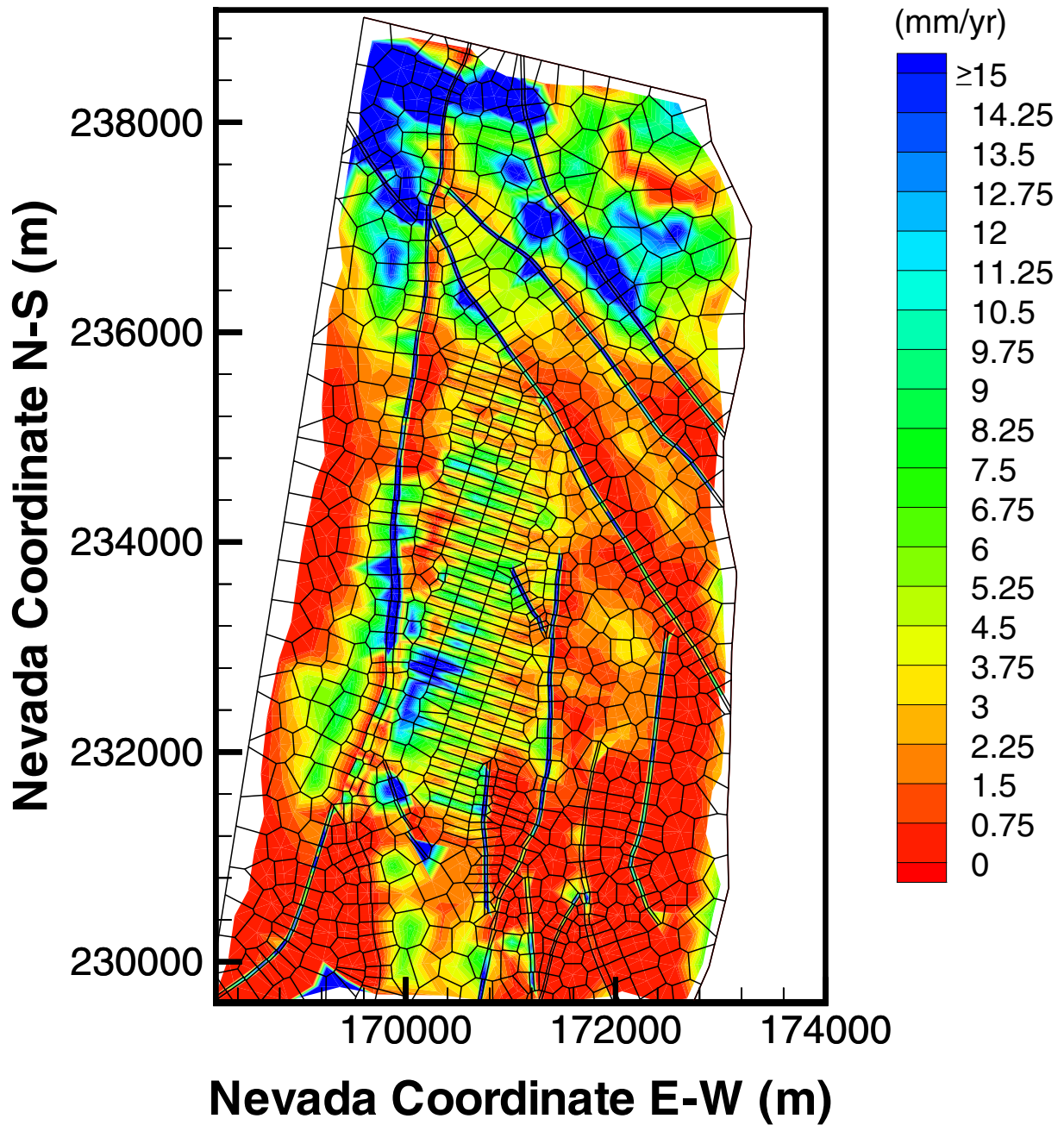


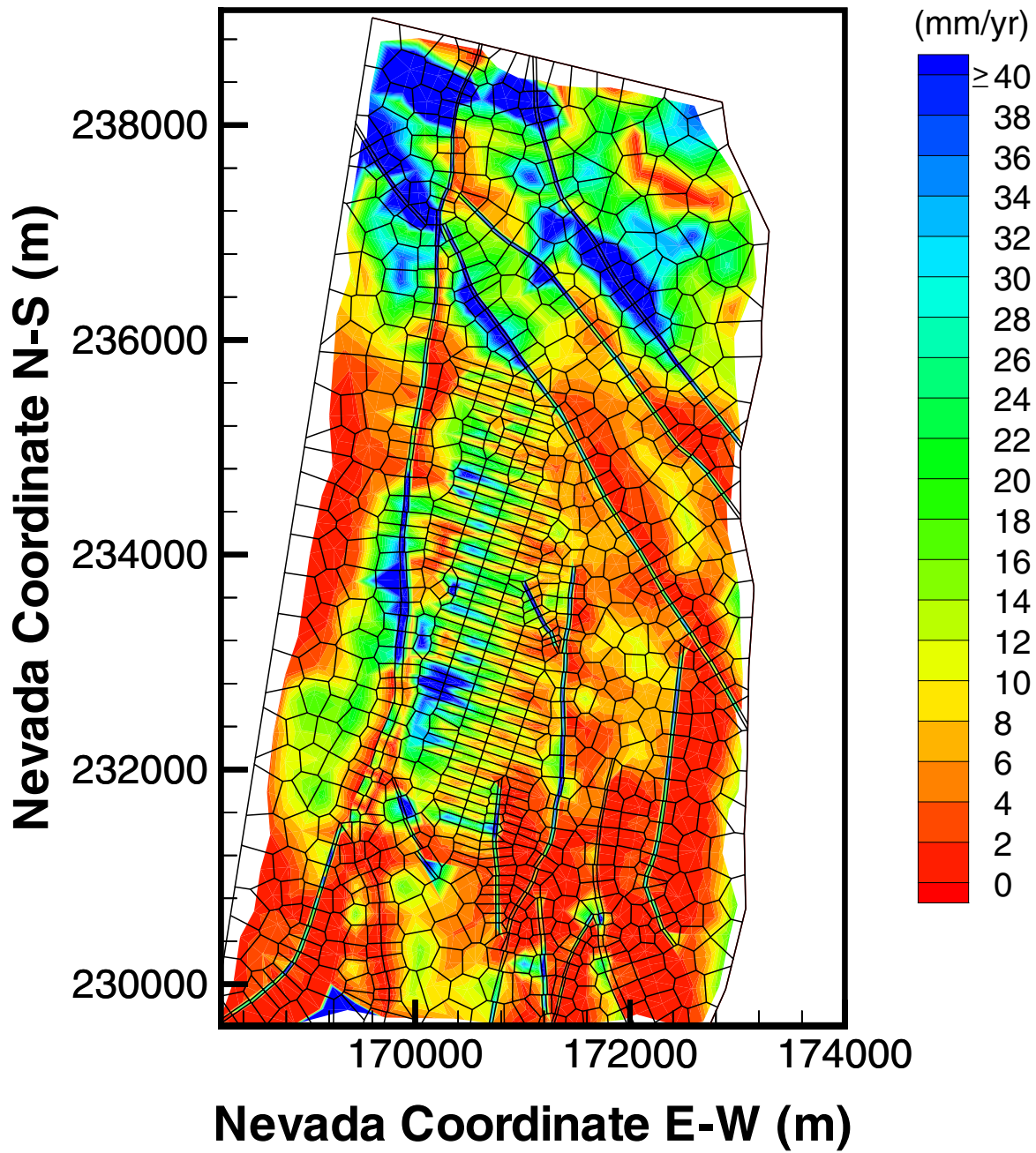
Figure 6-41. Comparison to the Simulated and Observed Matrix Liquid Saturations and Perched Water Elevations for Borehole UZ-14, Using the Results of pa_pchm1, pa_monm1 and pa_glam1 Simulations for Three Mean Infiltration Scenarios of Three Climates.

Percolation Fluxes and Fracture-Matrix Flow Components: Percolation fluxes at the potential repository horizon, simulated using the three mean infiltration scenarios of the present-day and two future climates, are shown in Figures 6-42, 6-43, and 6-44. The figures show that simulated total (matrix+fracture) percolation fluxes at the potential repository level have very nonuniform distributions, similar to the infiltration maps used for the top boundary conditions. By comparing the three percolation fluxes at the potential repository horizon with the corresponding surface-infiltration maps (Figures 6-3, 6-4 and 6-5), we find that little lateral diversion, except near faults, occurs during flow from surface to potential repository level, as predicted in these three simulations with the 3-D calibration grid.



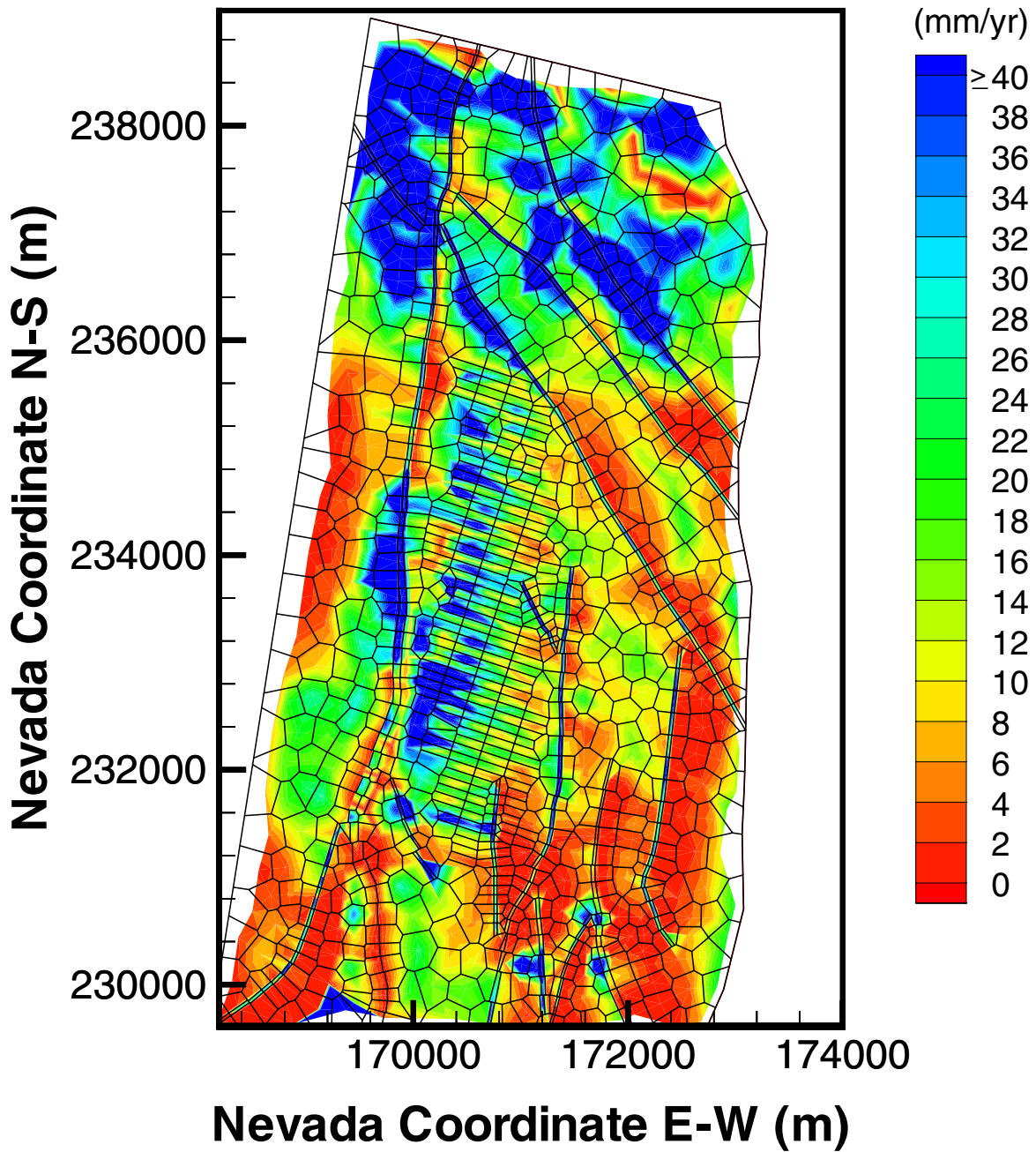
Based on DTN: LB990801233129.003

Figure 6-42. Simulated Percolation Fluxes at the Potential Repository Horizon Under Present-Day, Mean Infiltration Using the Results of Simulation pa_pchm1.



Based on DTN: LB990801233129.015

Figure 6-43. Simulated Percolation Fluxes at the Potential Repository Horizon Under Monsoon, Mean Infiltration Using the Results of Simulation pa_monm1.

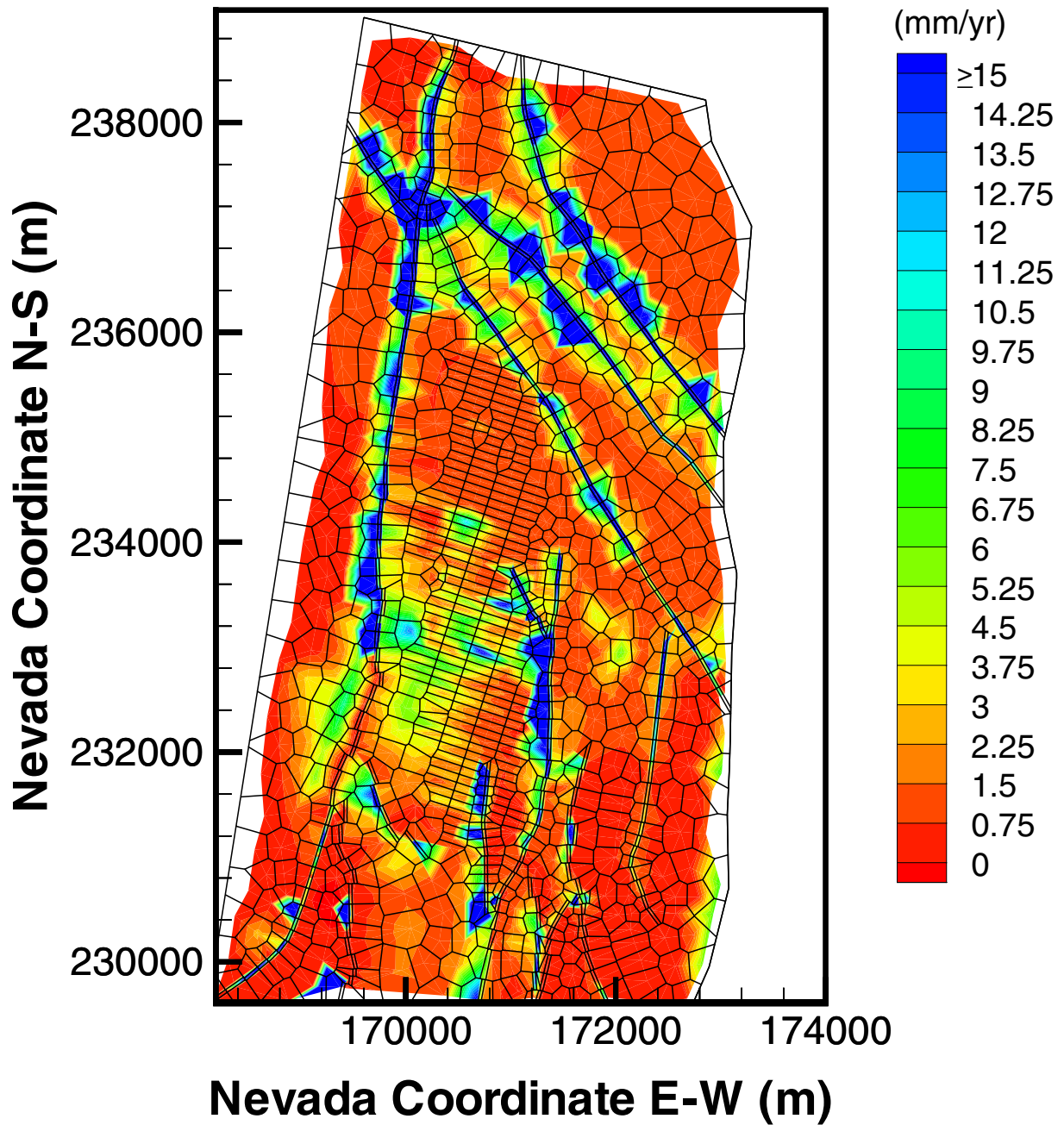


Based on DTN: LB990801233129.009

Figure 6-44. Simulated Percolation Fluxes at the Potential Repository Horizon Under Glacial Transition, Mean Infiltration Using the Results of Simulation pa_glam1.

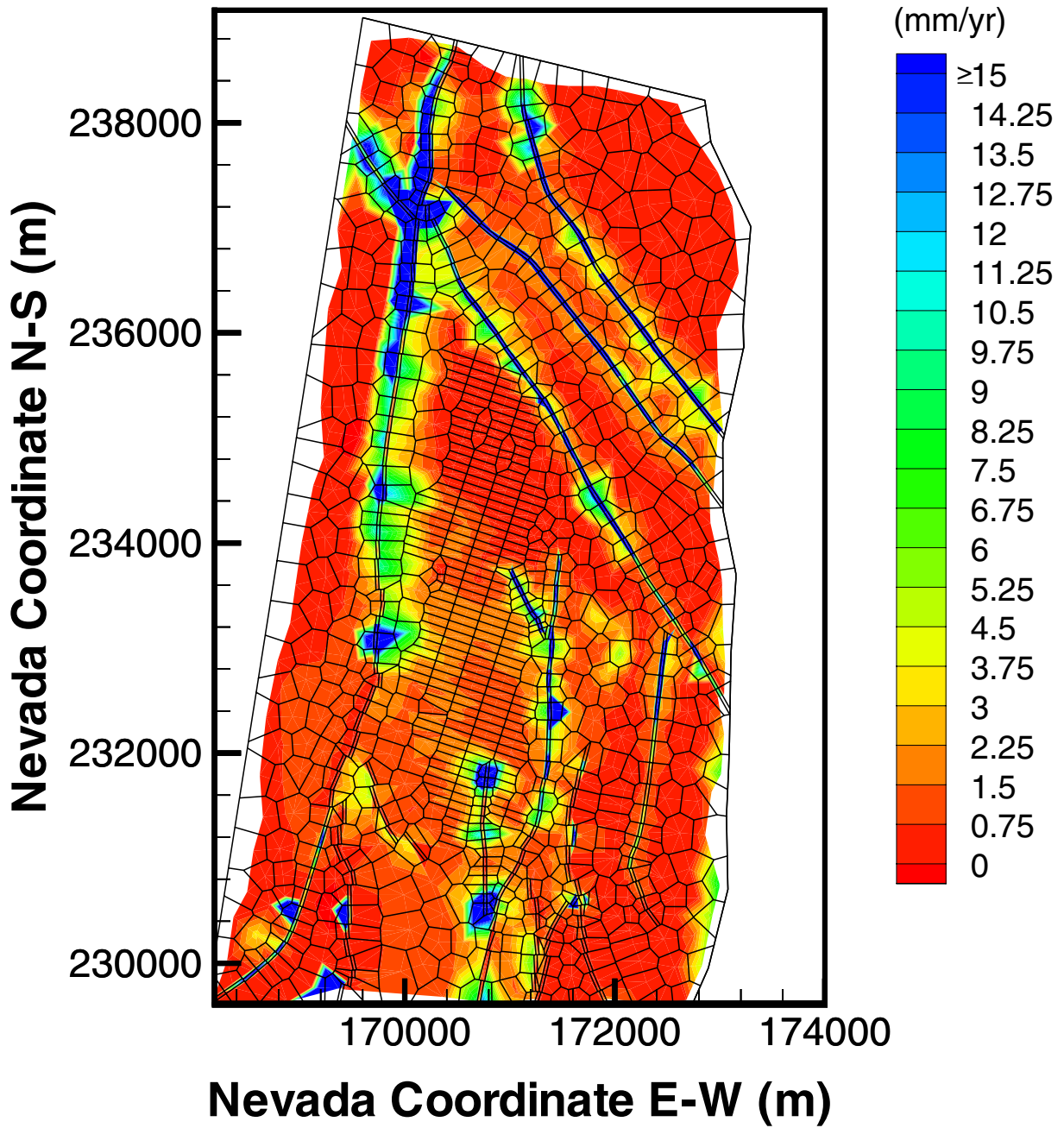
Figures 6-45 through 6-53 show the simulated percolation fluxes at the water table also using the three mean infiltration scenarios with the three conceptual models. When comparing the percolation fluxes at the potential repository (e.g., Figures 6-42, 6-43, and 6-44) we find the following:

- Conceptual Model #3 (non-perching model) predicts a possible maximum, nearly vertical flow through the CHn zeolitic rocks.
- Conceptual Model #2 (by-passing model) predicts the least flowing-through or maximum by-passing of perched water zones or zeolites of flow through the CHn.
- Conceptual Model #1 (flow-through model) predicts significant vertical flow-through in the southern part of the vitric zones, and large lateral diversion occurring in the northern portion of the potential repository (where thick zeolitic layers are located), but an overall much higher vertical flow rate and much less lateral flow than Conceptual Model #2.



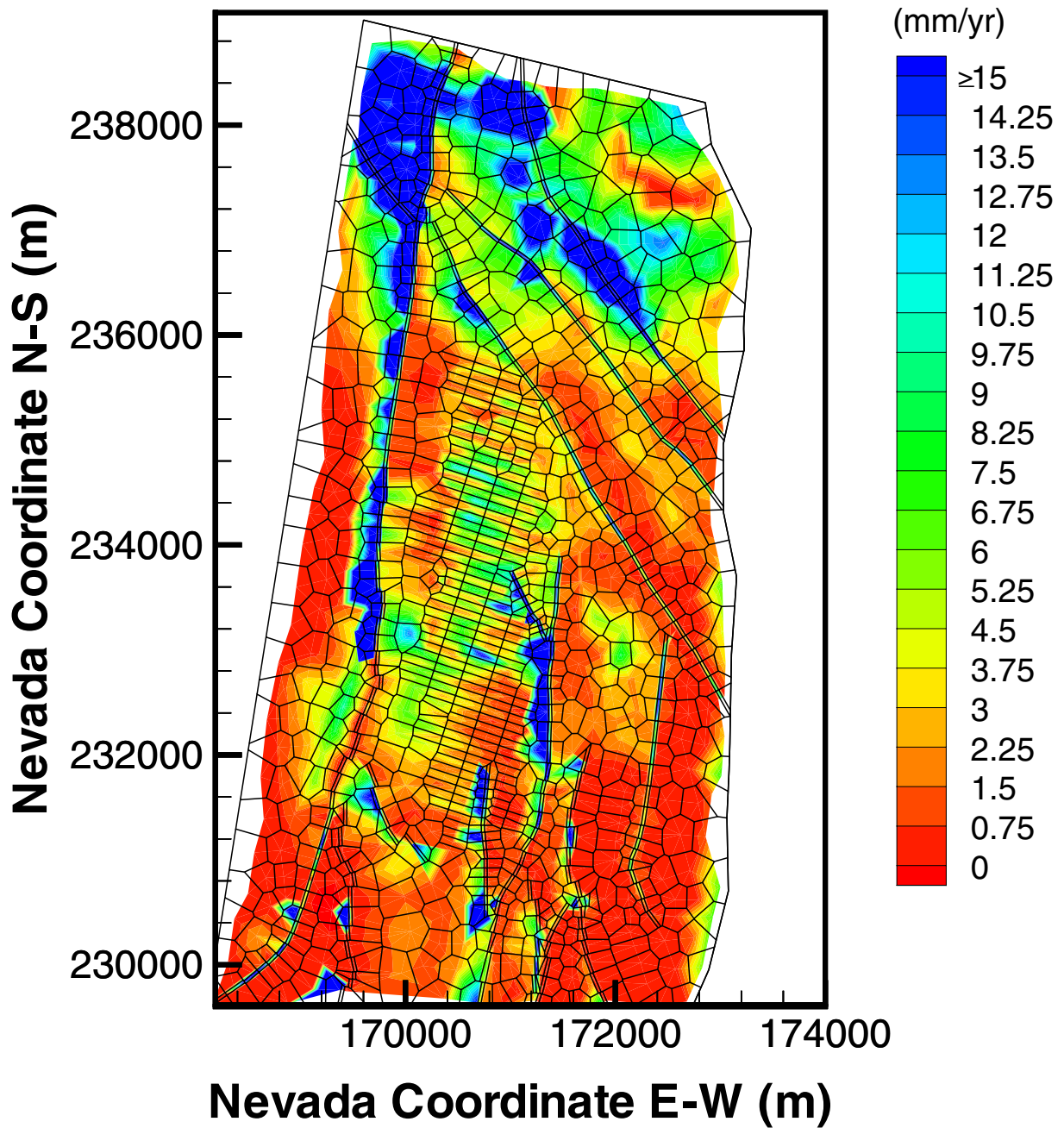
Based on DTN: LB990801233129.003

Figure 6-45. Simulated Percolation Fluxes at the Water Table Under Present-Day, Mean Infiltration Using the Results of Simulation pa_pchm1–Conceptual Model #1.



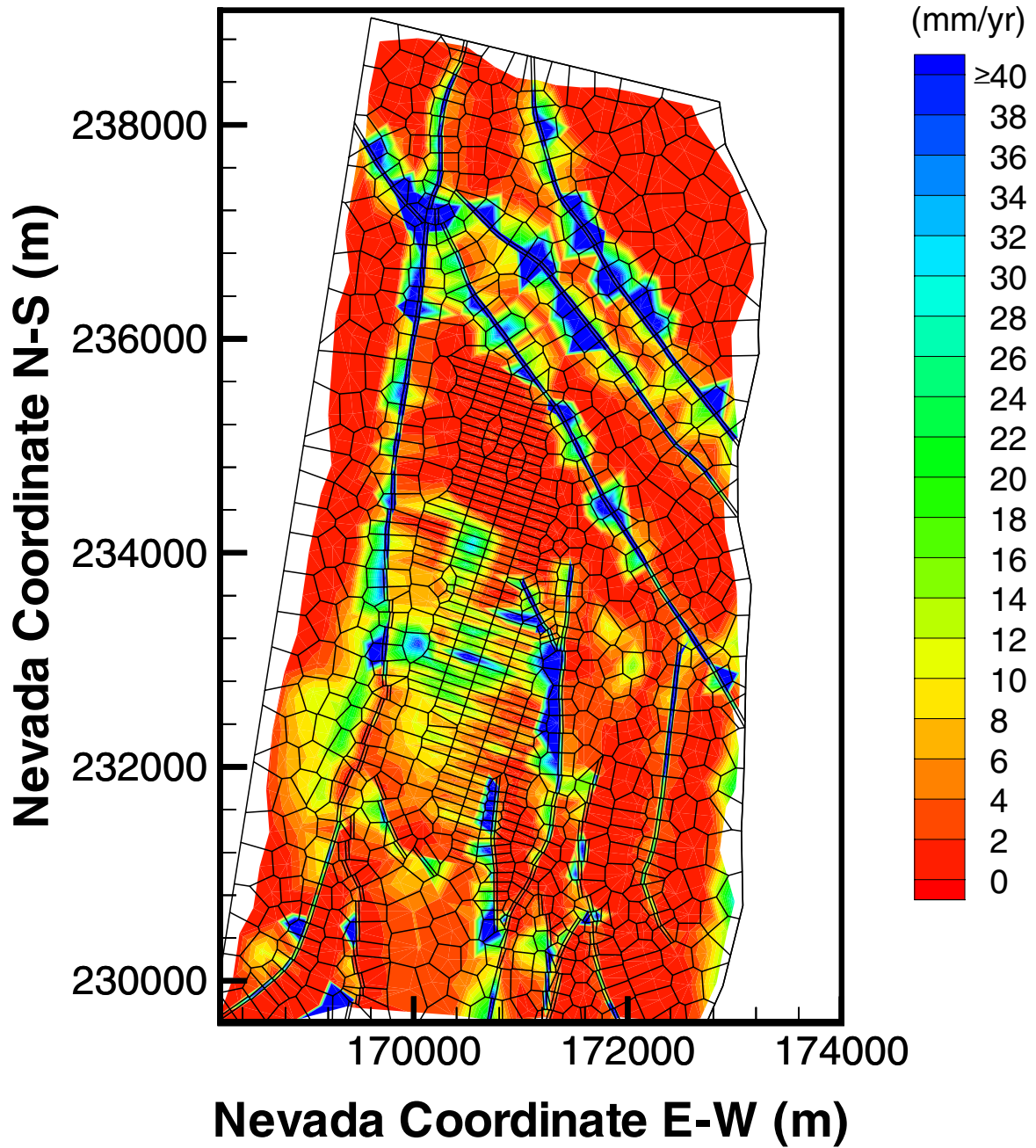
Based on DTN: LB990801233129.004

Figure 6-46. Simulated Percolation Fluxes at the Water Table Under Present-Day, Mean Infiltration Using the Results of Simulation pa_pchm2 – Conceptual Model #2.



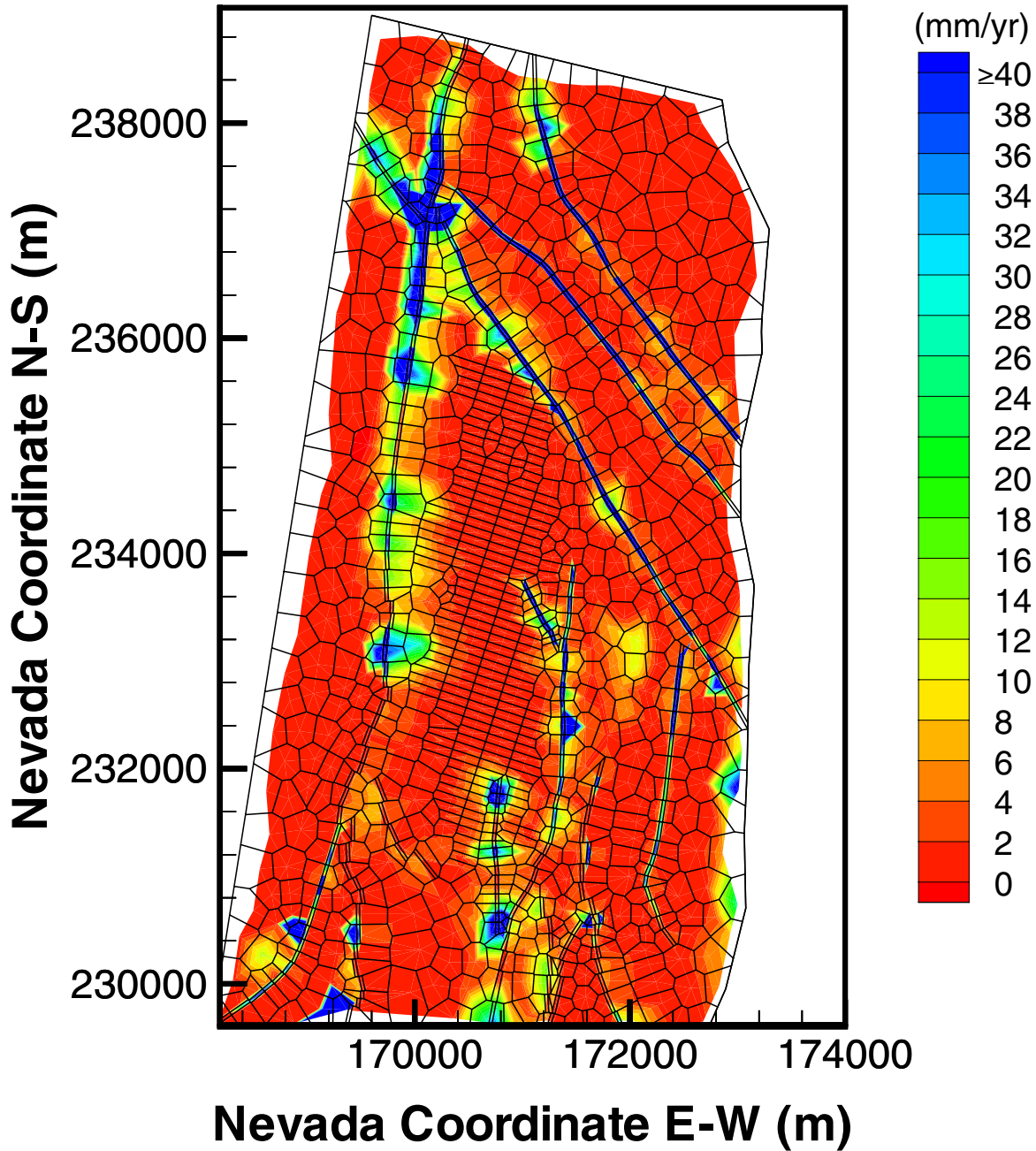
Based on DTN: LB990801233129.019

Figure 6-47. Simulated Percolation Fluxes at the Water Table Under Present-Day, Mean Infiltration Using the Results of Simulation pa99_m – Conceptual Model #3.



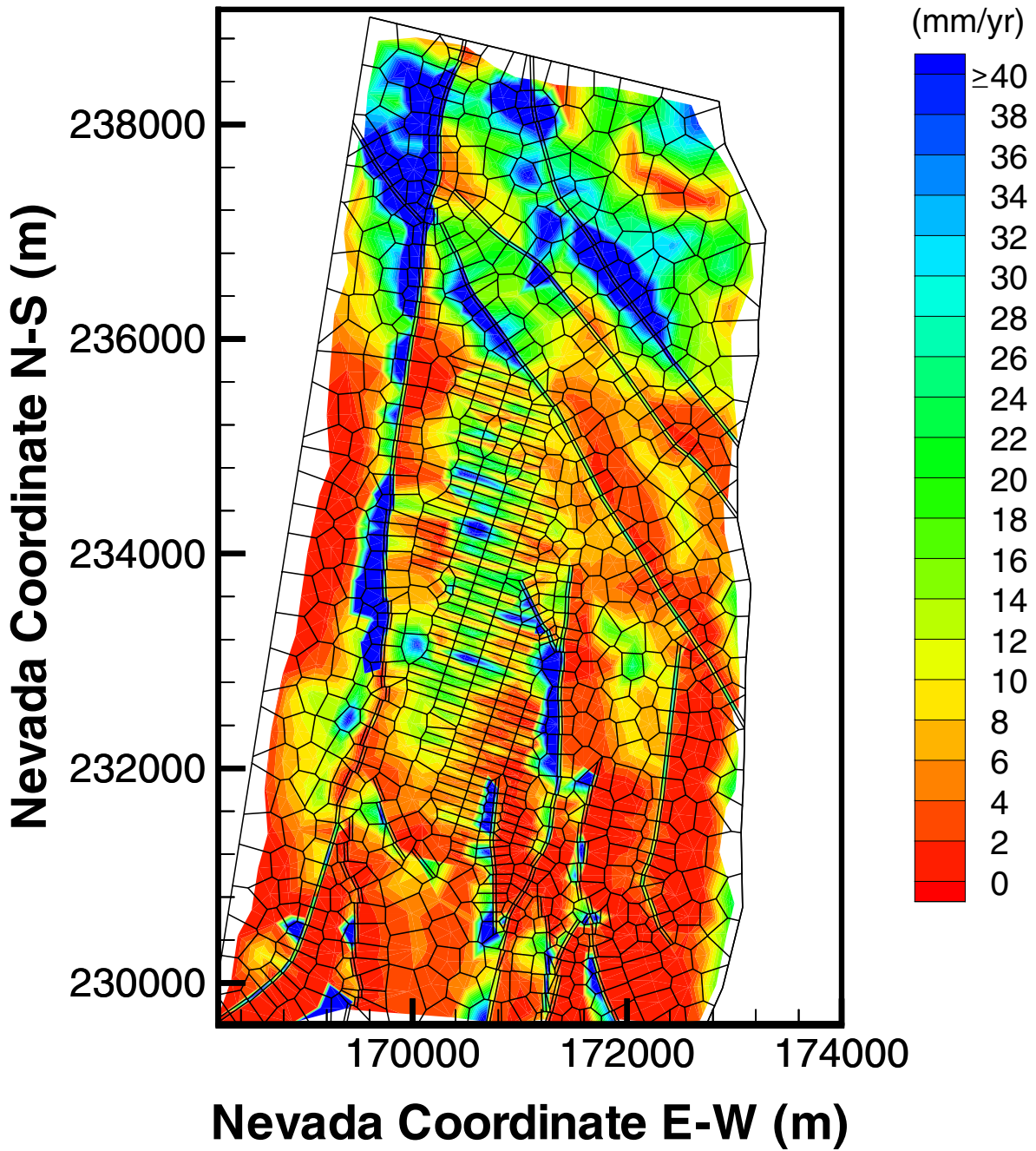
Based on DTN: LB990801233129.015

Figure 6-48. Simulated Percolation Fluxes at the Water Table Under Monsoon, Mean Infiltration Using the Results of Simulation pa_monm1 – Conceptual Model #1.



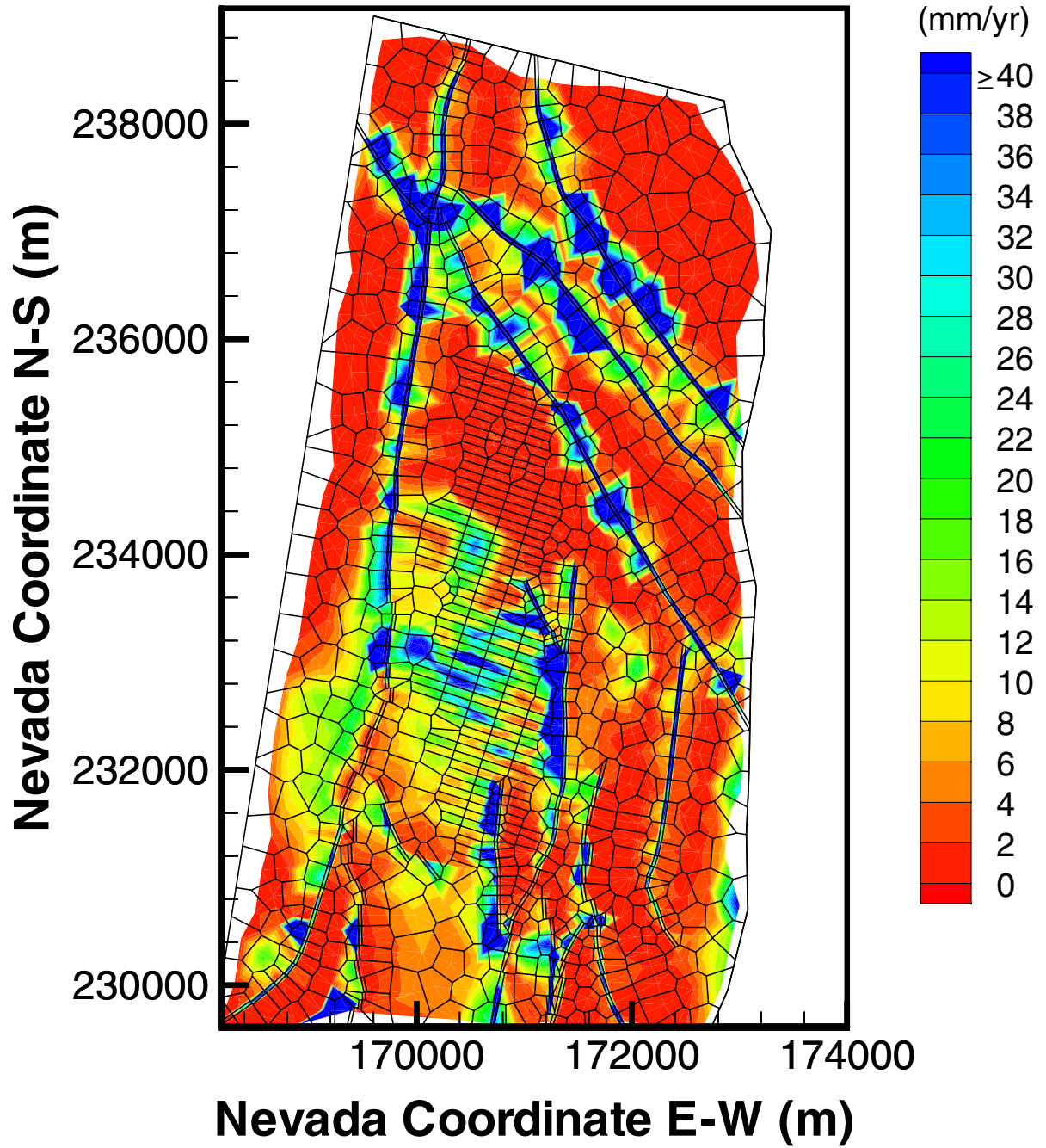
Based on DTN: LB990801233129.016

Figure 6-49. Simulated Percolation Fluxes at the Water Table Under Monsoon, Mean Infiltration Using the Results of Simulation pa_monm2 – Conceptual Model #2.



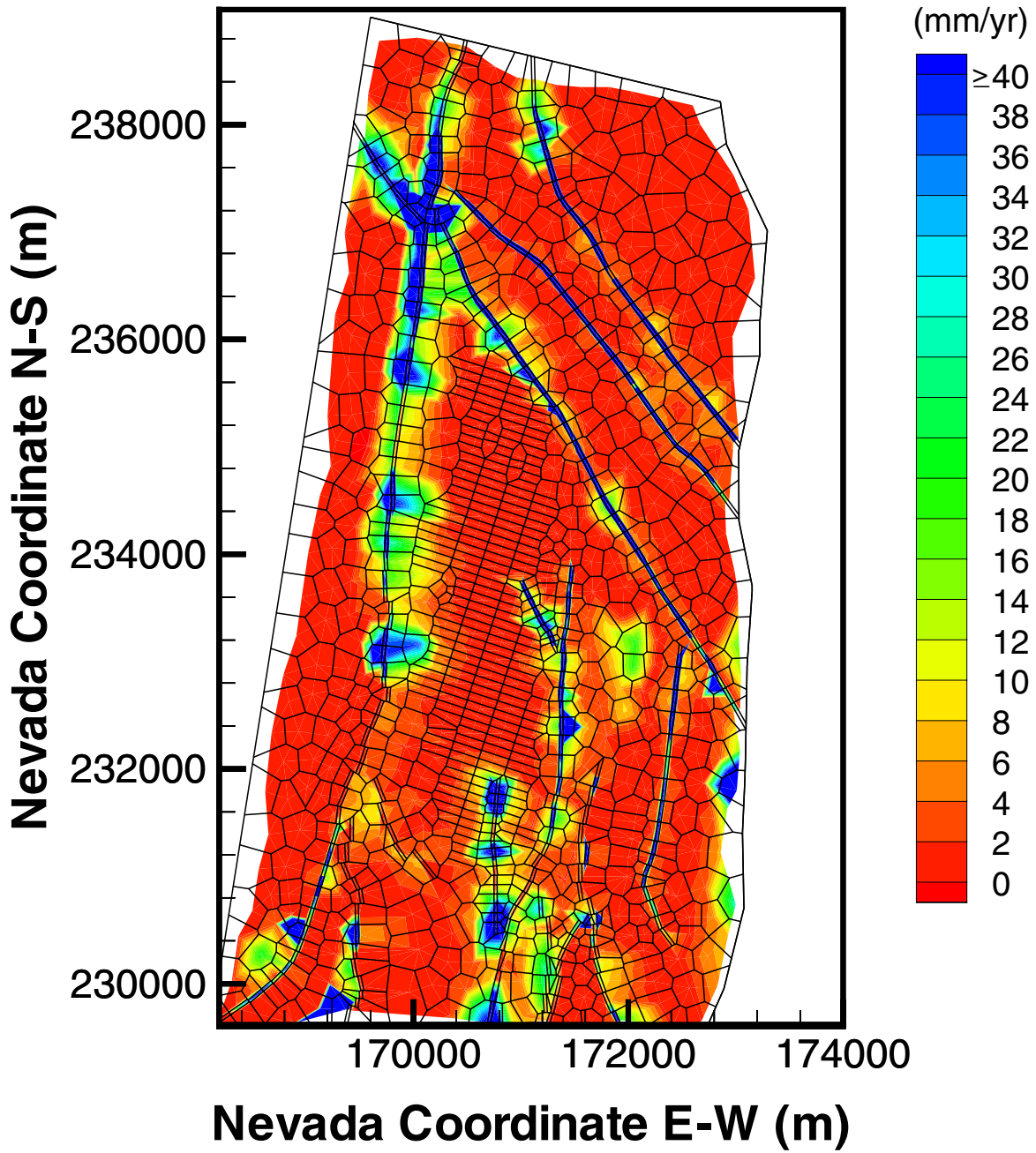
Based on DTN: LB990801233129.020

Figure 6-50. Simulated Percolation Fluxes at the Water Table Under Monsoon, Mean Infiltration Using the Results of Simulation mon99_m – Conceptual Model #3.



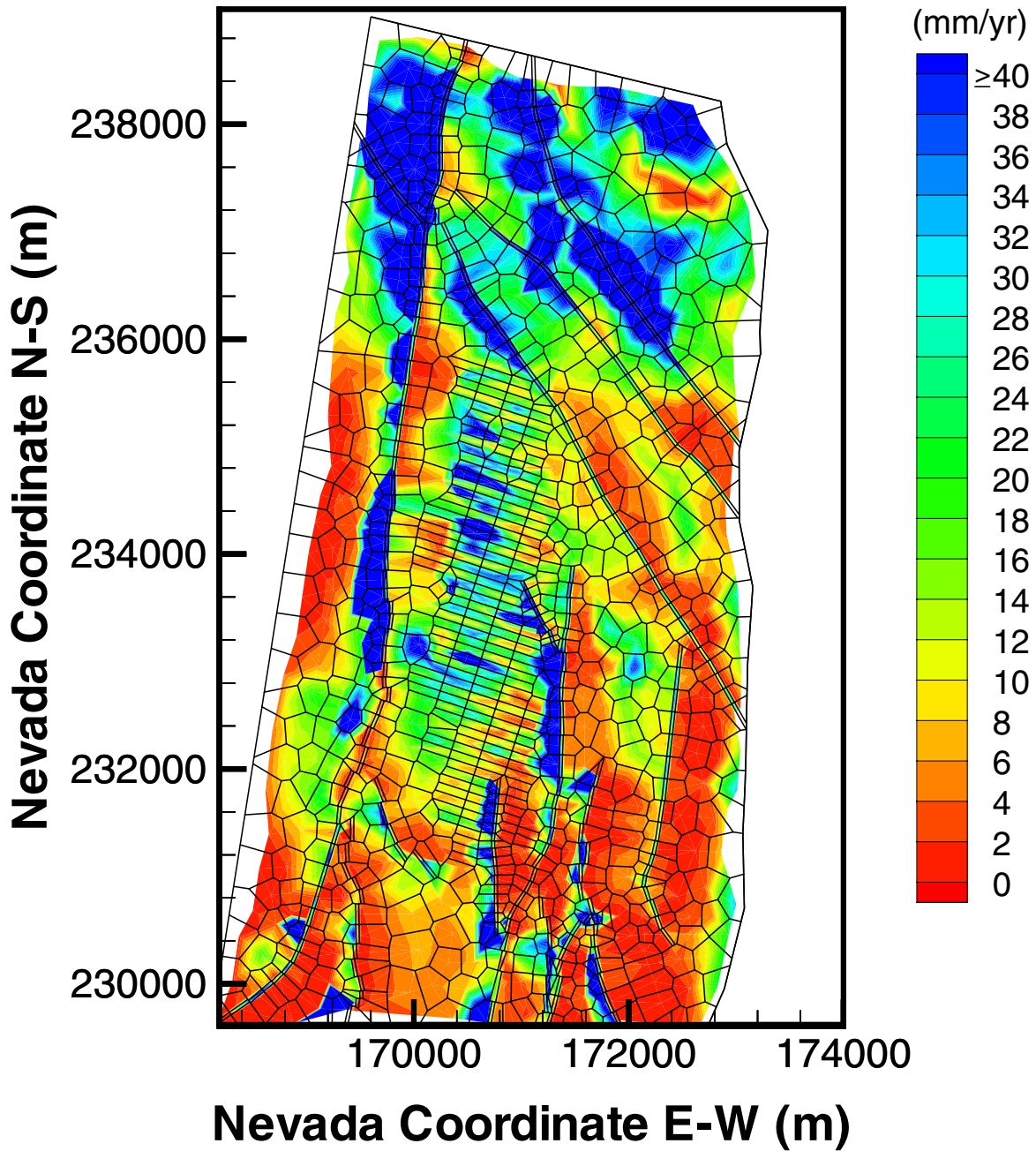
Based on DTN: LB990801233129.009

Figure 6-51. Simulated Percolation Fluxes at the Water Table Under Glacial Transition, Mean Infiltration Using the Results of Simulation pa_glam1 – Conceptual Model #1.



Based on DTN: LB990801233129.010

Figure 6-52. Simulated Percolation Fluxes at the Water Table Under Glacial Transition, Mean Infiltration Using the Results of Simulation pa_glam2 – Conceptual Model #2.



Based on DTN: LB990801233129.021

Figure 6-53. Simulated Percolation Fluxes at the Water Table Under Glacial Transition, Mean Infiltration Using the Results of Simulation gla99_m – Conceptual Model #3.

Tables 6-22, 6-23, and 6-24 list the percentage of fracture-matrix flow components at the potential repository horizon and the water table, respectively, predicted using the 21 simulation results. These statistics show that fracture flow is dominant both at the potential repository horizon and at the water table in all the 21 flow fields. Specific predictions are as follows:

- Table 6-22 indicates that for the three present-day infiltration scenarios, simulated fracture-matrix flow components with the TSPA grid are similar to those (Table 6-11) using the calibration grid. At the potential repository level, fracture flow consists of more than 80% of the total flow; at the water table, consists of about 70-90% of the total flow.
- Tables 6-23 and 6-24 show, for two future climatic scenarios, a higher percentage of fracture flow at both the potential repository (86-96%) and water table level (71-96%) compared to the results of the present-day infiltration (Table 6-22). The second perched water conceptual model predicts consistently lower fracture-flow components by more than 8% for the two climatic scenarios.

Table 6-22. Comparison of the Water Flux through Matrix and Fractures as a Percentage of the Total Flux at two Different Horizons (1) at the Potential Repository and (2) at the Water Table, using the Three Present-Day Infiltration Scenarios.

Simulation Designation	Flux at Potential Repository (%)		Flux at Water Table (%)	
	Fracture	Matrix	Fracture	Matrix
pa99_m	83.76	16.24	80.35	19.65
pa_pchL1	86.61	13.39	84.66	15.34
pa_pchL2	86.38	13.62	69.37	30.63
pa_pchm1	83.69	16.31	86.69	13.31
pa_pchm2	83.66	16.34	71.19	28.81
pa_pchu1	94.45	5.55	95.40	4.60
pa_pchu2	94.32	5.68	82.07	17.93

Model Results - DTNs: LB990801233129.001, LB990801233129.002, LB990801233129.003, LB990801233129.004, LB990801233129.005, LB990801233129.006, LB990801233129.019

Table 6-23. Comparison of the Water Flux through Matrix and Fractures as a Percentage of the Total Flux at Two Different Horizons (1) at the Potential Repository and (2) at the Water Table, using the Three Monsoon Infiltration Scenarios.

Simulation Designation	Flux at potential repository (%)		Flux at Water Table (%)	
	Fracture	Matrix	Fracture	Matrix
mon99_m	89.60	10.40	85.31	14.69
pa_monL1	89.97	10.03	90.10	9.90
pa_monL2	89.90	10.10	76.55	23.45
pa_monm1	89.53	10.47	90.21	9.79
pa_monm2	89.50	10.50	80.87	19.13
pa_monu1	95.61	4.39	96.47	3.53
pa_monu2	95.50	4.50	83.86	16.14

Model Results - DTNs: LB990801233129.013, LB990801233129.014, LB990801233129.015, LB990801233129.016, LB990801233129.017, LB990801233129.018, LB990801233129.020

Table 6-24. Comparison of the Water Flux through Matrix and Fractures as a Percentage of the Total Flux at Two Different Horizons (1) at the Potential Repository and (2) at the Water Table, using the Three Glacial Transition Infiltration Scenarios.

Simulation Designation	Flux at potential repository (%)		Flux at Water Table (%)	
	Fracture	Matrix	Fracture	Matrix
gla99_m	91.46	8.54	83.26	16.74
pa_glaL1	86.92	13.08	87.15	12.85
pa_glaL2	86.78	13.22	71.38	28.62
pa_glam1	91.38	8.62	90.47	9.53
pa_glam2	91.37	8.63	83.43	16.57
pa_glau1	96.53	3.47	96.92	3.08
pa_glau2	96.44	3.56	88.97	11.03

Model Results - DTNs: LB990801233129.007, LB990801233129.008, LB990801233129.009, LB990801233129.010, LB990801233129.011, LB990801233129.012, LB990801233129.022

6.7 GROUNDWATER TRAVEL TIMES AND TRACER TRANSPORT

This section summarizes our studies of groundwater travel times and tracer transport using the 21 TSPA flow fields as well as one flow field with the calibration grid (Figure 6-1) for chloride-36 studies. These studies are conducted to obtain insights into groundwater travel times and radionuclide transport from (a) the potential repository to the water table, and (b) the ground surface to the potential repository level. The results present an evaluation of transport processes of

radionuclides from the potential repository to the water table (saturated zone) and groundwater travels within the mountain, including effects of different perched water conceptual models, infiltration scenarios, and adsorption. Methodology and Transport Parameters. Studies of this section on tracer transport are intended for insight of the transport processes and PA may use other models/codes for radionuclide transport predictions in TSPA.

6.7.1 Methodology and Transport Parameters

Simulation results and analyses of this section are based on transport studies of conservative and reactive tracers using the T2R3D V1.4 code. The dual-permeability modeling approach, the 3-D TSPA grid (Figure 6-2) and the calibration grid (Figure 6-1) are used in the transport simulations. The 21 steady-state, 3-D flow fields, as discussed in Section 6.6, are directly used as input to the T2R3D code for runs for transport from the potential repository to the water table. Groundwater travel times or ^{36}Cl transport is modeled using the calibration grid with the present-day, mean infiltration rate.

Transport from the potential repository to the water table: This study is to assess groundwater travel times from the potential repository to the water table. Tracer or radionuclides are treated as conservative (nonadsorbing) and reactive (adsorbing) components transported through the UZ. For both cases, the hydrodynamic dispersion effect through the fracture-matrix system is ignored because sensitive studies indicate insignificant effect of hydrodynamic dispersion on the cumulative breakthrough curves of tracers at the water table. A constant molecular diffusion coefficient of 3.2×10^{-11} (m^2/s) is used for matrix diffusion of the conservative component, and 1.6×10^{-10} (m^2/s) and is used for the reactive component (DTN: LAIT831341AQ96.001). In the case of a reactive or adsorbing tracer, several K_d values are used, as given in Table 6-25, and these values were selected to approximate those for neptunium (^{237}Np) transport (DTN: LAIT831341AQ96.001). For a conservative tracer, K_d is set to zero. These molecular diffusions coefficients and K_d values are selected to represent technitium and neptunium, respectively. All transport simulations were conducted for 1,000,000 years with a constant infiltration and an initial, constant source concentration condition injected into the fracture continuum at the potential repository horizon. A tracer is released at the starting time of a simulation.

Table 6-25. K_d Values used for Reactive Tracer Transport in Different Hydrogeologic Units.

Hydrogeologic Unit	K_d (cc/g)
Zeolitic matrix in CHn	4.0
Vitric matrix in CHn	1.0
Matrix in TSw	1.0
Fault matrix in CHn	1.0
Fractures and the matrix in the rest of units	0.0

DTN: LAIT831341AQ96.001

Transport from the ground surface: This is to investigate groundwater travel times from the ground surface to the potential repository level as well as ^{36}Cl transport phenomena under steady-

state UZ flow conditions. A tracer with ^{36}Cl transport properties (Section 6.4.2) is introduced into the second top grid or infiltration layer of the calibration grid with the climate scenario of the present-day, mean infiltration for the modeling studies. There are four simulation scenarios with different surface tracer boundary conditions specified with a small area above the potential repository and the entire model domain, respectively. Use of the small area of the tracer source boundary condition on the land surface is to reduce the possible effects of lateral boundaries and to focus on transport behavior in the immediate vicinity above the potential repository. The small tracer-source area is defined as an area directly above the potential repository, bounded by the Solitario Canyon, Drill Hole Wash and Ghost Dance faults in the western, northern and eastern directions, with the southern boundary in alignment with the south ramp of the ESF. Two types of boundary conditions were specified for the tracer, one being constant initial tracer concentration and the other constant tracer mass injection rate in the fracture gridblocks of the boundary. In the four simulations, the tracer was treated as a conservative, (nonadsorbing) and decaying component. For all cases, the hydrodynamic dispersion effect through the fracture-matrix system was included with longitudinal dispersivities of 20 and 5 m and transverse dispersivities of 4 and 1 m, respectively, for fracture and matrix systems. Also, transport simulations were conducted for 1,000,000 years.

6.7.2 Simulation Scenarios

For each TSPA flow simulation, as listed in [Tables 6-16, 6-17 and 6-18](#), there are two transport runs, one for conservative (*_tr1) and one for reactive (*_tr2) tracer transport, respectively. [Tables 6-26, 6-27 and 6-28](#) summarize a total of 21×2 simulation scenarios, associated with conceptual models/grids and corresponding TSPA flow fields for the nine infiltration maps of three climates, respectively.

[Table 6-26](#) also includes the four simulations using the calibration grid for studies of groundwater travel or ^{36}Cl transport times from the land surface. Among the four scenarios, cam1_CL1 uses a constant initial tracer concentration boundary condition within the small source area; cam1_CL2 uses a constant tracer mass flux boundary condition that is proportional to net infiltration rate for each fracture block, within the small source area; cam1_CL3 uses a constant initial tracer concentration boundary condition over the entire top model area; and cam1_CL4 uses a constant

tracer mass flux boundary condition (Section 6.4.1.2) with each fracture block, over the entire top model area.

Table 6-26. Transport Simulation Scenarios: Data Files, Conceptual Models/Grids, Corresponding TSPA Flow Fields with Three Present-Day Infiltration Rates.

Designation/ Transport Simulation	Designation/ Flow Simulation	Perched Water Conceptual Model/Grid	Infiltration Map (DTN: GS000399991221.002)
pa99_tr1 pa99_tr2	pa99_m	#3 Non-perching model/ 3d2kpa.mesh DTN: LB990701233129.001	Present-day, mean infiltration (Figure 6-3)
paL1_tr1 paL1_tr2	pa_pchL1	#1 Flow-through perched water model/ 3d2kpa_pc1.mesh DTN: LB990701233129.001	Present-day, lower- bound infiltration
paL2_tr1 paL2_tr2	Pa_pchL2	#2 By-passing perched water model/ 3d2kpa_pc2.mesh DTN: LB990701233129.001	Present-day, lower- bound infiltration
pam1_tr1 pam1_tr2	pa_pchm1	#1 Flow-through perched water model/ 3d2kpa_pc1.mesh DTN: LB990701233129.001	Present-day, mean infiltration (Figure 6-3)
pam2_tr1 pam2_tr2	pa_pchm2	#2 By-passing perched water model/ 3d2kpa_pc2.mesh DTN: LB990701233129.001	Present-day, mean infiltration (Figure 6-3)
pau1_tr1 pau1_tr2	pa_pchu1	#1 Flow-through perched water model/ 3d2kpa_pc1.mesh DTN: LB990701233129.001	Present-day, upper- bound infiltration
pau2_tr1 pau2_tr2	pa_pchu2	#2 By-passing perched water model/ 3d2kpa_pc2.mesh DTN: LB990701233129.001	Present-day, upper- bound infiltration
cam1_CL1	pch!_m2	#1 Flow through perched water model/ 3d2kcalib_pc1.mesh (DTN: LB997141233129.001)	Present-day, mean infiltration (Figure 6.1.3)
cam1_CI2	pch1_m2	#1 Flow-through perched water model/ 3d2kcalib_pc1.mesh DTN:LB997141233129.001)	Present-day, lower- bound infiltration (Figure 6.1.3)

Table 6-26. Transport Simulation Scenarios: Data Files, Conceptual Models/Grids, Corresponding TSPA Flow Fields with Three Present-Day Infiltration Rates.

Designation/ Transport Simulation	Designation/ Flow Simulation	Perched Water Conceptual Model/Grid	Infiltration Map (DTN: GS000399991221.002)
cam1_CL3	pch1_m2	#1 Flow through perched water model/ 3d2kcalib_pc1.mesh DTN: LB997141233129.001	Present-day, lower-bound infiltration (Figure 6.1.3)
cam1_CL4	pch1_m2	#1 Flow-through perched water model/ 3d2kpa_pc1.mesh DTN: LB990701233129.001	Present-day, mean infiltration (Figure 6.1.3)

(Cont) JEH 4/7/00

Table 6-27. Transport Simulation Scenarios: Data Files, Conceptual Models/Grids, Corresponding TSPA Flow Fields with Three Monsoon Infiltration Rates

Designation/ Transport Simulation	Designation/ Flow Simulation	Conceptual Model/Grid	Infiltration Map
mon99_tr1 mon99_tr2	mon99_m	#3 Non-perching model/ 3d2kpa.mesh DTN: LB990701233129.001	Monsoon, mean infiltration (Figure 6-4)
monL1_tr1 monL1_tr2	pa_monL1	#1 Flow-through perched water model/ 3d2kpa_pc1.mesh DTN: LB990701233129.001	Monsoon, lower- bound infiltration
monL2_tr1 monL2_tr2	pa_monL2	#2 By-passing perched water model/ 3d2kpa_pc2.mesh DTN: LB990701233129.001	Monsoon, lower- bound infiltration
monm1_tr1 monm1_tr2	pa_monm1	#1 Flow-through perched water model/ 3d2kpa_pc1.mesh DTN: LB990701233129.001	Present-day, mean infiltration (Figure 6-4)
monm2_tr1 monm2_tr2	pa_monm2	#2 By-passing perched water model/ 3d2kpa_pc2.mesh DTN: LB990701233129.001	Monsoon, mean infiltration (Figure 6-4)
monu1_tr1 monu1_tr2	pa_monu1	#1 Flow-through perched water model/ 3d2kpa_pc1.mesh DTN: LB990701233129.001	Monsoon, upper- bound infiltration
monu2_tr1 monu2_tr2	pa_monu2	#2 By-passing perched water model/ 3d2kpa_pc2.mesh DTN: LB990701233129.001	Monsoon, upper- bound infiltration

Table 6-28. Transport Simulation Scenarios: Data Files, Conceptual Models/Grids, Corresponding TSPA Flow Fields with Three Glacial Transition Infiltration Rates.

Designation/ Transport Simulation	Designation/ Flow Simulation	Conceptual Model/Grid	Infiltration Map
gla99_tr1 gla99_tr2	gla99_m	#3 Non-perching model/ 3d2kpa.mesh DTN: LB990701233129.001	Glacial Transition, mean infiltration (Figure 6-5)
glaL1_tr1 glaL1_tr2	pa_glaL1	#1 Flow-through perched water model/ 3d2kpa_pc1.mesh DTN: LB990701233129.001	Glacial Transition, lower-bound infiltration
glaL2_tr1 glaL2_tr2	pa_glaL2	#2 By-passing perched water model/ 3d2kpa_pc2.mesh DTN: LB990701233129.001	Glacial Transition, lower-bound infiltration
glam1_tr1 glam1_tr2	pa_glam1	#1 Flow-through perched water model/ 3d2kpa_pc1.mesh DTN: LB990701233129.001	Glacial Transition, mean infiltration (Figure 6-5)
glam2_tr1 glam2_tr2	pa_glam2	#2 By-passing perched water model/ 3d2kpa_pc2.mesh DTN: LB990701233129.001	Glacial Transition, mean infiltration (Figure 6-5)
glau1_tr1 glau1_tr2	pa_glau1	#1 Flow-through perched water model/ 3d2kpa_pc1.mesh DTN: LB990701233129.001	Glacial Transition, upper-bound infiltration
glau2_tr1 glau2_tr2	pa_glau2	#2 By-passing perched water model/ 3d2kpa_pc2.mesh DTN: LB990701233129.001	Glacial Transition, upper-bound infiltration

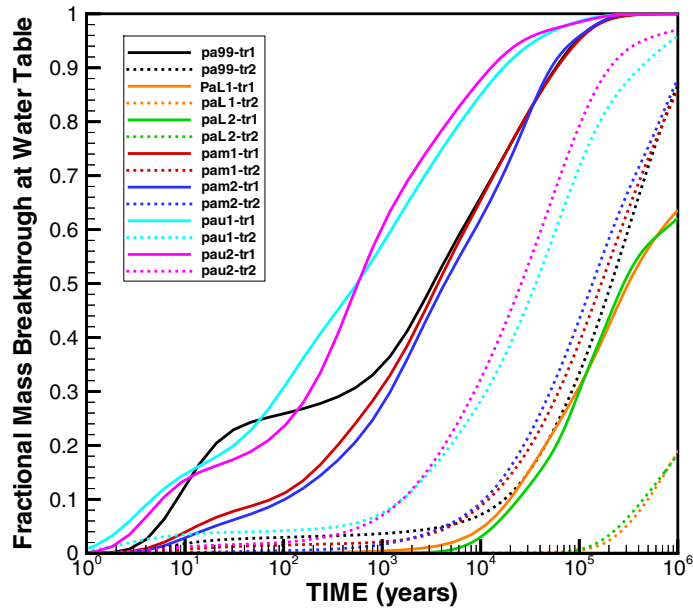
6.7.3 Simulation Results and Analyses

Groundwater travel and tracer transport times from the potential repository to water table:

Groundwater travel times (since release from the potential repository to the water table) may be analyzed using a cumulative or fractional breakthrough curve, as shown in [Figures 6-54, 6-55, and 6-56](#) for 1 million years. The fractional mass breakthrough in these figures is defined as the cumulative mass of a tracer or radionuclide arriving at the water table over the entire bottom model boundary over time, normalized by the total mass of the component initially introduced at the potential repository. In the figures, solid-line curves represent simulation results of conservative/nonadsorbing tracer transport and dotted-line plots represents reactive, adsorbing tracer transport. The three figures show a wide range of groundwater travel or tracer transport times with different infiltration rates, tracers, and perched water conceptual models from the 42 simulations. The predominant factors in groundwater travel times or tracer transport, as indicated by [Figures 6-54, 6-55 and 6-56](#), are (1) surface-infiltration rates or net water recharge and (2) adsorption effects, whether the tracer is conservative or reactive. To a certain extent, perched water conceptual models also affect groundwater travel/ transport times. However, the overall impact of the perched water conceptual models on tracer breakthrough at the water table is secondary compared to effects of infiltration and adsorption.

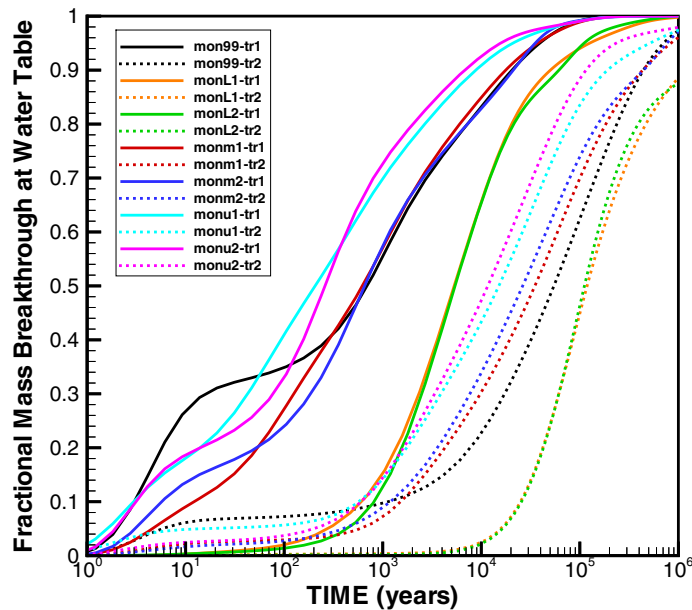
Statistics of groundwater travel or tracer transport times of 10% and 50% mass breakthrough at the water table for the 42 simulation scenarios are given in [Tables 6-29, 6-30 and 6-31](#), respectively. [Figure 6-57](#) correlates average infiltration rates and groundwater travel or tracer transport times at 50% mass breakthrough for the 42 simulation scenarios. [Figures 6-54 to 6-57](#) and the statistical data of [Tables 6-29, 6-30 and 6-31](#) show the following:

Groundwater travel or tracer transport times are inversely proportional to average surface infiltration (net water recharge) rate over the model domain ([Figure 6-57](#)). When an average infiltration rate increases from 5 to 35 (mm/yr), average groundwater travel (50% breakthrough) times decrease by one to two orders of magnitude. As infiltration decreases, the adsorbing species has a lower increasing rate in transport times than that of a nonadsorbing tracer because of retardation effects.



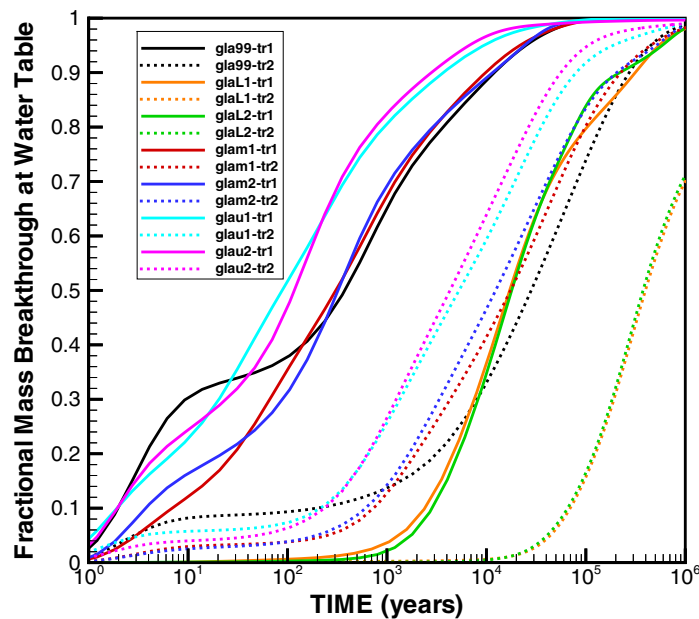
Based on DTN: LB9908T1233129.001

Figure 6-54. Simulated Breakthrough Curves of Cumulative Tracer Mass Arriving at the Water Table, Since Release from the Potential Repository, Using the Three Present-Day Infiltration Scenarios and Three Conceptual Models for Nonadsorbing and Adsorbing Transport



Based on DTN: LB9908T1233129.001

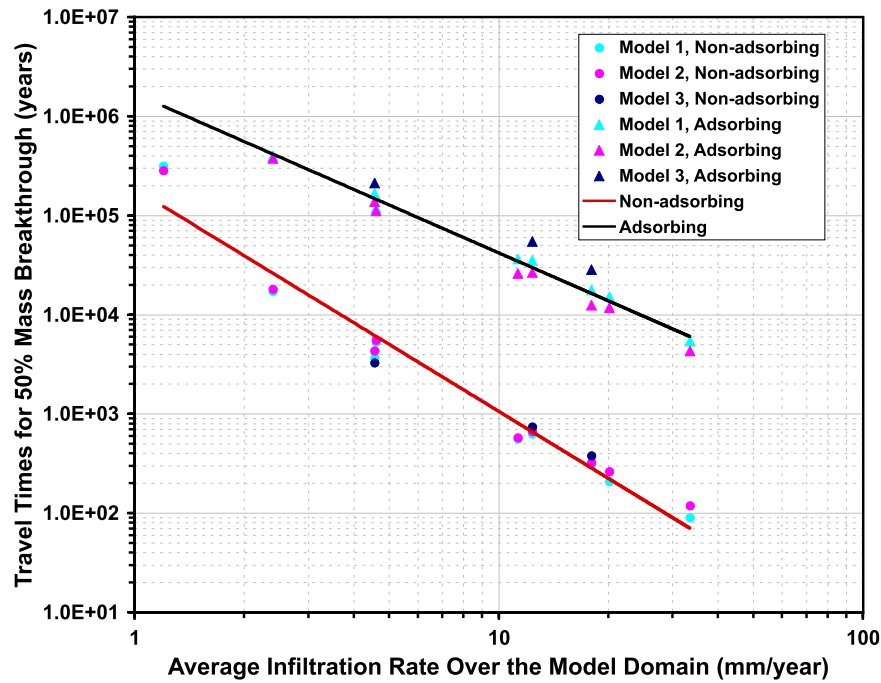
Figure 6-55. Simulated Breakthrough Curves of Cumulative Tracer Mass Arriving at the Water Table, Since Release from the Potential Repository, Using the Three Monsoon Infiltration Scenarios and Three Conceptual Models for Nonadsorbing and Adsorbing Transport.



Based on DTN: LB9908T1233129.001

Figure 6-56. Simulated Breakthrough Curves of Cumulative Tracer Mass Arriving at the Water Table, Since Release from the Potential Repository, Using the Three Glacial Transition Infiltration Scenarios and Three Conceptual Models for Nonadsorbing and Adsorbing Transport.

- Nonadsorbing tracers migrate one to two orders of magnitude faster than an adsorbing tracer when traveling from the potential repository to the water table under the same infiltration condition.
- The non-perching-water conceptual model (Conceptual Model #3) predicts the shortest arrival times for both nonadsorbing and adsorbing tracers during the first 1,000 years, using the results of the three conceptual models for the three mean infiltration scenarios of the three climates.
- In later times (>1,000 years), the results are mixed when comparing travel/transport times from the different conceptual perched water models. For nonadsorbing tracers, Conceptual Model #1 in general has a longer arrival time than Conceptual Model #2. For adsorbing tracers with retardation effects, however, Conceptual Model #1 predicts shorter travel times than Conceptual Model #2 for lower-bound and mean infiltration scenarios.



Based on DTN: LB9908T1233129.001

Figure 6-57. Correlations of Average Infiltration Rates and Groundwater Travel or Tracer Transport Times at 50% Mass Breakthrough for the 42 Simulation Scenarios.

Table 6-29. Groundwater Travel/Tracer Transport Times at 10% and 50% Mass Breakthrough Times for 14 Transport Simulation Scenarios, Corresponding to TSPA Flow Fields with Three Present-Day Infiltration Rates.

Designation/ Transport Simulation	Types of Tracer	10% Breakthrough Times (years)	50% Breakthrough Times (years)
pa99_tr1	Nonadsorbing	8	3,300
pa99_tr2	Adsorbing	17,000	210,000
paL1_tr1	Nonadsorbing	20,000	320,000
paL1_tr2	Adsorbing	500,000	> 1,000,000
paL2_tr1	Nonadsorbing	24,000	280,000
paL2_tr2	Adsorbing	450,000	> 1,000,000
pam1_tr1	Nonadsorbing	75	3,700
pam1_tr2	Adsorbing	12,000	170,000
pam2_tr1	Nonadsorbing	100	4,300
pam2_tr2	Adsorbing	11,000	140,000
pau1_tr1	Nonadsorbing	5	560
pau1_tr2	Adsorbing	1,600	36,000
pau2_tr1	Nonadsorbing	6	570
pau2_tr2	Adsorbing	1,600	26,000

Model Results - DTN: LB9908T1233129.001

Table 6-30. Groundwater Travel/Tracer Transport Times at 10% and 50% Mass Breakthrough Times for 14 Transport Simulation Scenarios, Corresponding to TSPA Flow Fields with Three Monsoon Infiltration Rates. _

Designation/ Transport Simulation	Types of Tracer	10% Breakthrough Times (years)	50% Breakthrough Times (years)
mon99_tr1	Nonadsorbing	3	740
mon99_tr2	Adsorbing	1,100	55,000
monL1_tr1	Nonadsorbing	600	5,300
monL1_tr2	Adsorbing	25,000	120,000
monL2_tr1	Nonadsorbing	820	5,500
monL2_tr2	Adsorbing	26,000	110,000
monm1_tr1	Nonadsorbing	12	630
monm1_tr2	Adsorbing	1,500	35,000
monm2_tr1	Nonadsorbing	6	670
monm2_tr2	Adsorbing	1,200	26,000
monu1_tr1	Nonadsorbing	3	210
monu1_tr2	Adsorbing	570	15,000
monu2_tr1	Nonadsorbing	3	260
monu2_tr2	Adsorbing	600	12,000

Model Results - DTN: LB9908T1233129.001

Table 6-31. Groundwater Travel/Tracer Transport times at 10% and 50% Mass Breakthrough for 14 Transport Simulation Scenarios, Corresponding to TSPA Flow Fields with Three Glacial Transition Infiltration Rates.

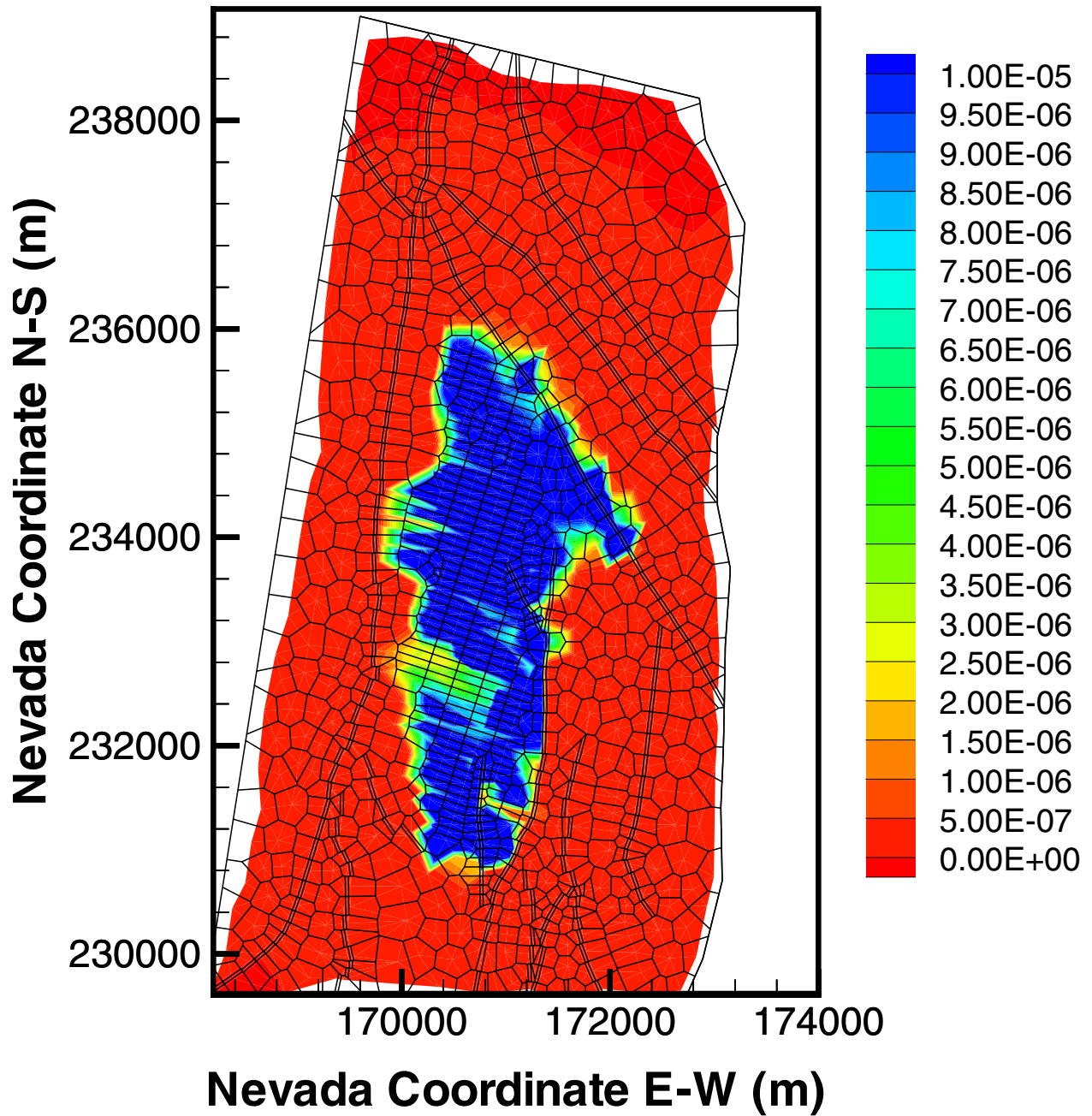
Designation/ Transport Simulation	Types of Tracer	10% Breakthrough Times (years)	50% Breakthrough Times (years)
gla99_tr1	Nonadsorbing	2	380
gla99_tr2	Adsorbing	200	28,000
glaL1_tr1	Nonadsorbing	2,400	17,000
glaL1_tr2	Adsorbing	70,000	400,000
glaL2_tr1	Nonadsorbing	2,900	18,000
glaL2_tr2	Adsorbing	66,000	380,000
glam1_tr1	Nonadsorbing	7	310
glam1_tr2	Adsorbing	740	18,000
glam2_tr1	Nonadsorbing	4	330
glam2_tr2	Adsorbing	620	12,000
glau1_tr1	Nonadsorbing	2	90
glau1_tr2	Adsorbing	220	5,400
glau2_tr1	Nonadsorbing	2	120
glau2_tr2	Adsorbing	240	4,300

DTN: LB9908T1233129.001

Potential locations of tracer breakthrough at the water table: The 42 tracer-transport simulation results can also be used to estimate potential locations or areas where radionuclides are most likely to break through at the water table. This information may be useful for modeling saturated zone transport. Figures 6-58a, 6-58b, 6-59a, and 6-59b show mass fraction contours at the water table at 1,000 years as examples after release from the potential repository for conservative and reactive tracer transport with Conceptual Models #1 and 2, respectively, using the present-day, mean infiltration rate.

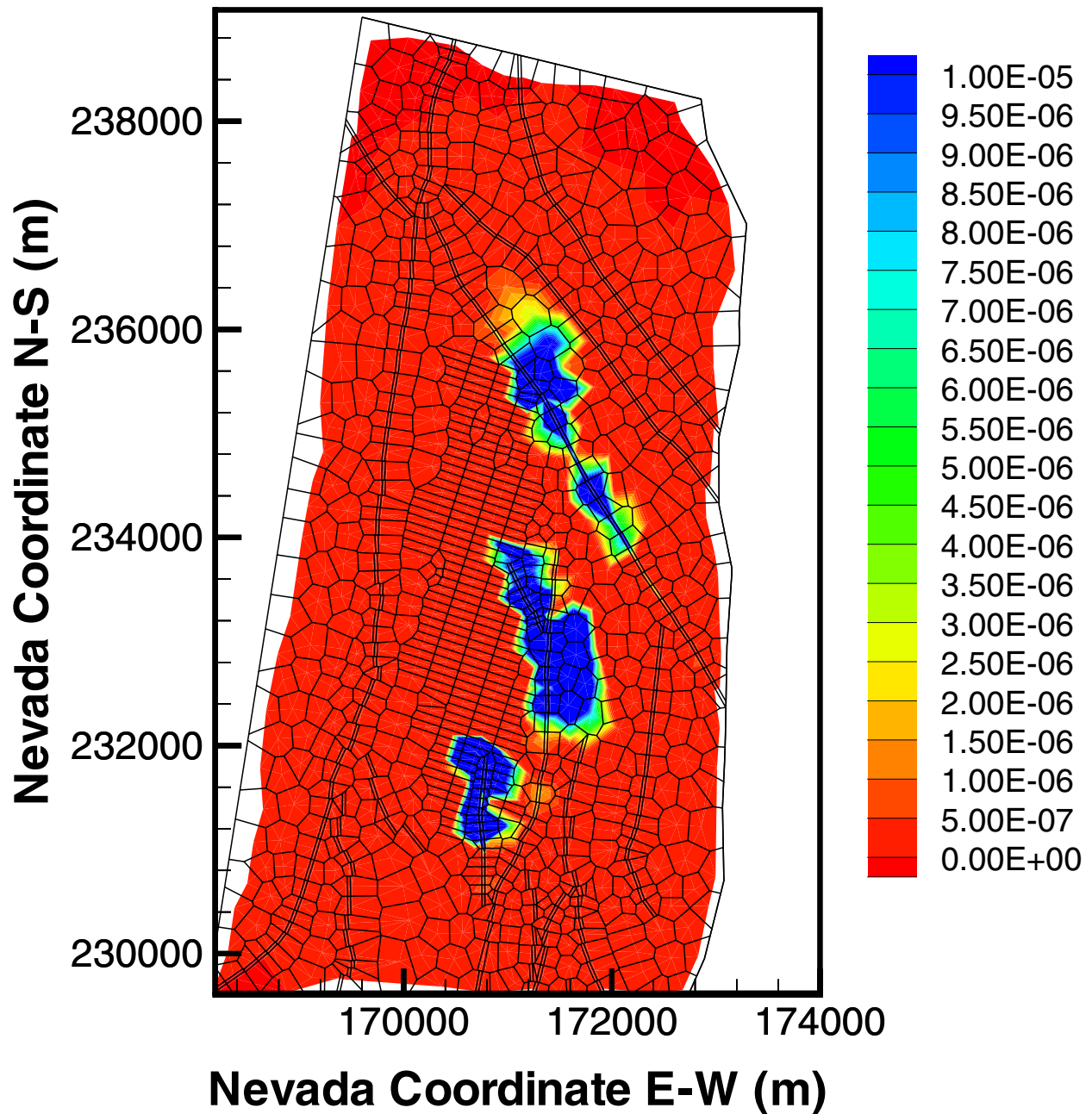
Figures 6-58a and 6-58b are for comparison between mass fraction contours of a conservative tracer at the water table after 1,000 years, simulated using the present-day, mean infiltration and Conceptual Model #1 (flow-through), and Conceptual Model #2 (by-passing), respectively. The two figures clearly indicate a significant difference in distributions of tracer mass fraction or concentration along the water table with the two conceptual model results. Conceptual Model #1 (Figure 6-58a) predicts a large area of high concentration covering the entire area directly below the potential repository, indicating that transport is predominantly vertical for this case. In contrast Conceptual Model #2 (Figure 6-58b) shows only three high-concentration areas, which are associated mainly with faults. This indicates the significant effects of by-passing flow in the CHn unit on the tracer transport using Conceptual Model #2 (by-passing model).

For an adsorbing tracer, Figures 6-59a and 6-59b show similar concentration contours to those on Figures 6-58a and 6-58b for a nonadsorbing tracer, but smaller areas and much lower concentration values for the same flow conditions. Figure 6-59a indicates that after 1,000 years, breakthrough occurs mainly below the southern portion of the potential repository in the vitric zones. In the northern part below the potential repository, breakthrough occurs along only a small portion of the Drillhole Wash fault. A comparison between high-concentration contours in Figures 6-58a and 6-59a shows that adsorption effects are expected to have a significant impact on arriving concentration values and distributions on the water table for the same flow conceptual model (flow-through model). This impact is especially apparent in the northern part below the potential repository, where thick zeolitic layers are located. The tracer has not yet broken through in 1,000 years (with retardation effects included – Figure 6-59a), when compared with Figure 6-58a without adsorbing effects using the same flow field. Since Conceptual Model #1 predicts a higher percentage of flow-through in the zeolites than Conceptual Model #2, as discussed in Section 6.2, these zeolitic units may effectively retard further transport of the tracer, carried (with this conceptual model) by flow-through waters even under water perching conditions.



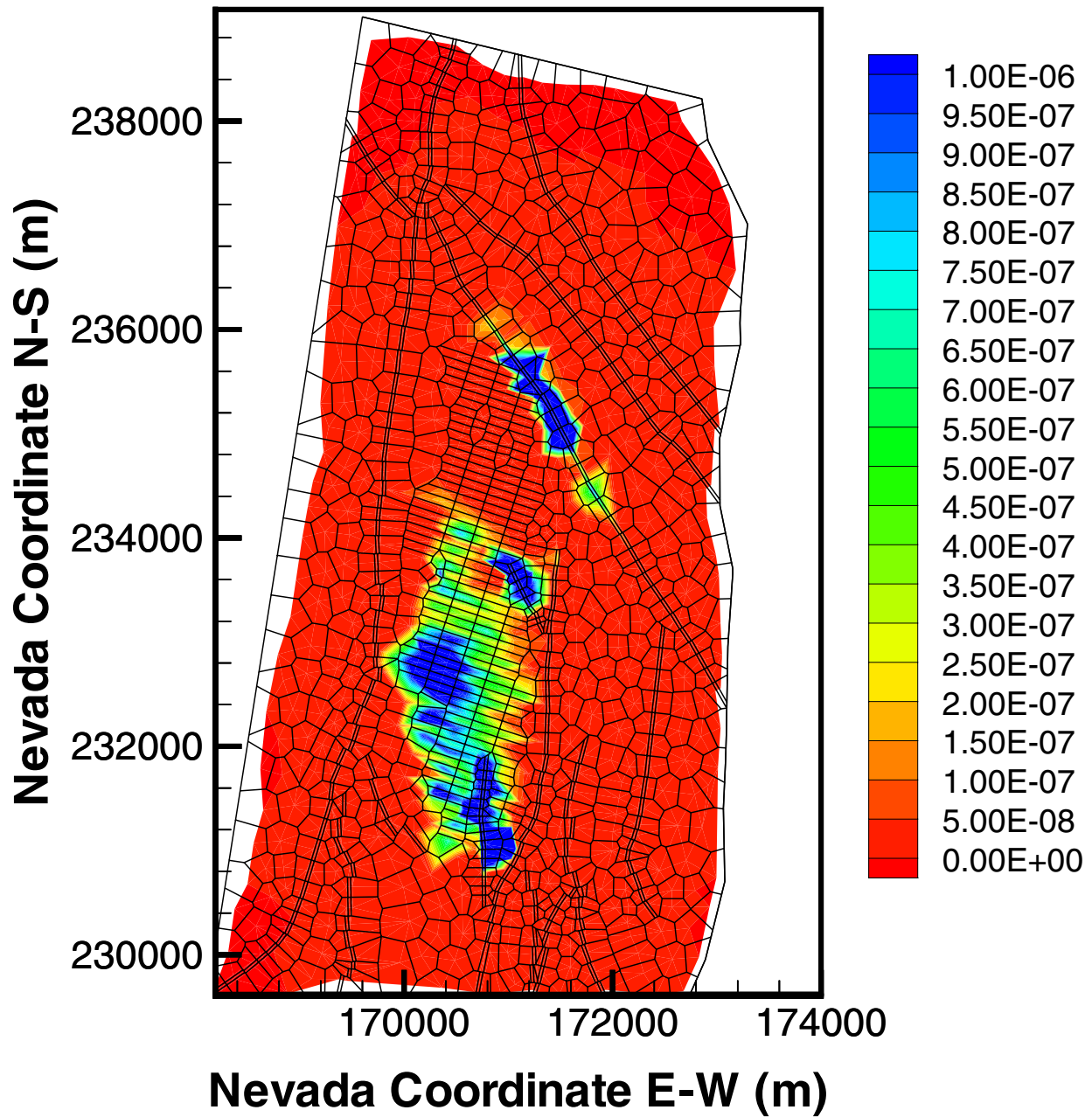
Based on DTN: LB9908T1233129.001

Figure 6-58. (a) Simulated Mass Fraction Contours of a Conservative Tracer at the Water Table after 1,000 Years, Indicating Potential Breakthrough Locations at the Time, Using the Present-Day, Mean Infiltration with Conceptual Model #1.



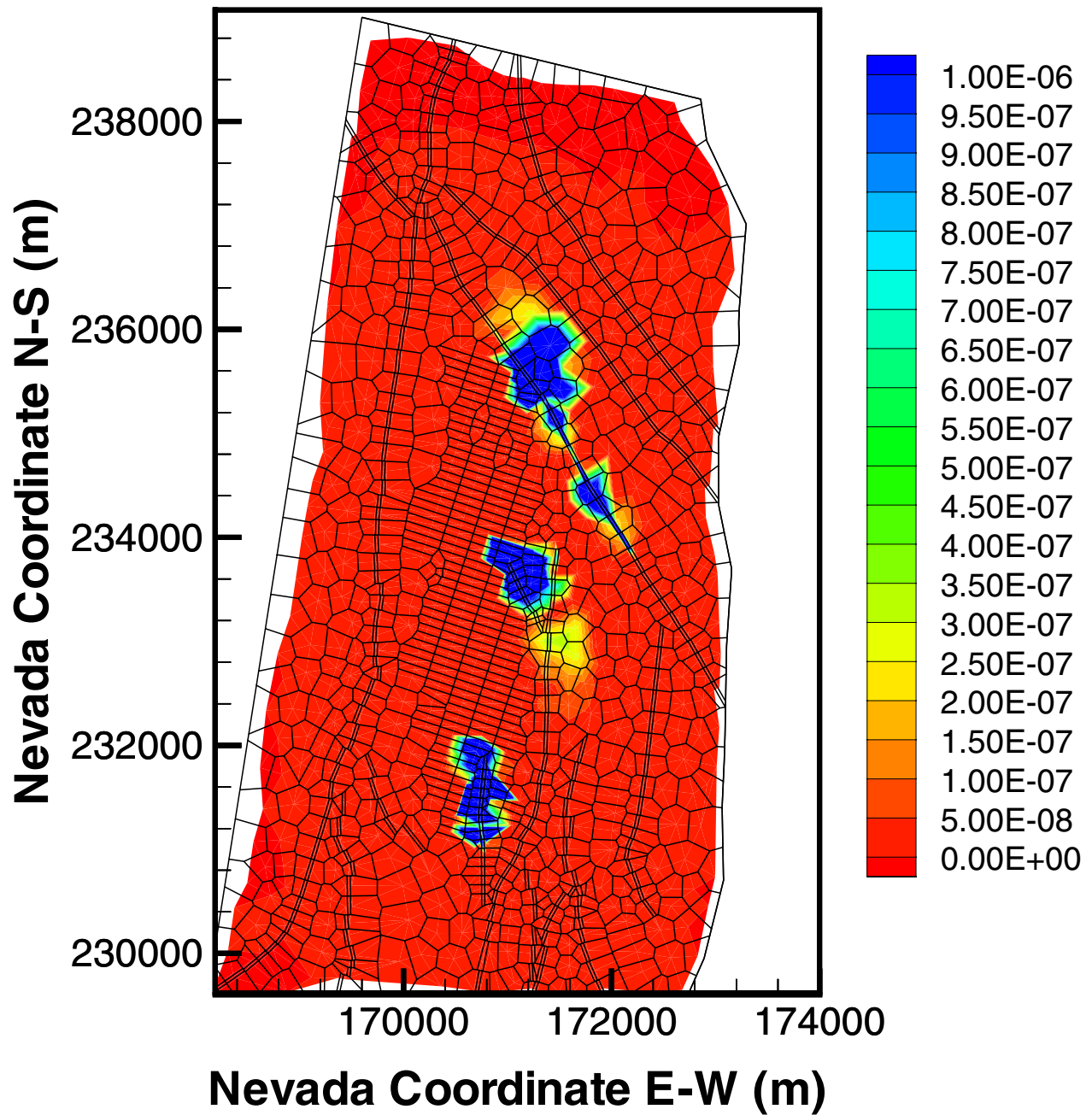
Based on DTN: LB9908T1233129.001

Figure 6-58 (b) Simulated Mass Fraction Contours of a Conservative Tracer at the Water Table after 1,000 Years, Indicating Potential Breakthrough Locations at the Time, Using the Present-Day, Mean Infiltration with Conceptual Model #2.



Based on DTN: LB9908T1233129.001

Figure 6-59. (a) Simulated Mass Fraction Contours of a Reactive Tracer at the Water Table after 1,000 Years, Indicating Potential Breakthrough Locations at the Time, Using the Present-Day, Mean Infiltration with Conceptual Model #1.

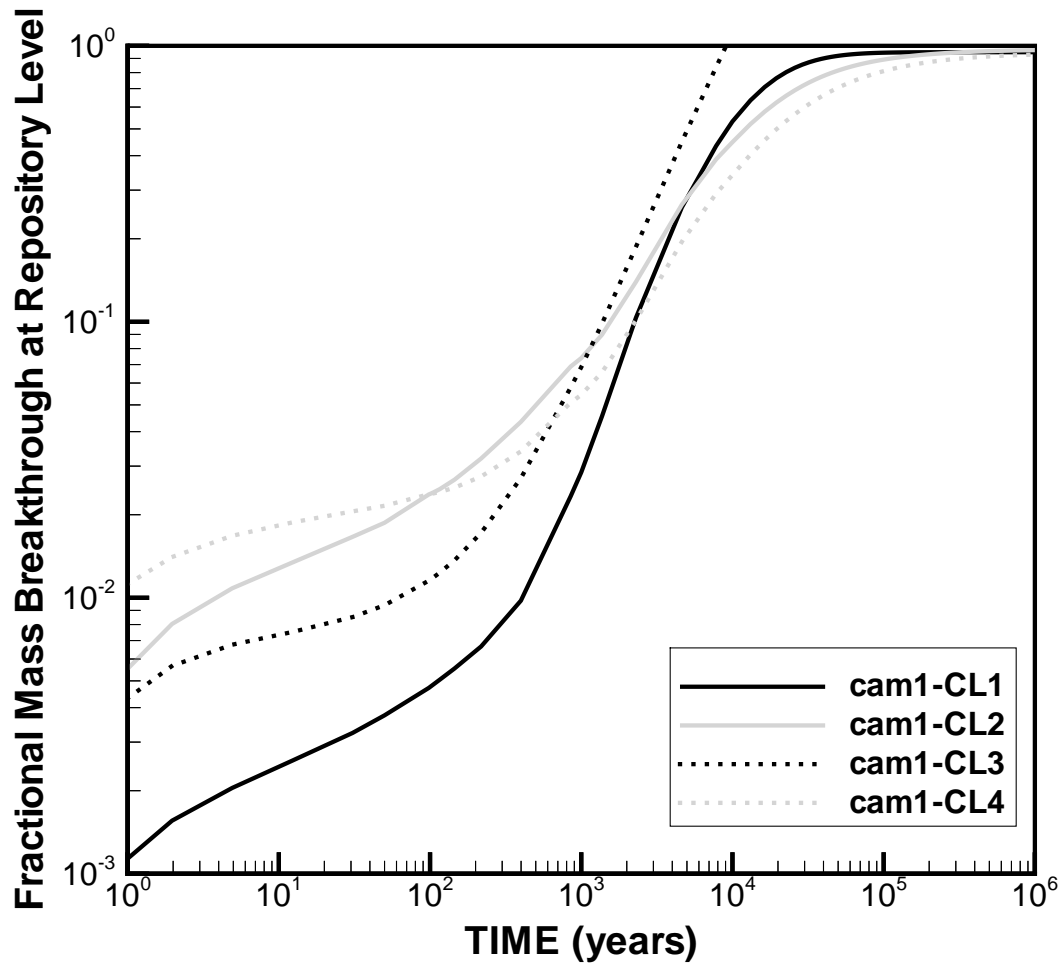


Based on DTN: LB9908T1233129.001

Figure 6-59 (b) Simulated Mass Fraction Contours of a Reactive Tracer at the Water Table after 1,000 Years, Indicating Potential Breakthrough Locations at the Time, Using the Present-Day, Mean Infiltration with Conceptual Model #2.

Groundwater travel and ^{36}Cl transport times from the land surface: Groundwater travel or ^{36}Cl transport times to the potential repository since release from the ground surface may be estimated using a cumulative or fractional breakthrough curve, as shown in [Figures 6-60](#) for the four simulation scenarios. The figure shows a similar range of groundwater travel or tracer transport times for the four different surface source conditions with the same present-day, mean infiltration rate. Except for the scenario with a constant initial concentration within the small surface source area (cam1_CL1), there is about 1% mass breakthrough during 10 to 100 years after tracer release on the ground. This indicates the existence of possible fast flow pathways with a travel time of 50 years, travelling from the ground surface to the potential repository level, under the steady-state UZ flow condition. However, the cumulative mass breakthrough is small (~1% of the total mass released on the ground) for the early breakthrough at 50 years. The average groundwater travel times from the surface to the potential repository level is estimated between 5,000 to 20,000 year using the 50% mass breakthrough curves of [Figure 6-60](#) from the four simulation results.

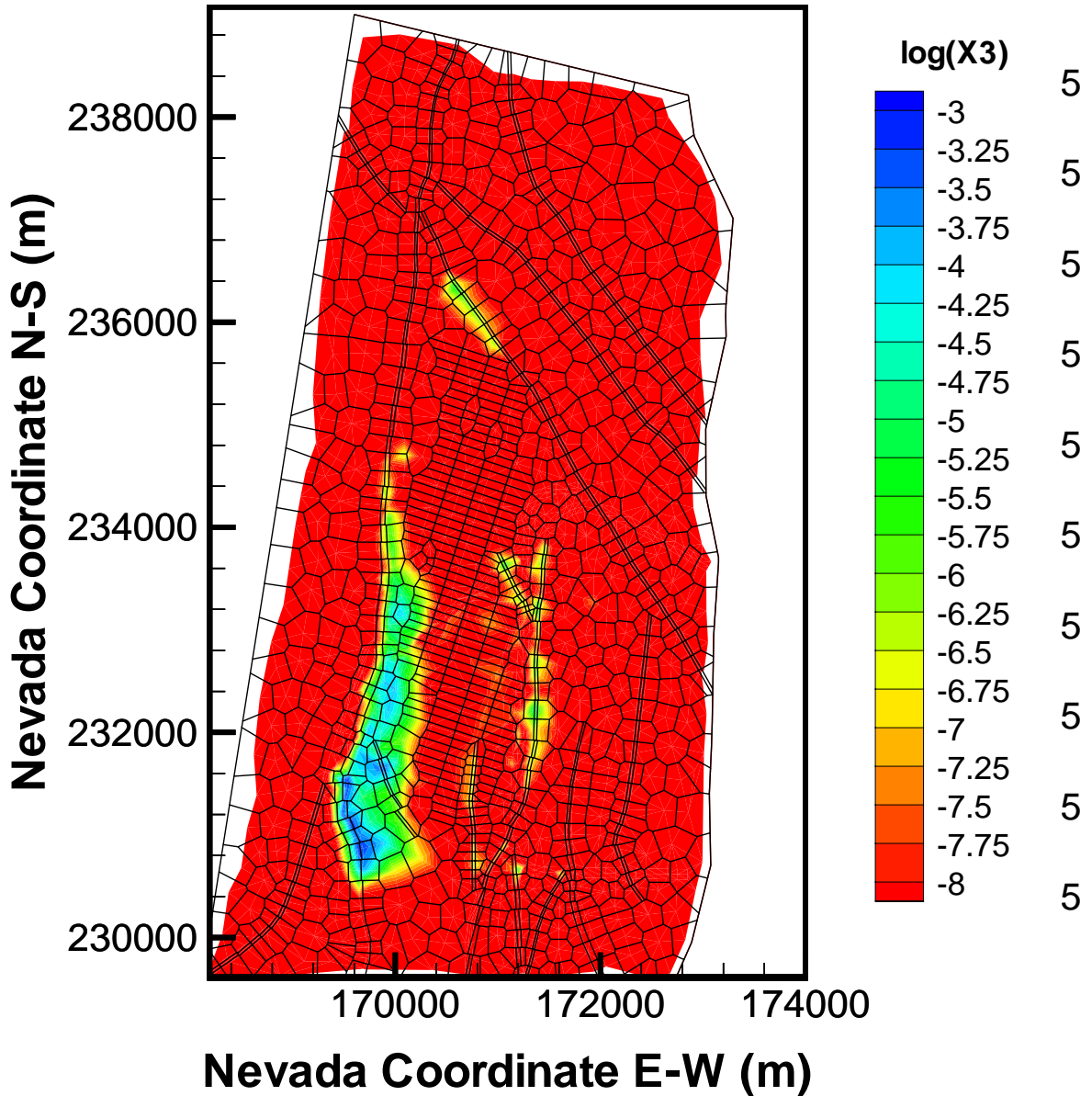
[Figures 6-61](#) shows spatial profiles of tracer mass fraction or concentrations in the UZ model at 50 years of release from the small source area of the top boundary. In a plan view, [Figure 6-61](#) indicates very localized breakthrough at the potential repository level, with all the high mass fraction/concentration zones associated with faults. Examination of the simulated tracer concentration distributions along vertical cross sections, and the ESF and ECRB tunnels indicates that in the vertical direction, tracer plumes penetrates faster only along high-permeability faults during the earlier travel times of 50 to 1000 years



Based on DTN: LB9908T1233129.001

Figure 6-60. Simulated Breakthrough Curves of Cumulative Tracer (³⁶Cl) Mass Arriving at the Potential Repository Level, Since Release from the Ground Surface, Using the Present-Day, Mean Infiltration and Four Simulation Scenarios

FRACTURE MASS FRACTION AT REPOSITORY LEVEL



Based on DTN: LB9908T1233129.001

Figure 6-61. Simulated Spatial Distribution of Tracer (³⁶Cl) in the US System at 50 Years since Release from the Ground Surface, Simulated Normalized Mass Fraction Contours at the Potential Repository Level (Note X3 denotes tracer mass fraction normalized to mass fraction values at source).

6.8 MODEL VALIDATION

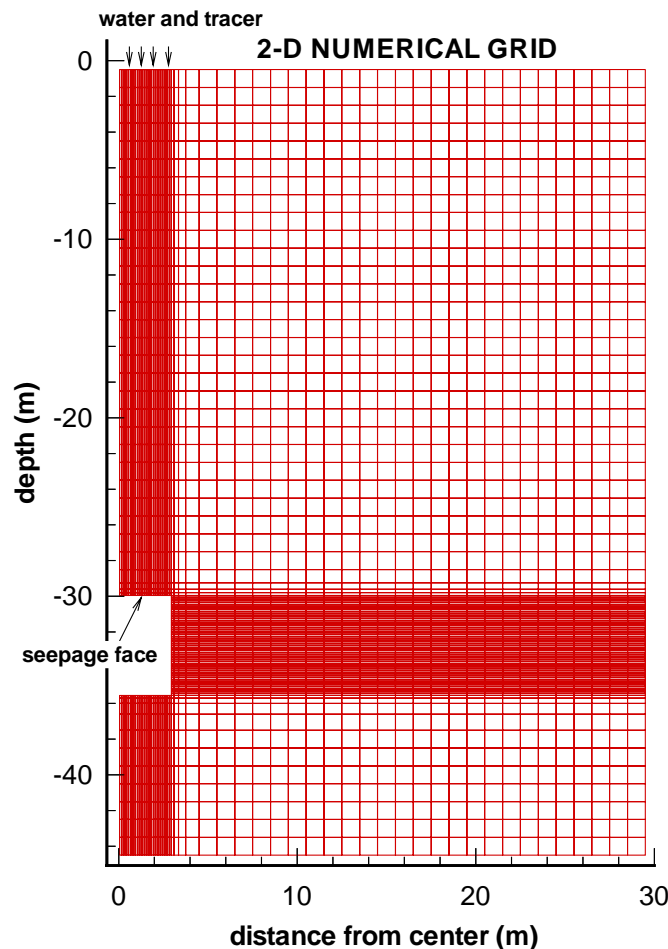
6.8.1 Alcove 1 Test Results

The continuum approach has been used in the UZ Flow and Transport Model. The reasons for using this approach are documented in the AMR describing conceptual and numerical models for UZ flow and transport (CRWMS M&O 2000c). One way to confirm the validity of the continuum approach is to compare simulation results based on these approaches with field observations (Pruess et al. 1999, p. 312). The same continuum concept is used in this modeling study, although grid spacings near the alcove are significantly smaller than those used in the site-scale model.

Recently, an infiltration and tracer transport test was performed in the ESF Alcove 1. Alcove 1 is located near the North Portal of the ESF in the upper lithophysal zone of the Tiva Canyon Tuff (Tpcpul) unit, corresponding to hydrogeologic unit CUL (Flint, 1998, p. 3). The Tpcpul unit extends above the alcove to the ground surface, with the crown of the drift approximately 30 m below the ground surface. The infiltration test at Alcove 1 involved applying water at the ground surface directly over the end of Alcove 1. At a late stage of the test, a conservative bromide tracer was introduced into the infiltrating water. The seepage into the alcove and the tracer arrival time were recorded. The experimental observations are directly related to the flow and transport processes in the unsaturated fractured rocks and, therefore, provide a useful data set for evaluating the continuum approaches used in the UZ flow and transport model. The test consisted of two phases. Phase I was performed from March to August in 1998 and corresponds to a relatively large degree of temporal variability in the infiltration-rate data. Phase II was performed from January to June in 1999. This study was documented in Scientific Notebooks (YMP-LBNL-JSW-CFA-6.1 pp. 1-26; 39-48; 72-88, YMP-LBNL-GSB-1.12 p. 153, YMP-LBNL-GSB-1.6.3 pp. 74-78, and YMP-LBNL-GSB-LHH-2 pp. 67-73).

6.8.1.1 Numerical Model

A radially symmetric, two-dimensional (2-D) grid in cylindrical coordinates was constructed for simulation of the infiltration test (Figure 6-62). The grid extended 45 m in the vertical dimension and 30 m in the radial (horizontal) dimension (the diameter is 60 m). The ground surface was approximated as horizontal. A square opening representing the alcove has created in the grid from 30 m to 35.5 m below the ground surface. The grid was regular, with 10-cm grid spacing around the alcove and 1-m grid spacing away from the alcove. The active fracture model (Liu et al. 1998, pp.2633-2646) was employed to describe flow and transport within fractures and between fractures and the matrix. Because of the highly transient nature of the infiltration test, the multiple interacting continua (MINC) approach was used. Three matrix continua were used for developing the numerical grid. The development of the grid is documented in Scientific Notebooks (YMP-LBNL-JSW-CFA-6.1 pp. 9; 17-18; 45-46 and YMP-LBNL-GSB-1.1.2 p. 153).



DTN: LB991131233129.002

Figure 6-62. Numerical Grid for the Model of the Infiltration Test

Because the test site is located in the same hydrogeological unit, hydraulic properties for fractures and the matrix are assumed to be homogeneously distributed within the model domain. The initial estimate for these properties was taken from different sources for the model calibration (Table 6-32) because a systematic calibrated property set for the CUL unit, where the test site is located, was not available. Matrix properties were directly taken from those for hydrologic unit CUL in (DTN: GS960908312231.004.) Fracture permeability, residual saturation and van Genuchten α were from DTN: LB971212001254.006 (Table A-2a, tcw11) and fracture van Genuchten m was taken from DTN: LB990501233129.001. The initial estimates of fracture porosity was assumed to be 0.01, based on the porosity data in DTN: LB980912332245.002. The fracture spacing was calculated using fracture-frequency data between ESF stations 0 + 60 m and 0 + 80 m [from the Detailed Line Survey (DTN: GS971108314224.020)]. Software routines Read_TDB (version 1.0) and Frac_Calc (Version 1.1), were used for calculating the fracture frequency. Since the objective of this study is mainly to evaluate the numerical approach, it should be considered as a corroborative study.

Table 6-32. Initial Estimated Hydrologic Properties for Infiltration Test Model

Parameter	Fracture	Matrix
Porosity [-]	0.01	0.164
Permeability ^a [m ²]	2.29 x10 ⁻¹¹	1.2Ex10 ⁻¹⁵
Van Genuchten α [Pa ⁻¹]	2.37 x10 ⁻³	7.12x10 ⁻⁶
Van Genuchten m [-]	0.633	0.346
Residual saturation [-]	0.01	0.06
Fracture spacing [m]	0.377	NA

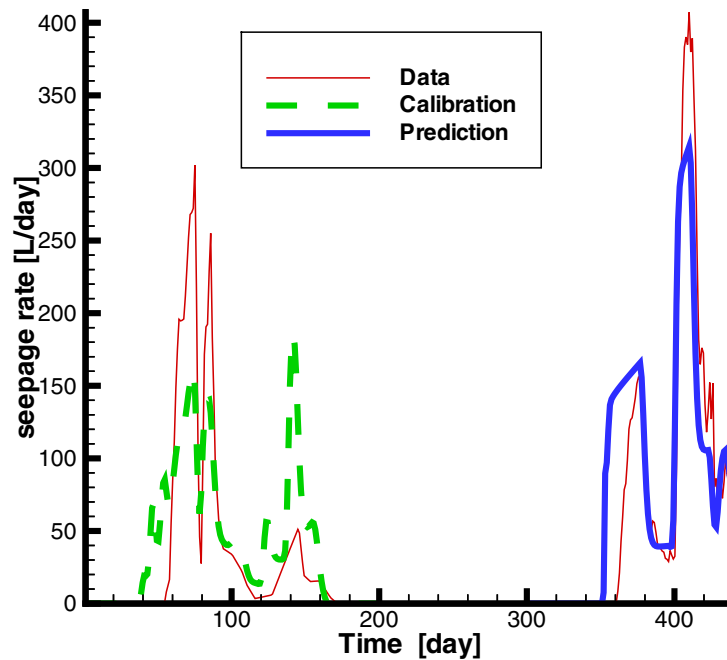
DTNs: GS960908312231.004; LB971212001254.006; LB990501233129.001; LB980912332245.002
GSa71108314224.020

NOTES: ^aIn both the vertical and horizontal directions

The temporally variable inflow rates are imposed on the top boundary, representing the infiltration condition. The side boundary away from the alcove corresponds to a zero-flow condition in the radial direction, considering that the side boundary is far away from the alcove. The alcove wall boundary is modeled using a zero-capillary-pressure condition, corresponding to 100% humidity within the alcove. The bottom boundary was assigned a constant matrix saturation of 0.61, which is the average matrix saturation of the unit CUL (DTN: GS960908312231.004). Initially, rock mass within the model domain was considered to be in gravity-capillary equilibrium with the low boundary and to be solute-free.

6.8.1.2 Results and Discussion

Figure 6-63 shows a comparison between observed seepage rate data for Phase I of the test and the simulation result from model calibration with ITOUGH2 (version 3.2). Table 6-33 gives the rock properties calibrated with Phase I data. Although arrival times of three major peaks in the Phase I seepage rate data are matched, large differences exist between the simulated and observed seepage rate values at these peaks. While it is possible that the homogeneity assumption and the continuum approach underestimates the variability of seepage rates, we believe that the more important reason is the simplicity of the model in representing the site conditions during the Phase I test.



Data - CRWMS M&O (1999f) Model Results - DTN: LB991131233129.002

Figure 6-63. Model Calibration Using the Seepage Rate Data of the Phase I of the Test and Prediction for Phase II of the Test.

We modeled liquid-water flow with the EOS9 module, which ignores vapor transport. An isothermal condition was also assumed for simplicity. Since the Phase I test was conducted from March to August in 1998, temperatures were relatively high in the late stage of the test, which may have caused considerable vapor transport and evaporation through highly permeable and well-connected fractures. The matrix saturation near the fracture-matrix interface becomes very high with time between the alcove's ceiling and the ground surface, resulting in very small simulated matrix imbibition between 100 and 200 days. Simulated results consequently show a strong response to the infiltration pulses during this period. In reality, the vapor transport might remove a portion of the liquid water from the fractures and the matrix near the fracture-matrix interface area. This could give rise to a weaker response of the seepage to the infiltration, as indicated by the data (Figure 6-63). Because of the temporally variable infiltration rates in Phase I of the test, a complex wetting and drying process was involved in the matrix. Under these conditions, hysteresis might considerably affect seepage into the alcove. However, not enough data were available for characterizing the matrix hysteresis. Instead, a single matrix water retention curve was used for both the wetting and drying procedure. However, these issues are not specific to the continuum approach used for this study.

Table 6-33. Calibrated Hydrologic Properties for Infiltration Test Model Based on the Phase I Seepage Rate Data^a

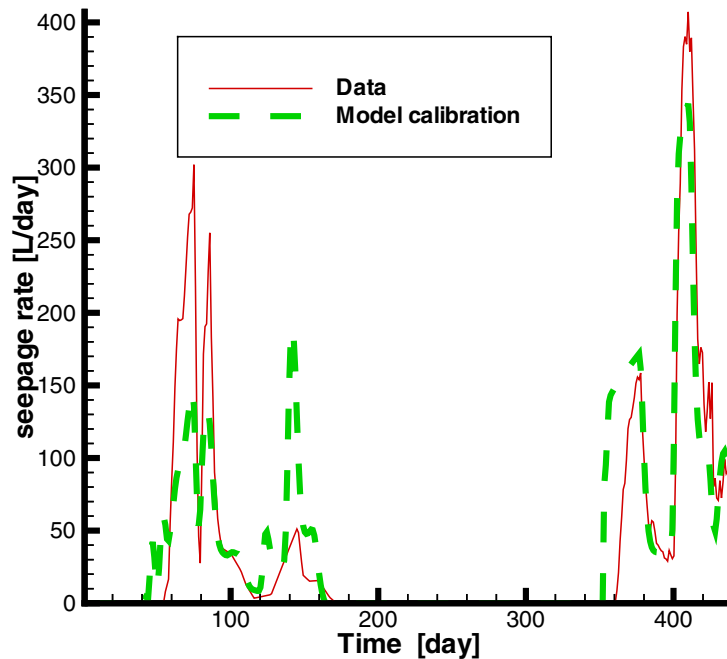
Parameter	Fracture	Matrix
Porosity [-]	0.028	0.164
Vertical Permeability [m ²]	2.90E×10 ⁻¹¹	3.64×10 ⁻¹⁶
Horizontal Permeability [m ²]	3.14E×10 ⁻¹¹	9.35×10 ⁻¹⁶
Van Genuchten α [Pa ⁻¹]	2.07E×10 ⁻³	1.43×10 ⁻⁵
Active fracture parameter γ [-]	0.28	NA

DTN: LB991131233129.002

NOTE: ^aParameters that are not shown in this table are the same as those in Table 6-32. They are fixed in the inversion.

Figure 6-63 also shows a comparison between the predicted seepage rates and the data for Phase II of the test. Properties calibrated against Phase I test data were used for the prediction. The comparison is fairly reasonable considering that a relatively poor match was obtained for the Phase I test using the inverse modeling. The comparison confirms that ignoring water loss through evapotranspiration for periods of high temperature is a major reason for the poor match of the Phase I data. For the Phase II test, simulated seepage occurs earlier than the observation, and the simulated seepage rates are generally higher in the 350—380 day period (Figure 6-63). As a result of the model's inability to deal with vapor transport, the fracture-matrix system in the numerical model was wetter than the actual system during the initial stage of the Phase II test. The wetter condition reduces the matrix imbibition and therefore increases the seepage rate. After 380 days, the performance of the model prediction improves, possibly because during this period the actual system is very wet, and actual matrix saturations approximate the modeled results.

The Phase II test data, shown in Figure 6-63, were collected from January to May in 1999. In this period, the vapor transport is not considered to be important because the temperature is not very high. More importantly, Figure 6-63 shows that the infiltration and seepage processes can be reasonably represented by the model, considering the complexities of the problem and the simplicity of the model. In other words, a continuum approach is shown to be valid for capturing the complex flow and transport processes in an unsaturated fractured porous medium.



Data - DTN: GS000399991221.003 Model Results - DTN: LB991131233129.002

Figure 6-64. Model Calibration Using Seepage Rate Data from Phases I and II Test.

To further improve the accuracy of rock property estimates, we conducted the second inversion based on data from both Phase I and Phase II of the test. The initial estimate for rock properties, used in the model calibration, was based on those in Table 6-32. Figure 6-64 shows the comparison between the simulated and observed seepage rates, which is similar to that in Figure 6-63. The calibrated properties are given in Table 6-34. Note that these properties are very comparable to the base case properties of model layer tcw11 (DTN: LB990501233129.001) in terms of order of magnitude.

Table 6-34. Calibrated Hydrologic Properties for Infiltration Test Model Based on the Phases I and II Seepage Rate Data^a

Parameter	Fracture	Matrix
Porosity [-]	0.03	0.164
Vertical Permeability [m ²]	3.23x10 ⁻¹¹	3.23x10 ⁻¹⁶
Horizontal Permeability [m ²]	3.53x10 ⁻¹¹	8.08x10 ⁻¹⁶
Van Genuchten α [Pa ⁻¹]	2.04x10 ⁻³	1.84x10 ⁻⁵
Active fracture parameter γ	0.23	NA

DTN: LB991131233129.002

NOTE: ^a Parameters that are not shown in this table are the same as those in Table 6-32. They are fixed in the inversion.

Figure 6-65 shows tracer transport simulation results obtained with T2R3D (Version 1.4). The tracer test was carried out over a 51 day period, beginning on May 18, 1999. First detection of the tracer within the seepage occurred after 28 days. To predict the tracer arrival time, we assumed zero dispersivity for the fracture continuum since no data for the dispersivity are available. Note that Figure 6-65 shows the predicted breakthrough curve is not sensitive to the fracture dispersivity value. A molecular diffusion coefficient of $2.0E-9 \text{ m}^2/\text{s}$ was used for bromide (Domenico and Schwartz 1990, p. 368). According to Francis (1997, p. 5), while experimental data for tortuosity are not available for the Yucca Mountain tuff, a representative value of the matrix tortuosity is 0.7. Figure 6-65 shows simulation results for a number of tortuosity values. Since pore velocities in the matrix are generally small, the mechanical dispersion is ignored for the matrix. The calibrated hydrologic properties based on both Phases I and II seepage data (Table 6-34) were used in the simulation.

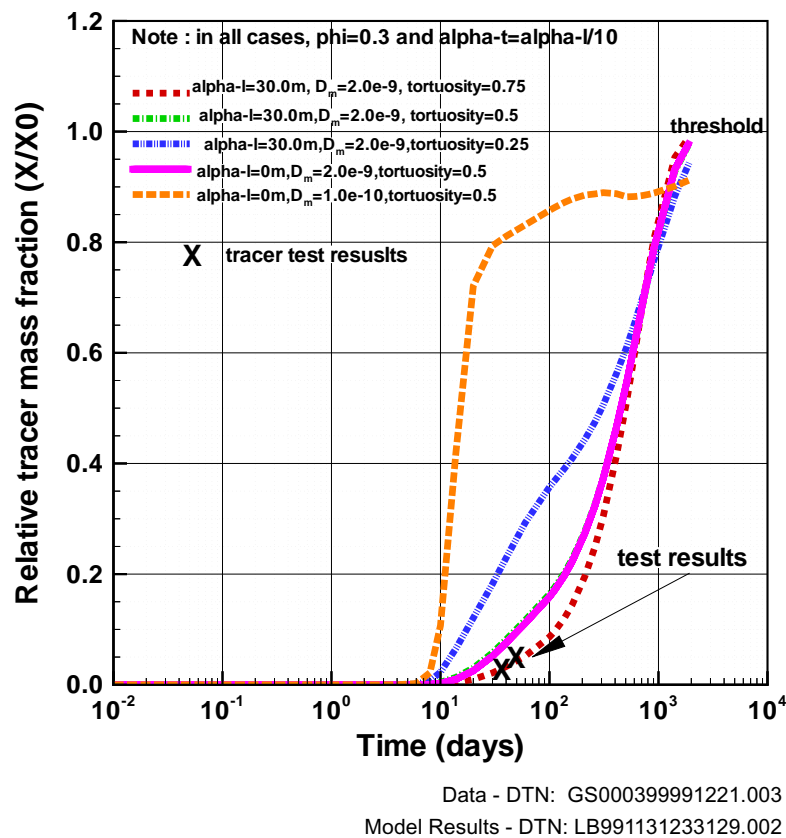


Figure 6-65. Comparison between Simulation Results of Tracer Transport and Observations. (Note that $\alpha-l$, $\alpha-t$, ϕ refer to longitudinal dispersivity, transverse dispersivity and fracture porosity, respectively.)

As shown in Figure 6-65, the simulated breakthrough curve is closely matched with the tracer concentration data for a tortuosity value of 0.75, which is close to the representative value of 0.7 given by Francis (1997, p. 5). This indicates that our model correctly predicts the tracer transport

behavior without calibration of transport parameters. Again, this validates the continuum approach and shows that it can capture important features of the UZ transport processes.

An important finding from the tracer simulations is that the breakthrough curve is considerably sensitive to the matrix molecular diffusion coefficient and tortuosity (Figure 6-65), suggesting that matrix diffusion is an important mechanism for UZ transport. This sensitivity also implies that flow and transport between the two continua (fracture-matrix interaction) is correctly simulated with the active fracture model, although complex fingering of flow and transport occurred in the fracture networks during the Alcove 1 test. On the other hand, the simulation result is not sensitive to the fracture dispersivity, possibly because in a dual-continua system, the chemical transport is mainly determined by the largest heterogeneity, the property difference between the matrix and fracture continua. In this case, heterogeneity in each continuum, resulting in the corresponding macroscopic dispersion process, becomes secondary.

In summary, the results from this study indicate that the continuum approach is valid for modeling flow and transport in unsaturated fractured rock. The use of an active-fracture model can capture the major features of fingering flow and transport in fractures. The matrix diffusion has a significant effect on the overall transport behavior in unsaturated fractured rocks, while the dispersion in fractures does not.

6.8.2 ECRB Results

An east and west cross drift was constructed in 1997 as part of the Enhanced Characterization of the Repository Block (ECRB) program (see Figure 6-1 for the location of the ECRB tunnel). Water-potential data (DTN: GS980908312242.036) were collected from heat dissipation probes installed in the tunnel wall (at a depth of 2 meters) along the ECRB tunnel inside ESF. The probe locations were transferred from station number to Nevada Coordinates system through ECRB-XYZ Version 03 (STN: 30093).

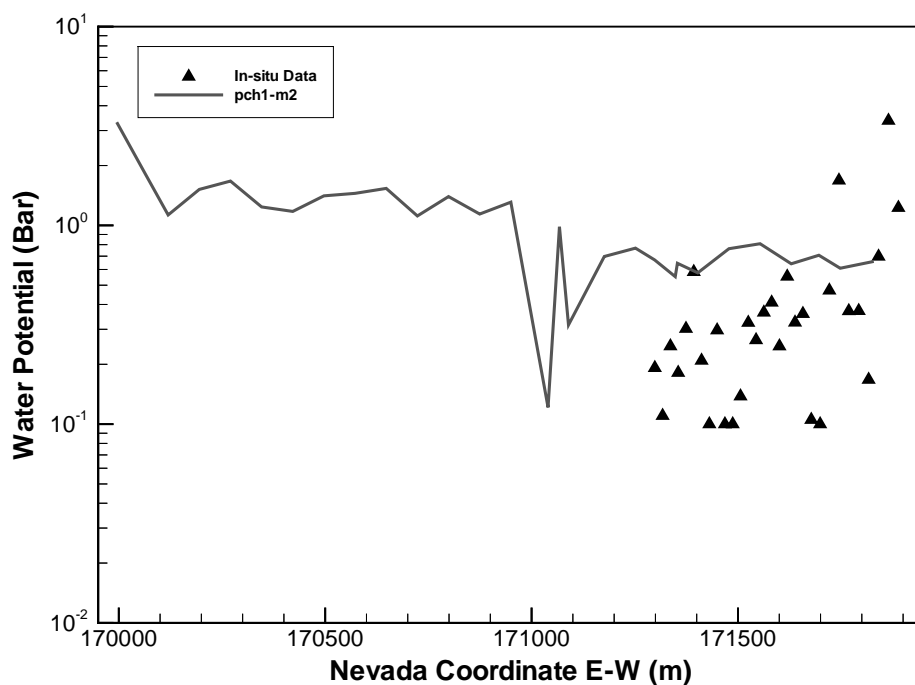
Water potential data were collected from heat dissipation sensors that have been calibrated for matrix potential. At installation, the borehole was dry drilled, however the sensor was not installed with the wet cement. Thus the sensor was fully saturated and surrounded with contact media to ensure good contact with rock. The sensor then equilibrated with the matrix potential of the rock (took about two to six weeks). Often following the equilibration, the probe would gradually dry out. Since this was the first group of probes installed in the tunnel wall, there were no steps taken to reduce the effects of ventilation drying in the tunnel. Extra steps such as installing double doors were taken during installation and monitoring the first group of probes in the ECRB tunnel. Accuracy of heat dissipation probes calibrated intensively and as a function of temperature is plus or minus 10% of the matrix potential reading.

As part of the 3-D flow and transport modeling validation process, modeling results were compared to the field observation data collected from the wall of the tunnel to check the accuracy of the modeling predictions.

The 3-D mesh with perched water flow-through model adjustment for the Calibration flow-fields was used (DTN: LB990501233129.004). Infiltration boundary conditions were the same as those documented in Section 6.1.3 and 6.1.4 for the present-day, base-case infiltration scenario

CRWMS M&O 1999e, (DTN: GS000399991221.002). The calibrated properties used for the 3-D prediction are those developed by inversion of saturation, water potential, and pneumatic data using 1-D and 2-D models for the present-day, base-case infiltration scenario. The detail of the model development is documented in Section 6.1 and 6.2.

Figure 6-66 shows a comparison of matrix water potential along the wall of the ECRB drift. As shown in the figure, observation data are available only along part of the tunnel. Most of the observed water-potential data are distributed between 0.1 and 1 bar, with a maximum of 3.4 bar. The model predicted approximately 1 bar for the same section of tunnel, which is higher than most of the observed data. The predicted water-potential data from the UZ Model ranged between 0.1 and 3.3 bar.



Data - DTN: GS980908312242.036 Model Results - DTN: LB990801233129.003

Figure 6-66. Predicted Water Potential along ECRB Using the Present-Day Mean Infiltration Rate and Perched Water Conceptual Model #1

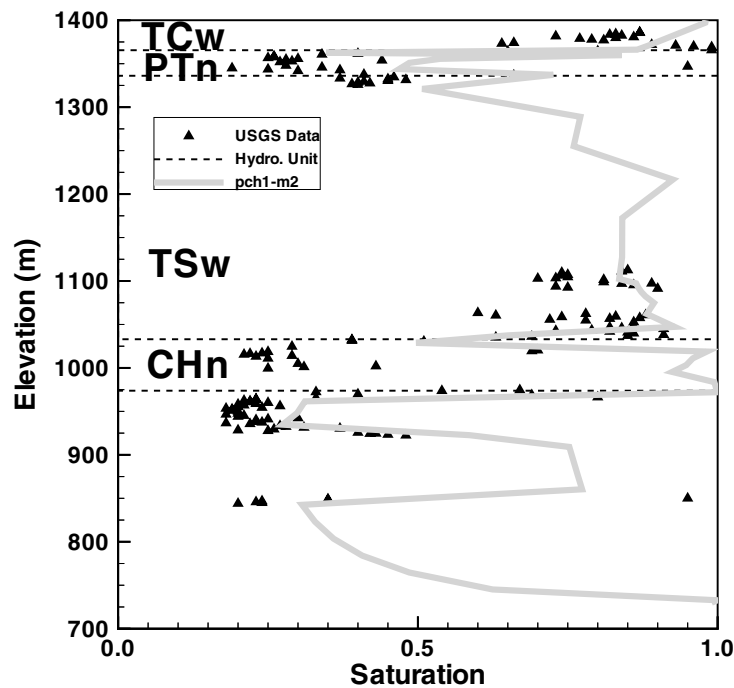
Since the probe measurements have an error of plus and minus 10%, field heterogeneity will play an important role for a range of data between 0.1 and 1 bar. Even though the data available for comparison at the ECRB drift are limited, results indicated that the UZ Model generally predicted the range of the water-potential data from *in situ* measurements. Even though the data available for comparison at the ECRB drift are limited, results indicated that the UZ Model results were within the range of the water-potential data from *in situ* measurements.

6.8.3 SD-6 and WT-24 Modeling Results

Boreholes WT-24 and SD-6 were drilled in 1997 as part of the ECRB program (see Figure 6-1 for borehole locations). Observed saturation data were collected from these two boreholes (see Section 4-1 for DTNs). No perched water was detected in borehole SD-6. However, perched water was detected within the basal vitrophyre of the TSw at an elevation of approximately 985 m for borehole WT-24 (DTN: GS980508312313.001). As part of the modeling validation process, modeling results were compared to the field-observation data to check the accuracy of the modeling predictions.

The 3-D mesh with perched water flow-through model adjustment for the calibration flow-fields was used (DTN: LB990501233129.004). Infiltration boundary conditions were the same as those documented in Section 6.1.3 and 6.1.4 for the present-day, base-case infiltration scenario (DTN: GS000399991221.002). The details of the model development are documented in Section 6.1 and 6.2.

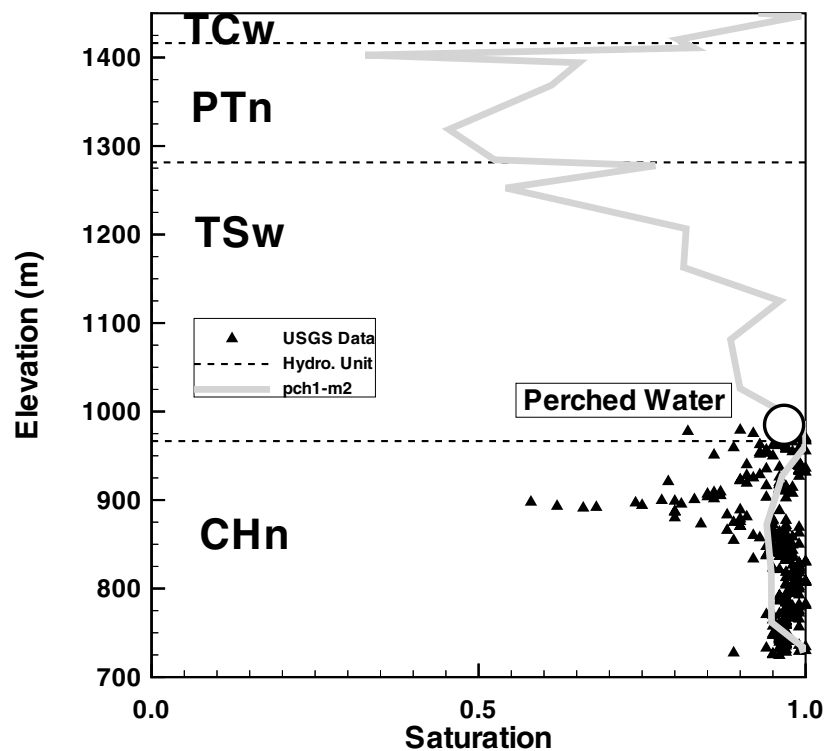
Figure 6-67 shows a comparison of matrix saturation results with field measurement data at borehole SD-6. As shown on the figure, the modeling prediction is generally consistent with field measurements. The model does not predict perched water occurrence at this borehole, which is consistent with field observation. The modeling result predicts higher saturation in this CHn unit; however, the field measurement indicates a dry condition in the same unit. This is a result of the current geological framework model which specifies this layer as zeolitic layer at the location of SD-6.



Data - DTN: GS980808312242.014; Model Results - DTN: LB990801233129.003

Figure 6-67. Predicted Matrix Saturation for Borehole SD-6 using the Present-Day Mean Infiltration Rate and Perched Water Model #1

Figure 6-68 compares matrix saturation results with the field measurement data at borehole WT-24. The observed location of perched water is also shown on the figure. As shown on the figure, the field-measurement data for saturation are limited to the deeper section of the borehole (mostly in the CHn unit). The UZ Model predicts a saturated condition at the location of observed perched water, which matches the field measurement. Even though several low saturation data points appear in the vicinity of perched water elevation, most of the data points collected in the same vicinity have much higher saturations. There is a low saturation layer within the CHn unit (according to the field measurement data) that was not predicted by the UZ Model.



Data - DTN: GS980708312242.010 Model Results - DTN: LB990801233129.003

Figure 6-68. Predicted Matrix Saturation for Borehole WT-24 using the Present-Day Mean Infiltration Rate and Perched Water Model #1

The data gaps at the particular units (i.e., CHn) for these two boreholes are due to the inaccuracy of the 3-D geological model GFM3.1 at certain locations. High saturations within the CHn are strongly correlated with the presence of zeolites (portions of the CHn that are vitric tend to show much lower saturations than the zeolitic portions of the CHn). During development of the mountain-scale numerical grids, data on the abundance of zeolites within SD-6 of WT-24 in the CHn were not available. It was assumed that ch1 through ch6 were zeolitic in WT-24 and that ch2 through ch6 were zeolitic in SD-6 (based on geostatistically determined hydraulic conductivity data from the Rock Properties Model (RPM3.0 of ISM3.0)). The accuracy of UZ Model depends partly on the accuracy of the Integrated Site Model, which is assumed to represent subsurface geology as well as rock properties. The spatial heterogeneity of low-permeability alteration products such as zeolites has a profound impact on flow and transport calculations, yet the nature

of their distribution is not fully understood. The data gaps should be resolved with the updated version of the Integrated Site Model (ISM3.1).

In general, the UZ Model accurately predicts the location of perched water at borehole WT-24. Consistent with field data, this model also indicates no perched water at borehole SD-6. The modeling predictions are generally consistent with field measurements for both boreholes.

6.8.4 3-D Pneumatic Prediction

As part of the validation effort to build confidence that the calibrated property sets documented in the *AMR Calibrated Properties Model* (CRWMS M&O 2000b), a fully 3-D pneumatic simulation was performed. The results of this simulation are compared to both the pneumatic data used for the calibration and the pneumatic data for the 30 days immediately following the calibration data. Differences between the 3-D pneumatic prediction and the 1-D and 2-D calibrated pneumatic simulations (CRWMS M&O 2000b, Sections 6.1 and 6.3) were also assessed. Data from 27 instrument stations in six boreholes were then compared to the 3-D prediction.

The 3-D mesh for the TSPA flow-fields was used. This mesh is documented in *AMR Development of Numerical Grids for UZ Flow and Transport Modeling* (CRWMS M&O 1999d, pp. VI-1 to VI-7; DTN: LB990701233129.001).

The calibrated properties used for the 3-D pneumatic prediction are those developed by inversion of saturation, water potential, and pneumatic data using 1-D and 2-D models for the present-day, base-case infiltration scenario (CRWMS M&O 2000b, Sections 6.1 and 6.3; DTNs LB997141233129.001 and LB991091233129.004). Infiltration boundary conditions were the same as those documented in Section 6.1.3 for the present-day, base-case infiltration scenario. Pneumatic boundary conditions are developed using the routine TBgas3D (MOL. 19991012.0222) and atmospheric barometric pressure data from boreholes USW NRG-6 and USW NRG-7a, (YMP-LBNL-GSB-1.1.2, pp. 155-156).

The 3-D pneumatic predictions were compared to pneumatic data from six boreholes. [Table 6-35](#) shows the start and end dates for the data used to calibrate the property sets and for validation. Data from the first 30 days of each are used for the inversion, as documented in the *AMR Calibrated Properties Model* (CRWMS M&O 2000b, pp. 41 and 62). Data from the second 30 days are compared to the prediction for validation.

Table 6-35. Pneumatic Data Used for Inversion (First Thirty Days) and Validation (Last Thirty Days).

Borehole	Date/Range
UE-25 NRG#5	7/17 – 9/15/95
USW NRG-6	3/27 – 5/26/95
USW NRG-7a	3/27 – 5/26/95
USW SD-7	4/5 – 6/4/96

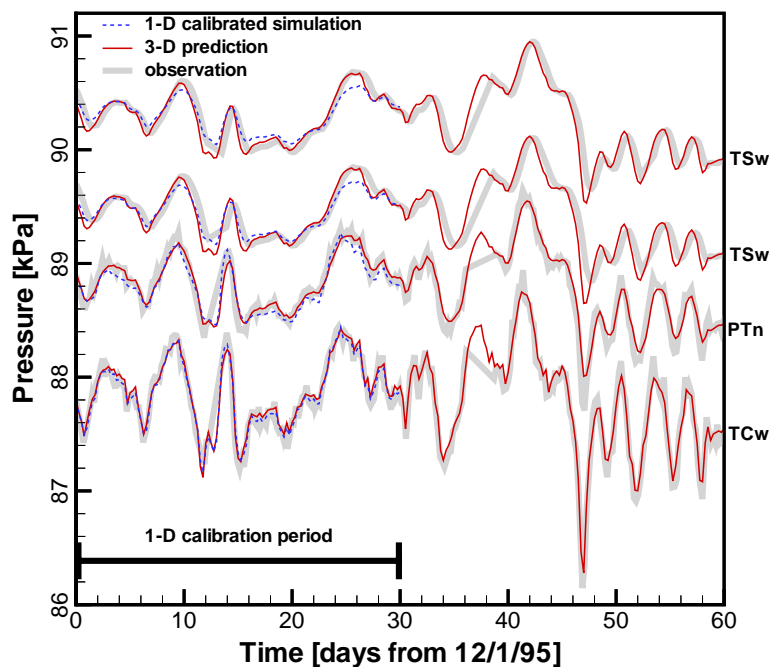
NOTE: DTNs are provided in [Table 4-1](#).

Table 6-35. Pneumatic Data Used for Inversion (First Thirty Days) and Validation (Last Thirty Days).

USW SD-12	12/1/95 – 1/29/96
USW UZ-7a	12/1/95 – 1/29/96

NOTE: DTNs are provided in Table 4-1.

Comparisons of the 3-D prediction and the data for boreholes USW SD-12 and USW UZ-7a are shown in Figures 6-69 and 6-70, respectively. Both figures show a good match between the prediction and the data. Also shown are the 1-D and 2-D calibrated simulation results documented in the AMR “*Calibrated Properties Model*” (CRWMS M&O 2000b, Figures 4 and 11). At USW SD-12, the 3-D simulation predicts a larger amplitude signal in the TSw than the calibrated 1-D simulation. This difference can be attributed to the presence of the nearby Ghost Dance fault, which has a higher permeability through the PTn than does the formation (non fault zone) rock at USW SD-12 (CRWMS M&O 2000b, Sections 6.1 and 6.3). At USW UZ-7a, in the Ghost Dance fault, the 3-D simulation predicts a slightly smaller amplitude signal in the TSw than the calibrated 2-D simulation. This difference can be attributed to lateral losses within the fault zone to the north where the PTn is thicker and thus further restricts the propagation of the barometric signal.



Observation - GS960308312232.001 Model Results - DTN: DTNs: LB991121233129.007

Figure 6-69. Comparison of 3-D Pneumatic Prediction to Data (Observation) from Borehole USW SD-12 and 1-D Calibrated Simulation.

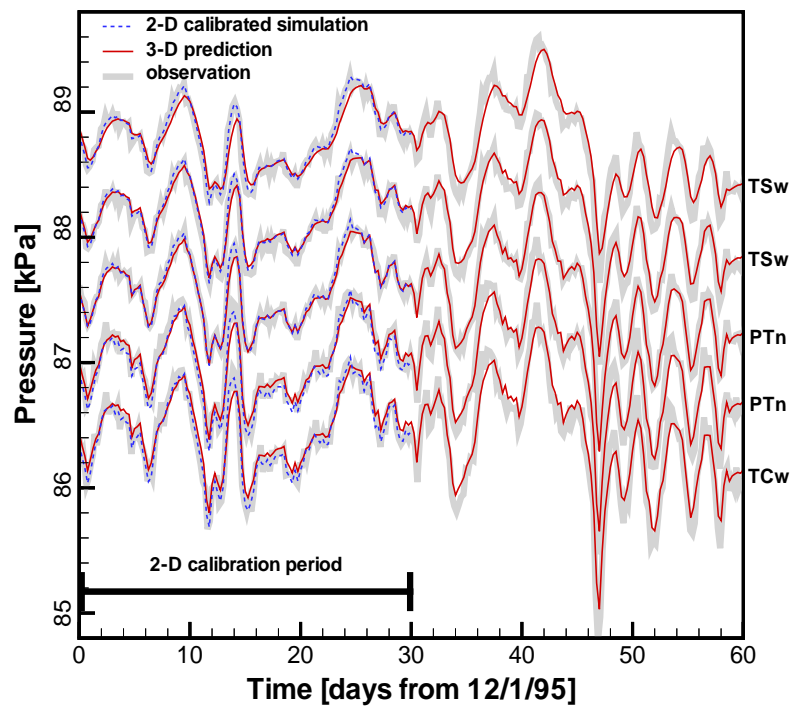


Figure 6-70. Comparison of 3-D Pneumatic Prediction to Data (Observation) from Borehole USW UZ-7a and 2-D Calibrated Simulation.

The good match between the 3-D pneumatic prediction and the pneumatic data builds confidence that the base-case infiltration-scenario calibrated properties are appropriate for gas-flow simulations. The simulations using the upper- and lower-bound infiltration-scenario calibrated properties produced results that were virtually identical to those from simulations using the base-case infiltration-scenario calibrated properties (CRWMS M&O 2000b, Section 6.1). This is not expected to change for the 3-D simulations, and thus the upper- and lower-bound infiltration-scenario calibrated properties are also appropriate for gas-flow simulations. While the comparisons of the 3-D pneumatic predictions with the 1-D and 2-D calibrated pneumatic simulations show that the assumptions of 1-D and 2-D flow (CRWMS M&O 2000b, Section 5), respectively, are not completely correct, they do show that they provide reasonable estimates of fracture permeability for the 3-D UZ Model.

INTENTIONALLY LEFT BLANK

7. CONCLUSIONS

This AMR documents the development, results, and analyses of the UZ flow model and submodels, including the:

- 3-D UZ flow calibration model
- Geothermal calibration model
- Chloride submodel
- Calcite submodel
- 3-D UZ flow model for generating 18 flow fields
- Groundwater travel and tracer transport model
- Model validation.

The UZ flow model and its submodels are developed to simulate past, present, and future hydrogeologic, geothermal, and geochemical conditions within the unsaturated zone of Yucca Mountain to support various TSPA activities. In particular, as part of the output of this AMR, 18 3-D steady-state flow fields of the Yucca Mountain UZ system have been generated for TSPA-SR calculations. This report has documented the UZ flow model and its submodels in terms of modeling approach, hydrogeological conceptual model, data source and incorporation, methodology of model calibrations, perched water parameter estimation, and model results and analysis of the 18 flow fields and associated analyses on groundwater travel times and tracer transport.

7.1 UZ FLOW MODEL CALIBRATION

As a critical step, field-measured saturation, water potential and perched water data have been used to calibrate the UZ Model. Such calibrations are part of the important iterative processes of model development in order to increase confidence in model predictions of site condition. This AMR continues the model calibration effort using the 1-D inversions reported in CRWMS M&O (2000b) and focuses on 3-D perched water calibrations using a 3-D calibration grid.

The calibration was conducted using three sets of parameters CRWMS M&O (1999d), three present-day infiltration rates, and the geological model and numerical grid for calibration (CRWMS M&O 2000b). Two water-perching models were investigated, in which rock properties were locally modified in several gridlayers near the observed perched zones. In addition, one non-perching model was also used for comparative studies.

The model calibration efforts conclude that the UZ Model can reproduce moisture conditions in the unsaturated zone of Yucca Mountain in terms of liquid saturations and water potentials, as verified by observations. In general, the modeled results from all the six calibration simulations with perched water Conceptual Models #1 and #2 are in good agreement with the measured water-perching elevations at seven boreholes with perched water occurrence for upper-bound and mean present-day infiltration scenarios. However, under the lower-bound present-day infiltration rate, the models did not match the perched water data very well in boreholes SD-7, SD-9, and UZ-14 because of the low percolation fluxes at these locations. Conceptual Model #1 is a preferred one because it has a minimum calibration and match perched water data better.

The UZ Flow model provides steady-state results of flow of fluids and heat as well as tracer transport. The steady-state results for model layers above the TSw may be subject to episodic infiltration. These model results may not reflect actual conditions; that are scale-dependent and so the results are not intended to be valid for other scales such as drift-scale studies. In this report, the uncertainties in the results due to input parameter and model gridding uncertainties are evaluated by generating a number of flow fields with various parameter sets, infiltration maps, and conceptual models. Using the dual permeability model, the matrix is represented by one gridblock which is only valid for steady-state flow according to Doughty (1999); and any others that apply to this modeling approach.

7.2 GEOTHERMAL MODEL CALIBRATION

Field-measured temperature data was used to calibrate the geothermal conditions of the UZ Model, using the base-case present-day infiltration parameter set with a 3-D ECM model. The calibration results are in good agreement with the observed temperature profiles from boreholes and provide the ambient temperature distributions for determining boundary and initial conditions for thermohydrologic models.

7.3 CHLORIDE SUBMODEL

Pore-water chemical-concentration data have been analyzed by 3-D chemical transport numerical simulations. Surface infiltration rate calibrations were performed using the pore-water Cl concentrations. Modeled results of chemical distributions were improved when using the calibrated infiltration map. In addition, an analytical method has been applied to transient transport analysis. The analytic analysis, validated by 3-D simulations under the same flow and transport conditions, was able to capture major Cl and Cl³⁶ transient transport behavior and trends. This work indicates that chemical transport studies provides an alternative interpretation by which to estimate the distribution of net infiltration. The calibration results can be important at places where a significant amount of measured pore-water chemical data are available. Additional information on infiltration, flow mechanism, and climate effects may be helpful to further investigate chemical transport in the UZ system of Yucca Mountain.

7.4 CALCITE SUBMODEL

Analysis of calcite deposition using a transport-reaction model not only gives us some constraints on hydrology, but also provides useful insights into the hydrogeochemical processes in the system. The model considers: (1) fracture-matrix interaction, (2) gaseous CO₂ diffusive transport and partitioning in liquid and gas phases, (3) ambient geothermal gradient, and (4) kinetics of fluid-rock interaction. Calcite deposition values obtained from simulations can reproduce the measured data. The calcite precipitation generally increases as percolation increases. This interconnection depends on boundary-water types and reaction rates. Calcite deposition is sensitive to boundary-water chemical composition indicated by CO₂ partial pressure. The higher the partial pressure, the lower the calcite precipitation. Calcite depth-dependent distribution varies with reaction rate. Simple mineralogy simulations considering most relevant minerals may reproduce the calcite deposition condition better than complex mineralogy simulations. A

thorough understanding of complex mineralogy may be complicated by the uncertainty of thermodynamic and kinetic data for clay minerals that are poorly known at present.

7.5 TSPA FLOW FIELDS

Eighteen 3-D UZ flow fields are generated for TSPA_SR calculations. These flow fields are based on (1) the TSPA grid CRWMS M&O (1999d), (2) nine infiltration maps representing three climates; (3) the three parameter sets in CRWMS M&O (2000b); and (4) the two conceptual models of perched water with the calibrated perched water parameters. The purpose of studying a large number of flow fields for various modeling scenarios is to cover all TSPA-SR scenarios and to account for possible current and future site conditions. The main uncertainties currently considered in the UZ Model include fracture-matrix properties, present-day and future infiltration rates over the mountain, and conceptual models for perched water occurrence.

The simulation results for 18 flow fields were checked and compared against observed matrix liquid saturation, water potential, and perched water data. In general, model results from the 18 3-D simulations were able to match observed saturation and water potential data. For calibrations with perched water data, the simulations with mean and upper infiltration rates of the three climates with both perched water conceptual models can reproduce water-perching conditions in all the observation boreholes. For lower-bound infiltration runs, the models are also able to match perched water data from most boreholes, except at SD-7 or UZ-14 boreholes (which have zero infiltration rates).

A detailed analysis of simulated percolation fluxes at the potential repository level and at the water table was conducted for 18 simulation scenarios of TSPA flow fields. These percolation fluxes and their distributions at the potential repository level indicate that there is relatively small lateral flow or diversion by the PTn unit for all the 18 simulations using both the perched water conceptual models. However, comparing simulated percolation fluxes at the potential repository level with those at the water table, using the two perched water conceptual models, we verified that perched water Conceptual Model #2 (by-passing model) predicts significant lateral flow at perched or zeolitic layers, while Conceptual Model #1 (flow-through model) predicts significantly higher vertical flow crossing perched water or zeolitic zones than Conceptual Model #2 (by-passing model).

Fracture-matrix flow components at the potential repository horizon and at the water table were also analyzed for the 18 simulation results. The statistics show that fracture flow is dominant in the welded tuffs, both at the potential repository horizon and at the water table, in all the 18 flow fields. For three present-day infiltration scenarios – fracture-matrix flow components simulated at the potential repository level – fracture flow consists of more than 80% of total flow and at the water table 70–90% of the total flow. For two future climatic scenarios, a higher percentage of fracture flow at both the potential repository (about 86–96%) and water table level (about 70–96%), compared to the case with the present-day infiltration, was predicted. At the water table, the second perched water conceptual model consistently estimates lower fracture-flow components (by 8% or more under the same infiltration).

7.6 GROUNDWATER TRAVEL TIMES AND TRACER TRANSPORT

A total of 42 tracer transport simulations were conducted to obtain insight into the various impacts of infiltration rates, perched water conceptual models, and retardation effects on tracer migration from the potential repository to the water table. All the 18 TSPA flow fields and three additional, non-perching flow simulations were incorporated into these 42 transport runs. For each flow run, there were two tracer transport runs, one for conservative or nonadsorbing and the other for reactive or adsorbing tracer transport, respectively. These tracer-transport studies indicate that there exist a wide range of groundwater travel or tracer transport times associated with different infiltration rates, type of tracers, and perched water conceptual models. The most important factors for groundwater travel/tracer-transport times are (1) surface infiltration rates and (2) adsorption effects in the CHn unit. Compared with effects from infiltration and adsorption, perched water conceptual effects are of secondary importance to the overall impact on groundwater travel/tracer-transport times, but have a primary impact on determining potential breakthrough areas of tracers at the water table.

Statistics of groundwater travel or tracer transport times at 10% and 50% mass breakthrough at the water table from the 42 simulations show that groundwater travel or tracer-transport times are inversely proportional to average surface infiltration. When an average infiltration rate increases from 5 to 35 (mm/yr), average groundwater travel (50% breakthrough) times decrease by two to three orders of magnitude. Nonadsorbing tracers migrate two orders of magnitude faster than adsorbing tracer when traveling from the potential repository to the water table under the same infiltration conditions. The non-perching conceptual model predicts the shortest travel times for both nonadsorbing and adsorbing tracers during the first 1,000 years of escape from the potential repository.

In addition, four tracer (^{36}Cl) transport simulations were performed to investigate groundwater travel and tracer transport times from the land surface to the potential repository level under steady-state flow conditions. These studies indicate the existence of possible fast flow pathways with travel times of 50 years, for groundwater to travel from the ground surface to the potential repository level. However, the cumulative mass breakthrough carried by the fast flow is relative small (1%) for the early times of 50 years. The 50% mass breakthrough times to the potential repository level since release from the surface is estimated between 5,000 to 20,000 years under the present-day, mean infiltration scenario. The fast flow breakthrough at the earlier time occurs mainly along faults.

7.7 MODEL VALIDATION

The current model validation efforts have been documented in this AMR. These activities include simulation studies of the following: (1) Alcove 1 Test; (2) ECRB observation data; (3) SD-6 and WT-24 data; and (4) 3-D gas flow. In all these cases, the results of the UZ Model can reasonably match different types of data, such as water potentials, liquid saturation, seepage rate, breakthrough concentrations, and pneumatic pressures, as observed from the mountain. These efforts have provided validation of the UZ Model and its submodels for their accuracy and reliability in describing and predicting flow and transport processes in the UZ system of Yucca Mountain.

7.8 LIMITATIONS AND UNCERTAINTIES

The UZ Model and its submodels are appropriate tools for characterizing flow and transport processes at Yucca Mountain. The accuracy and reliability of the UZ Model predictions are critically dependent on the accuracy of estimated model properties, other types of input data, and conceptual models. These models are limited mainly by the current understanding of the mountain system, including the geological and conceptual models, the volume-average modeling approach, and the available field and laboratory data.

Past site investigations have shown that large variabilities exists in the flow and transport parameters over the spatial and temporal scales of the mountain. Even though considerable progress has been made in this area, uncertainty associated with the UZ Model input parameters will continue to be a key issue for future studies. The major uncertainties in model parameters are: (1) accuracy in estimated current, past and future net-infiltration rates over the mountain; (2) quantitative descriptions of heterogeneity of welded and nonwelded tuffs, their flow properties, and detailed spatial distributions within the mountain, especially below the potential repository; (3) fracture properties in zeolitic units and faults from field studies; (4) evidence of lateral diversion caused by zeolites in the CHn units; and (5) transport properties: (e.g., adsorption or K_d coefficients in different rock types, matrix molecular diffusion coefficients in different units for different radionuclides, dispersivities in fracture and matrix systems). These uncertainties have been addressed with the modeling studies in this AMR.

This document and its conclusion may be affected by technical product input information that requires confirmation (identified as TBV in [Attachment I](#)). Any changes to the document or its conclusion that may occur as a result of completing the confirmation activities will be reflected in subsequent revisions. The status of the input information quality may be confirmed by review of the Document Input Reference System database. However, the results and conclusions of the UZ flow fields will not be affected by the status of temperature and geochemistry data used in the calibration studies, because these flow fields are based on flow simulations under isothermal and different climate conditions.

INTENTIONALLY LEFT BLANK

8. REFERENCES

8.1 DOCUMENTS CITED

- Bodvarsson, G.S.; Boyle, W.; Patterson, R.; and Williams, D. 1999. "Overview of Scientific Investigations at Yucca Mountain—the Potential Repository for High-Level Nuclear Waste." *Journal Of Contaminant Hydrology* 38 (1–3), 3–24. Amsterdam, The Netherlands: Elsevier Science Publishers. TIC: 244160.
- CRWMS M&O (Civilian Radioactive Waste Management System, Management & Operating Contractor) 1999a. *Analysis & Modeling Development Plan (DP) for U0050, UZ Flow Models and Submodels, Rev. 00*. TDP-NBS-HS-000011. Las Vegas, Nevada: CRWMS M&O. ACC: MOL.19991013.0353.
- CRWMS M&O 1999b. *M&O Site Investigations*. Activity Evaluation, January 23, 1999. Las Vegas, Nevada: CRWMS M&O. ACC: MOL.19990317.0330.
- CRWMS M&O 1999c. *M&O Site Investigations*. Activity Evaluation, September 28, 1999. Las Vegas, Nevada: CRWMS M&O. ACC: MOL.19990928.0224.
- CRWMS M&O 1999d. *Development of Numerical Grids for UZ Flow and Transport Modeling*. ANL-NBS-HS-000015. Las Vegas, Nevada: CRWMS M&O. ACC: MOL.19990721.0517.
- CRWMS M&O 2000a. *Analysis of Geochemistry Data for the Unsaturated Zone*. ANL-NBS-HS-000017. Las Vegas, Nevada: CRWMS M&O. URN-0048.
- CRWMS M&O 2000b. *Calibrated Properties Model*. MDL-NBS-HS-000003. Las Vegas, Nevada: CRWMS M&O. ACC: 19990720.0520.
- CRWMS M&O 2000c. *Conceptual and Numerical Model for the Unsaturated Zone Flow and Transport*. MDL-NBS-HS-000005. Las Vegas, Nevada: CRWMS M&O. ACC: MOL.19990721.0526.
- CRWMS M&O 2000d *Drift-Scale Coupled Processes (DST, THC Seepage) Models*. MDL-NBS-HS-000001. Las Vegas, Nevada: CRWMS M&O ACC: MOL.19990721.0523.
- CRWMS M&O 2000e. *Repository Safety Strategy: Plan to Prepare the Postclosure Safety Case to Support Yucca Mountain Site recommendation and Licensing Considerations*. TDR-WIS-RL-000001 REV. 3. Las Vegas, Nevada: CRWMS M&O. ACC: MOL.20000119.0189.
- CRWMS M&O 2000f. *Analyses of Hydrologic Properties Data*. ANL-NBS-HS-000002. Las Vegas, Nevada: CRWMS M&O URN-0057.
- Domenico, P.A. and Schwartz, F.W. 1990. *Physical and Chemical Hydrogeology*. New York, New York: John Wiley and Sons. TIC: 234782.
- Doughty, C. 1999. "Investigation of Conceptual and Numerical Approaches for Evaluating Moisture, Gas, Chemical, and Heat Transport in Fractured Unsaturated Rock." *Journal of*

Contaminant Hydrology 38 (1-3), 69-106. Amsterdam, The Netherlands: Elsevier Science Publishers. TIC: 244160.

Driscoll, Fletcher G. 1986. *Groundwater and Wells*, 2nd Edition. St. Paul, Minnesota: Johnson Filtration Systems. TIC: 225919.

Dyer, J.R. 1999. "Revised Interim Guidance Pending Issuance of New U.S. Nuclear Regulatory Commission (NRC) Regulations (Revision 01, July 22, 1999), for Yucca Mountain, Nevada." Letter from J.R. Dyer (DOE) to D.R. Wilkins (CRWMS M&O), September 9, 1999, OL&RC:SB-1714, with enclosure, "Interim Guidance Pending Issuance of New U.S. Nuclear Regulatory Commission (NRC) Regulations (Revision 01)." ACC: MOL.19990910.0079.

Flint, A.L. and Flint, L.E. 1994. "Spatial Distribution of Potential Near Surface Moisture Flux at Yucca Mountain." *Proceedings of the Fifth Annual International Conference on High Level Radioactive Waste Management, 4, Las Vegas, Nevada, May 22–26, 1994*, 2352–2358. La Grange Park, Illinois: American Nuclear Society. TIC: 224142.

Flint, L.E. 1998. *Characterization of Hydrogeologic Units Using Matrix Properties, Yucca Mountain, Nevada*. Water-Resources Investigations Report 97-4243. Denver, Colorado: U.S. Geological Survey. ACC: MOL.19980429.0512.

Francis, N.D. 1997. "The Base-Case Thermal Properties for TSPA-VA Modeling." Memo from N.D. Francis (SNL) to Distribution, April 16, 1997. Albuquerque, New Mexico: Sandia National Laboratories. ACC: MOL.19980518.0229.

Hevesi, J.A.; Flint, A.L.; and Istock, J.D. 1992. "Precipitation Estimation in Mountainous Terrain Using Multivariate Geostatistics, Part II: Isohyetal Maps." *Journal of Applied Meteorology*, 31, 677–688. Boston, Massachusetts: American Meteorological Society. TIC: 225248.

Javandel, I.; Doughty, C.; and Tsang, C.F. 1984. "Groundwater Transport: Handbook of Mathematical Models." *Water Resources Monograph*, 10. Washington, D.C.: American Geophysical Union. TIC: 209908.

Lasaga, A.C. 1998. *Kinetic Theory in the Earth Sciences*. Princeton, New Jersey: Princeton University Press. TIC: 246279.

Liu, H.H.; Doughty, C.; and Bodvarsson, G.S. 1998. "An Active Fracture Model for Unsaturated Flow and Transport in Fractured Rocks." *Water Resources Research* 34 (10), 2633-2646. Washington, D.C.: American Geophysical Union. TIC: 243012.

Montazer, P. and Wilson, W.E. 1984. *Conceptual Hydrologic Model of Flow in the Unsaturated Zone, Yucca Mountain, Nevada*. Water Resources Investigations Report 84-4345. Denver, Colorado: U.S. Geological Survey. TIC: 203223.

Pruess, K. and Narasimhan, T.N. 1985. "A Practical Method for Modeling Fluid and Heat Flow in Fractured Porous Media." *Society of Petroleum Engineers Journal*, 25 (1), 14–26. Dallas, Texas: Society of Petroleum Engineers. TIC: 221917.

Pruess, K. 1991. *"TOUGH2, a General-Purpose Numerical Simulator for Multiphase Fluid and Heat Flow."* Report LBL-29400. Berkeley, California: Lawrence Berkeley National Laboratory. ACC: NNA.19940202.0088.

Pruess, K.; Faybishenko, B.; and Bodvarsson, G.S. 1999. "Alternative Concepts and Approaches for Modeling Flow and Transport in Thick Unsaturated Zones of Fractured Rocks." *Journal of Contaminant Hydrology* (38) 1–3, 281–322. Amsterdam, The Netherlands: Elsevier Science Publishers. TIC: 244160.

Sass, J.H.; Lachenbruch, A.H.; Dudley, W.W., Jr.; Priest, S.S.; and Munroe, R.J. 1988. *Temperature, Thermal Conductivity and Heat Flow Near Yucca Mountain, Nevada: Some Tectonic and Hydrologic Implications.* Open File Rep. 87-649. Denver, Colorado: U.S. Geological Survey. TIC: 203195.

Sonnenthal, E. L. and Bodvarsson, G. S. 1999. "Constraints on the Hydrology of the Unsaturated Zone at Yucca Mountain, NV from Three-Dimensional Models of Chloride and Strontium Geochemistry." *Journal of Contaminant Hydrology* 38 (1–3), 107–156. Amsterdam, Netherlands: Elsevier Science Publishers. TIC: 244160.

Steeffel, C.I. and Lichtner, P.C. 1998. "Multicomponent Reactive Transport in Discrete Fractures: II: Infiltration of Hyperalkaline Groundwater at Maqarin, Jordan, a Natural Analogue Site." *Journal of Hydrology*, 209, 200–224. Amsterdam, The Netherlands: Elsevier Science Publishers. TIC: applied for.

Tyler, S.W.; Chapman, J.B.; Conrad, S.H.; Hammermeister, D.P.; Blout, D.O.; Miller, J.J.; Sully, M.J.; and Ginanni, J.M. 1996. "Soil-Water Flux in the Southern Great Basin, United States: Temporal and Spatial Variations over the Last 120,000 Years." *Water Resources Research* 32 (6), 1481–1499. Washington, DC: American Geophysical Union. TIC: 235938.

van Genuchten, M. 1980. "A Closed-Form Equation for Predicting the Hydraulic Conductivity of Unsaturated Soils." *Soil Science Society of America Journal*, 44 (5), 892–898. Madison, Wisconsin: Soil Science Society of America. TIC: 217327.

Wemheuer, R.F. 1999. "First Issue of FY00 NEPO QAP-2-0 Activity Evaluations." Interoffice correspondence from R.F. Wemheuer (CRWMS M&O) to R.A. Morgan (CRWMS M&O), October 1, 1999, LV.NEPO.RTPS.TAG.10/99-155, with attachments, Activity Evaluation for Work Package #1401213UM1. ACC: MOL.19991028.0162.

Wu, Y.S.; Ahlers, C.F.; Fraser, P.; Simmons, A.; and Pruess, K. 1996. *Software Qualification of Selected TOUGH2 Modules.* Report LBNL-39490, UC-800. Berkeley, California: Lawrence Berkeley National Laboratory. ACC: MOL.19970219.0104.

Wu, Y.S.; Haukwa, C. and Bodvarsson, G.S. 1999a. "A Site-Scale Model for Fluid and Heat Flow in the Unsaturated Zone of Yucca Mountain, Nevada." *Journal of Contaminant Hydrology* 38 (1–3), 185–215. Amsterdam, The Netherlands: Elsevier Science Publishers. TIC: 244160.

Wu, Y.S.; Ritcey, A.C. and Bodvarsson, G.S. 1999b. "A Modeling Study of Perched Water Phenomena in the Unsaturated Zone at Yucca Mountain." *Journal of Contaminant Hydrology* 38 (1-3), 157-184. Amsterdam, The Netherlands: Elsevier Science Publishers. TIC: 244160.

Yang, I.C.; Yu, P.; Rattray, G.W.; Ferarese, J.S.; Rayn, J.N. 1998. *Hydrochemical Investigations in Characterizing the Unsaturated Zone at Yucca Mountain, Nevada*. Water Resources Investigation Report 98-4132. Denver, Colorado: U.S. Geological Survey. TIC: 243710.

Software Cited:

Software Code: EARTHVISION V4.0. STN: 30035-2 V4.0.

Software Code: EXT V1.0_MEOS9. STN: 10227-1.0MEOS9-00.

Software Code: infil2grd V1.6. STN: 10077-1.6-00.

Software Code: ITOUGH2 V3.2. STN: 10054-3.2-00

Software Code: T2R3D V1.4. STN: 10006-1.4-00.

Software Code: TOUGH2 V1.4. STN: 10007-1.4-00.

Software Code: TOUGHREACT V2.2. STN: 10154-2.2-00.

Software Code: TOUGHREACTE9 V1.0. STN: 10153-1.0-00.

Software Routine: ECRB-XYZ V03. STN: 30093-V.03.

Software Routine: TBgas3D V1.1. ACC: MOL.19991012.0222.

Software Routine: Read_TDB V1.0. ACC: MOL.19990903.0031.

Software Routine: Frac_Calc V1.1. ACC: MOL.19990903.0032.

8.2 CODES, STANDARDS, REGULATIONS, AND PROCEDURES

AP-3.10Q, Rev. 1, ICN 1. *Analyses and Models*. Washington, D.C.: U.S. Department of Energy, Office of Civilian Radioactive Waste Management. ACC: MOL.19991019.0467.

AP-SI.1Q, Rev. 1, ICN 0. *Software Management*. Las Vegas, Nevada: CRWMS M&O. ACC: MOL.19990630.0395.

DOE 1999. *Quality Assurance Requirements and Description*. DOE/RW-0333P, REV 9. Washington D.C.: DOE OCRWM. ACC: MOL.19991028.0012.

QAP-2-0, Rev. 5. *Conduct of Activities*. Las Vegas, Nevada: CRWMS M&O. ACC: MOL.19980826.0209.

8.3 SOURCE DATA, LISTED BY DATA TRACKING NUMBER

GS000399991221.002. *Rainfall/Runoff/Runon 1999 Simulations.*

GS000399991221.003. *Preliminary Alcove 1 Infiltration Experiment Data.*

GS000399991221.004. *Preliminary Developed Matrix Properties.*

GS910908315214.003. Meteorological, Stream-Discharge, and Water-Quality Data for 1986 through 1991 from Two Small Basins in Central Nevada. Submittal date: 09/04/1991. Initial use.

GS931008315214.032 Meteorological, Stream-Discharge, and Water-Quality Data for Water Year 1992 from Two Small Basins in Central Nevada. Submittal date: 10/08/1993. Initial use.

GS950208312232.003. Data, including Water Potential, Pressure and Temperature, Collected from Boreholes USW NRG-6 and USW NRG -7a from Instrumentation through March 31, 1995. Submittal date: 02/13/1995.

GS951108312232.008. Data, including Water Potential, Pressure and Temperature, Collected from Boreholes UE-25 UZ#4 & UZ#5 from Instrumentation through September 30, 1995, and from USW NRG-6 & NRG-7a from April 1 through September 30, 1995. Submittal date: 11/21/1995.

GS960208312261.001. Shut-in Pressure Test Data from April 1995 to December 1995 from Select Wells and Boreholes at Yucca Mountain, NV. Submittal date: 02/07/1996.

GS960308312232.001. Deep Unsaturated Zone Surface-Based Borehole Instrumentation Program Data from Boreholes USW NRG-7A, USW NRG-6, UE-25 UZ#4, UE-25 UZ#5, USW UZ-7A, and USW SD-12 for the Time Period 10/01/95 through 3/31/96. Submittal date: 04/04/1996.

GS960308312312.005. Water-Level, Discharge Rate and Related Data from the Pump Tests Conducted at Well USW UZ-14, August 17 through August 30, 1993. Submittal date: 03/15/1996.

GS960808312232.004. Deep Unsaturated Zone Surface-Based Borehole Instrumentation Program Data for Boreholes USW NRG-7A, USW NRG-6, UE-25, UZ#4, UE-25 UZ#5, USW UZ-7A and USW SD-12 for the Time Period 4/1/96 through 8/15/96. Submittal date: 08/30/1996.

GS960908312231.004. Characterization of Hydrogeologic Units Using Matrix Properties at Yucca Mountain, Nevada. Submittal date: 09/12/1996.

GS960908312232.006. In-Situ Pneumatic Tests of Boreholes. Submittal Date: 09/18/1996.

GS960908312261.004. Shut-In Pressure Test Data from UE-25 NRG#5 And USW SD-7 from November 1995 to July 1996. Submittal date: 09/24/1996.

GS961108312261.006. Gas Chemistry, ESF Alcoves 2 and 3, 11/95 - 4/96; Water Chemistry, Alcove 2 (Tritium), Alcove 3, and ESF Tunnel; and Pneumatic Pressure Response from Boreholes in Exploratory Studies Facility Alcoves 2 and 3, 10/95 - 5/96. Submittal date: 11/12/1996.

GS970108312232.002. Deep Unsaturated Zone, Surface-Based Borehole Instrumentation Program - Raw Data Submittal For Boreholes USW NRG-7A, USW NRG-6, UE-25 UZ#4, UE-25 UZ#5, USW UZ-7A, and USW SD-12, for the Period 8/16/96 through 12/31/96. Submittal date: 01/22/1997.

GS970208312312.003. Water-Level and Related Data from Pump Tests Conducted at Well USW G-2, 4/8/96 - 12/17/96. Submittal date: 02/05/1997.

GS970808312232.005. Deep Unsaturated Zone Surface-Based Borehole Instrumentation Program Data from Boreholes USW NRG-7A, UE-25 UZ#4, UE-25 UZ#5, USW UZ-7A and USW SD-12 for the Time Period 1/1/97 - 6/30/97. Submittal date: 08/28/1997.

GS971108312232.007. Deep Unsaturated Zone Surface-Based Borehole Instrumentation Program Data from Boreholes USW NRG-7A, UE-25 UZ #4, UE-25 UZ #5, USW UZ-7A and USW SD-12 for the Time Period 7/1/97 - 9/30/97. Submittal date: 11/18/1997.

GS971108314224.020. Revision 1 of Detailed Line Survey Data, Station 0+60 to Station 4+00, North Ramp Starter Tunnel, Exploratory Studies Facility. Submittal date: 12/03/1997.

GS980408312232.001. Deep Unsaturated Zone Surface-Based Borehole Instrumentation Program Data From Boreholes USW NRG-7A, UE-25 UZ #4, USW NRG-6, UE-25 UZ #5, USW UZ-7A and USW SD-12 for the Time Period 10/01/97 - 03/31/98. Submittal date: 04/16/1998.

GS980508312313.001. Water-Level and Related Data Collected in Support of Perched-Water Testing in Borehole USW WT-24, September 10, 1997 through February 3, 1998. Submittal date: 05/07/1998.

GS980708312242.010. Physical Properties of Borehole Core Samples, and Water Potential Measurements Using the Filter Paper Technique, for Borehole Samples from USW WT-24. Submittal date: 07/27/1998.

GS980808312242.014. Physical Properties of Borehole Core Samples and Water Potential Measurements Using the Filter Paper Technique for Borehole Samples from USW SD-6. Submittal date: 08/11/1998.

GS980908312242.036. Water Potentials Measured With Heat Dissipation Probes in ECRB Holes from 4/23/98 to 7/31/98. Submittal date: 09/22/1998.

GS981008312313.003. Manually Measured Water-Level Data from Borehole USW G-2 on 02/03/98, Collected in Support of Perched-Water Testing in Borehole USW WT-24. Submittal date: 10/20/1998.

LAIT831341AQ96.001. Radionuclide Retardation. Measurements of Batch Sorption Distribution Coefficients for Barium, Cesium, Selenium, Strontium, Uranium, Plutonium, and Neptunium. Submittal date: 11/12/1996.

LASL831151AQ98.001. Mineralogic Characterization of the ESF Single Heater Test Block. Submittal date: 08/31/1998.

LASL831222AQ98.002. Mineralogic Data Chlorine-36 Studies. Submittal date: 09/10/1998.

LA9908JC831321.001. Mineralogic Model "MM3.0" Version 3.0. Submittal Date: 08/16/1999.

LB971212001254.006. Three Files Using DKM Weeps Parameter Sets with Mean Fracture Permeability, Present Day Infiltration, and Estimated Global FMX for Present Day and Long Term Average and Superpluvial Infiltration. Submittal date: 12/12/1997.

LB980912332245.002. Gas Tracer Data from Niche 3107 of the ESF. Submittal date: 09/30/1998.

LB990501233129.001. Fracture Properties for the UZ Model Grids and Uncalibrated Fracture and Matrix Properties for the UZ Model Layers for AMR U0090, "Analysis of Hydrologic Properties Data." Submittal date: 08/25/1999.

LB990501233129.002. 1-D Grids For Hydrogeologic Property Set Inversions and Calibrations for AMR U0000, "Development of Numerical Grids For UZ Flow and Transport Modeling." Submittal date: 09/24/1999.

LB990501233129.004. 3-D UZ Model Calibration Grids for AMR U0000, "Development of Numerical Grids of UZ Flow and Transport Modeling." Submittal date: 09/24/1999.

LB990701233129.001. 3-D UZ Model Grids for Calculation of Flow Fields for PA for AMR U0000, "Development of Numerical Grids for UZ Flow and Transport Modeling." Submittal date: 09/24/1999.

LB990701233129.002. 3-D UZ Model Calibration Grid for Calculation of Flow Fields using #3 Perched Water Conceptual Model (Non-Perched Water Model). Submittal date: Will be submitted with AMR.

LB991091233129.003. Two-Dimensional Fault Calibration For AMR U0035, "Calibrated Properties Model." Submittal date: 10/22/1999.

LB991091233129.004. Calibrated Fault Properties for the UZ Flow and Transport Model for AMR U0035, "Calibrated Properties Model." Submittal date: 10/22/1999.

LB991121233129.001. Calibrated parameters for the present-day, mean infiltration scenario, used for simulations with perched water conceptual model #1 (flow through) for the mean infiltration scenarios of the present-day, Monsoon and Glacial transition climates. Submittal date: will be submitted with AMR.

LB991121233129.002. Calibrated parameters for the present-day, mean infiltration scenario, used for simulations with perched water conceptual model #2 (by passing) for the mean infiltration scenarios of the present-day, Monsoon and Glacial transition climates. Submittal date: will be submitted with AMR.

LB991121233129.003. Calibrated parameters for the present-day, upper-bound infiltration scenario, used for simulations with perched water conceptual model #1 (flow through) for the upper-bound infiltration scenarios of the present-day, Monsoon and Glacial transition climates. Submittal date: will be submitted with AMR.

LB991121233129.004. Calibrated parameters for the present-day, upper-bound infiltration scenario, used for simulations with perched water conceptual model #2 (by passing) for the upper-bound infiltration scenarios of the present-day, Monsoon and Glacial transition climates. Submittal date: will be submitted with AMR.

LB991121233129.005. Calibrated parameters for the present-day, lower-bound infiltration scenario, used for simulations with perched water conceptual model #1 (flow through) for the lower-bound infiltration scenarios of the present-day, Monsoon and Glacial transition climates. Submittal date: will be submitted with AMR.

LB991121233129.006. Calibrated parameters for the present-day, lower-bound infiltration scenario, used for simulations with perched water conceptual model #2 (by passing) for the lower-bound infiltration scenarios of the present-day, Monsoon and Glacial transition climates. Submittal date: will be submitted with AMR.

LB991121233129.007. Calibrated parameters for the present-day, mean infiltration scenario, used for simulations with perched water conceptual model #3 (non-perching) for the mean infiltration scenarios of the present-day, Monsoon and Glacial transition climates. Submittal date: will be submitted with AMR.

LB991200DSTTHC.001. Pore water composition and CO₂ partial pressure input to Thermal-Hydrological-Chemical (THC) simulations: Table 3 of AMR N0120/U0110, "Drift-Scale Coupled Processes (DST and TH Seepage) Models." Submittal date: will be submitted with AMR.

LB997141233129.001. Calibrated Basecase Infiltration 1-D Parameter Set for the UZ Flow and Transport Model, FY99. Submittal date: 07/21/1999.

LB997141233129.002. Calibrated Upper-Bound Infiltration 1-D Parameter Set for the UZ Flow and Transport Model, FY99. Submittal date: 07/21/1999.

LB997141233129.003. Calibrated Lower-Bound Infiltration 1-D Parameter Set for the UZ Flow and Transport Model, FY99. Submittal date: 07/21/1999.

8.4 OUTPUT DATA, LISTED BY DATA TRACKING NUMBER

LB9908T1233129.001. Transport Simulations for mean, low, and upper infiltration maps from AMR U0050. Submittal date: will be submitted with AMR.

LB990801233129.001. TSPA Grid Flow Simulations for AMR U0050, "UZ Flow Models and Submodels." Flow Field #1: Present Day Low Infiltration Map for Flow-Through Perched-Water Conceptual Model. Submittal date: will be submitted with AMR.

LB990801233129.002. TSPA Grid Flow Simulations for AMR U0050, "UZ Flow Models and Submodels." Flow Field #2: Present Day Low Infiltration Map for Unfractured Zeolite Perched-Water Conceptual Model. Submittal date: will be submitted with AMR.

LB990801233129.003. TSPA Grid Flow Simulations for AMR U0050, "UZ Flow Models and Submodels." Flow Field #3: Present Day Mean Infiltration Map for Flow-Through Perched-Water Conceptual Model. Submittal date: will be submitted with AMR.

LB990801233129.004. TSPA Grid Flow Simulations for AMR U0050, "UZ Flow Models and Submodels." Flow Field #4: Present Day Mean Infiltration Map for Unfractures Zeolite Perched-Water Conceptual Model. Submittal date: will be submitted with AMR.

LB990801233129.005. TSPA Grid Flow Simulations for AMR U0050, "UZ Flow Models and Submodels." Flow Field #5: Present Day Upper Infiltration Map for Flow-Through Perched-Water Conceptual Model. Submittal date: will be submitted with AMR.

LB990801233129.006. TSPA Grid Flow Simulations for AMR U0050, "UZ Flow Models and Submodels." Flow Field #6: Present Day Upper Infiltration Map for Unfractured Zeolite Perched-Water Conceptual Model. Submittal date: will be submitted with AMR.

LB990801233129.007. TSPA Grid Flow Simulations for AMR U0050, "UZ Flow Models and Submodels." Flow Field #7: Glacial Low Infiltration Map for Flow-Through Perched-Water Conceptual Model. Submittal date: will be submitted with AMR.

LB990801233129.008. TSPA Grid Flow Simulations for AMR U0050, "UZ Flow Models and Submodels." Flow Field #8: Glacial Low Infiltration Map for Unfractured Zeolite Perched-Water Conceptual Model. Submittal date: will be submitted with AMR.

LB990801233129.009. TSPA Grid Flow Simulations for AMR U0050, "UZ Flow Models and Submodels." Flow Field #9: Glacial Mean Infiltration Map for Flow-Through Perched-Water Conceptual Model. Submittal date: will be submitted with AMR.

LB990801233129.010. TSPA Grid Flow Simulations for AMR U0050, "UZ Flow Models and Submodels." Flow Field #10: Glacial Mean Infiltration Map for Unfractured Zeolite Perched-Water Conceptual Model. Submittal date: will be submitted with AMR.

LB990801233129.011. TSPA Grid Flow Simulations for AMR U0050, "UZ Flow Models and Submodels." Flow Field #11: Glacial Upper Infiltration Map for Flow-Through Perched-Water Conceptual Model. Submittal date: will be submitted with AMR.

LB990801233129.012. TSPA Grid Flow Simulations for AMR U0050, "UZ Flow Models and Submodels." Flow Field #12: Glacial Upper Infiltration Map for Unfractured Zeolite Perched-Water Conceptual Model. Submittal date: will be submitted with AMR.

LB990801233129.013. TSPA Grid Flow Simulations for AMR U0050, "UZ Flow Models and Submodels." Flow Field #13: Monsoon Low Infiltration Map for Flow-Through Perched-Water Conceptual Model. Submittal date: will be submitted with AMR.

LB990801233129.014. TSPA Grid Flow Simulations for AMR U0050, "UZ Flow Models and Submodels." Flow Field #14: Monsoon Low Infiltration Map for Unfractured Zeolite Perched-Water Conceptual Model. Submittal date: will be submitted with AMR.

LB990801233129.015. TSPA Grid Flow Simulations for AMR U0050, "UZ Flow Models and Submodels." Flow Field #15: Monsoon Mean Infiltration Map for Flow-Through Perched-Water Model. Submittal date: will be submitted with AMR.

LB990801233129.016. TSPA Grid Flow Simulations for AMR U0050, "UZ Flow Models and Submodels." Flow Field #16: Monsoon Mean Infiltration Map for Unfractured Zeolite Perched-Water Conceptual Model. Submittal date: will be submitted with AMR.

LB990801233129.017. TSPA Grid Flow Simulations for AMR U0050, "UZ Flow Models and Submodels." Flow Field #17: Monsoon Upper Infiltration Map for Flow-Through Perched-Water Conceptual Model. Submittal date: will be submitted with AMR.

LB990801233129.018. TSPA Grid Flow Simulations for AMR U0050, "UZ Flow Models and Submodels." Flow Field #18: Monsoon Upper Infiltration Map for Unfractured Zeolite Perched-Water Conceptual Model. Submittal date: will be submitted with AMR.

LB990801233129.019. Present day mean infiltration map; #3 or non-perched water model. Submittal date: will be submitted with AMR.

LB990801233129.020. Monsoon mean infiltration map; #3 or non-perched water model. Submittal date: will be submitted with AMR.

LB990801233129.021. Glacial mean infiltration map; #3 or non-perched water model. Submittal date: will be submitted with AMR.

LB990801233129.022. Present day mean infiltration map; #3 non-perched water model. Submittal date: will be submitted with AMR.

LB990801233129.023. Present day low infiltration map; #1 perched water conceptual model. Submittal date: will be submitted with AMR.

LB990801233129.024. Present day low infiltration map; #2 perched water conceptual model. Submittal date: will be submitted with AMR.

LB990801233129.025. Present day mean infiltration map; #1 perched water conceptual model. Submittal date: will be submitted with AMR.

LB990801233129.026. Present day mean infiltration map; #2 perched water conceptual model. Submittal date: will be submitted with AMR.

LB990801233129.027. Present day upper infiltration map; #1 perched water conceptual model. Submittal date: will be submitted with AMR.

LB990801233129.028. Present day upper infiltration map; #2perched water conceptual model. Submittal date: will be submitted with AMR.

LB991131233129.001. Modeling calcite deposition and percolation. Submittal date: will be submitted with AMR.

LB991131233129.002. Modeling seepage and tracer tests at Alcove 1. Submittal date: will be submitted with AMR.

LB991131233129.003. Analytical and Simulation Results of Cl and Cl36 Analysis. Submittal date: will be submitted with AMR.

LB991131233129.004. Modeling of Thermo-Hydrological Data to Simulate Flow, Transport, and Geothermal Conditions of the UZ. Submittal date: will be submitted with AMR.

INTENTIONALLY LEFT BLANK

9. ATTACHMENTS

Attachment I - Document Input References Sheet

Attachment II - Calibrated parameter sets, combining from one-dimensional inversions and three-dimensional perched water modeling, used in generating the 18 flow fields, groundwater travel and tracer transport times

Attachment III - Software Routines

INTENTIONALLY LEFT BLANK

ATTACHMENT I-DOCUMENT INPUT REFERENCE SHEET

DIRS as of the issue date of this AMR. Refer to the DIRS database for the current status of these inputs

OFFICE OF CIVILIAN RADIOACTIVE WASTE MANAGEMENT DOCUMENT INPUT REFERENCE SYSTEM									
1. Document Identifier No./Rev.: MDL-NBS-HS-000006/Rev. 00			Change: <i>924 4/700</i> N/A	Title: UZ Flow Models and Submodels					
Input Document			4. Input Status	5. Section Used in	6. Input Description	7. TBV/TBD Priority	8. TBV Due To		
2. Technical Product Input Source Title and Identifier(s) with Version		3. Section					Unqual.	From Uncontrolled Source	Un-confirmed
2a									
1.	DTN: GS000399991221.002. <i>Rainfall/Runoff/Runon 1999 Simulations.</i>	base-case, present day simulation	N/A- Qualification Level 2	6.1 6.2 6.3 6.6 6.7, 6.8.2, 6.8.3	Top boundary condition for modeling	N/A	N/A	N/A	N/A
2.	DTN: GS000399991221.002. <i>Rainfall/Runoff/Runon 1999 Simulations.</i>	lower bound, present day simulation	N/A- Qualification Level 2	6.1 6.2 6.6 6.7	Top boundary condition for modeling	N/A	N/A	N/A	N/A
3.	DTN: GS000399991221.002. <i>Rainfall/Runoff/Runon 1999 Simulations.</i>	upper bound, present day simulation	N/A- Qualification Level 2	6.1 6.2 6.6 6.7	Top boundary condition for modeling	N/A	N/A	N/A	N/A
4.	DTN: GS000399991221.002. <i>Rainfall/Runoff/Runon 1999 Simulations.</i>	base-case, future monsoon simulation	N/A- Qualification Level 2	6.1 6.6 6.7	Top boundary condition for modeling	N/A	N/A	N/A	N/A

OFFICE OF CIVILIAN RADIOACTIVE WASTE MANAGEMENT DOCUMENT INPUT REFERENCE SYSTEM									
1. Document Identifier No./Rev.: MDL-NBS-HS-000006/Rev. 00			Change: N/A	Title: UZ Flow Models and Submodels					
Input Document			4. Input Status	5. Section Used in	6. Input Description	7. TBV/TBD Priority	8. TBV Due To		
2. Technical Product Input Source Title and Identifier(s) with Version		3. Section					Unqual.	From Uncontrolled Source	Un-confirmed
2a									
5.	DTN: GS000399991221.002. Rainfall/Runoff/Runon 1999 Simulations.	lower bound, future monsoon simulation	N/A- Qualification Level 2	6.1 6.6 6.7	Top boundary condition for modeling	N/A	N/A	N/A	N/A
6.	DTN: GS000399991221.002. Rainfall/Runoff/Runon 1999 Simulations.	upper bound, future monsoon simulation	N/A- Qualification Level 2	6.1 6.6 6.7	Top boundary condition for modeling	N/A	N/A	N/A	N/A
7.	DTN: GS000399991221.002. Rainfall/Runoff/Runon 1999 Simulations.	Base-case, future glacial transition simulation	N/A- Qualification Level 2	6.1 6.6 6.7	Top boundary condition for modeling	N/A	N/A	N/A	N/A
8.	DTN: GS000399991221.002. Rainfall/Runoff/Runon 1999 Simulations.	Lower bound, future glacial transition simulation	N/A- Qualification Level 2	6.1 6.6 6.7	Top boundary condition for modeling	N/A	N/A	N/A	N/A
9.	DTN: GS000399991221.002. Rainfall/Runoff/Runon 1999 Simulations.	Upper bound, future glacial transition simulation	N/A- Qualification Level 2	6.1 6.6 6.7	Top boundary condition for modeling	N/A	N/A	N/A	N/A

OFFICE OF CIVILIAN RADIOACTIVE WASTE MANAGEMENT DOCUMENT INPUT REFERENCE SYSTEM									
1. Document Identifier No./Rev.: MDL-NBS-HS-000006/Rev. 00			Change: N/A	Title: UZ Flow Models and Submodels					
Input Document		3. Section	4. Input Status	5. Section Used in	6. Input Description	7. TBV/TBD Priority	8. TBV Due To		
2. Technical Product Input Source Title and Identifier(s) with Version							Unqual.	From Uncontrolled Source	Un-confirmed
2a									
10.	DTN: GS000399991221.003. <i>Preliminary Alcove 1 Infiltration Experiment Data.</i>	Entire	N/A- Qualification Level 2	6.8.1	Alcove 1 infiltration and tracer test data	N/A	N/A	N/A	N/A
11.	DTN: GS000399991221.004. <i>Preliminary Developed Matrix Properties.</i>	Entire	N/A- Qualification Level 2	6.1 6.2 6.6	Saturation data from cores for borcholes USW SD-7, USW SD-9, USW SD-12, USW UZ-14, UE-25 UZ#16 & USW UZ-7a	N/A	N/A	N/A	N/A
12.	DTN: GS910908315214.003. Meteorological, Stream-Discharge, and Water-Quality Data for 1986 through 1991 from Two Small Basins in Central Nevada. Submittal date: 09/04/1991. Initial use.	Entire	TBV-3608	6.4.4.3	SO ₂ infiltration flux	1	✓	N/A	N/A
13.	DTN: GS931008315214.032 Meteorological, Stream-Discharge, and Water-Quality Data for Water Year 1992 from Two Small Basins in Central Nevada. Submittal date: 10/08/1993. Initial use.	Entire	TBV-3609	6.4.4.3	SO ₂ infiltration flux	1	N/A	N/A	✓

284 4/7/00

OFFICE OF CIVILIAN RADIOACTIVE WASTE MANAGEMENT DOCUMENT INPUT REFERENCE SYSTEM									
1. Document Identifier No./Rev.: MDL-NBS-HS-000006/Rev. 00		Change: N/A		Title: UZ Flow Models and Submodels					
Input Document		4. Input Status	5. Section Used in	6. Input Description	7. TBV/TBD Priority	8. TBV Due To			
2. Technical Product Input Source Title and Identifier(s) with Version	3. Section					Unqual.	From Uncontrolled Source	Un-confirmed	
2a									
14.	DTN: GS950208312232.003. Data, including Water Potential, Pressure and Temperature, Collected from Boreholes USW NRG-6 and USW NRG -7a from Instrumentation through March 31, 1995. Submittal date: 02/13/1995.	NRG-6 and NRG-7a pneumatic pressure and temperature	TBV-1101	4 6.3 6.8.4	NRG-6 and NRG-7a pneumatic pressure and temperature	1	N/A	N/A	✓
15.	DTN: GS951108312232.008. Data, including Water Potential, Pressure and Temperature, Collected from Boreholes UE-25 UZ#4 & UZ#5 from Instrumentation through September 30, 1995, and from USW NRG-6 & NRG-7a from April 1 through September 30, 1995. Submittal date: 11/21/1995.	NRG-6 and NRG-7a pneumatic pressure and temperature	TBV-807	6.3 6.8.4	NRG-6 and NRG-7a pneumatic pressure and temperature	1	N/A	N/A	✓
16.	DTN: GS960208312261.001. Shut-in Pressure Test Data from April 1995 to December 1995 from Select Wells and Boreholes at Yucca Mountain, NV. Submittal date: 02/07/1996.	NRG#5 pneumatic pressure	TBV-536 TBV-817	6.8.4	NRG#5 pneumatic pressure	1	N/A	N/A	✓

OFFICE OF CIVILIAN RADIOACTIVE WASTE MANAGEMENT DOCUMENT INPUT REFERENCE SYSTEM										
1. Document Identifier No./Rev.: MDL-NBS-HS-000006/Rev. 00			Change: N/A	Title: UZ Flow Models and Submodels						
Input Document		3. Section	4. Input Status	5. Section Used in	6. Input Description	7. TBV/TBD Priority	8. TBV Due To			
2. Technical Product Input Source Title and Identifier(s) with Version							Unqual.	From Uncontrolled Source	Un-confirmed	
2a										
17.	DTN: GS960308312232.001. Deep Unsaturated Zone Surface-Based Borehole Instrumentation Program Data from Boreholes USW NRG-7A, USW NRG-6, UE-25 UZ#4, UE-25 UZ#5, USW UZ-7A, and USW SD-12 for the Time Period 10/01/95 through 3/31/96. Submittal date: 04/04/1996.		SD-12, UZ-7a, NRG-6, and NRG-7a pneumatic pressure and temperature	TBV-538 TBV-819	6.2 6.3 6.6 6.8.4	SD-12, UZ-7a, NRG-6, and NRG-7a pneumatic pressure and temperature	I	N/A	N/A	✓
18.	DTN: GS960308312312.005. Water-Level, Discharge Rate and Related Data from the Pump Tests Conducted at Well USW UZ-14, August 17 through August 30, 1993. Submittal date: 03/15/1996.		Entire	TBV-544 TBV-822	6.2 6.6	Perched water elevation – UZ-14	I	N/A	N/A	✓
19.	DTN: GS960808312232.004. Deep Unsaturated Zone Surface-Based Borehole Instrumentation Program Data for Boreholes USW NRG-7A, USW NRG-6, UE-25, UZ#4, UE-25 UZ#5, USW UZ-7A and USW SD-12 for the Time Period 4/1/96 through 8/15/96. Submittal date: 08/30/1996.		NRG-6 and NRG-7a pneumatic pressure and temperature	TBV-833	6.3 6.8.4	NRG-6 and NRG-7a pneumatic pressure and temperature	I	N/A	N/A	✓

OFFICE OF CIVILIAN RADIOACTIVE WASTE MANAGEMENT DOCUMENT INPUT REFERENCE SYSTEM										
1. Document Identifier No./Rev.: MDL-NBS-HS-000006/Rev. 00			Change: <i>2EA 4/7/00</i> N/A		Title: UZ Flow Models and Submodels					
Input Document			4. Input Status	5. Section Used in	6. Input Description	7. TBV/TBD Priority	8. TBV Due To			
2. Technical Product Input Source Title and Identifier(s) with Version		3. Section					Unqual.	From Uncontrolled Source	Un-confirmed	
2a										
20.	DTN: GS960908312231.004. Characterization of Hydrogeologic Units Using Matrix Properties at Yucca Mountain, Nevada. Submittal date: 09/12/1996.		Entire	N/A- Qualified-Verification Level 2	6.2 6.3 6.6 6.7 6.8.1, 6.8.2, 6.8.3	Matrix hydrologic property data	N/A	N/A	N/A	N/A
21.	DTN: GS960908312232.006. In-Situ Pneumatic Tests of Boreholes. Submittal Date: 09/18/1996.		Perched water elevation for SD-12	N/A- Qualified-Verification Level 2	3.2 3.6 6.2 6.6	Observation data Perched water elevation - SD-12	1	N/A	N/A	✓
22.	DTN: GS960908312261.004. Shut-In Pressure Test Data from UE-25 NRG#5 And USW SD-7 from November 1995 to July 1996. Submittal date: 09/24/1996.		SD-7 pneumatic pressure	TBV-534 TBV-844	6.8.4	In situ gas pressure - SD-7	1	N/A	N/A	✓

OFFICE OF CIVILIAN RADIOACTIVE WASTE MANAGEMENT DOCUMENT INPUT REFERENCE SYSTEM										
1. Document Identifier No./Rev.: MDL-NBS-HS-000006/Rev. 00			Change: N/A		Title: UZ Flow Models and Submodels					
Input Document			4. Input Status	5. Section Used in	6. Input Description	7. TBV/TBD Priority	8. TBV Due To			
2. Technical Product Input Source Title and Identifier(s) with Version		3. Section					Unqual.	From Uncontrolled Source	Un-confirmed	
2a										
23.	DTN: GS961108312261.006. Gas Chemistry, ESF Alcoves 2 and 3, 11/95 - 4/96; Water Chemistry, Alcove 2 (Tritium), Alcove 3, and ESF Tunnel; and Pneumatic Pressure Response from Boreholes in Exploratory Studies Facility Alcoves 2 and 3, 10/95 - 5/96. Submittal date: 11/12/1996.		Entire	TBV	6.4.2.1	Chemical composition of pore water samples	1	N/A	N/A	✓
24.	DTN: GS970108312232.002. Deep Unsaturated Zone, Surface-Based Borehole Instrumentation Program - Raw Data Submittal For Boreholes USW NRG-7A, USW NRG-6, UE-25 UZ#4, UE-25 UZ#5, USW UZ-7A, and USW SD-12, for the Period 8/16/96 through 12/31/96. Submittal date: 01/22/1997.		Temperature	TBV-3162	6.3	In situ temperature	1	N/A	N/A	✓
25.	DTN: GS970208312312.003. Water-Level and Related Data from Pump Tests Conducted at Well USW G-2, 4/8/96 - 12/17/96. Submittal date: 02/05/1997.		Entire	TBV-849	6.2 6.6	Perched water elevation - G-2	1	N/A	N/A	✓

OFFICE OF CIVILIAN RADIOACTIVE WASTE MANAGEMENT DOCUMENT INPUT REFERENCE SYSTEM										
1. Document Identifier No./Rev.: MDL-NBS-HS-000006/Rev. 00		Change: N/A		Title: UZ Flow Models and Submodels						
Input Document		3. Section	4. Input Status	5. Section Used in	6. Input Description	7. TBV/TBD Priority	8. TBV Due To			
2. Technical Product Input Source Title and Identifier(s) with Version							Unqual.	From Uncontrolled Source	Un-confirmed	
2a										
26.	DTN: GS970808312232.005. Deep Unsaturated Zone Surface-Based Borehole Instrumentation Program Data from Boreholes USW NRG-7A, UE-2 5 UZ#4, UE-25 UZ#5, USW UZ-7A and USW SD-12 for the Time Period 1/1/97 - 6/30/97. Submittal date: 08/28/1997.		Temperature	TBV-0858	6.3	In situ temperature	1	N/A	N/A	✓
27.	DTN: GS971108312232.007. Deep Unsaturated Zone Surface-Based Borehole Instrumentation Program Data from Boreholes USW NRG-7A, UE-2 5 UZ #4, UE-25 UZ #5, USW UZ-7A and USW SD-12 for the Time Period 7/1/97 - 9/30/97. Submittal date: 11/18/1997.		Temperature	N/A- Qualified-Verification Level 2	6.3	In situ temperature	N/A	N/A	N/A	N/A
28.	DTN: GS971108314224.020. Revision 1 of Detailed Line Survey Data, Station 0+60 to Station 4+00, North Ramp Starter Tunnel, Exploratory Studies Facility. Submittal date: 12/03/1997.		Entire	N/A- Qualified-Verification Level 2	6.8.1	Detailed line survey data from ESF station 0+60m to 0+80m	N/A	N/A	N/A	N/A

REV 4/7/00

OFFICE OF CIVILIAN RADIOACTIVE WASTE MANAGEMENT DOCUMENT INPUT REFERENCE SYSTEM										
1. Document Identifier No./Rev.: MDL-NBS-HS-000006/Rev. 00			Change: N/A	Title: UZ Flow Models and Submodels						
Input Document		3. Section	4. Input Status	5. Section Used in	6. Input Description	7. TBV/TBD Priority	8. TBV Due To			
2. Technical Product Input Source Title and Identifier(s) with Version							Unqual.	From Uncontrolled Source	Un-confirmed	
2a										
29.	DTN: GS980408312232.001. Deep Unsaturated Zone Surface-Based Borehole Instrumentation Program Data From Boreholes USW NRG-7A, UE-2 5 UZ #4, USW NRG-6, UE-25 UZ #5, USW UZ-7A and USW SD-12 for the Time Period 10/01/97 - 03/31/98. Submittal date: 04/16/1998.		Temperature	N/A- Qualified-Verification Level 2	6.3	In situ temperature	N/A	N/A	N/A	N/A
30.	DTN: GS980508312313.001. Water-Level and Related Data Collected in Support of Perched-Water Testing in Borehole USW WT-24, September 10, 1997 through February 3, 1998. Submittal date: 05/07/1998.		Entire	TBV-3310	6.2 6.6 6.8.3	WT-24 perched water observations	1	N/A	N/A	✓
31.	DTN: GS980708312242.010. Physical Properties of Borehole Core Samples, and Water Potential Measurements Using the Filter Paper Technique, for Borehole Samples from USW WT-24. Submittal date: 07/27/1998.		Entire	TBV-3161	6.2 6.6 6.8.3	WT-24 saturation data	1	N/A	N/A	✓

OFFICE OF CIVILIAN RADIOACTIVE WASTE MANAGEMENT DOCUMENT INPUT REFERENCE SYSTEM									
1. Document Identifier No./Rev.: MDL-NBS-HS-000006/Rev. 00			Change: N/A		Title: UZ Flow Models and Submodels				
Input Document		3. Section	4. Input Status	5. Section Used in	6. Input Description	7. TBV/TBD Priority	8. TBV Due To		
2. Technical Product Input Source Title and Identifier(s) with Version							Unqual.	From Uncontrolled Source	Un-confirmed
2a									
32.	DTN: GS980808312242.014. Physical Properties of Borehole Core Samples and Water Potential Measurements Using the Filter Paper Technique for Borehole Samples from USW SD-6. Submittal date: 08/11/1998.	Entire	TBV-3160	6.2 6.6 6.8.3	SD-6 saturation data	1	N/A	N/A	✓
33.	DTN: GS980908312242.036. Water Potentials Measured With Heat Dissipation Probes in ECRB Holes from 4/23/98 to 7/31/98. Submittal date: 09/22/1998. Initial use.	Entire	N/A- Qualified- Verification Level 2	6.8.2	Water potential data along ECRB tunnel	N/A	N/A	N/A	N/A
34.	DTN: GS981008312313.003. Manually Measured Water-Level Data from Borehole USW G-2 on 02/03/98, Collected in Support of Perched-Water Testing in Borehole USW WT-24. Submittal date: 10/20/1998. Initial use.	Entire	TBV-3612	6.2 6.6	Perched water elevation - G-2	1	N/A	N/A	✓

OFFICE OF CIVILIAN RADIOACTIVE WASTE MANAGEMENT DOCUMENT INPUT REFERENCE SYSTEM										
1. Document Identifier No./Rev.: MDL-NBS-HS-000006/Rev. 00			Change: N/A	Title: UZ Flow Models and Submodels						
Input Document			4. Input Status	5. Section Used in	6. Input Description	7. TBV/TBD Priority	8. TBV Due To			
2. Technical Product Input Source Title and Identifier(s) with Version		3. Section					Unqual.	From Uncontrolled Source	Un-confirmed	
2a										
35.	DTN: LAIT831341AQ96.001. Radionuclide Retardation. Measurements of Batch Sorption Distribution Coefficients for Barium, Cesium, Selenium, Strontium, Uranium, Plutonium, and Neptunium. Submittal date: 11/12/1996.		Tc and ²³⁷ Np	TBV-0473 TBV-0869	6.7	Matrix diffusion coefficients for Tc and ²³⁷ Np	1	N/A	N/A	✓
36.	DTN: LASL831151AQ98.001. Mineralogic Characterization of the ESF Single Heater Test Block. Submittal date: 08/31/1998. Initial use.		Entire	N/A- Qualified- Verification Level 2	6.5	Mineral abundances in fractures	N/A	N/A	N/A	N/A
37.	DTN: LASL831222AQ98.002. Mineralogic Data Chlorine-36 Studies. Submittal date: 09/10/1998.		Entire	N/A- Reference Only	6.4.2.1	Chemical composition of pore water samples	N/A	N/A	N/A	N/A
38.	DTN: LA9908JC831321.001. Mineralogic Model "MM3.0" Version 3.0. Submittal Date: 08/16/1999.		Borehole SD-9 XRD data	N/A- Technical Product Output	6.5	Model input and output files for Mineralogic Model (borehole SD-9 XRD data.	N/A	N/A	N/A	N/A

OFFICE OF CIVILIAN RADIOACTIVE WASTE MANAGEMENT DOCUMENT INPUT REFERENCE SYSTEM									
1. Document Identifier No./Rev.: MDL-NBS-HS-000006/Rev. 00			Change: N/A		Title: UZ Flow Models and Submodels				
Input Document		3. Section	4. Input Status	5. Section Used in	6. Input Description	7. TBV/TBD Priority	8. TBV Due To		
2. Technical Product Input Source Title and Identifier(s) with Version	2a						Unqual.	From Uncontrolled Source	Un-confirmed
39.	DTN: LB971212001254.006. Three Files Using DKM Weeps Parameter Sets with Mean Fracture Permeability, Present Day Infiltration, and Estimated Global FMX for Present Day and Long Term Average and Superpluvial Infiltration. Submittal date: 12/12/1997. Initial Use.	Entire	N/A-Reference Only	6.8.1	Flow fields and calibrated hydrologic properties	N/A	N/A	N/A	N/A
40.	DTN: LB980912332245.002. Gas Tracer Data from Niche 3107 of the ESF. Submittal date: 09/30/1998.	Entire	TBV-3251	6.2 6.3 6.6 6.7 6.8	Air-injection, tracer test, and fracture porosity data	I	N/A	N/A	✓
41.	DTN: LB990501233129.001. Fracture Properties for the UZ Model Grids and Uncalibrated Fracture and Matrix Properties for the UZ Model Layers for AMR U0090, "Analysis of Hydrologic Properties Data." Submittal date: 08/25/1999.	Entire	N/A-Technical Product Output	6.2 6.3 6.6 6.7 6.8	Uncalibrated hydrologic property data	N/A	N/A	N/A	N/A

OFFICE OF CIVILIAN RADIOACTIVE WASTE MANAGEMENT DOCUMENT INPUT REFERENCE SYSTEM									
1. Document Identifier No./Rev.: MDL-NBS-HS-000006/Rev. 00			Change: <i>234 4/7/00</i> N/A	Title: UZ Flow Models and Submodels					
Input Document		3. Section	4. Input Status	5. Section Used in	6. Input Description	7. TBV/FBD Priority	8. TBV Due To		
2. Technical Product Input Source Title and Identifier(s) with Version							Unqual.	From Uncontrolled Source	Un-confirmed
2a									
42.	DTN: LB990501233129.002. 1-D Grids For Hydrogeologic Property Set Inversions and Calibrations for AMR U0000, "Development of Numerical Grids For UZ Flow and Transport Modeling." Submittal date: 09/24/1999.	Entire	N/A- Technical Product Output	6.5	1-D grid for flow property calibration	N/A	N/A	N/A	N/A
43.	DTN: LB990501233129.004. 3-D UZ Model Calibration Grids for AMR U0000, "Development of Numerical Grids of UZ Flow and Transport Modeling." Submittal date: 09/24/1999.	Entire	N/A- Technical Product Output	6.1 6.2 6.3, 6.8.2, 6.8.3,	3-D UZ Model Calibration Grid	N/A	N/A	N/A	N/A
44.	DTN: LB990701233129.001. 3-D UZ Model Grids for Calculation of Flow Fields for PA for AMR U0000, "Development of Numerical Grids for UZ Flow and Transport Modeling." Submittal date: 09/24/1999.	Entire	N/A- Technical Product Output	6.1 6.6 6.7 6.8.4,	3-D UZ Model TSPA Grids	N/A	N/A	N/A	NA

OFFICE OF CIVILIAN RADIOACTIVE WASTE MANAGEMENT DOCUMENT INPUT REFERENCE SYSTEM									
1. Document Identifier No./Rev.: MDL-NBS-HS-000006/Rev. 00			Change: N/A		Title: UZ Flow Models and Submodels				
Input Document		3. Section	4. Input Status	5. Section Used in	6. Input Description	7. TBV/TBD Priority	8. TBV Due To		
2. Technical Product Input Source Title and Identifier(s) with Version							Unqual.	From Uncontrolled Source	Un-confirmed
2a									
45.	DTN: LB990701233129.002. 3-D UZ Model Calibration Grid for Calculation of Flow Fields using #3 Perched Water Conceptual Model (Non-Perched Water Model). Submittal date: Will be submitted with AMR. Initial use.	Entire	N/A- Technical Product Output	6.1 6.2 6.3, 6.8.2, 6.8.3,	3-D UZ Model Calibration Grid for Non water-perching model	N/A	N/A	N/A	N/A
46.	DTN: LB991091233129.003. Two-Dimensional Fault Calibration For AMR U0035. "Calibrated Properties Model." Submittal date: 10/22/1999. Initial use.	Entire	N/A- Technical Product Output	6.2 6.3 6.6 6.7 6.8	Calibrated fault property	N/A	N/A	N/A	N/A
47.	DTN: LB991091233129.004. Calibrated Fault Properties for the UZ Flow and Transport Model for AMR U0035, "Calibrated Properties Model." Submittal date: 10/22/1999.	Entire	N/A- Technical Product Output	6.8.4	Calibrated fault property	N/A	N/A	N/A	N/A

OFFICE OF CIVILIAN RADIOACTIVE WASTE MANAGEMENT DOCUMENT INPUT REFERENCE SYSTEM										
1. Document Identifier No./Rev.: MDL-NBS-HS-000006/Rev. 00			Change: N/A	Title: UZ Flow Models and Submodels						
Input Document			4. Input Status	5. Section Used in	6. Input Description	7. TBV/TBD Priority	8. TBV Due To			
2. Technical Product Input Source Title and Identifier(s) with Version		3. Section					Unqual.	From Uncontrolled Source	Un-confirmed	
2a										
48.	DTN: LB991121233129.001. Calibrated parameters for the present-day, mean infiltration scenario, used for simulations with perched water conceptual model #1 (flow through) for the mean infiltration scenarios of the present-day, Monsoon and Glacial transition climates. Submittal date: will be submitted with AMR.		Entire	N/A- Technical Product Output	6.2, 6.3, 6.4, 6.6, 6.7, 6.8.2, 6.8.3, 6.8.4	Calibrated parameters for the base case infiltration scenario - flow through perched water conceptual model	N/A	N/A	N/A	N/A
49.	DTN: 1.B991121233129.002. Calibrated parameters for the present-day, mean infiltration scenario, used for simulations with perched water conceptual model #2 (by passing) for the mean infiltration scenarios of the present-day, Monsoon and Glacial transition climates. Submittal date: will be submitted with AMR.		Entire	N/A- Technical Product Output	6.2, 6.3, 6.4, 6.6, 6.7, 6.8.4	Calibrated parameters for the base case infiltration scenario - by-passing perched water conceptual model	N/A	N/A	N/A	N/A

OFFICE OF CIVILIAN RADIOACTIVE WASTE MANAGEMENT DOCUMENT INPUT REFERENCE SYSTEM										
1. Document Identifier No./Rev.: MDL-NBS-HS-000006/Rev. 00			Change: <i>JEH 4/7/00</i> N/A		Title: UZ Flow Models and Submodels					
Input Document			4. Input Status	5. Section Used in	6. Input Description	7. TBV/TBD Priority	8. TBV Due To			
2. Technical Product Input Source Title and Identifier(s) with Version		3. Section					Unqual.	From Uncontrolled Source	Un-confirmed	
2a										
50.	DTN: LB991121233129.003. Calibrated parameters for the present-day, upper-bound infiltration scenario, used for simulations with perched water conceptual model #1 (flow through) for the upper-bound infiltration scenarios of the present-day, Monsoon and Glacial transition climates. Submittal date: will be submitted with AMR.		Entire	N/A- Technical Product Output	6.2, 6.6, 6.7	Calibrated parameters for the upper bound infiltration scenario - flow through perched water conceptual model	N/A	N/A	N/A	N/A
51.	DTN: LB991121233129.004. Calibrated parameters for the present-day, upper-bound infiltration scenario, used for simulations with perched water conceptual model #2 (by passing) for the upper-bound infiltration scenarios of the present-day, Monsoon and Glacial transition climates. Submittal date: will be submitted with AMR.		Entire	N/A- Technical Product Output	6.2, 6.6, 6.7	Calibrated parameters for the upper bound infiltration scenario - by-passing perched water conceptual model	N/A	N/A	N/A	N/A

OFFICE OF CIVILIAN RADIOACTIVE WASTE MANAGEMENT DOCUMENT INPUT REFERENCE SYSTEM									
1. Document Identifier No./Rev.: MDL-NBS-HS-000006/Rev. 00		Change: N/A		Title: UZ Flow Models and Submodels					
Input Document		4. Input Status	5. Section Used in	6. Input Description	7. TBV/TBD Priority	8. TBV Due To			
2. Technical Product Input Source Title and Identifier(s) with Version	3. Section					Unqual.	From Uncontrolled Source	Un-confirmed	
2a									
52.	DTN: LB991121233129.005. Calibrated parameters for the present-day, lower-bound infiltration scenario, used for simulations with perched water conceptual model #1 (flow through) for the lower-bound infiltration scenarios of the present-day, Monsoon and Glacial transition climates. Submittal date: will be submitted with AMR.	Entire	N/A- Technical Product Output	6.2, 6.6, 6.7	Calibrated parameters for the lower bound infiltration scenario - flow through perched water conceptual model	N/A	N/A	N/A	N/A
53.	DTN: 1.B991121233129.006. Calibrated parameters for the present-day, lower-bound infiltration scenario, used for simulations with perched water conceptual model #2 (by passing) for the lower-bound infiltration scenarios of the present-day, Monsoon and Glacial transition climates. Submittal date: will be submitted with AMR.	Entire	N/A- Technical Product Output	6.2, 6.6, 6.7	Calibrated parameters for the lower bound infiltration scenario - by-passing perched water conceptual model	N/A	N/A	N/A	N/A

224 4/7/00

OFFICE OF CIVILIAN RADIOACTIVE WASTE MANAGEMENT DOCUMENT INPUT REFERENCE SYSTEM									
1. Document Identifier No./Rev.: MDL-NBS-HS-000006/Rev. 00			Change: JEH N/A	Title: UZ Flow Models and Submodels					
Input Document		3. Section	4. Input Status	5. Section Used in	6. Input Description	7. TBV/TBD Priority	8. TBV Due To		
2. Technical Product Input Source Title and Identifier(s) with Version	2a						Unqual.	From Uncontrolled Source	Un-confirmed
54.	DTN: LB991121233129.007. Calibrated parameters for the present-day, mean infiltration scenario, used for simulations with perched water conceptual model #3 (non-perching) for the mean infiltration scenarios of the present-day, Monsoon and Glacial transition climates. Submittal date: will be submitted with AMR.	Entire	N/A- Technical Product Output	6.2, 6.6, 6.7	Calibrated parameters for the base case infiltration scenario - non-perching perched water conceptual model	N/A	N/A	N/A	N/A
55.	DTN: LB991200DSTTHC.001. Pore water composition and CO2 partial pressure input to Thermal-Hydrological-Chemical (THC) simulations: Table 3 of AMR N0120/U0110, "Coupled Processes (DST and TH Seepage) Models." Submittal date: will be submitted with AMR.	Entire	N/A- Technical Product Output	6.5	Kinetic data	N/A	N/A	N/A	N/A

OFFICE OF CIVILIAN RADIOACTIVE WASTE MANAGEMENT DOCUMENT INPUT REFERENCE SYSTEM									
1. Document Identifier No./Rev.: MDL-NBS-HS-000006/Rev. 00			Change: N/A	Title: UZ Flow Models and Submodels					
Input Document		3. Section	4. Input Status	5. Section Used in	6. Input Description	7. TBV/TBD Priority	8. TBV Due To		
2. Technical Product Input Source Title and Identifier(s) with Version	2a						Unqual.	From Uncontrolled Source	Un-confirmed
56.	DTN: 1.B997141233129.001. Calibrated Basecase Infiltration 1-D Parameter Set for the UZ Flow and Transport Model, FY99. Submittal date: 07/21/1999.	Entire	N/A- Technical Product Output	6.2 6.3 6.4 6.6 6.7 6.8.2 6.8.3 6.8.4	Calibrated flow and thermal parameters - base case	N/A	N/A	N/A	N/A
57.	DTN: 1.B997141233129.002. Calibrated Upper-Bound Infiltration 1-D Parameter Set for the UZ Flow and Transport Model, FY99. Submittal date: 07/21/1999. Initial use.	Entire	TBV-3947	6.2 6.6 6.7	Calibrated flow and thermal parameters - upper bound	1	N/A	N/A	✓
58.	DTN: 1.B997141233129.003. Calibrated Lower-Bound Infiltration 1-D Parameter Set for the UZ Flow and Transport Model, FY99. Submittal date: 07/21/1999. Initial use.	Entire	TBV-3948	6.2 6.6 6.7	Calibrated flow and thermal parameters - lower bound	1	N/A	N/A	✓

OFFICE OF CIVILIAN RADIOACTIVE WASTE MANAGEMENT DOCUMENT INPUT REFERENCE SYSTEM									
1. Document Identifier No./Rev.: MDL-NBS-HS-000006/Rev. 00			Change: N/A	Title: UZ Flow Models and Submodels					
Input Document			4. Input Status	5. Section Used in	6. Input Description	7. TBV/TBD Priority	8. TBV Due To		
2. Technical Product Input Source Title and Identifier(s) with Version	3. Section	Unqual.					From Uncontrolled Source	Un-confirmed	
2a									
59.	Bodvarsson, G.S.; Boyle, W.; Patterson, R.; and Williams, D. 1999. "Overview of Scientific Investigations at Yucca Mountain—the Potential Repository for High-Level Nuclear Waste." <i>Journal Of Contaminant Hydrology</i> 38 (1–3), 3–24. Amsterdam, The Netherlands: Elsevier Science Publishers. TIC: 244160.	Entire	N/A-Reference only	6.8.1	TCw flow condition	N/A	N/A	N/A	N/A
60.	CRWMS M&O (Civilian Radioactive Waste Management System, Management & Operating Contractor) 1999a. <i>Analysis & Modeling Development Plan (DP) for U0050, UZ Flow Models and Submodels, Rev. 00</i> . TDP-NBS-HS-000011. Las Vegas, Nevada: CRWMS M&O. ACC: MOL.19991013.0353.	Entire	N/A - Reference only	2	Standards, Codes & Regulations	N/A	N/A	N/A	N/A

OFFICE OF CIVILIAN RADIOACTIVE WASTE MANAGEMENT DOCUMENT INPUT REFERENCE SYSTEM										
1. Document Identifier No./Rev.: MDL-NBS-HS-000006/Rev. 00			Change: N/A	Title: UZ Flow Models and Submodels						
Input Document			4. Input Status	5. Section Used in	6. Input Description	7. TBV/TBD Priority	8. TBV Due To			
2. Technical Product Input Source Title and Identifier(s) with Version		3. Section					Unqual.	From Uncontrolled Source	Un-confirmed	
2a										
61.	CRWMS M&O 1999b. <i>M&O Site Investigations. Activity Evaluation. Las Vegas, Nevada: CRWMS M&O. ACC: MOL.19990317.0330.</i>		Entire	N/A - Reference only	2	Standards, Codes & Regulations	N/A	N/A	N/A	N/A
62.	CRWMS M&O 1999c. <i>M&O Site Investigations. Activity Evaluation. Las Vegas, Nevada: CRWMS M&O. ACC: MOL.19990928.0224.</i>		Entire	N/A - Reference only	2	Standards, Codes & Regulations	N/A	N/A	N/A	N/A
63.	CRWMS M&O 1999d. <i>Development of Numerical Grids for UZ Flow and Transport Modeling. ANL-NBS-HS-000015. Las Vegas, Nevada: CRWMS M&O. ACC: MOL.19990721.0517.</i>		Entire	N/A-Reference only	6.1 6.2 6.3 6.4 6.6 6.7 6.8.2 6.8.3 6.8.4	Model grids	N/A	N/A	N/A	N/A

OFFICE OF CIVILIAN RADIOACTIVE WASTE MANAGEMENT DOCUMENT INPUT REFERENCE SYSTEM									
1. Document Identifier No./Rev.: MDL-NBS-HS-000006/Rev. 00			Change: 92H 4/7/00 N/A		Title: UZ Flow Models and Submodels				
Input Document		3. Section	4. Input Status	5. Section Used in	6. Input Description	7. TBV/TBD Priority	8. TBV Due To		
2. Technical Product Input Source Title and Identifier(s) with Version							Unqual.	From Uncontrolled Source	Un-confirmed
2a									
64.	CRWMS M&O 2000a. <i>Analysis of Geochemistry Data for the Unsaturated Zone.</i> ANL-NBS-HS-000017. Las Vegas, Nevada: CRWMS M&O. URN-0048.	Table 4 Table 5 Table 6-1	TBV	6.4.2.1	Chemical composition of pore water samples	1	N/A	✓	N/A
65.	CRWMS M&O 2000b. <i>Calibrated Properties Model.</i> MDL-NBS-HS-000003. Las Vegas, Nevada: CRWMS M&O. ACC: 19990720.0520. URN-0028.	Entire	N/A-Reference only	6.1 6.2 6.3 6.4 6.6 6.7 6.8.2 6.8.3 6.8.4	Model properties and parameters	N/A	N/A	N/A	N/A
66.	CRWMS M&O 2000c. <i>Conceptual and Numerical Model for the Unsaturated Zone Flow and Transport.</i> MDL-NBS-HS-000005 REV 00. Las Vegas, Nevada: CRWMS M&O. URN-0036.	Entire	N/A-Reference only	6.1	Conceptual Model description	N/A	N/A	N/A	N/A

OFFICE OF CIVILIAN RADIOACTIVE WASTE MANAGEMENT DOCUMENT INPUT REFERENCE SYSTEM									
1. Document Identifier No./Rev.: MDL-NBS-HS-000006/Rev. 00			Change: N/A	Title: UZ Flow Models and Submodels					
Input Document		3. Section	4. Input Status	5. Section Used in	6. Input Description	7. TBV/TBD Priority	8. TBV Due To		
2. Technical Product Input Source Title and Identifier(s) with Version							Unqual.	From Uncontrolled Source	Un-confirmed
2a									
67.	CRWMS M&O 2000d. <i>Drift-Scale Coupled Processes (DST, THC Seepage) Models</i> . MDL-NBS-HS-000001. Las Vegas, Nevada: CRWMS M&O. ACC: MOL.19990721.0523.	Entire	N/A-Reference only	6.5	Referring to the conceptual model and approaches for reactive transport.	N/A	N/A	N/A	N/A
68.	CRWMS M&O 2000e. <i>Repository Safety Strategy: Plan to Prepare the Postclosure Safety Case to Support Yucca Mountain Site recommendation and Licensing Considerations</i> . TDR-WIS-RL-000001 REV. 3. Las Vegas, Nevada: CRWMS M&O. ACC: MOL.20000119.0189.	Entire	N/A-Reference only	6 6.6.1	Referring to the plan as a standard for models.	N/A	N/A	N/A	N/A
69.	CRWMS M&O 2000f. <i>Analyses of Hydrologic Properties Data</i> . ANL-NBS-HS-000002. Las Vegas, Nevada: CRWMS M&O URN-0057.	Entire	N/A-Reference only	6.5.3	Development of fracture properties and matrix porosities	N/A	N/A	N/A	N/A

OFFICE OF CIVILIAN RADIOACTIVE WASTE MANAGEMENT DOCUMENT INPUT REFERENCE SYSTEM										
1. Document Identifier No./Rev.: MDL-NBS-HS-000006/Rev. 00			Change: N/A	Title: UZ Flow Models and Submodels						
Input Document			4. Input Status	5. Section Used in	6. Input Description	7. TBV/TBD Priority	8. TBV Due To			
2. Technical Product Input Source Title and Identifier(s) with Version		3. Section					Unqual.	From Uncontrolled Source	Un-confirmed	
2a										
70.	Domenico, P.A. and Schwartz, F.W. 1990. <i>Physical and Chemical Hydrogeology</i> . New York, New York: John Wiley and Sons. TIC: 234782.		p. 368	N/A-Reference only	6.8.1	Molecule diffusion coefficient	N/A	N/A	N/A	N/A
71.	Doughty, C. 1999. "Investigation of Conceptual and Numerical Approaches for Evaluating Moisture, Gas, Chemical, and Heat Transport in Fractured Unsaturated Rock." <i>Journal of Contaminant Hydrology</i> 38 (1-3), 69-106. Amsterdam, The Netherlands: Elsevier Science Publishers. TIC: 244160.		p. 69-106	N/A-Reference only	6.1	Conceptual and numerical model in fracture and matrix interaction	N/A	N/A	N/A	N/A
72.	Driscoll, Fletcher G. 1986. <i>Groundwater and Wells, 2nd Edition</i> . St. Paul, Minnesota: Johnson Filtration Systems. TIC: 225919.		p. 50	N/A-Reference only	6.3	Dry adiabatic atmospheric lapse rate	N/A	N/A	N/A	N/A

OFFICE OF CIVILIAN RADIOACTIVE WASTE MANAGEMENT DOCUMENT INPUT REFERENCE SYSTEM										
1. Document Identifier No./Rev.: MDL-NBS-HS-000006/Rev. 00			Change: N/A		Title: UZ Flow Models and Submodels					
Input Document			4. Input Status	5. Section Used in	6. Input Description	7. TBV/TBD Priority	8. TBV Due To			
2. Technical Product Input Source Title and Identifier(s) with Version		3. Section					Unqual.	From Uncontrolled Source	Un-confirmed	
2a										
73.	Dyer, J.R. 1999. "Revised Interim Guidance Pending Issuance of New U.S. Nuclear Regulatory Commission (NRC) Regulations (Revision 01, July 22, 1999), for Yucca Mountain, Nevada." Letter from J.R. Dyer (DOE) to D.R. Wilkins (CRWMS M&O), September 9, 1999. OL&RC:SB-1714, with enclosure, "Interim Guidance Pending Issuance of New U.S. Nuclear Regulatory Commission (NRC) Regulations (Revision 01)." ACC: MOL.19990910.0079.		Entire	N/A Reference only	4.2	Interim Guidance	N/A	N/A	N/A	N/A

OFFICE OF CIVILIAN RADIOACTIVE WASTE MANAGEMENT DOCUMENT INPUT REFERENCE SYSTEM									
1. Document Identifier No./Rev.: MDL-NBS-HS-000006/Rev. 00			Change: N/A	Title: UZ Flow Models and Submodels					
Input Document		3. Section	4. Input Status	5. Section Used in	6. Input Description	7. TBV/TBD Priority	8. TBV Due To		
2. Technical Product Input Source Title and Identifier(s) with Version	2a						Unqual.	From Uncontrolled Source	Un-confirmed
74.	Flint, A.L. and Flint, L.E. 1994. "Spatial Distribution of Potential Near Surface Moisture Flux at Yucca Mountain." <i>Proceedings of the Fifth Annual International Conference on High Level Radioactive Waste Management, 4, Las Vegas, Nevada, May 22-26, 1994, 2352-2358.</i> La Grange Park, Illinois: American Nuclear Society. TIC: 224142.	Entire	N/A-Reference only	6.4.1	Water Infiltration Flux	N/A	N/A	N/A	N/A
75.	Flint, L.E. 1998. <i>Characterization of Hydrogeologic Units Using Matrix Properties, Yucca Mountain, Nevada.</i> Water-Resources Investigations Report 97-4243. Denver, Colorado: U.S. Geological Survey. ACC: MOL.19980429.0512.	p.3	N/A-Reference only	6.8.1	Evaluation of numerical approach	N/A	N/A	N/A	N/A

OFFICE OF CIVILIAN RADIOACTIVE WASTE MANAGEMENT DOCUMENT INPUT REFERENCE SYSTEM									
1. Document Identifier No./Rev.: MDL-NBS-HS-000006/Rev. 00			Change: N/A	Title: UZ Flow Models and Submodels					
Input Document		3. Section	4. Input Status	5. Section Used in	6. Input Description	7. TBV/TBD Priority	8. TBV Due To		
2. Technical Product Input Source Title and Identifier(s) with Version	2a						Unqual.	From Uncontrolled Source	Un-confirmed
76.	Francis, N.D. 1997. "The Base-Case Thermal Properties for TSPA-VA Modeling." Memo from N.D. Francis (SNL) to Distribution, April 16, 1997. Albuquerque, New Mexico: Sandia National Laboratories. ACC: MOL.19980518.0229.	p. 5	N/A-Reference only	6.8.1	Tortuosity for the matrix	N/A	N/A	N/A	N/A
77.	Hevesi, J.A.; Flint, A.L.; and Istock, J.D. 1992. "Precipitation Estimation in Mountainous Terrain Using Multivariate Geostatistics, Part II: Isohyetal Maps." <i>Journal of Applied Meteorology</i> , 31, 677-688. Boston, Massachusetts: American Meteorological Society. TIC: 225248.	Entire	N/A-Reference only	6.4.1	Water Infiltration Flux	N/A	N/A	N/A	N/A
78.	Javandel, I.; Doughty, C.; and Tsang, C.F. 1984. "Groundwater Transport: Handbook of Mathematical Models." <i>Water Resources Monograph</i> , 10. Washington, D.C.: American Geophysical Union. TIC: 209908.	p. 9-34	N/A-Reference only	6.4.3.2	1D chemical transport analytical model	N/A	N/A	N/A	N/A

OFFICE OF CIVILIAN RADIOACTIVE WASTE MANAGEMENT DOCUMENT INPUT REFERENCE SYSTEM									
I. Document Identifier No./Rev.: MDL-NBS-HS-000006/Rev. 00		Change: N/A	Title: UZ Flow Models and Submodels						
Input Document		4. Input Status	5. Section Used in	6. Input Description	7. TBV/TBD Priority	8. TBV Due To			
2. Technical Product Input Source Title and Identifier(s) with Version	3. Section					Unqual.	From Uncontrolled Source	Un-confirmed	
2a									
79.	Lasaga, A.C. 1998. <i>Kinetic Theory in the Earth Sciences</i> . Princeton, New Jersey: Princeton University Press. TIC: 246279.	p. 315	N/A-Reference only	6.4.4.1	Diffusion coefficients of chemical ions	N/A	N/A	N/A	N/A
80.	Liu, H.H.; Doughty, C.; and Bodvarsson, G.S. 1998. "An Active Fracture Model for Unsaturated Flow and Transport in Fractured Rocks." <i>Water Resources Research</i> 34 (10), 2633-2646. Washington, D.C.: American Geophysical Union. TIC: 243012.	p. 2633-2646	N/A-Reference only	6.8.1	Active fracture model	N/A	N/A	N/A	N/A
81.	Montazer, P. and Wilson, W.E. 1984. <i>Conceptual Hydrologic Model of Flow in the Unsaturated Zone, Yucca Mountain, Nevada</i> . Water Resources Investigations Report 84-4345. Denver, Colorado: U.S. Geological Survey. TIC: 203223.	Entire	N/A-Reference only	6.1	Geological model description	N/A	N/A	N/A	N/A

JEA 4/7/00

OFFICE OF CIVILIAN RADIOACTIVE WASTE MANAGEMENT DOCUMENT INPUT REFERENCE SYSTEM									
1. Document Identifier No./Rev.: MDL-NBS-HS-000006/Rev. 00			Change: N/A	Title: UZ Flow Models and Submodels					
Input Document			4. Input Status	5. Section Used in	6. Input Description	7. TBV/TBD Priority	8. TBV Due To		
2. Technical Product Input Source Title and Identifier(s) with Version		3. Section					Unqual.	From Uncontrolled Source	Un-confirmed
2a									
82.	PLACEHOLDER								
83.	Pruess, K. and Narasimhan, T.N. 1985. "A Practical Method for Modeling Fluid and Heat Flow in Fractured Porous Media." <i>Society of Petroleum Engineers Journal</i> , 25 (1), 14-26. Dallas, Texas: Society of Petroleum Engineers. TIC: 221917.		Entire	N/A-Reference only	6.1	MINC model	N/A	N/A	N/A

JEH 4/7/00

OFFICE OF CIVILIAN RADIOACTIVE WASTE MANAGEMENT DOCUMENT INPUT REFERENCE SYSTEM									
1. Document Identifier No./Rev.: MDL-NBS-HS-000006/Rev. 00		Change: N/A		Title: UZ Flow Models and Submodels					
Input Document		4. Input Status	5. Section Used in	6. Input Description	7. TBV/TBD Priority	8. TBV Due To			
2. Technical Product Input Source Title and Identifier(s) with Version	3. Section					Unqual.	From Uncontrolled Source	Un-confirmed	
2a									
84.	Pruess, K. 1991. "TOUGH2, a General-Purpose Numerical Simulator for Multiphase Fluid and Heat Flow." Report LBL-29400. Berkeley, California: Lawrence Berkeley National Laboratory. ACC: NNA.19940202.0088.	Entire	N/A-Reference only	6.1 6.5	TOUGH2 model	N/A	N/A	N/A	N/A
85.	Pruess, K.; Faybishenko, B.; and Bodvarsson, G.S. 1999. "Alternative Concepts and Approaches for Modeling Flow and Transport in Thick Unsaturated Zones of Fractured Rocks." <i>Journal of Contaminant Hydrology</i> (38) 1-3. 281-322. Amsterdam. The Netherlands: Elsevier Science Publishers. TIC: 244160.	p. 132	N/A-Reference only	6.8.1	Validation method	N/A	N/A	N/A	N/A

JEH 4/7/00

OFFICE OF CIVILIAN RADIOACTIVE WASTE MANAGEMENT DOCUMENT INPUT REFERENCE SYSTEM									
1. Document Identifier No./Rev.: MDL-NBS-HS-000006/Rev. 00			Change: N/A	Title: UZ Flow Models and Submodels					
Input Document		3. Section	4. Input Status	5. Section Used in	6. Input Description	7. TBV/TBD Priority	8. TBV Due To		
2. Technical Product Input Source Title and Identifier(s) with Version							Unqual.	From Uncontrolled Source	Un-confirmed
2a									
86.	Sass, J.H.; Lachenbruch, A.H.; Dudley, W.W., Jr.; Priest, S.S.; and Munroe, R.J. 1988. <i>Temperature, Thermal Conductivity and Heat Flow Near Yucca Mountain, Nevada: Some Tectonic and Hydrologic Implications</i> . Open File Rep. 87-649. Denver, Colorado: U.S. Geological Survey. TIC: 203195.	Entire	N/A-Reference only	6.3	Temperature, thermal conductivity, and heat flow	N/A	N/A	N/A	N/A
87.	Sonnenthal, E. L. and Bodvarsson, G. S. 1999. "Constraints on the Hydrology of the Unsaturated Zone at Yucca Mountain, NV from Three-Dimensional Models of Chloride and Strontium Geochemistry." <i>Journal of Contaminant Hydrology</i> 38 (1-3), 107-156. Amsterdam, Netherlands: Elsevier Science Publishers. TIC: 244160.	Entire	N/A-Reference only	6.4.1 6.4.2.2 6.4.4.1	Introduction to porewater chemical model Climate change effect on porewater chemicals Modern time and glacial time ³⁶ Cl/Cl ratios hydraulic dispersivity	N/A	N/A	N/A	N/A

JEH 4/7/00

**OFFICE OF CIVILIAN RADIOACTIVE WASTE MANAGEMENT
DOCUMENT INPUT REFERENCE SYSTEM**

get 4/7/00

1. Document Identifier No./Rev.: MDL-NBS-HS-000006/Rev. 00		Change: <i>N/A</i>	Title: UZ Flow Models and Submodels						
Input Document		4. Input Status	5. Section Used in	6. Input Description	7. TBV/TBD Priority	8. TBV Due To			
2. Technical Product Input Source Title and Identifier(s) with Version	3. Section					Unqual.	From Uncontrolled Source	Un-confirmed	
2a									
88.	Steefel, C.I. and Lichtner, P.C. 1998. "Multicomponent Reactive Transport in Discrete Fractures: II: Infiltration of Hyperalkaline Groundwater at Maqarin, Jordan, a Natural Analogue Site." <i>Journal of Hydrology</i> , 209, 200-224. Amsterdam, The Netherlands: Elsevier Science Publishers. TIC: applied for.	Entire	N/A-Reference only	6.5	Mineralogical data	N/A	N/A	N/A	N/A
89.	Tyler, S.W.; Chapman, J.B.; Conrad, S.H.; Hammermeister, D.P.; Blout, D.O.; Miller, J.J.; Sully, M.J.; and Ginanni, J.M. 1996. "Soil-Water Flux in the Southern Great Basin, United States: Temporal and Spatial Variations over the Last 120,000 Years." <i>Water Resources Research</i> 32 (6), 1481-1499. Washington, DC: American Geophysical Union. TIC: 235938.	Entire	N/A-Reference only	6.4.2.2	Cl infiltration flux	N/A	N/A	N/A	N/A

OFFICE OF CIVILIAN RADIOACTIVE WASTE MANAGEMENT DOCUMENT INPUT REFERENCE SYSTEM									
1. Document Identifier No./Rev.: MDL-NBS-HS-000006/Rev. 00			Change: N/A	Title: UZ Flow Models and Submodels					
Input Document		3. Section	4. Input Status	5. Section Used in	6. Input Description	7. TBV/TBD Priority	8. TBV Due To		
2. Technical Product Input Source Title and Identifier(s) with Version							Unqual.	From Uncontrolled Source	Un-confirmed
2a									
90.	van Genuchten, M. 1980. "A Closed-Form Equation for Predicting the Hydraulic Conductivity of Unsaturated Soils." <i>Soil Science Society of America Journal</i> , 44 (5), 892-898. Madison, Wisconsin: Soil Science Society of America. TIC: 217327.	Entire	N/A-Reference only	6.1 6.2 6.6	van Genuchten model	N/A	N/A	N/A	N/A
91.	Wemheuer, R.F. 1999. "First Issue of FY00 NEPO QAP-2-0 Activity Evaluations." Interoffice correspondence from R.F. Wemheuer (CRWMS M&O) to R.A. Morgan (CRWMS M&O), October 1, 1999. LV.NEPO.RTPS.TAG.10/99-155, with attachments. Activity Evaluation for Work Package #1401213UM1. ACC: MOL.19991028.0162.	Work Package #1401213UM1	N/A-Reference only	2	Activity Evaluation	N/A	N/A	N/A	N/A

JRH 4/7/00

OFFICE OF CIVILIAN RADIOACTIVE WASTE MANAGEMENT DOCUMENT INPUT REFERENCE SYSTEM									
1. Document Identifier No./Rev.: MDL-NBS-HS-000006/Rev. 00			Change: N/A	Title: UZ Flow Models and Submodels					
Input Document		3. Section	4. Input Status	5. Section Used in	6. Input Description	7. TBV/TBD Priority	8. TBV Due To		
2. Technical Product Input Source Title and Identifier(s) with Version	2a						Unqual.	From Uncontrolled Source	Un-confirmed
92.	Wu, Y.S.; Ahlers, C.F.; Fraser, P.; Simmons, A.; and Pruess, K. 1996. <i>Software Qualification of Selected TOUGH2 Modules</i> . Report LBNL-39490, UC-800. Berkeley, California: Lawrence Berkeley National Laboratory. ACC: MOL.19970219.0104.	Entire	N/A-Reference only	6.1	Tough2 EOS9 module	N/A	N/A	N/A	N/A
93.	Wu, Y.S.; Haukwa, C. and Bodvarsson, G.S. 1999a. "A Site-Scale Model for Fluid and Heat Flow in the Unsaturated Zone of Yucca Mountain, Nevada." <i>Journal of Contaminant Hydrology</i> 38 (1-3), 185-215. Amsterdam, The Netherlands: Elsevier Science Publishers. TIC: 244160.	p. 188-196	N/A-Reference only	6.1 6.2	3-D UZ model Surface temperature correlation	N/A	N/A	N/A	N/A

93H 4/7/00

**OFFICE OF CIVILIAN RADIOACTIVE WASTE MANAGEMENT
DOCUMENT INPUT REFERENCE SYSTEM**

JEH 4/7/00

1. Document Identifier No./Rev.: MDL-NBS-HS-000006/Rev. 00		Change: <i>N/A</i>	Title: UZ Flow Models and Submodels						
Input Document		4. Input Status	5. Section Used in	6. Input Description	7. TBV/TBD Priority	8. TBV Due To			
2. Technical Product Input Source Title and Identifier(s) with Version	3. Section					Unqual.	From Uncontrolled Source	Un-confirmed	
2a									
94.	Wu, Y.S.; Ritcey, A.C. and Bodvarsson, G.S. 1999b. "A Modeling Study of Perched Water Phenomena in the Unsaturated Zone at Yucca Mountain." <i>Journal of Contaminant Hydrology</i> 38 (1-3), 157-184. Amsterdam, The Netherlands: Elsevier Science Publishers. TIC: 244160.	p. 163-165	N/A-Reference only	6.2	Perched water conceptual model	N/A	N/A	N/A	N/A
95.	Yang, I.C.; Yu, P.; Rattray, G.W.; Ferarese, J.S.; Rayn, J.N. 1998. <i>Hydrochemical Investigations in Characterizing the Unsaturated Zone at Yucca Mountain, Nevada</i> . Water Resources Investigation Report 98-4132. Denver, Colorado: U.S. Geological Survey. TIC: 243710.	Entire	N/A-Reference only	6.4.2.1 6.5	Pore water chemical concentrations Water chemistry for initial and boundary conditions	N/A	N/A	N/A	N/A
96.	Software Code: EARTHVISION V4.0. STN: 30035-2 V4.0.	Entire	N/A-Qualified/Confirmed/Verified	6.2	General software use	N/A	N/A	N/A	N/A

OFFICE OF CIVILIAN RADIOACTIVE WASTE MANAGEMENT DOCUMENT INPUT REFERENCE SYSTEM									
1. Document Identifier No./Rev.: MDL-NBS-HS-000006/Rev. 00			Change: <i>JCH 4/7/00</i> N/A	Title: UZ Flow Models and Submodels					
Input Document		3. Section	4. Input Status	5. Section Used in	6. Input Description	7. TBV/TBD Priority	8. TBV Due To		
2. Technical Product Input Source Title and Identifier(s) with Version							Unqual.	From Uncontrolled Source	Un-confirmed
2a									
97.	Software Code: EXT V1.0_MEOS9. STN: 10227-1.0MEOS9-00.	Entire	N/A- Qualified/ Confirmed/ Verified	6.2 6.3 6.6 6.7 6.8.3	General software use	N/A	N/A	N/A	N/A
98.	Software Code: infil2grd V1.6. STN: 10077-1.6-00.	Entire	TBV	6.1 6.2 6.3 6.4 6.6 6.7 6.8.2 6.8.3 6.8.4	General software use	1	✓	N/A	N/A
99.	Software Code: ITOUGH2 V3.2, STN: 10054-3.2-00	Entire	N/A- Qualified/ Confirmed/ Verified	6.8.1	General software use	N/A	N/A	N/A	N/A
100.	Software Code: T2R3D V1.4. STN: 10006-1.4-00.	Entire	N/A- Qualified/ Confirmed/ Verified	6.4 6.7 6.8.1	General software use	N/A	N/A	N/A	N/A

OFFICE OF CIVILIAN RADIOACTIVE WASTE MANAGEMENT DOCUMENT INPUT REFERENCE SYSTEM									
1. Document Identifier No./Rev.: MDL-NBS-HS-000006/Rev. 00			Change: <i>N/A</i>	Title: UZ Flow Models and Submodels					
Input Document		3. Section	4. Input Status	5. Section Used in	6. Input Description	7. TBV/TBD Priority	8. TBV Due To		
2. Technical Product Input Source Title and Identifier(s) with Version	2a						Unqual.	From Uncontrolled Source	Un-confirmed
101.	Software Code: TOUGH2 V1.4. STN: 10007-1.4-00.	Entire	N/A- Qualified/ Confirmed/ Verified	6.2 6.3 6.4 6.6 6.8.2, 6.8.3, 6.8.4	General software use	N/A	N/A	N/A	N/A
102.	Software Code: TOUGHREACT V2.2. STN: 10154-2.2-00.	Entire	N/A- Qualified/ Confirmed/ Verified	6.5	General software use	N/A	N/A	N/A	N/A
103.	Software Code: TOUGHREACTE9 V1.0. STN: 10153-1.0-00.	Entire	TBV	6.5	General software use	1	✓	N/A	N/A
104.	Software Routine: ECRB-XYZ V03. STN: 30093-V.03.	Entire	N/A- Qualified/ Confirmed/ Verified	6.8.2	General software use	N/A	N/A	N/A	N/A
105.	Software Routine: TBgas3D V.1.1.1. ACC: MOL.19991012.0222.	Entire	N/A- Qualified/ Confirmed/ Verified	6.8.4	General software use	N/A	N/A	N/A	N/A

OFFICE OF CIVILIAN RADIOACTIVE WASTE MANAGEMENT DOCUMENT INPUT REFERENCE SYSTEM									
1. Document Identifier No./Rev.: MDL-NBS-HS-000006/Rev. 00			Change: <i>28H 4/7/00</i> N/A	Title: UZ Flow Models and Submodels					
Input Document		3. Section	4. Input Status	5. Section Used in	6. Input Description	7. TBV/TBD Priority	8. TBV Due To		
2. Technical Product Input Source Title and Identifier(s) with Version	2a						Unqual.	From Uncontrolled Source	Un-confirmed
106.	Software Routine: Read_TDB V1.0. ACC: MOL.19990903.0031	Entire	N/A- Qualified/ Confirmed/ Verified	6.8.1	General software use	N/A	N/A	N/A	N/A
107.	Software Routine: Frac_Calc V1.1. ACC: MOL.19990903.0032.	Entire	N/A- Qualified/ Confirmed/ Verified	6.8.1	General software use	N/A	N/A	N/A	N/A

AP-3.15Q.1

Rev. 06/30/1999

ATTACHMENT II

Calibrated parameter sets, combining from one-dimensional inversions and three-dimensional perched water modeling, used in generating the 18 flow fields, groundwater travel and tracer transport times.

Table II-1. Calibrated parameters for the present-day, mean infiltration scenario, used for simulations with perched water conceptual model #1 (flow-through) for the mean infiltration scenarios of the present-day, Monsoon and Glacial transition climates.

Model Layer	k_M (m ²)	α_M (1/Pa)	m_M (-)	k_F (m ²)	α_F (1/Pa)	m_F (-)	γ (-)
tcw11	3.86E-15	4.00E-5	0.470	2.41E-12	3.15E-3	0.627	0.30
tcw12	2.74E-19	1.81E-5	0.241	1.00E-10	2.13E-3	0.613	0.30
tcw13	9.23E-17	3.44E-6	0.398	5.42E-12	1.26E-3	0.607	0.30
ptn21	9.90E-13	1.01E-5	0.176	1.86E-12	1.68E-3	0.580	0.09
ptn22	2.65E-12	1.60E-4	0.326	2.00E-11	7.68E-4	0.580	0.09
ptn23	1.23E-13	5.58E-6	0.397	2.60E-13	9.23E-4	0.610	0.09
ptn24	7.86E-14	1.53E-4	0.225	4.67E-13	3.37E-3	0.623	0.09
ptn25	7.00E-14	5.27E-5	0.323	7.03E-13	6.33E-4	0.644	0.09
ptn26	2.21E-13	2.49E-4	0.285	4.44E-13	2.79E-4	0.552	0.09
tsw31	6.32E-17	3.61E-5	0.303	3.21E-11	2.49E-4	0.566	0.06
tsw32	5.83E-16	3.61E-5	0.333	3.56E-11	1.27E-3	0.608	0.41
tsw33	3.08E-17	2.13E-5	0.298	3.86E-11	1.46E-3	0.608	0.41
tsw34	4.07E-18	3.86E-6	0.291	1.70E-11	5.16E-4	0.608	0.41
tsw35	3.04E-17	6.44E-6	0.236	4.51E-11	7.39E-4	0.611	0.41
tsw36	5.71E-18	3.55E-6	0.380	7.01E-11	7.84E-4	0.610	0.41
tsw37	4.49E-18	5.33E-6	0.425	7.01E-11	7.84E-4	0.610	0.41
tsw38	4.53E-18	6.94E-6	0.324	5.92E-13	4.87E-4	0.612	0.41
tsw39	5.46E-17	2.29E-5	0.380	4.57E-13	9.63E-4	0.634	0.41
ch1z	1.96E-19	2.68E-7	0.316	3.40E-13	1.43E-3	0.631	0.10
ch1v	9.90E-13	1.43E-5	0.350	1.84E-12	1.09E-3	0.624	0.13
ch2v	9.27E-14	5.13E-5	0.299	2.89E-13	5.18E-4	0.628	0.13
ch3v	9.27E-14	5.13E-5	0.299	2.89E-13	5.18E-4	0.628	0.13
ch4v	9.27E-14	5.13E-5	0.299	2.89E-13	5.18E-4	0.628	0.13
ch5v	9.27E-14	5.13E-5	0.299	2.89E-13	5.18E-4	0.628	0.13
ch2z	6.07E-18	3.47E-6	0.244	3.12E-14	4.88E-4	0.598	0.10
ch3z	6.07E-18	3.47E-6	0.244	3.12E-14	4.88E-4	0.598	0.10
ch4z	6.07E-18	3.47E-6	0.244	3.12E-14	4.88E-4	0.598	0.10
ch5z	6.07E-18	3.47E-6	0.244	3.12E-14	4.88E-4	0.598	0.10

NOTE: These data have been developed as documented in this AMR and submitted under DTN: LB991121233129.001.

Table II-1. Calibrated parameters for the present-day, mean infiltration scenario, used for simulations with perched water conceptual model #1 (flow-through) for the mean infiltration scenarios of the present-day, Monsoon and Glacial transition climates. (Cont.)

Model Layer	k_M (m ²)	α_M (1/Pa)	m_M (-)	k_F (m ²)	α_F (1/Pa)	m_F (-)	γ (-)
ch6	4.23E-19	3.38E-7	0.510	1.67E-14	7.49E-4	0.604	0.10
pp4	4.28E-18	1.51E-7	0.676	3.84E-14	5.72E-4	0.627	0.10
pp3	2.56E-14	2.60E-5	0.363	7.60E-12	8.73E-4	0.655	0.46
pp2	1.57E-16	2.67E-6	0.369	1.38E-13	1.21E-3	0.606	0.46
pp1	6.40E-17	1.14E-6	0.409	1.12E-13	5.33E-4	0.622	0.10
bf3	2.34E-14	4.48E-6	0.481	4.08E-13	9.95E-4	0.624	0.46
bf2	2.51E-17	1.54E-7	0.569	1.30E-14	5.42E-4	0.608	0.10
pcM38/ pcF38	3.00E-19	6.94E-6	0.324	3.00E-18	6.94E-6	0.324	0.00
pcM39/ pcF39	6.20E-18	2.29E-5	0.381	6.20E-17	2.29E-5	0.381	0.00
pcM1z/ pcF1z	9.30E-20	2.68E-7	0.316	9.30E-19	2.68E-7	0.316	0.00
pcM2z/ pcF2z	2.40E-18	3.47E-6	0.245	2.40E-17	3.47E-6	0.245	0.00
pcM5z/ pcF5z	2.40E-18	3.47E-6	0.245	2.40E-18	3.47E-6	0.245	0.00
pcM6z/ pcF6z	1.10E-19	3.38E-7	0.510	1.10E-19	3.38E-7	0.510	0.00
pcM4p/ pcF4p	7.70E-19	1.51E-7	0.676	7.70E-19	1.51E-7	0.676	0.00

NOTE: These data have been developed as documented in this AMR and submitted under DTN: LB991121233129.001.

Table II-2. Calibrated parameters for the present-day, mean infiltration scenario, used for simulations with perched water conceptual model #2 (by-passing) for the mean infiltration scenarios of the present-day, Monsoon and Glacial transition climates

Model Layer	k_M (m ²)	α_M (1/Pa)	m_M (-)	k_F (m ²)	α_F (1/Pa)	m_F (-)	γ (-)
tcw11	3.86E-15	4.00E-5	0.470	2.41E-12	3.15E-3	0.627	0.30
tcw12	2.74E-19	1.81E-5	0.241	1.00E-10	2.13E-3	0.613	0.30
tcw13	9.23E-17	3.44E-6	0.398	5.42E-12	1.26E-3	0.607	0.30
ptn21	9.90E-13	1.01E-5	0.176	1.86E-12	1.68E-3	0.580	0.09
ptn22	2.65E-12	1.60E-4	0.326	2.00E-11	7.68E-4	0.580	0.09
ptn23	1.23E-13	5.58E-6	0.397	2.60E-13	9.23E-4	0.610	0.09
ptn24	7.86E-14	1.53E-4	0.225	4.67E-13	3.37E-3	0.623	0.09

NOTE: These data have been developed as documented in this AMR and submitted under DTN: LB991121233129.002

Table II-2. Calibrated parameters for the present-day, mean infiltration scenario, used for simulations with perched water conceptual model #2 (by-passing) for the mean infiltration scenarios of the present-day, Monsoon and Glacial transition climates (Cont.)

Model Layer	k_M (m ²)	α_M (1/Pa)	m_M (-)	k_F (m ²)	α_F (1/Pa)	m_F (-)	γ (-)
ptn25	7.00E-14	5.27E-5	0.323	7.03E-13	6.33E-4	0.644	0.09
ptn26	2.21E-13	2.49E-4	0.285	4.44E-13	2.79E-4	0.552	0.09
tsw31	6.32E-17	3.61E-5	0.303	3.21E-11	2.49E-4	0.566	0.06
tsw32	5.83E-16	3.61E-5	0.333	3.56E-11	1.27E-3	0.608	0.41
tsw33	3.08E-17	2.13E-5	0.298	3.86E-11	1.46E-3	0.608	0.41
tsw34	4.07E-18	3.86E-6	0.291	1.70E-11	5.16E-4	0.608	0.41
tsw35	3.04E-17	6.44E-6	0.236	4.51E-11	7.39E-4	0.611	0.41
tsw36	5.71E-18	3.55E-6	0.380	7.01E-11	7.84E-4	0.610	0.41
tsw37	4.49E-18	5.33E-6	0.425	7.01E-11	7.84E-4	0.610	0.41
tsw38	4.53E-18	6.94E-6	0.324	5.92E-13	4.87E-4	0.612	0.41
tsw39	5.46E-17	2.29E-5	0.380	4.57E-13	9.63E-4	0.634	0.41
ch1z	1.96E-19	2.68E-7	0.316	1.96E-19	2.68E-7	0.316	0.00
ch1v	9.90E-13	1.43E-5	0.350	1.84E-12	1.09E-3	0.624	0.13
ch2v	9.27E-14	5.13E-5	0.299	2.89E-13	5.18E-4	0.628	0.13
ch3v	9.27E-14	5.13E-5	0.299	2.89E-13	5.18E-4	0.628	0.13
ch4v	9.27E-14	5.13E-5	0.299	2.89E-13	5.18E-4	0.628	0.13
ch5v	9.27E-14	5.13E-5	0.299	2.89E-13	5.18E-4	0.628	0.13
ch2z	6.07E-18	3.47E-6	0.244	6.07E-18	3.47E-6	0.244	0.00
ch3z	6.07E-18	3.47E-6	0.244	6.07E-18	3.47E-6	0.244	0.00
ch4z	6.07E-18	3.47E-6	0.244	6.07E-18	3.47E-6	0.244	0.00
ch5z	6.07E-18	3.47E-6	0.244	6.07E-18	3.47E-6	0.244	0.00
ch6	4.23E-19	3.38E-7	0.510	4.23E-19	3.38E-7	0.510	0.00
pp4	4.28E-18	1.51E-7	0.676	4.28E-18	1.51E-7	0.676	0.00
pp3	2.56E-14	2.60E-5	0.363	7.60E-12	8.73E-4	0.655	0.46
pp2	1.57E-16	2.67E-6	0.369	1.38E-13	1.21E-3	0.606	0.46
pp1	6.40E-17	1.14E-6	0.409	6.40E-17	1.14E-6	0.409	0.00
bf3	2.34E-14	4.48E-6	0.481	4.08E-13	9.95E-4	0.624	0.46
bf2	2.51E-17	1.54E-7	0.569	2.51E-17	1.54E-7	0.569	0.00
pcM38/ pcF38	3.00E-19	6.94E-6	0.324	3.00E-18	6.94E-6	0.324	0.00
pcM39/ pcF39	6.20E-18	2.29E-5	0.381	6.20E-17	2.29E-5	0.381	0.00

NOTE: These data have been developed as documented in this AMR and submitted under DTN: LB991121233129.002

Table II-3. Calibrated parameters for the present-day, upper-bound infiltration scenario, used for simulations with perched water conceptual model #1 (flow-through) for the upper-bound infiltration scenarios of the present-day, Monsoon and Glacial transition climates

Model Layer	k_M (m ²)	α_M (1/Pa)	m_M (-)	k_F (m ²)	α_F (1/Pa)	m_F (-)	γ (-)
tcw11	3.98E-15	4.27E-5	0.484	2.75E-12	4.67E-3	0.636	0.31
tcw12	3.26E-19	2.18E-5	0.229	1.00E-10	2.18E-3	0.633	0.31
tcw13	1.63E-16	2.17E-6	0.416	2.26E-12	1.71E-3	0.631	0.31
ptn21	1.26E-13	1.84E-4	0.199	1.00E-11	2.38E-3	0.611	0.08
ptn22	5.98E-12	2.42E-5	0.473	1.00E-11	1.26E-3	0.665	0.08
ptn23	3.43E-13	4.06E-6	0.407	1.96E-13	1.25E-3	0.627	0.08
ptn24	3.93E-13	5.27E-5	0.271	4.38E-13	2.25E-3	0.631	0.08
ptn25	1.85E-13	2.95E-5	0.378	6.14E-13	1.00E-3	0.637	0.08
ptn26	6.39E-13	3.54E-4	0.265	3.48E-13	3.98E-4	0.367	0.08
tsw31	9.25E-17	7.79E-5	0.299	2.55E-11	1.78E-4	0.577	0.09
tsw32	5.11E-16	4.90E-5	0.304	2.83E-11	1.32E-3	0.631	0.38
tsw33	1.24E-17	1.97E-5	0.272	3.07E-11	1.50E-3	0.631	0.38
tsw34	7.94E-19	3.32E-6	0.324	1.35E-11	4.05E-4	0.579	0.38
tsw35	1.42E-17	7.64E-6	0.209	3.58E-11	9.43E-4	0.627	0.38
tsw36	1.34E-18	3.37E-6	0.383	5.57E-11	8.21E-4	0.623	0.38
tsw37	7.04E-19	2.70E-6	0.447	5.57E-11	8.21E-4	0.623	0.38
tsw38	4.47E-18	5.56E-7	0.314	4.06E-13	7.69E-4	0.622	0.38
tsw39	3.12E-17	1.82E-5	0.377	5.89E-13	1.30E-3	0.633	0.38
ch1z	8.46E-20	4.23E-7	0.336	5.70E-13	1.29E-3	0.631	0.10
ch1v	4.36E-14	4.23E-5	0.363	7.90E-13	1.66E-3	0.656	0.10
ch2v	3.89E-13	4.86E-5	0.312	4.64E-13	1.45E-3	0.626	0.10
ch3v	3.89E-13	4.86E-5	0.312	4.64E-13	1.45E-3	0.626	0.10
ch4v	3.89E-13	4.86E-5	0.312	4.64E-13	1.45E-3	0.626	0.10
ch5v	3.89E-13	4.86E-5	0.312	4.64E-13	1.45E-3	0.626	0.10
ch2z	1.16E-17	1.13E-6	0.229	2.64E-14	8.45E-4	0.628	0.10
ch3z	1.16E-17	1.13E-6	0.229	2.64E-14	8.45E-4	0.628	0.10
ch4z	1.16E-17	1.13E-6	0.229	2.64E-14	8.45E-4	0.628	0.10
ch5z	1.16E-17	1.13E-6	0.229	2.64E-14	8.45E-4	0.628	0.10
ch6	3.32E-20	3.57E-7	0.502	2.21E-14	1.31E-3	0.631	0.10
pp4	2.00E-18	1.83E-7	0.683	1.07E-13	7.99E-4	0.633	0.10
pp3	1.47E-14	1.02E-5	0.395	7.10E-12	1.29E-3	0.749	0.56
pp2	1.05E-16	2.43E-6	0.367	2.53E-13	1.65E-3	0.629	0.56
pp1	5.49E-17	1.01E-6	0.393	6.25E-13	8.18E-4	0.630	0.10
bf3	2.98E-14	3.83E-6	0.490	1.43E-12	1.50E-3	0.636	0.56

NOTE: These data have been developed as documented in this AMR and submitted under DTN: LB991121233129.003

Table II-3. Calibrated parameters for the present-day, upper-bound infiltration scenario, used for simulations with perched water conceptual model #1 (flow-through) for the upper-bound infiltration scenarios of the present-day, Monsoon and Glacial transition climates (Cont.)

Model Layer	k_M (m ²)	α_M (1/Pa)	m_M (-)	k_F (m ²)	α_F (1/Pa)	m_F (-)	γ (-)
bf2	3.86E-17	2.29E-7	0.582	2.26E-14	8.18E-4	0.631	0.10
pcM38/ pcF38	3.00E-19	5.56E-7	0.314	3.00E-18	5.56E-7	0.314	0.00
pcM39/ pcF39	6.20E-18	1.82E-5	0.377	6.20E-17	1.82E-5	0.377	0.00
pcM1z/ pcF1z	9.30E-20	4.23E-7	0.336	9.30E-19	4.23E-7	0.336	0.00
pcM2z/ pcF2z	2.40E-18	1.13E-6	0.229	2.40E-17	1.13E-6	0.229	0.00
pcM5z/ pcF5z	2.40E-18	1.13E-6	0.229	2.40E-18	1.13E-6	0.229	0.00
pcM6z/ pcF6z	1.10E-19	3.57E-7	0.502	1.10E-19	3.57E-7	0.502	0.00
pcM4p/ pcF4p	7.70E-19	1.83E-7	0.683	7.70E-19	1.83E-7	0.683	0.00

NOTE: These data have been developed as documented in this AMR and submitted under DTN: LB991121233129.003

Table II-4. Calibrated parameters for the present-day, upper-bound infiltration scenario, used for simulations with perched water conceptual model #2 (by-passing) for the upper-bound infiltration scenarios of the present-day, Monsoon and Glacial transition climates

Model Layer	k_M (m ²)	α_M (1/Pa)	m_M (-)	k_F (m ²)	α_F (1/Pa)	m_F (-)	γ (-)
tcw11	3.98E-15	4.27E-5	0.484	2.75E-12	4.67E-3	0.636	0.31
tcw12	3.26E-19	2.18E-5	0.229	1.00E-10	2.18E-3	0.633	0.31
tcw13	1.63E-16	2.17E-6	0.416	2.26E-12	1.71E-3	0.631	0.31
ptn21	1.26E-13	1.84E-4	0.199	1.00E-11	2.38E-3	0.611	0.08
ptn22	5.98E-12	2.42E-5	0.473	1.00E-11	1.26E-3	0.665	0.08
ptn23	3.43E-13	4.06E-6	0.407	1.96E-13	1.25E-3	0.627	0.08
ptn24	3.93E-13	5.27E-5	0.271	4.38E-13	2.25E-3	0.631	0.08
ptn25	1.85E-13	2.95E-5	0.378	6.14E-13	1.00E-3	0.637	0.08
ptn26	6.39E-13	3.54E-4	0.265	3.48E-13	3.98E-4	0.367	0.08
tsw31	9.25E-17	7.79E-5	0.299	2.55E-11	1.78E-4	0.577	0.09
tsw32	5.11E-16	4.90E-5	0.304	2.83E-11	1.32E-3	0.631	0.38
tsw33	1.24E-17	1.97E-5	0.272	3.07E-11	1.50E-3	0.631	0.38
tsw34	7.94E-19	3.32E-6	0.324	1.35E-11	4.05E-4	0.579	0.38

NOTE: These data have been developed as documented in this AMR and submitted under DTN: LB991121233129.004

Table II-4. Calibrated parameters for the present-day, upper-bound infiltration scenario, used for simulations with perched water conceptual model #2 (by-passing) for the upper-bound infiltration scenarios of the present-day, Monsoon and Glacial transition climates (Cont.)

Model Layer	k_M (m ²)	α_M (1/Pa)	m_M (-)	k_F (m ²)	α_F (1/Pa)	m_F (-)	γ (-)
tsw35	1.42E-17	7.64E-6	0.209	3.58E-11	9.43E-4	0.627	0.38
tsw36	1.34E-18	3.37E-6	0.383	5.57E-11	8.21E-4	0.623	0.38
tsw37	7.04E-19	2.70E-6	0.447	5.57E-11	8.21E-4	0.623	0.38
tsw38	4.47E-18	5.56E-7	0.314	4.06E-13	7.69E-4	0.622	0.38
tsw39	3.12E-17	1.82E-5	0.377	5.89E-13	1.30E-3	0.633	0.38
ch1z	8.46E-20	4.23E-7	0.336	8.46E-20	4.23E-7	0.336	0.00
ch1v	4.36E-14	4.23E-5	0.363	7.90E-13	1.66E-3	0.656	0.10
ch2v	3.89E-13	4.86E-5	0.312	4.64E-13	1.45E-3	0.626	0.10
ch3v	3.89E-13	4.86E-5	0.312	4.64E-13	1.45E-3	0.626	0.10
ch4v	3.89E-13	4.86E-5	0.312	4.64E-13	1.45E-3	0.626	0.10
ch5v	3.89E-13	4.86E-5	0.312	4.64E-13	1.45E-3	0.626	0.10
ch2z	1.16E-17	1.13E-6	0.229	1.16E-17	1.13E-6	0.229	0.00
ch3z	1.16E-17	1.13E-6	0.229	1.16E-17	1.13E-6	0.229	0.00
ch4z	1.16E-17	1.13E-6	0.229	1.16E-17	1.13E-6	0.229	0.00
ch5z	1.16E-17	1.13E-6	0.229	1.16E-17	1.13E-6	0.229	0.00
ch6	3.32E-20	3.57E-7	0.502	3.32E-20	3.57E-7	0.502	0.00
pp4	2.00E-18	1.83E-7	0.683	2.00E-18	1.83E-7	0.683	0.00
pp3	1.47E-14	1.02E-5	0.395	7.10E-12	1.29E-3	0.749	0.56
pp2	1.05E-16	2.43E-6	0.367	2.53E-13	1.65E-3	0.629	0.56
pp1	5.49E-17	1.01E-6	0.393	5.49E-17	1.01E-6	0.393	0.00
bf3	2.98E-14	3.83E-6	0.490	1.43E-12	1.50E-3	0.636	0.56
bf2	3.86E-17	2.29E-7	0.582	3.86E-17	2.29E-7	0.582	0.00
pcM38/ pcF38	3.00E-19	5.56E-7	0.314	3.00E-18	5.56E-7	0.314	0.00
pcM39/ pcF39	6.20E-18	1.82E-5	0.377	6.20E-17	1.82E-5	0.377	0.00

NOTE: These data have been developed as documented in this AMR and submitted under DTN: LB991121233129.004

Table II-5. Calibrated parameters for the present-day, lower-bound infiltration scenario, used for simulations with perched water conceptual model #1 (flow-through) for the lower-bound infiltration scenarios of the present-day, Monsoon and Glacial transition climates

Model Layer	k_M (m ²)	α_M (1/Pa)	m_M (-)	k_F (m ²)	α_F (1/Pa)	m_F (-)	γ (-)
tcw11	4.63E-15	1.61E-5	0.460	2.70E-12	2.40E-3	0.598	0.25
tcw12	8.87E-20	2.89E-5	0.241	1.00E-10	2.05E-3	0.608	0.25
tcw13	6.61E-17	1.42E-6	0.368	1.79E-12	9.21E-4	0.600	0.25
ptn21	1.86E-13	6.13E-5	0.165	1.00E-11	1.66E-3	0.503	0.01
ptn22	3.27E-12	1.51E-5	0.390	1.00E-11	9.39E-4	0.651	0.01
ptn23	4.20E-13	2.04E-6	0.387	1.84E-13	1.28E-3	0.518	0.01
ptn24	3.94E-13	2.32E-5	0.210	4.31E-13	2.02E-3	0.594	0.01
ptn25	2.22E-13	2.04E-5	0.296	7.12E-13	7.42E-4	0.555	0.01
ptn26	5.43E-13	1.82E-4	0.264	3.08E-13	2.00E-4	0.401	0.01
tsw31	6.38E-17	2.81E-5	0.317	2.55E-11	4.42E-4	0.545	0.06
tsw32	6.28E-16	6.35E-5	0.279	2.83E-11	1.21E-3	0.603	0.23
tsw33	1.82E-17	2.44E-5	0.248	3.07E-11	1.36E-3	0.600	0.23
tsw34	3.50E-19	3.54E-6	0.309	1.35E-11	2.48E-4	0.515	0.23
tsw35	1.27E-17	7.57E-6	0.187	3.58E-11	6.26E-4	0.612	0.23
tsw36	1.19E-18	3.74E-6	0.328	5.57E-11	4.90E-4	0.540	0.23
tsw37	5.63E-19	3.28E-6	0.423	5.57E-11	4.90E-4	0.540	0.23
tsw38	1.44E-18	3.72E-6	0.291	5.65E-13	4.00E-4	0.603	0.23
tsw39	1.09E-17	2.37E-5	0.321	3.12E-13	6.43E-4	0.605	0.23
ch1z	2.75E-20	7.26E-7	0.304	1.87E-13	1.00E-3	0.611	0.12
ch1v	2.05E-14	9.86E-6	0.402	9.03E-13	1.43E-3	0.658	0.12
ch2v	3.17E-13	1.91E-5	0.326	1.94E-13	6.84E-4	0.544	0.12
ch3v	3.17E-13	1.91E-5	0.326	1.94E-13	6.84E-4	0.544	0.12
ch4v	3.17E-13	1.91E-5	0.326	1.94E-13	6.84E-4	0.544	0.12
ch5v	3.17E-13	1.91E-5	0.326	1.94E-13	6.84E-4	0.544	0.12
ch2z	6.28E-18	2.44E-6	0.135	4.10E-14	2.08E-4	0.613	0.12
ch3z	6.28E-18	2.44E-6	0.135	4.10E-14	2.08E-4	0.613	0.12
ch4z	6.28E-18	2.44E-6	0.135	4.10E-14	2.08E-4	0.613	0.12
ch5z	6.28E-18	2.44E-6	0.135	4.10E-14	2.08E-4	0.613	0.12
ch6	8.20E-20	5.06E-7	0.445	1.12E-14	6.10E-4	0.604	0.12
pp4	2.05E-18	1.83E-7	0.653	3.40E-14	4.86E-4	0.635	0.12
pp3	1.91E-14	1.53E-5	0.355	2.23E-12	5.93E-4	0.699	0.43
pp2	1.08E-16	2.08E-6	0.399	1.42E-13	7.62E-4	0.608	0.43
pp1	6.52E-17	9.40E-7	0.392	7.15E-14	3.90E-4	0.638	0.12
bf3	9.47E-15	3.75E-6	0.509	3.43E-13	7.60E-4	0.611	0.43

NOTE: These data have been developed as documented in this AMR and submitted under DTN: LB991121233129.005

Table II-5. Calibrated parameters for the present-day, lower-bound infiltration scenario, used for simulations with perched water conceptual model #1 (flow-through) for the lower-bound infiltration scenarios of the present-day, Monsoon and Glacial transition climates (Cont.)

Model Layer	k_M (m ²)	α_M (1/Pa)	m_M (-)	k_F (m ²)	α_F (1/Pa)	m_F (-)	γ (-)
bf2	1.27E-17	1.38E-7	0.568	9.21E-15	4.18E-4	0.598	0.12
pcM38/ pcF38	3.00E-19	3.72E-6	0.291	3.00E-19	3.72E-6	0.291	0.00
pcM39/ pcF39	6.20E-18	2.37E-5	0.321	6.20E-18	2.37E-5	0.321	0.00
pcM1z/ pcF1z	9.30E-20	7.26E-7	0.304	9.30E-20	7.26E-7	0.304	0.00
pcM2z/ pcF2z	2.40E-18	2.44E-6	0.135	2.40E-18	2.44E-6	0.135	0.00
pcM5z/ pcF5z	2.40E-18	2.44E-6	0.135	2.40E-18	2.44E-6	0.135	0.00
pcM6z/ pcF6z	1.10E-19	5.06E-7	0.445	1.10E-19	5.06E-7	0.445	0.00
pcM4p/ pcF4p	7.70E-19	1.83E-7	0.653	7.70E-19	1.83E-7	0.653	0.00

NOTE: These data have been developed as documented in this AMR and submitted under DTN: LB991121233129.005

Table II-6. Calibrated parameters for the present-day, lower-bound infiltration scenario, used for simulations with perched water conceptual model #2 (by-passing) for the lower-bound infiltration scenarios of the present-day, Monsoon and Glacial transition climates

Model Layer	k_M (m ²)	α_M (1/Pa)	m_M (-)	k_F (m ²)	α_F (1/Pa)	m_F (-)	γ (-)
tcw11	4.63E-15	1.61E-5	0.460	2.70E-12	2.40E-3	0.598	0.25
tcw12	8.87E-20	2.89E-5	0.241	1.00E-10	2.05E-3	0.608	0.25
tcw13	6.61E-17	1.42E-6	0.368	1.79E-12	9.21E-4	0.600	0.25
ptn21	1.86E-13	6.13E-5	0.165	1.00E-11	1.66E-3	0.503	0.01
ptn22	3.27E-12	1.51E-5	0.390	1.00E-11	9.39E-4	0.651	0.01
ptn23	4.20E-13	2.04E-6	0.387	1.84E-13	1.28E-3	0.518	0.01
ptn24	3.94E-13	2.32E-5	0.210	4.31E-13	2.02E-3	0.594	0.01
ptn25	2.22E-13	2.04E-5	0.296	7.12E-13	7.42E-4	0.555	0.01
ptn26	5.43E-13	1.82E-4	0.264	3.08E-13	2.00E-4	0.401	0.01
tsw31	6.38E-17	2.81E-5	0.317	2.55E-11	4.42E-4	0.545	0.06
tsw32	6.28E-16	6.35E-5	0.279	2.83E-11	1.21E-3	0.603	0.23
tsw33	1.82E-17	2.44E-5	0.248	3.07E-11	1.36E-3	0.600	0.23
tsw34	3.50E-19	3.54E-6	0.309	1.35E-11	2.48E-4	0.515	0.23

NOTE: These data have been developed as documented in this AMR and submitted under DTN: LB991121233129.006

Table II-6. Calibrated parameters for the present-day, lower-bound infiltration scenario, used for simulations with perched water conceptual model #2 (by-passing) for the lower-bound infiltration scenarios of the present-day, Monsoon and Glacial transition climates (Cont.)

Model Layer	k_M (m ²)	α_M (1/Pa)	m_M (-)	k_F (m ²)	α_F (1/Pa)	m_F (-)	γ (-)
tsw35	1.27E-17	7.57E-6	0.187	3.58E-11	6.26E-4	0.612	0.23
tsw36	1.19E-18	3.74E-6	0.328	5.57E-11	4.90E-4	0.540	0.23
tsw37	5.63E-19	3.28E-6	0.423	5.57E-11	4.90E-4	0.540	0.23
tsw38	1.44E-18	3.72E-6	0.291	5.65E-13	4.00E-4	0.603	0.23
tsw39	1.09E-17	2.37E-5	0.321	3.12E-13	6.43E-4	0.605	0.23
ch1z	2.75E-20	7.26E-7	0.304	2.75E-20	7.26E-7	0.304	0.00
ch1v	2.05E-14	9.86E-6	0.402	9.03E-13	1.43E-3	0.658	0.12
ch2v	3.17E-13	1.91E-5	0.326	1.94E-13	6.84E-4	0.544	0.12
ch3v	3.17E-13	1.91E-5	0.326	1.94E-13	6.84E-4	0.544	0.12
ch4v	3.17E-13	1.91E-5	0.326	1.94E-13	6.84E-4	0.544	0.12
ch5v	3.17E-13	1.91E-5	0.326	1.94E-13	6.84E-4	0.544	0.12
ch2z	6.28E-18	2.44E-6	0.135	6.28E-18	2.44E-6	0.135	0.00
ch3z	6.28E-18	2.44E-6	0.135	6.28E-18	2.44E-6	0.135	0.00
ch4z	6.28E-18	2.44E-6	0.135	6.28E-18	2.44E-6	0.135	0.00
ch5z	6.28E-18	2.44E-6	0.135	6.28E-18	2.44E-6	0.135	0.00
ch6	8.20E-20	5.06E-7	0.445	8.20E-20	5.06E-7	0.445	0.00
pp4	2.05E-18	1.83E-7	0.653	2.05E-18	1.83E-7	0.653	0.00
pp3	1.91E-14	1.53E-5	0.355	2.23E-12	5.93E-4	0.699	0.43
pp2	1.08E-16	2.08E-6	0.399	1.42E-13	7.62E-4	0.608	0.43
pp1	6.52E-17	9.40E-7	0.392	6.52E-17	9.40E-7	0.392	0.00
bf3	9.47E-15	3.75E-6	0.509	3.43E-13	7.60E-4	0.611	0.43
bf2	1.27E-17	1.38E-7	0.568	1.27E-17	1.38E-7	0.568	0.00
pcM38/ pcF38	3.00E-19	3.72E-6	0.291	3.00E-19	3.72E-6	0.291	0.00
pcM39/ pcF39	6.20E-18	2.37E-5	0.321	6.20E-18	2.37E-5	0.321	0.00

NOTE: These data have been developed as documented in this AMR and submitted under DTN: LB991121233129.006

Table II-7. Calibrated parameters for the present-day, mean infiltration scenario, used for simulations with perched water conceptual model #3 (non-perching) for the mean infiltration scenarios of the present-day, Monsoon and Glacial transition climates

Model Layer	k_M (m ²)	α_M (1/Pa)	m_M (-)	k_F (m ²)	α_F (1/Pa)	m_F (-)	γ (-)
tcw11	3.86E-15	4.00E-5	0.470	2.41E-12	3.15E-3	0.627	0.30
tcw12	2.74E-19	1.81E-5	0.241	1.00E-10	2.13E-3	0.613	0.30
tcw13	9.23E-17	3.44E-6	0.398	5.42E-12	1.26E-3	0.607	0.30
ptn21	9.90E-13	1.01E-5	0.176	1.86E-12	1.68E-3	0.580	0.09
ptn22	2.65E-12	1.60E-4	0.326	2.00E-11	7.68E-4	0.580	0.09
ptn23	1.23E-13	5.58E-6	0.397	2.60E-13	9.23E-4	0.610	0.09
ptn24	7.86E-14	1.53E-4	0.225	4.67E-13	3.37E-3	0.623	0.09
ptn25	7.00E-14	5.27E-5	0.323	7.03E-13	6.33E-4	0.644	0.09
ptn26	2.21E-13	2.49E-4	0.285	4.44E-13	2.79E-4	0.552	0.09
tsw31	6.32E-17	3.61E-5	0.303	3.21E-11	2.49E-4	0.566	0.06
tsw32	5.83E-16	3.61E-5	0.333	3.56E-11	1.27E-3	0.608	0.41
tsw33	3.08E-17	2.13E-5	0.298	3.86E-11	1.46E-3	0.608	0.41
tsw34	4.07E-18	3.86E-6	0.291	1.70E-11	5.16E-4	0.608	0.41
tsw35	3.04E-17	6.44E-6	0.236	4.51E-11	7.39E-4	0.611	0.41
tsw36	5.71E-18	3.55E-6	0.380	7.01E-11	7.84E-4	0.610	0.41
tsw37	4.49E-18	5.33E-6	0.425	7.01E-11	7.84E-4	0.610	0.41
tsw38	4.53E-18	6.94E-6	0.324	5.92E-13	4.87E-4	0.612	0.41
tsw39	5.46E-17	2.29E-5	0.380	4.57E-13	9.63E-4	0.634	0.41
ch1z	1.96E-19	2.68E-7	0.316	3.40E-13	1.43E-3	0.631	0.10
ch1v	9.90E-13	1.43E-5	0.350	1.84E-12	1.09E-3	0.624	0.13
ch2v	9.27E-14	5.13E-5	0.299	2.89E-13	5.18E-4	0.628	0.13
ch3v	9.27E-14	5.13E-5	0.299	2.89E-13	5.18E-4	0.628	0.13
ch4v	9.27E-14	5.13E-5	0.299	2.89E-13	5.18E-4	0.628	0.13
ch5v	9.27E-14	5.13E-5	0.299	2.89E-13	5.18E-4	0.628	0.13
ch2z	6.07E-18	3.47E-6	0.244	3.12E-14	4.88E-4	0.598	0.10
ch3z	6.07E-18	3.47E-6	0.244	3.12E-14	4.88E-4	0.598	0.10
ch4z	6.07E-18	3.47E-6	0.244	3.12E-14	4.88E-4	0.598	0.10
ch5z	6.07E-18	3.47E-6	0.244	3.12E-14	4.88E-4	0.598	0.10
ch6	4.23E-19	3.38E-7	0.510	1.67E-14	7.49E-4	0.604	0.10
pp4	4.28E-18	1.51E-7	0.676	3.84E-14	5.72E-4	0.627	0.10
pp3	2.56E-14	2.60E-5	0.363	7.60E-12	8.73E-4	0.655	0.46
pp2	1.57E-16	2.67E-6	0.369	1.38E-13	1.21E-3	0.606	0.46
pp1	6.40E-17	1.14E-6	0.409	1.12E-13	5.33E-4	0.622	0.10
bf3	2.34E-14	4.48E-6	0.481	4.08E-13	9.95E-4	0.624	0.46

NOTE: These data have been developed as documented in this AMR and submitted under DTN: LB991121233129.007

Table II-7. Calibrated parameters for the present-day, mean infiltration scenario, used for simulations with perched water conceptual model #3 (non-perching) for the mean infiltration scenarios of the present-day, Monsoon and Glacial transition climates (Cont.)

Model Layer	k_M (m ²)	α_M (1/Pa)	m_M (-)	k_F (m ²)	α_F (1/Pa)	m_F (-)	γ (-)
bf2	2.51E-17	1.54E-7	0.569	1.30E-14	5.42E-4	0.608	0.10

NOTE: These data have been developed as documented in this AMR and submitted under DTN: LB991121233129.007

ATTACHMENT III
SOFTWARE ROUTINES

111-1 JED 4/7/00

Read_TDB V1.0
Routine/Macro Documentation Form*

Note: All relevant scientific notebook (SN) pages are included in this records package. In some instances, the included SN pages cross-reference other pages that are not included here because these were not essential to the documentation of this routine.

1. Name of routine/macro with version/OS/hardware environment:
Read_TDB / Version 1.0 / DOS (or Windows with DOS) / PC
2. Name of commercial software with version/OS/hardware used to develop routine/macro:
FORTRAN 77 / FORTRAN Powerstation 4.0 (see SN YMP-LBNL-GSB-MC-1.2, p. 48)
3. Description and Test Plan.
 - Explain whether this is a routine or macro and describe what it does: (**Read_TDB is a routine**)
The software routine Read_TDB is a FORTRAN code that reads a text file (ASCII format) downloaded from the Technical Data Management System (TDMS), extracts the selected columns and rows of data for use in standard spreadsheet packages, and converts stations into linear meters. It excludes any rows that have incomplete or missing information and notes the rows excluded with a print out to the screen. It is described on pages 52 and 58 in YMP-LBNL-GSB-MC-1. To install the software, copy frac_calc11.f and datablk11.f from a disk onto the hard drive of a PC. Then, compile frac_calc using a FORTRAN 77 compiler and run executable.

This software routine is documented in the following scientific notebook pages:

YMP-LBNL-GSB-MC-1	pp. 52, 58, 82-87
YMP-LBNL-GSB-MC-1.2	pp. 48-50
Reference Binder YMP-LBNL-GSB-MC-1.2A	pp. 120-124

Inputs:

The code is designed to use fracture property data text files as directly downloaded from the TDMS. The test input which is in this very specific TDMS format is provided on pp. 120-124, Reference Binder YMP-LBNL-GSB-MC-1.2A.

- Source code: (including equations or algorithms from software setup (LabView, Excel, etc.):
The FORTRAN code is included on pp. 82-87 in YMP-LBNL-GSB-MC-1
 - Description of test(s) to be performed (be specific):
A test case is to use a downloaded file from the TDMS that has stations to be converted to linear distance and includes some columns with incomplete data (that are to be excluded by the routine). The test case downloaded file is DTN: GS951108314224.005. It was saved as test.dat and is included as pages 121-122 in Reference Binder YMP-LBNL-GSB-MC-1.2A. This routine is primarily used for processing of Detailed Line Survey (DLS) data and the test case uses a DLS file. The acceptance criteria are that it (1) extract the proper columns, (2) print the correct values for the selected columns, (3) exclude rows that have incomplete data, and (4) convert stations into linear distance.
 - Specify the range of input values to be used and why the range is valid:
The input is a direct sample from the TDMS and includes the columns with incomplete data and station values to be converted to linear distance. It is considered valid because it is the type of the data that the routine was designed to use.
4. **Test Results.**
 - Output from test (explain difference between input range used and possible input):

111-2 JEH 4/7/00

Read_TDB V1.0
Routine/Macro Documentation Form*

Test results are shown on pages 49-50 in YMP-LBNL-GSB-MC-1.2 and in Reference Binder YMP-LBNL-GSB-MC-1.2A, pp. 120-124.

- Description of how the testing shows that the results are correct for the specified input:
The routine correctly (1) extracted the proper columns (see columns/datatypes selected on p. 50 in YMP-LBNL-GSB-MC-1.2 and output on pp. 123-124 in Reference Binder YMP-LBNL-GSB-MC-1.2A, (2) printed the correct values for the selected columns in output file frac.dat (compare values in output with input pp. 123-124, 121-122 in Reference Binder YMP-LBNL-GSB-MC-1.2A, respectively (3) excluded rows that have incomplete data (see p. 50 in YMP-LBNL-GSB-MC-1.2 and output which excludes these rows on pp. 123-124 in Reference Binder YMP-LBNL-GSB-MC-1.2A, and (4) converted stations into linear distance (compare values under LOCATION in output as a linear distance in meters with input as stations on pp. 123-124, 121-122 in Reference Binder YMP-LBNL-GSB-MC-1.2A, respectively).
 - List limitations or assumptions to this test case and code in general:
The input file must be a downloaded file (ASCII or text) from the TDMS. It also assumes that the TDMS will not change its formatting of having the column heading align directly with the value or text within the column. It also assumes that station measurements correspond to meters (which has been used for the ESF, ECRB and their alcoves)
 - Electronic files identified by name and location (include disc if necessary):
test.dat and frac.dat (input and output) listed on pp. 120-124 in Reference Binder YMP-LBNL-GSB-MC-1.2A. File sizes and other information given on p. 49 of YMP-LBNL-GSB-MC-1.2.
5. Supporting Information. Include background information, such as revision to a previous routine or macro, or explanation of the steps performed to run the software. Include listings of all electronic files and codes used. Attach Scientific Notebook pages with appropriate information annotated:
See attached pages for technical review forms, referenced scientific notebook pages and other supporting documentation.

MAINTAIN PAGES IN THIS ORDER:

- | | |
|---|-------------------|
| 1) This 2 page "Routine Documentation" summarization form | |
| 2) YMP-LBNL-GSB-MC-1 | pp. 52, 58, 82-87 |
| 3) YMP-LBNL-GSB-MC-1.2 | pp. 48-50 |
| 4) Reference Binder YMP-LBNL-GSB-MC-1.2A | pp. 120-124 |

*Note that ~~the~~ supplement includes:

-Addition of this 2-page "Routine Documentation" summarization form

5/1/2000

111-3 2EA 4/7/00

TDB - Developed code to read in
data from DLS of ESF

4/1/98

This code uses the headings to determine
the spacing between parameters. This
code extracts:

STATION (only 1st if range.)
STRIKE
DIP
LENGTH ABOVE TRACE
LENGTH BELOW TRACE
HEIGHT
WIDTH

If any of the above are Not Recorded (NR) or
NA (Not Available) then the entire line is
excluded.

If an * is present indicating a possible
range for the value, the value given in the
table is used.

All of the above data manipulations are printed
to the file index.txt

The code allows the concatenation of data
files so that all can be placed together
for analysis.

This program was necessary because of the
text that is present in the TDB files and
allows for direct use of the data as numbers.

Read-DLS

is the prototype
for Read-TDB
which is a
single user
macro checked
on page 87
by R. Ahlers

MC 3/31/99

The code was tested on 11 DLS files
available from the TDB. Spot checks
were performed and the program was
found to work properly.

The following code and executable is on

NWD-Cushey

shared folder DLS \read_dls & DLS \read_dls.f

and

d:\code\read_dls\read_dls.f

d:\code\read_dls\read_dls

SIGNATURE _____

READ AND UNDERSTOOD _____

DATE _____

19

DATE _____

19

TDB - development of code to read any TDB text file 4/13/98

The previous code, read_dls.f (p. 52) was revised extensively to allow the extract of any parameter from any data file.

Again, the header is used as a basis for spacing.

The new code allows the user to select any parameter(s) (assumes all names are unique after 8 letters) and print these separately to a file.

If any of the selected parameters is not recorded (NR) or not available (NA), the entire line of data is excluded. (noted in file index. *txt) MC 4/13/98

If a * is present, the number is used by a note is recorded in index.txt

Any files can be concatenated.
number of

This code is called read_tdb.f and resides in both

D:\code\read_tdb
and
share folder dls
on NWD-Cushey

The code was tested on DLS files and spot checked. It appears to work properly.

The code will put in this Scientific Notebook once it is further tested.

SIGNATURE (SIGNATURE REMOVED)
READ AND UNDERSTOOD

DATE
DATE

4/13/98
19

Version 1.0 (MC 7/9/99)

This code is a single user macro MC 3/31/99

program Read_TDB

c This program reads the data files from the
 c Technical Database. Output are written
 c unformatted to selected output file. All messages are
 c recorded to the screen and file 'index.txt'
 c Mark Cushey 4/98

c Output is limited to 10 numerical datatypes
 c It is assumed that the maximum line length is less than 250

```

real anum,bnum,value(10),limvalue(10,2)
character*4 first
character*25 filename
character*250 all
character*250 datastring
character*8 astat,bstat,avalue,limtext(10)
character*1 onestring(250),onedata(8),plus(8),ans
character*8 dataname(10),limitname(10)
integer row,iname,istring,idata,icolumn(10),i,loc,rowused,
+ im,limnum,limtxt,loctype

```

c -----

c open output files
 write(*,*)'Enter name of output file:'
 read(*,1000)filename
 open(unit=20,file=filename)
 open(unit=21,file='index.txt')
 write(*,*)'Details on data retrieval are in index.txt'

c -----

c query for different data types to be stored

c

c write(*,*)'List names of data types to be retrieved - up to 10'
 write(*,*)' Enter only the first 8 letters for each'
 write(*,*)' Enter the word end for last entry'
 i = 0

40 i = i + 1
 read(*,1010)dataname(i)
 if ((dataname(i).ne.'end').and.
 & (dataname(i).ne.'END')) go to 40
 iname = i - 1
 write(*,1040)iname
 write(21,1040)iname
 write(20,1041) (dataname(i),i=1,iname)
 write(*,*)'Should header be printed in output file - Y or N'
 read(*,1011)ans
 if ((ans.eq.'Y').or.(ans.eq.'y'))
 & write(21,1041) (dataname(i),i=1,iname)

1010 format(a8)
 1011 format(a1)
 1040 format(1x,i7,' datatypes selected')
 1041 format(10(2x,a8))

c -----

see p87
 reviewed
 by
 F. Allers
 MC
 7/1/98

see
 p.52 and
 p.58 for
 initial development
 & planning
 of these
 code
 MC
 6/28/99

SIGNATURE

READ AND UNDERSTOOD

DATE

19

DATE

19

111-6 JEH 4/7/00

```

c      query for limits on outputting data
      limnum = iname
      limtxt = iname
      write(*,*)'Are there limits for the output - Y or N ?'
      read(*,1011)ans
      if ((ans.eq.'Y').or.(ans.eq.'y')) then
c          i = iname
c          write(*,*)'Enter the parameter names for numerical limits
c
c          write(*,*)'  Enter only the first 8 letters for each'
c          write(*,*)'  Enter the word end for last entry'
c45         i = i + 1
c          read(*,1010)dataname(i)
c          if ((dataname(i).eq.'end').or.
c          & (dataname(i).eq.'END')) go to 46
c          write(*,*)'Enter upper and lower value for limit'
c          read(*,*)limvalue(i,1),limvalue(i,2)
c          write(*,*)'Enter next limit or end'
c          go to 45
c46         i = i - 1
c          limnum = i
c          write(*,*)'Enter the parameter names for text-defined lim
its'
c          write(*,*)'  Enter only the first 8 letters for each'
c          write(*,*)'  Enter the word end for last entry'
47         i = i + 1
c          read(*,1010)dataname(i)
c          if ((dataname(i).eq.'end').or.
c          & (dataname(i).eq.'END')) go to 49
c          write(*,*)'Enter text to exclude - up to 8 characters'
c          read(*,1010)limtext(i)
c          write(*,*)'Enter next limit or end'
c          go to 47
49         limtxt = i - 1
c          do i=(iname+1),limtxt
c              if (i.le.limnum) then
c                  write(*,1045)dataname(i),limvalue(i,1),li
mvalue(i,2)
c                  write(21,1045)dataname(i),limvalue(i,1),l
imvalue(i,2)
c                  else
c                      write(*,1046)dataname(i),limtext(i)
c                      write(21,1046)dataname(i),limtext(i)
c                  end if
c              end do
1045        format(1x,'Limits on',a8,1x,f9.3,1x,f9.3)
1046        format(1x,'Limits on',a8,1x,'exclude',1x,a8)
c
c      -----
c      query for input filename and open
50         write(*,*)'Enter next data filename (use MS-DOS filename) or quit
c
c          read(*,1000)filename
c          if ((filename.eq.'quit').or.(filename.eq.'QUIT'))go to 990

```

SIGNATURE _____
 READ AND UNDERSTOOD _____

DATE _____ 19____
 DATE _____ 19____

111-7 224 4/7/00

```

open(unit=10,file=filename,action='READ',
&      form='FORMATTED',status='old',err=75)
write(*,*)filename
write(21,*)'-----'
write(21,*)filename
write(21,*)'-----'
1000  format(a25)
      go to 80
75    write(*,*)'File does not exist'
      go to 50

c      -----
c      If one of the parameters is LOCATION, determine type.
c      If LOCATION is station number along DLS, loctype = 0
c      If LOCATION is along alcove, loctype = alcove #.
c      If other, then loctype = -1.
80    loctype = -1
      Do i = 1,iname
          if (dataname(i).eq.'LOCATION') then
              write(*,*)'Is LOCATION a station number along the
+ ' DLS, alcove, or other - d, a, or o'
              read(*,*)ans
              if ((ans.eq.'d').or.(ans.eq.'D')) then
                  loctype = 0
              else
                  if ((ans.eq.'a').or.(ans.eq.'A')) then
                      write(*,*)'Which alcove #'
                      read(*,*)loctype
                  else
                      loctype = -1
                  end if
              end if
          end if
      End Do
c      -----
c      find header line (between rows of asteriks)
82    read(10,1001)first
      if (first.ne.'*****') go to 82
1001  format(a4)
c      -----
c      find location where different data starts (use header)

do i=1,limtxt
    icolumn(i)=0
end do

read(10,1020)datastring
read(datastring,1021)(onestring(istring),istring=1,250)
do i = 1,limtxt
    read(dataname(i),1022)(onedata(idata),idata=1,8)
    do istring = 1,250
        do idata = 1,8

```

SIGNATURE _____
 READ AND UNDERSTOOD _____

DATE _____ 19____
 DATE _____ 19____

111-8 224 4/2/00

```

        if( (onestring(istring+idata-1).ne.onedata(idata)) )
&          go to 98
        end do
98        if (idata.eq.9) go to 99
        end do
99        if (istring.ne.251) then
            icolumn(i)=istring
        else
            write(*,1023)dataname(i)
            pause
            stop
        end if
    end do

    write(*,1003)(icolumn(i),i=1,iname)
    write(21,1003)(icolumn(i),i=1,iname)
1003    format(1x,'Column headers at',10(1x,i5))
1020    format(a250)
1021    format(250(a1))
1022    format(8(a1))
1023    format(1x,a8,' not found in file -- stopped')

c      -----
c      move forward to first data row

105    read(10,1001)first
        if (first.ne.'****') go to 105
c      skip blank line
        read(10,1002)all
1002    format(a72)

c      -----

c      read data lines from file and get values
        rowused = 0
        row = 0
200    read(10,2001,err=900,end=900)datastring
        if (datastring.eq.'End of Report') go to 900
        if (datastring.eq.'          ') go to 200
        row = row + 1
        write(*,*)row

c      first see if data is within text-defined limits
        do ii=(limnum+1),limtxt
            loc = icolumn(ii)
            read(datastring,1999)all
            if (all.eq.limtext(ii)) then
                write(*,2025)row,dataname(ii),limtext(ii)
                write(*,2026)datastring
                write(21,2025)row,dataname(ii),limtext(ii)
                write(21,2026)datastring
                go to 200
            end if
        end do
    end do

```

SIGNATURE _____

READ AND UNDERSTOOD _____

DATE _____

19

DATE _____

19

111-9 JEH 4/7/00

```

open(unit=10,file=filename,action='READ',
& form='FORMATTED',status='old',err=75)
write(*,*)filename
write(21,*)'-----'
write(21,*)filename
write(21,*)'-----'
1000 format(a25)
go to 80
75 write(*,*)'File does not exist'
go to 50

c -----
c If one of the parameters is LOCATION, determine type.
c If LOCATION is station number along DLS, loctype = 0
c If LOCATION is along alcove, loctype = alcove #.
c If other, then loctype = -1.
80 loctype = -1
Do i = 1,iname
if (dataname(i).eq.'LOCATION') then
write(*,*)'Is LOCATION a station number along the
+' DLS, alcove, or other - d, a, or o'
read(*,*)ans
if ((ans.eq.'d').or.(ans.eq.'D')) then
loctype = 0
else
if ((ans.eq.'a').or.(ans.eq.'A')) then
write(*,*)'Which alcove #'
read(*,*)loctype
else
loctype = -1
end if
end if
End Do
c -----
c find header line (between rows of asteriks)
82 read(10,1001)first
if (first.ne.'*****') go to 82
1001 format(a4)
c -----
c find location where different data starts (use header)
do i=1,limtxt
icolumn(i)=0
end do

read(10,1020)datastring
read(datastring,1021)(onestring(istring),istring=1,250)
do i = 1,limtxt
read(dataname(i),1022)(onedata(idata),idata=1,8)
do istring = 1,250
do idata = 1,8

```

SIGNATURE _____

READ AND UNDERSTOOD _____

DATE _____

19

DATE _____

19

111-8 JEH 4/2/00

```

        if( (onestring(istring+idata-1).ne.onedata(idata)) )
    &      go to 98
        end do
98      if (idata.eq.9) go to 99
        end do
99      if (istring.ne.251) then
            icolumn(i)=istring
        else
            write(*,1023)dataname(i)
            pause
            stop
        end if
    end do

    write(*,1003)(icolumn(i),i=1,iname)
    write(21,1003)(icolumn(i),i=1,iname)
1003   format(1x,'Column headers at',10(1x,i5))
1020   format(a250)
1021   format(250(a1))
1022   format(8(a1))
1023   format(1x,a8,' not found in file -- stopped')

c     -----
c     move forward to first data row

105   read(10,1001)first
        if (first.ne.'****') go to 105
c     skip blank line
        read(10,1002)all
1002   format(a72)

c     -----
c     read data lines from file and get values
        rowused = 0
        row = 0
200   read(10,2001,err=900,end=900)datastring
        if (datastring.eq.'End of Report') go to 900
        if (datastring.eq.'          ') go to 200
        row = row + 1
        write(*,*)row

c     first see if data is within text-defined limits
        do ii=(limnum+1),limtxt
            loc = icolumn(ii)
            read(datastring,1999)all
            if (all.eq.limtext(ii)) then
                write(*,2025)row,dataname(ii),limtext(ii)
                write(*,2026)datastring
                write(21,2025)row,dataname(ii),limtext(ii)
                write(21,2026)datastring
                go to 200
            end if
        end do
    end do

```

SIGNATURE _____

DATE _____

19

READ AND UNDERSTOOD _____

DATE _____

19

111-9 JEH 4/7/00

```

do i=1,iname
  loc = icolumn(i)
  read(datastring,1999)avalue

c      first check to see if any are not recorded (NR) or
c      special (*) -- exclude NR and use *
      read(avalue,2002)(onedata(idata),idata=1,8)
do idata=1,8
  if ((onedata(idata)).eq.'N') then
c      the entire line is excluded
      write(*,2020)row,onedata(idata),onedata(idata+1)
      &      dataname(i)
      write(21,2020)row,onedata(idata),onedata(idata+1)
  ),
  &      dataname(i)
  go to 200
end if
if (onedata(idata).eq.'*') then
  write(*,2021)row
  write(21,2021)row
  read(avalue,2024)avalue
end if
end do

c      check if entry is a station number -- if loctype = 0
c      LOCATION is station number along DLS, if loctype = +#
c      LOCATION is along alcove (number loctype)

c      If ((loctype.ge.0).and.(dataname(i).eq.'LOCATION')) then
      get station number
      read(avalue,2005)(plus(ip),ip=1,8)
      do ip=1,8
        if (plus(ip).eq.'+') go to 215
      end do
215      read(avalue,2010)astat,all,bstat
      read(astat,*)anum
      read(bstat,2005)(plus(im),im=1,(8-ip))
      do im = 1, (8-ip)
        if (plus(im).eq.'-') go to 216
      end do
216      read(bstat,2011)astat
      read(astat,*)bnum

      if (loctype.eq.0) then
        value(i) = anum*100 + bnum
      else
        value(i) = real(loctype)*10000 + anum*100
+ bnum
      end if
    else
      read(avalue,*)value(i)
    end if

  end do

```

SIGNATURE _____

READ AND UNDERSTOOD _____

DATE _____

19 _____

DATE _____

19 _____

111-10 JEH 4/7/60

```

2001  format(a250)
c      change a8 to larger value if number is more than 8 digits
1999  format(<loc-1>x,a8)
2002  format(8(a1))
2005  format(8(a1))
2010  format(a<ip-1>,a1,a8)
2011  format(a<im-1>)
2020  format(1x,'Row',i5,' has a ',a1,a1,' for ',a8,
&      ' - this data row is not used')
2021  format(1x,'Row',i5,' has a * - printed value will be used')
2024  format(a<idata-1>)

2025  format(1x,'Row',i5,' excluded ',a8,' is ',a8)
2026  format(5x,a40)

c      write data to output file and read next line

write(20,3000)(value(i),i=1,iname)

3000  format(10(f10.3))
rowused = rowused + 1
go to 200

900   close(10)
write(*,*)row,' rows read and',rowused,' used'
write(21,*)row,' rows read and',rowused,' used'
c      ask for next file
go to 50

990   close(20)
close(21)
pause
stop

999   write(*,*)'Error in file formatting -- stopped'
write(*,*)'Error in file formatting -- stopped'
close(20)
close(21)
close(10)
pause
stop
end

```

This code has been reentered, and performs the task intended

(SIGNATURE REMOVED) 7/1/98

SIGNATURE (SIGNATURE REMOVED)
 READ AND UNDERSTOOD

DATE 5/7 19 98
 DATE 19

111-11 JEH 4/1/00

48

PROJECT NAME _____

QA: L

NOTEBOOK NO. _____

Computer information for Read_TDB.f

12/2/99

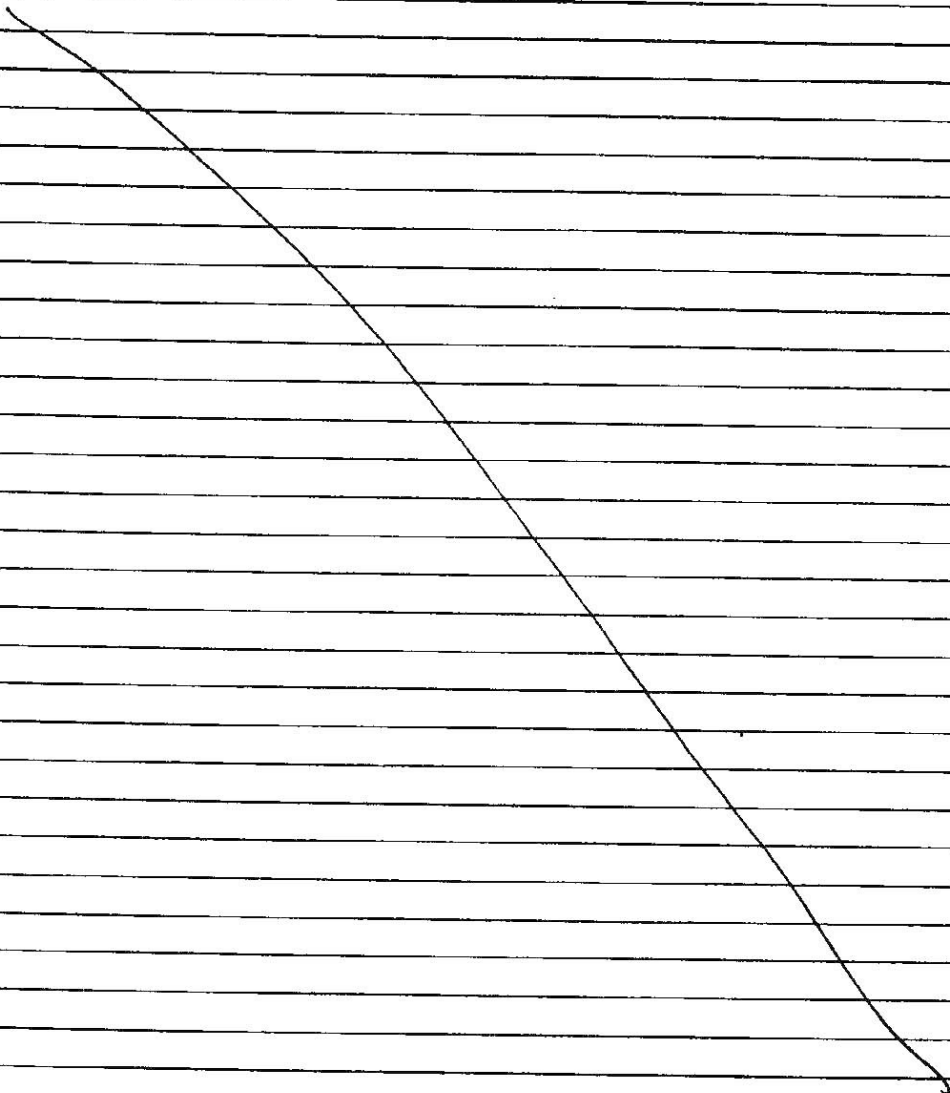
The routine Read_TDB Version 1.0 was compiled
using:

FORTAN Powerstation 4.0

Microsoft 1994-1995

Product ID: 36785-411-0083773-30563

(part of Microsoft Developer Studio)



SIGNATURE (SIGNATURE ON FILE) _____

READ AND UNDERSTOOD _____

DATE

12/2/99

DATE

19

✓ 111-12
QA 4/7/00

Files used in testing Read-TDB Version 1.0 12/2/97

Read-TDB was previously tested (see YMP-LBNL-GSB-MC-1, p. 58) and reviewed. The test case though was not included in the notebook, though. The files used to test are given below. This case was run on 4/13/98.

Volume in drive D is YMP
Volume Serial Number is 0758-0AD0
Directory of D:\code\read_tdb

		<DIR>	04-13-98	11:11a	.
		<DIR>	04-13-98	11:11a	..
			8,675	05-21-98	4:31p read_tdb.f
			4,797	04-13-98	2:36p read_tdb.mak
				04-13-98	12:16p Debug
		<DIR>			
input file	→	TEST	49,900	04-13-98	12:48p test.txt
output file	→	FRAC	7,488	04-13-98	2:56p frac.dat
		DIR	0	12-02-99	3:22p dir.txt
		READ_TDB	33,792	06-11-98	2:41p read_tdb.mdp
		DUMMY	24,800	04-20-98	3:19p dummy
		DLS	16,596	04-29-98	3:19p dls.dat
		ALCOVE3	4,960	05-04-98	3:16p alcove3.dat
			9 file(s)		151,008 bytes
			3 dir(s)		1,693,548,544 bytes free

The files test.dat and frac.dat are in Reference Binder YMP-LBNL-MC-1.2A pp. 120-124

test.dat is the input - it is a direct example from the TDMS
frac.dat is the output

These can be used to test Read-TDB on other personal computers.

The screen printout that is saved to 'index.txt' is on the next page.

SIGNATURE _____

READ AND UNDERSTOOD _____

11-13 test 4/7/00

DATE _____

DATE _____

19

19

```

7 datatypes selected
LOCATION STRIKE DIP LENGTH A LENGTH B HEIGHT WIDTH
-----
d:\code\read_tdb\test.txt
-----
Column headers at 28 70 87 104 121 138 155
Row 2 has a NR for LENGTH A - this data row is not used
Row 4 has a * - printed value will be used
Row 5 has a NR for LENGTH B - this data row is not used
Row 18 has a NR for LENGTH B - this data row is not used
Row 19 has a NR for LENGTH B - this data row is not used
Row 20 has a NR for LENGTH B - this data row is not used
Row 24 has a NR for LENGTH B - this data row is not used
Row 26 has a NR for LENGTH B - this data row is not used
Row 29 has a NR for LENGTH B - this data row is not used
Row 30 has a NR for LENGTH B - this data row is not used
Row 31 has a NR for LENGTH B - this data row is not used
Row 34 has a NR for LENGTH A - this data row is not used
Row 63 has a NR for LENGTH A - this data row is not used
Row 70 has a NR for LENGTH B - this data row is not used
Row 72 has a NR for LENGTH B - this data row is not used
Row 81 has a NR for LENGTH B - this data row is not used
Row 82 has a NR for LENGTH B - this data row is not used
Row 84 has a NR for LENGTH B - this data row is not used
Row 86 has a NR for LENGTH B - this data row is not used
Row 87 has a NR for LENGTH B - this data row is not used
Row 95 has a NR for LENGTH B - this data row is not used
123 rows read and 103 used

```

↑ from file 'index.txt'

SIGNATURE (SIGNATURE REMOVED)

DATE 12/2 19 99

READ AND UNDERSTOOD

J 11-14 Jan 1999

DATE 19

Files used in checking Read-TDB Version 1.0
(a software routine)

test.dat - input test file

frac.dat - output test file

These files were created on 4/13/98

frac.dat

LOCATION	STRIKE	DIP	LENGTH A	LENGTH B	HEIGHT	WIDTH
801.360	200.000	86.000	2.450	.700	3.100	.400
802.580	.000	90.000	.700	.200	.900	.100
803.180	325.000	83.000	.850	3.000	3.500	2.600
804.150	220.000	73.000	2.500	.900	3.000	.400
804.640	255.000	85.000	.750	1.300	1.900	.060
804.830	15.000	78.000	.270	.900	1.100	.030
805.600	170.000	50.000	2.500	.500	3.000	.400
806.290	220.000	84.000	1.400	1.100	2.500	.100
806.420	215.000	84.000	4.000	1.000	5.000	.500
806.860	220.000	85.000	1.500	.750	2.250	.080
807.750	210.000	74.000	2.200	2.500	4.500	1.500
808.340	225.000	80.000	4.000	1.300	5.000	.600
808.650	230.000	83.000	6.000	1.000	6.000	3.000
808.900	225.000	83.000	1.800	.900	2.400	.150
809.840	230.000	75.000	.660	.350	1.000	.030
814.960	30.000	84.000	1.200	.700	1.900	.100
815.310	235.000	75.000	4.000	.100	3.500	3.000
816.180	200.000	80.000	5.000	.200	5.000	4.000
817.880	180.000	48.000	1.900	.150	2.000	.100
819.450	230.000	75.000	2.500	1.200	3.500	.800
819.730	170.000	85.000	.950	.500	1.400	.050
824.180	176.000	56.000	.650	.600	1.250	.050
829.830	225.000	77.000	4.000	2.000	5.500	1.500
836.650	195.000	85.000	1.200	.170	1.330	.050
839.950	15.000	78.000	1.790	2.330	3.850	.900
843.310	225.000	77.000	3.000	2.100	4.800	.300
844.580	193.000	80.000	2.150	1.600	3.500	.100
845.000	300.000	84.000	5.400	1.900	7.000	8.000
849.920	197.000	65.000	2.900	1.600	4.400	.200
857.390	.000	40.000	.700	.850	1.500	.050
857.610	230.000	60.000	.550	1.250	1.750	.050
859.370	216.000	55.000	.470	1.500	1.970	.350
859.620	13.000	71.000	1.110	.210	1.300	.100
859.810	20.000	79.000	.730	1.020	1.700	.750
862.840	12.000	82.000	1.020	.220	1.170	.200
863.770	24.000	7.000	.340	2.800	3.000	.250
864.180	212.000	61.000	.570	.800	1.200	.080
864.700	21.000	15.000	.600	.490	1.000	.030
865.370	172.000	68.000	2.750	.490	3.000	.250
865.420	28.000	4.000	.030	.030	.060	.010
865.450	180.000	64.000	.150	.560	.650	.050
865.600	20.000	10.000	3.600	.200	3.400	.030
868.550	5.000	66.000	4.500	2.500	6.500	2.500
868.650	15.000	20.000	5.000	.100	5.000	.300
873.970	176.000	68.000	4.500	1.650	6.000	4.000
874.030	97.000	84.000	.560	.350	.850	.100
874.410	14.000	66.000	.230	.600	.780	.060
874.580	345.000	69.000	.570	.120	.650	.050
875.220	.000	74.000	2.600	.030	2.400	.400
879.700	20.000	8.000	2.000	6.000	8.000	1.500
882.370	184.000	78.000	3.500	1.670	4.000	2.000
893.860	20.000	49.000	.100	.330	.400	.010
893.920	22.000	80.000	.680	.620	1.250	.050
894.130	20.000	67.000	1.200	1.600	2.700	.900
896.190	225.000	50.000	2.660	1.480	3.800	.350

Page 1

111-16 22H 4/200

frac.dat

899.090	220.000	61.000	4.500	1.500	5.500	1.000
904.670	220.000	82.000	3.000	2.300	5.000	1.500
911.550	240.000	58.000	15.000	.200	6.000	10.000
916.700	300.000	49.000	5.000	2.500	7.200	9.000
921.670	165.000	76.000	15.000	2.000	8.000	7.000
922.000	205.000	90.000	1.000	1.800	2.500	1.400
923.570	5.000	85.000	1.700	1.800	3.100	1.300
923.950	30.000	80.000	6.000	1.650	7.000	2.700
926.550	15.000	83.000	2.700	1.400	3.500	.800
927.000	15.000	65.000	.400	.200	.500	.200
927.100	175.000	60.000	.500	.600	1.000	.150
929.570	195.000	87.000	13.000	10.000	8.000	8.000
931.760	220.000	90.000	2.700	1.500	3.500	.700
938.700	165.000	73.000	7.500	2.300	7.000	7.000
938.900	190.000	82.000	3.300	.800	3.000	.300
939.900	195.000	60.000	18.000	5.000	12.000	8.000
940.610	210.000	70.000	8.000	3.000	9.000	2.500
942.050	215.000	64.000	.700	.500	1.200	.150
942.430	210.000	65.000	5.000	.800	5.500	1.000
944.780	215.000	64.000	1.800	.900	2.600	.400
955.800	170.000	74.000	1.000	1.100	1.700	.300
956.430	188.000	66.000	18.000	5.000	12.000	8.000
958.020	330.000	82.000	4.000	1.400	5.000	2.200
962.000	200.000	90.000	.600	1.600	2.100	.200
963.230	150.000	84.000	3.500	1.800	5.000	1.000
965.390	160.000	66.000	1.000	1.200	2.000	.300
965.490	180.000	59.000	5.000	1.800	6.500	1.000
969.750	340.000	83.000	7.000	2.000	7.500	3.800
970.030	190.000	75.000	.500	.200	.700	.050
970.070	15.000	85.000	.700	.140	.800	.050
970.210	.000	80.000	4.000	1.900	5.900	1.000
973.600	190.000	70.000	1.200	1.100	2.200	.500
973.740	190.000	75.000	3.300	.220	3.000	.300
974.670	210.000	78.000	2.200	1.800	3.900	.900
983.470	200.000	58.000	5.000	1.900	6.000	1.000
984.760	350.000	88.000	.500	2.000	2.400	1.400
985.140	210.000	75.000	6.000	2.000	7.000	3.800
986.450	340.000	78.000	.700	2.300	2.200	1.900
986.850	210.000	87.000	.050	.900	.900	.300
987.860	190.000	74.000	.400	.600	1.000	.100
991.280	355.000	84.000	1.700	2.450	4.000	2.000
991.610	5.000	85.000	.900	2.400	3.000	2.000
991.870	215.000	88.000	4.000	2.400	6.000	1.500
994.150	340.000	82.000	2.000	2.200	4.000	2.100
995.940	195.000	64.000	.800	2.000	2.500	1.000
996.270	210.000	47.000	2.500	.400	2.700	.300
997.570	.000	82.000	2.400	2.600	4.500	2.200
998.430	340.000	76.000	2.700	3.200	4.500	2.200

View Unit Descriptions

Start of Report...

INGRES REPORT Copyright (c) 1981, 1995 Computer Associates Intl, Inc.
 Reading report specifications and preparing query . . .
 Retrieving data . . .

TECTONIC CHARACTERISTICS DATA REPORT

TABLE DESCRIPTION:

Fracture Type data from North Ramp Tunnel - ESF, and Yucca Mountain
 Project Detailed Line Survey-Data from Station 8+01.36 to 8+98.43;
 collected under GP-32, R3, SCP Study Number 8.3.1.4.2.2.4.. 06/02/1995 to
 06/20/1995.

TDIF: 305055

DTN: GS951108314224.005

FOOTNOTES: Traceline is generally 0.9 meters below right wall springline;
 BED-Bedding; F-Fracture; FLT-Fault; SH-Shear; RK-Ends blindly in rock
 mass; ST-End not visible behind ground support; IN Fracture extends under
 precast invert segments; Air-Fracture (usually subparallel to tunnel)
 termination has been excavated; CR-Crown; P-Planar; I-Irregular;
 U-Undulating; NR-Not recorded; R1-Stepped, Near-normal steps and ridges
 occur on the fracture surface; R2-Rough, Large, angular asperities can be
 seen; R3-Moderately rough, asperities are clearly visible and fracture
 surface feels abrasive; R4-Slightly rough, small asperities on the
 fracture surface are visible and can be felt; R5-Smooth, no asperities,
 smooth to the touch; R6- Polished, extremely smooth and shiny;
 Ja.11-Tightly healed, hard filling; Ja.12-unaltered surface stain only;
 Ja.13-slightly altered, non softening coating, sandy particles;
 Ja.14-silty or sandy clay coatings, little clay; Ja.15-softening or clay
 mineral coatings;

ADDNL FOOTNOTES: Ja.31 zones of disintegrated or crushed rock;
 Ja.32-zones of silty or sandy clay.

test.dat

ROW#	Q	FRACTURE TYPE	LOCATION	DATE	STRIKE (°)	DIP (°)	LENGTH ABOVE TR ACELINE (m)	LENGTH BELOW TR ACELINE (m)	HEIGHT (m)	WIDTH (m)	FRACTURE ENDS V ISIBLE	UPPER TERMINATI ON
1	Y	F	8+01.36	06/02/95 - 06/20/95	200	86	2.45	0.7	3.1	0.4	2	RK
2	Y	F	8+02.40	06/02/95 - 06/20/95	10	83	NR	1.5	1.3	1	2	RK
3	Y	F	8+02.58	06/02/95 - 06/20/95	0	90	0.7	0.2	0.9	0.1	2	RK
4	Y	F	8+03.18	06/02/95 - 06/20/95	125*	83	0.85	3	3.5	2.6	1	F
5	Y	F	8+03.60	06/02/95 - 06/20/95	210	77	3	NR	3	0.9	2	RK
6	Y	F	8+04.15	06/02/95 - 06/20/95	220	73	2.5	0.9	3	0.4	2	F
7	Y	F	8+04.64	06/02/95 - 06/20/95	245	85	0.75	1.3	1.9	0.06	2	F
8	Y	F	8+04.83	06/02/95 - 06/20/95	15	78	0.27	0.9	1.1	0.03	2	RK
9	Y	F	8+05.60	06/02/95 - 06/20/95	170	50	2.5	0.5	3	0.4	2	F
10	Y	F	8+06.29	06/02/95 - 06/20/95	220	84	1.4	1.1	2.5	0.13	2	F
11	Y	FLT	8+06.42	06/02/95 - 06/20/95	215	84	4	1	5	0.5	2	F
12	Y	FLT	8+06.86	06/02/95 - 06/20/95	220	85	1.5	0.75	2.25	0.08	2	RK
13	Y	F	8+07.75	06/02/95 - 06/20/95	210	74	2.2	2.5	4.5	1.5	1	F
14	Y	F	8+08.14	06/02/95 - 06/20/95	225	80	4	1.3	5	0.6	2	F
15	Y	F	8+08.65	06/02/95 - 06/20/95	230	81	6	1	6	3	2	RK
16	Y	F	8+08.93	06/02/95 - 06/20/95	225	83	1.8	0.9	2.4	0.15	2	F

(Abridged version of file included here.)

Full printout can be found on pp. 121-122 of Reference Notebook YMP-LBNL-GSR-MC-1.2A (for scientific Notebook YMP-LBNL-GSR-MC-1.2) under ACC: YOL.19990903.0031)

107	Y	F	9+73.60	06/02/95 - 06/20/95	190	70	1.2	1.1	2.2	0.5	2	F
108	Y	F	9+73.74	06/02/95 - 06/20/95	190	75	3.3	0.22	3	0.3	2	RK
109	Y	F	9+74.67	06/02/95 - 06/20/95	210	73	2.2	1.8	3.9	0.9	2	F
110	Y	F	9+83.47	06/02/95 - 06/20/95	201	58	5	1.9	6	1	2	RK
111	Y	F	9+84.76	06/02/95 - 06/20/95	350	88	0.5	2	2.4	1.4	2	RK
112	Y	F	9+85.14	06/02/95 - 06/20/95	210	75	6	2	7	3.8	1	RK
113	Y	F	9+86.45	06/02/95 - 06/20/95	340	78	0.7	2.3	2.2	1.9	1	RK
114	Y	F	9+86.85	06/02/95 - 06/20/95	210	87	0.05	0.9	0.9	0.3	2	RK
115	Y	F	9+87.86	06/02/95 - 06/20/95	190	74	0.4	0.6	1	0.1	2	RK
116	Y	F	9+91.28	06/02/95 - 06/20/95	355	84	1.7	2.45	4	2	1	F
117	Y	F	9+91.62	06/02/95 - 06/20/95	5	85	0.9	2.4	3	2	1	F
118	Y	F	9+91.87	06/02/95 - 06/20/95	215	88	4	2.4	6	1.5	0	ST
119	Y	F	9+94.15	06/02/95 - 06/20/95	340	82	2	2.2	4	2.1	1	F
120	Y	F	9+95.94	06/02/95 - 06/20/95	195	64	0.8	2	2.5	1	1	F
121	Y	F	9+96.27	06/02/95 - 06/20/95	210	47	2.5	0.4	2.7	3.3	2	RK
122	Y	F	9+97.57	06/02/95 - 06/20/95	0	82	2.4	2.6	4.5	2.2	1	RK
123	Y	F	9+98.43	06/02/95 - 06/20/95	340	76	2.7	3.2	4.5	2.2	1	RK

End of Report

III-19 JFH 4/1/00

CON	TERMINATI	PLANARITY	JOINT	ALTERATIO	FRACTURE	ROUGHN	MINIMUM APERTUR	MAXIMUM APERTUR
			N	NUMBER	ESS		E	E
							(mm)	(mm)
RK	P		14		4		0	0
RK	I		14		3		0	0
RK	I		15		3		0	0
IN	P		15		4		0	0
RK	I		15		4		0	0
RK	P		15		5		0	0
F	I		15		4		0	0
F	T		11		3		0	0
F	U		15		6		0	5
RK	P		13		4		0	3
RK	P		15		4		0	3
RK	U		13		4		0	0
IN	U		14		5		0	2
RK	P		15		4		0	10
RK	P		15		4		0	5
RK	P		15		4		0	0
					•			
					•			
					•			
					•			
RK	I		11		3		0	0
F	I		11		3		0	0
RK	I		12		3		0	0
RK	T		13		3		0	0
RK	I		13		3		0	0
IN	I		13		3		0	0
IN	I		13		3		0	0
RK	I		13		3		0	0
RK	I		15		3		0	0
IN	I		15		3		0	0
IN	I		15		3		0	0
IN	I		15		3		0	0
IN	P		14		3		0	0
IN	I		14		3		0	0
RK	T		14		3		0	0
IN	U		15		3		0	0
IN	I		15		3		0	0

COMMENTS

upper termination in stratigraphic pumice bed, 1 to 2mm clay coating, mostly in middle of fracture
 upper termination at trace line, has small finger fracture coming off which intersects fracture at sta. 8+02.58, finger comes off at 0.15m below trace line, 1 to 2mm clay coating
 at 0.65m above trace line fracture has finger that comes off with change in azimuth to 170, dip 90 degrees, this fracture can be traced from 3m to fracture
 upper termination in fracture 8+03.60, fracture thinning at bottom, 2 to 3mm clay infilling
 2 to 3mm altered clay infilling, zone of alteration on fracture sides, ends in highly altered zone
 up to 2mm soft orange colored clay infilling
 dip varies + or - 5 degrees along trace
 no coatings
 amplitude 0.04m, wave length 0.7m, up to 10mm orange clay infilling, fracture surface slicken sided, rake 70 degrees
 clean to local patches of up to 1mm thick orange clay infilling
 this has movement with 0.1m offset, west side down, up to 1mm clay infilling
 0.15m offset, west side down, locally clean, local 1mm clay infilling, unable to determine amplitude and wave length
 0 to 10mm orange clay infilling
 1mm to 3cm orange clay infilling
 0 to 10mm clay (average approx. 4mm) infilling
 1 to 3cm orange clay infilling

see next fracture 9+73.74, upper termination has apparent curves into 9+73.74, while the lower termination dies, next fracture is subparallel.
 see 9+73.60, the lower termination curves near tapeline to intersect 9+73.60
 hard to see ends
 bottom 1.0m (plus or minus) is in an altered, discolored zone, in local zones, especially at the bottom are up to 15mm mineralized infilling
 upper termination is faint, dies out, lower termination is in altered, discolored zone, bottom of fracture anastomoses, has mineralized infilling
 local mineralized infilling, especially in bottom altered zone
 mineralized infilling, especially in bottom altered zone, up to 30mm (plus or minus)
 mineralized infilling, up to 15mm thick, extending about 0.3m above altered zone
 mineralized infilling along total height, thickness of mineralized infilling up to 10cm
 mineralized infilling 0 to 5cm thick
 mineralized infilling 0 to 3.5cm, becomes very faint towards SW invert
 mineralized with dark minerals, varies from 0 to 3cm
 mineralized with dark minerals, varies from 0 to 4mm
 slightly mineralized 0 to 3mm
 slightly mineralized 0 to 2mm, fracture is faint and hard to trace in some locations
 mineralized 4 to 10mm, fracture terminates at top of hydrothermal alterations
 mineralized 3 to 5mm

YMP-LBNL DOCUMENT REVIEW/COMMENT RESOLUTION (DRCR) FORM

Document No. and Title: Software Macro Read_TDB Version 1.0 Page 1 of 1
 Date of Document / revision no. / draft revision no. (as applicable): Version 1.0 Author: Mark Cushey
 Are Scientific Notebooks or other background documents/data included in the scope of this review? Yes No (If yes, identify on Attachment 3)
 Specific Review Criteria or Governing Procedure: AP-SI.1Q, Rev 1, ICN 0 and YMP-LBNL-QIP-6.1, Rev. 4, Mod. 0
 General Review Criteria: (Identify relevant criteria on Attachment 4): Section 5.1 of AP-SI.1Q and Software Review Criteria S-7 to S-10
 Checker Technical Reviewer EA Reviewer OQA Reviewer
 Name: C.F. Ahlers Signature: (SIGNATURE REMOVED) Date: 9/23/99

REVIEWER'S COMMENTS		AUTHOR'S RESPONSE		Reviewer Disposition for Mandatory Comments	
COMMENT NO. MANDATORY (M) NON-MANDATORY (NM)	SECT. AND PAGE NO.	COMMENTS	REJECT Initial/Date	ACCEPT Initial/Date	REJECT Initial/Date
		No comments			

May be on separate sheets to be attached, in which case the comments shall be numbered and this form will be used to track the comments and their resolution according to such numbers.

Resolution of Disputed Comments

Office of Quality Assurance Date

Project Manager

Date

YMP-LBNL Management Approval (Project Manager or Designee)

(SIGNATURE REMOVED) for G.S. Bodvarsson 9/23/99

frac_calc V1.1
Routine/Macro Documentation Form*

Note: All relevant scientific notebook (SN) pages are included in this records package. In some instances, the included SN pages cross-reference other pages that are not included here because these were not essential to the documentation of this routine.

1. Name of routine/macro with version/OS/hardware environment:
frac_calc / Version 1.1 / DOS (or Windows with DOS) / PC
2. Name of commercial software with version/OS/hardware used to develop routine/macro:
FORTRAN 77 / FORTRAN Powerstation 4.0 (see SN YMP-LBNL-GSB-MC-1.1, p. 105)

3. Description and Test Plan.

- Explain whether this is a routine or macro and describe what it does: (**frac_calc is a routine**)
The software routine **frac_calc** is a FORTRAN code which performs simple calculations using Detailed Line Survey (DLS) data including fracture location, strike, dip, and trace lengths above and below the traceline to compute fracture hydrologic properties. The user can select a minimum and maximum fracture length to include in the calculations. Version 1.1 is a minor revision of Version 1.0 and calculates additional fracture properties from the same data. The fracture properties calculated include fracture frequency, aperture and other properties. These properties are listed and the computation methods are described on pages 60-65 in YMP-LBNL-GSB-MC-1, pp. 102-104 in YMP-LBNL-GSB-MC-1.1, and p. 14 in YMP-LBNL-GSB-MC-1.2. To install the software, copy **frac_calc11.f** and **datablk11.f** from a disk onto the hard drive of a PC. Then, compile **frac_calc** using a FORTRAN 77 compiler and run executable.

Changes between Version 1.1 and 1.0 are discussed on p. 14 in YMP-LBNL-GSB-MC-1.2 for the source code (filename: **frac_calc11.f**) and on pp. 12-13 in YMP-LBNL-GSB-MC-1.2 for the parameter dimensions file (filename: **datablk11.f**).

This software routine is documented in the following scientific notebook pages (the order below provides a chronology of the documentation from Version 1.1 back to Version 1.0):

YMP-LBNL-GSB-MC-1.2	pp. 14-16, 12-13
Reference Binder YMP-LBNL-GSB-MC-1.2A	pp. 67-87, 63-66
YMP-LBNL-GSB-MC-1.1	pp. 114-115, 105-109, 101-104
YMP-LBNL-GSB-MC-1	pp. 60-65

Inputs:

The code is designed to use an ASCII input file. The first row is a header and is not read. Each row represents a single fracture. It must have five columns of data for each fracture - location (in meters), strike (in degrees), dip (in degrees), length above (in meters), and length below (in meters) - in that order. The fractures must be in increasing order of location (distance along the ESF, an alcove, or the ECRB). All values must be numbers (no text, except the first row). All values must be positive. The limit on size of the input values is that the strike must be less than 360 degrees and the dip must be less than 90 degrees. For other values, there are no limits except those for double precision parameters and computations.

- Source code: (including equations or algorithms from software setup (LabView, Excel, etc.):
pp. 72-87, in Reference Binder YMP-LBNL-GSB-MC-1.2A for **frac_calc.f**, the source code.
pp. 63-66, in Reference Binder YMP-LBNL-GSB-MC-1.2A for **datablk11.f**, the include file that sets parameter dimensions and values.
- Description of test(s) to be performed (be specific):
A sample case using site data will be used to test the routine. The test case for Version 1.0 is rerun for Version 1.1 to test the new features as well as confirm that the previous computations

frac_calc V1.1
Routine/Macro Documentation Form*

are still performed correctly. The Version 1.0 test case included selecting a minimum fracture length of 1 meter to confirm that fractures smaller than 1 meter in the sample case will be excluded from the computations (the Version 1.0 test case is on pp. 105 – 108 in YMP-LBNL-GSB-MC-1.1). All new output from the output files all1.par and all2.par will be compared with computations performed using a calculator (previous output will be compared to Version 1.0). The acceptance criterion is that the values computed by hand and from the routine are the same within the round-off difference between the code and the calculator.

- Specify the range of input values to be used and why the range is valid:
The input values are a direct sample from the TDMS (see p. 105 in YMP-LBNL-GSB-MC-1) after pre-processing using the routine Read_TDB. The sample input includes small and large fracture lengths and a range of strikes and dips that are representative of the fracture parameters found at Yucca Mtn.

4. **Test Results.**

- Output from test :
Test results are shown on p. 15 in YMP-LBNL-GSB-MC-1.2 and in Reference Binder YMP-LBNL-GSB-MC-1.2A, pp. 67-71.
- Description of how the testing shows that the results are correct for the specified input:
Values from Version 1.1 matched exactly with those from Version 1.0 (regression testing), see p. 15 in YMP-LBNL-MC-1.2. Calculated values for new fracture calculations (gmlen and intarea) matched with rounding to 3 decimal places (the output format of frac_calc).
- List limitations or assumptions to this test case and code in general:
As noted above the fractures must be listed in order of their locations with increasing distances along a survey line.
- Electronic files identified by name and location (include disc if necessary):
See pp. 15-16 in YMP-LBNL-GSB-MC-1.2. No electronic files submitted.

5. **Supporting Information.** Include background information, such as revision to a previous routine or macro, or explanation of the steps performed to run the software. Include listings of all electronic files and codes used. Attach Scientific Notebook pages with appropriate information annotated:

See attached pages for technical review forms, referenced scientific notebook pages and other supporting documentation. Pages from YMP-LBNL-GSB-MC-1.1 and YMP-LBN-GSB-MC-1 are for Version 1.0 and provide the necessary background information for Version 1.1. The original qualification and references for Version 1.0 are provided on pp. 114-115 of YMP-LBNL-GSB-MC-1.1.

MAINTAIN PAGES IN THIS ORDER:

This 2 page "Routine Documentation" summarization form	
YMP-LBNL-GSB-MC-1.2	pp. 14-16, 12-13
Reference Binder YMP-LBNL-GSB-MC-1.2A	pp. 67-87, 63-66
YMP-LBNL-GSB-MC-1.1	pp. 114-115, 105-109, 101-104
YMP-LBNL-GSB-MC-1	pp. 60-65

***Note that supplement includes:**

- Addition of this 2-page "Routine Documentation" summarization form
- Addition of pp. 63-66, Reference Binder YMP-LBNL-GSB-MC-1.2A
- Addition of pp. 12-13, S/N YMP-LBNL-GSB-MC-1.2

3/1/2000

Version 1.1 of frac-calc

7/21/99

The following changes were made to Version 1.0
 (see p. 114 in YMP-LBNL-GSB-MC-1.1
 pp. 88-97 in YMP-LBNL-GSB-MC-1.1A)

- $k_f = k_{frc}(n) * freq$
 was replaced with
 $k_f = k_{frc}(n) * aper$
 see discussion on p. 103 in YMP-LBNL-GSB-MC-1.1

- The parameters $intarea$ & $gmlen$ were added.

$gmlen$ - geo metric mean of the fracture
 length

MC 7/21/99 ~~while fracture lengths are being~~

MC 7/21/99 summed added

MC 7/21/99 $gmlen = gmlen + \log(\text{trace length})$

$$\log[gmlen] = \frac{\sum_{i=1}^n \log(t_i)}{n}$$

t_i = trace length for fracture i
 n = number of fractures

$intarea$ - fracture interface area

$$intarea = \frac{\sum_{i=1}^n \pi r_i^2}{(block\ length)(gmlen)^2}$$

MC 7/21/99 along wall

essentially the fracture area
 divided by the block volume.
 $gmlen$ is used vertical length &
 depth into wall since these are
 unknown.

r_i = radius of fracture i

- The output file "calibrate.par" was revised
 to include "gmlen" & "intarea" and was
 reformatted

* All of these changes are marked with
 MAC V1.1 in the comments.

SIGNATURE _____

READ AND UNDERSTOOD _____

DATE _____

DATE _____

19

19

Reran ~~V~~-MC 7/21/99 test case ^{used} for Version 1.0

(pages 101-108 YMP-LBNL-GSB-MC-1.1)

[Using setting that limits calculations to 1m or larger]

Version 1.1 Version 1.0

all 1.par	min-m	0.93	0.43
	MinUse	1.00	1.00
	Max-m	8.00	8.00
	#Frac	5	5
	Spac-m	3.61	3.61
	SDSpac	2.78	2.78
	Fg-1/m	0.28	0.28
	SDFreq	0.21	0.21
	Leng-m	3.68	3.68
	SDLeng	2.91	2.91
all 2.par	Intens	0.16	0.16
	Apr-um	504	504.0
	Por-3D	5.93×10^{-5}	5.93×10^{-5}
	Por-2D	8.21×10^{-5}	8.21×10^{-5}
	Por-1D	1.40×10^{-9}	1.40×10^{-9}
	alpha	3.50×10^{-3}	3.50×10^{-3}
	kzz/kxx	1.69	1.69
	kxy/kxx	1.81	1.81
	kzz/kyy	0.93	0.93

~~MC 7/21/99 alpha~~
~~MC 7/21/99 alpha~~

Version 1.0 headers

Fr-porosity	8.21×10^{-5}	8.21×10^{-5}	Por-3D ^{2 MC 7/21/99}
Aperture	5.04×10^{-4} m	504.0 um	Apr-um
Frequency	0.28	0.28	Fg-1/m
Intr-Area	0.547	NA	
Gm-length	2.784	NA	
Fr-Alpha	3.50×10^{-3}	3.50×10^{-3}	alpha
SD-Alpha	2.41×10^{-9}	2.41×10^{-9}	sdalpha
Log Alpha	-2.54	^{MC 7/21/99} -2.46	loga
SD-Log Alpha	0.34	^{MC 7/21/99} -3.62	log sda

The output files & input files for this test case are in Reference Binder YMP-LBNL-GSB-MC-1.2A pp. 67-71. These are in d:\lls\code\calc.frac\frac-calc\1\Test Case ^{MC 7/21/99}

The above indicates that the calculations for Version 1.1

SIGNATURE _____

DATE _____

19

READ AND UNDERSTOOD _____

DATE _____

19

check for those included in Version 1.0.
The two new computations are checked below.

(formulas on p 14)

$$\log(gmlen) = \frac{[\log(8) + \log(5.17) + \log(1.11) + \log(0.43) + \log(1.3) + \log(2.8)]}{5}$$

$$gmlen = 2.7836 \text{ m}$$

$$intarea = \pi \frac{[(4)^2 + (2.585)^2 + (0.555)^2 + (0.215)^2 + (0.65)^2 + (1.4)^2]}{(18.8)(2.7836)^2}$$

$$= 0.5472 \text{ m}^2/\text{m}^3$$

frac_calc Version 1.1 gives

$$gmlen = 2.784 \text{ m}$$

$$intarea = 0.547 \text{ m}^2/\text{m}^3$$

frac_calc Version 1.1 checks

The code frac_calc Version 1.1 is included in
Reference binder YMP-LBNL-GSB-MC-1.2A pp. 72-87

The file is on "nwd-cuskey" in d:\code\frac_calc\frac_calc11

→ The filenames are frac_calc11.f & frac_calc11.exe

MC
9/23/99

SIGNATURE (SIGNATURE REMOVED)
READ AND UNDERSTOOD _____

DATE 7/21 19 99
DATE _____ 19 _____

Computing Fracture Frequencies - Preliminary 7/21/99

The multi-user macro frac_calc Version 1.0 ~~was~~ ^{MC} 7/21/99
(YMP-LBNL-MC-1.1 p.114) was updated to
reflect the new layering for the UZ model for
FY99. Essentially

GSB
MC
7/21/99

	FY98	FY99
	ptn 24	} ptn 24
	ptn 25	

ptn 26 → ptn 25

ptn 27 → ptn 26

The model layers for FY97, FY98 & FY99 are
summarized in Reference Binder YMP-LBNL-~~MC~~ GSB-MC-1.2A
on pp. 52-54. ^{MC} 7/21/99

The assignment of ESF stations to model layers was
also re-evaluated. An error was found in the
assignment of layers for the South Ramp. The
contacts given for the South Ramp are "exit" points
whereas these for the North Ramp & Main Drift
are "entrance" points. The South Ramp assignments
were therefore shifted. In particular tsw35 was
misassigned:

previous	57+29.2 - 63+08
correct	57+29.2 - 58+78.3

The original assignments are in YMP-LBNL-GSB-MC-1.1
pp. 36-39.

The new assignments are in Reference Binder
YMP-LBNL-GSB-MC-1.2A pp. 55-58
These were reviewed by Jennifer Hinds on 3/24/99

Intervals that were less than 5 meters were
considered too small & these data were
excluded.

Reference Binder YMP-LBNL-GSB-MC-1.2A p.59 gives a summary
of these assignments.

SIGNATURE _____
READ AND UNDERSTOOD _____

DATE _____ 19

DATE _____ 19

111-29 Jeth 4/2/00

MC 7/21/99

Fracture permeabilities in frac_calc were revised to reflect the new layer

	log k (k in m ²)
ptn 24	-11.53
ptn 25	-12.78
ptn 26	-12.66

old
old
previous value assigned to ptn 24 were for ptn 25 & considered analogous ∴ only old ptn 25 used for new ptn 24

The original fracture permeabilities are given in YMP-LBNL-GSB-MC-1.1 p. 61.

Page 65 in YMP-LBNL-GSB-MC-1.1 provides a summary of ~~where~~ the files and data used to determine fracture permeabilities

Pages 53-54 in Reference Binder YMP-LBNL-GSB-1.2A show how the model layers have changed from FY98 to FY99.

The file 'databk.f' which is part of 'frac_calc' was updated to reflect these changes and a new file was created 'databk11.f' which is for Version 1.1 of frac_calc. This file is included in Reference Binder YMP-LBNL-GSB-MC-1.2A pp. MC 7/21/99

The assignment of ECRB stations to model layers was completed using the locations of lithostratigraphic contacts from MOLA 19981229.0038. This is in Reference Binder YMP-LBNL-GSB-MC-1.2A pp. 60-62. The corresponding model layers are recorded on that page also. These were also put in 'databk11.f' with a header of "9" (see p. 10)

The file "databk11.f" is given in YMP-LBNL-GSB-MC-1.2A pp. 63-66 & stored on "nwd-cushey" in d:\code\frac_calc\frac_calc11

SIGNATURE (SIGNATURE REMOVED)
READ AND UNDERSTOOD

DATE 7/21 19 99
DATE 4/7/00 19

111-30 8/24/00

Input and Output files for test
case for frac_calc Version 1.1

Input: test.dat

Output: all1.par, all2.par, &
calibrate.par

file names are
frac_calc11.f and
frac_calc11.exe
MC
9/23/99

(S/N 101P 2302 0.58 -
410-1.24)

111-31 JEH 4/7/00

test

LOCATION	STRIKE	DIP	LENGTH A	LENGTH B
879.700	20.000	8.000	2.000	6.000
882.370	184.000	78.000	3.500	1.670
887.300	299.000	78.000	.000	1.110
893.860	20.000	49.000	.100	.330
893.920	22.000	80.000	.680	.620
894.130	20.000	67.000	1.200	1.600

← For test case run,
program excludes
this because
minimum fracture
length cutoff is set to
1 m (see next page)

Unit	MinUse	#Frac	Fq-1/m	Apr-um	Pot-3D	Pot-2D	Pot-1D	alpha	kzz/kxx	kyy/kxx	kzz/kyy
PUN24	1.00	5	.28	504.	5.93E-05	8.21E-05	1.40E-04	3.50E-03	1.69	1.81	93

all 2.par

111-33 JEH 4/7/00

70 #

Unit	Min-Fr-Length	Fr-Porosity	Aperture	Frequency	Inter-Area	Gm-Length	Fr-Alpha	SD-Alpha	LogAlpha	SD-LogAlpha
tcw11										
tcw12										
tcw13										
pcn21										
pcn22										
pcn23										
pcn24	1.00	8.21E-05	5.04E-04	.28	.547	2.784	3.50E-03	2.41E-04	-2.54	.34
pcn25										
pcn26										
csw31										
csw32										
csw33										
csw34										
csw35										
csw36										
csw37										

calibrate-par

111-34 284 4/7/00

74

Code for
Frac_calc
Version 1.1

111-35 JSH 4/7/00

```

program Frac_Calc

c   Version 1.1
c   All changes for Version 1.1 are indicated by MAC V1.1
c   See Scientific Notebook YMP-LBNL-GSB-MC-1.2 pages 14-16

c   Discussion for Version 1.0
c
c   The purpose of this program is to calculate means and variances
c   for fracture properties for UZ model layers based on detailed
c   line survey (DLS) data for the Exploratory Studies Facility (ESF)
c   that has been downloaded from the Technical Database (TDB).

c   This program was originally written by Eric Sonnenthal with
c   revisions and additions by Mark Cushey (4/98 to 7/98) which are
c   labeled MAC and dated. Major additions include using data
c   statements and coding to combine subunits for model layers
c   internally in the program; calculating additional parameters;
c   program recalculates all numbers for each model layer each time
c   it is executed; calculate apertures; calculate alpha & log alpha
c   and its statistics; calculates spacing, frequencies and intensity
c   for selected interval lengths; new input format for direct reading
c   of data from TDB after processing through read_tdb.f; and new
c   output formats.

c   MAC V1.1 - updated pages below for references for Version 1.0
c   See Scientific Notebook YMP-LBNL-GSB-MC-1 pages 60-69, 124-125, 137
c   See Scientific Notebook YMP-LBNL-GSB-MC-1.1 pages 98, 101-108, 114-115
c   See Reference Binder YMP-LBNL-GSB-MC-1.1A pages 88-97, 98-106

c   - Mark Cushey 7/98
c-----
c   Below comments by E.Sonnenthal
c... Program to read USGS ESF data and calculate fracture geometries
c... and densities for plotting (11/4/96: E. Sonnenthal)
c... Components of hydraulic conductivity tensor (de Marsily, 1986)
c... 11/11/96 E. Sonnenthal
c... revised 2/6/97 for a fracture size range
c   nf      = Number of fractures
c   blksiz = Block size (m)
c   kfrc   = Hydraulic conductivity of each fracture (m/s)
c   aper   = Aperture of each fracture (m)
c   strike = Strike of each fracture (azimuth in radians)
c   dip    = Dip of each fracture (dip in radians)
c   ktens  = Conductivity tensor (9 component)
c   k(9) = (kxx,kxy,kxz,kyx,kyy,kyz,kzx,kzy,kzz)
c   | kxx kxy kxz |
c   | kyx kyy kyz |
c   | kzx kzy kzz |
c-----

c Commented out variables no longer used MAC 7/98
c   integer nil,ni2
c   integer i,k,ni,n,nn,nml,nfr,nf,ns1,ns2
c   parameter (nf = 50000)
c   parameter (pi=3.1415926536d0)
c   parameter (ni = 199)

```

```
c Added MAC 4/13/98
  character*32 fname
```

```
c Commented out variables no longer used MAC 7/98
```

```
c   character*8 outfile, header2, fstat
c   character*200 header
c   integer dist1
c   double precision height(nf), dist2
```

```
integer nfrint(ni), ns
double precision blksize, kf, sdsq, stkrad, diprad, proptf
double precision fmin, fmax
double precision kfrc(nf), aper(nf)
double precision ktens(9)
double precision kxx, kxy, kxz, kyx, kyy, kyz, kzx, kzy, kzz
double precision endp1, endp2, totaltr, totalht, adip, bdip
double precision dist(nf), nfrc(nf)
double precision strike(nf), dip(nf), alen(nf), blen(nf)
double precision atrace(nf), btrace(nf), trace(nf)
double precision trlen, fmesf, frint, fgrpl, fgrp2, fsiz
double precision trcmax, dipmin, dipmax, aperture
double precision avgsp, frcint, varsp, sdspac
double precision freq, sdfreq, frcvol, frcrad, frcpor, blkht, blkdp
double precision sdlen, varlen, avglen, frarea, frcp2d
character*1 ans1, ans2
```

```
c   MAC V1.1
  double precision intarea, gmlen
```

```
c
```

```
c
```

```
-----
c   Below added by MAC 4/98 - 5/98
c   Data statements added to identify subunits and later combine
c   subunits for each model layer.
c   Moved to include MAC 6/98 so that various combinations could be
c   used by simply using a different file for include
c   Note that alcove stations are entered with Alcove # in the
c   ten thousandth location.
c   Assignment for model layers based on CRWSM M&O, 1998.
c   For most recent assignment see
c   Scientific Notebook YMP-LBNL-GSB-MC-1.1 pages 36-39.
c
c   Include file 'datblk.f' includes data statements for
c   unitname, modlayer, unitsta, unitend, and logairk
```

```
c   MAC V1.1
  include 'datblk11.f'
```

```
c
c   For testing, instead of 'datblk.f', include file 'uzmodel97.f'
c   for comparison with calculations performed for the July 97
c   milestone (Chapter 7, Sonnenthal et. al, 1997) or include
c   'sweetkind.f' for comparison with calculations in
c   Sweetkind et. al (1997). Use the data files ericdls.dat and
c   sweetdls.dat, respectively.
c   include 'uzmodel97.f'
c   include 'sweetkind.f'
```

```
c MAC 7/98 For the more detailed PTn model layers use
c include 'ptnblk.f'
```

```
-----
c Below added MAC 4/98 - 6/98
c ntotal is the total number of UZ model layers
c nlayers is the total number of segments along the ESF
c Both are used for the data statements and are defined in the
c file 'databl.f'
c npar is the number of parameters saved for calculating properties
c for entire model layer
c variables with 'int' are for calculating fracture properties for
c intervals
c variables for data statements [integer modlayer(ntotal);
c double precision logairk(nlayers),unitsta(nlayers),
c unitend(nlayers)] are in file 'databl.f'
```

```
integer layer,first,last,npar
c MAC V1.1 changed npar from 16 to 18
parameter(npar=18)
double precision spac,frcpid,trcmin, combine,kzzkxx,kyykxx,kzzkyy,
+ alpha,loga,logf,sdalpha
dimension combine(nlayers,npar)
character*5 outfile
```

```
integer intn,intmax,intnfr,intlayer
parameter(intmax=10000)
double precision intfreq,intspace, intlength, intrtrace
dimension intfreq(intmax),intspace(intmax),intnfr(intmax),
+ intrtrace(intmax)
```

```
c...Input file name
2 print *, 'Enter fracture data filename: '
read(*,*) fname
open(unit=12,file=fname,status='old',err=5)
go to 7
5 write(*,*)'File not found'
go to 2
7 continue
```

```
c Removed call to station file -- all in one file MAC 4/13/98
```

```
c revised MAC 4/13/98 - starting and end points for model layers
c now determined internally
```

```
c revised MAC 4/17/98 - changed input process
dipmin = 0.d0
dipmax = 90.d0
ans1 = 'n'
ans2 = 'y'
write(*,*)'Enter minimum and maximum fracture length to use'
read(*,*)fmin,fmax
```

```
c Added MAC 7/8/98 - query user for interval length
write(*,*)'Enter interval length (in meters) '
read(*,*)intlength
```

```

c-----
c... Read station file - Removed MAC 4/13/98

c   MAC 4/98 open output files
   open(13,file='all1.par',status='unknown')
   open(14,file='all2.par',status='unknown')
   write(13,441)
   write(14,442)
   open(18,file='interval.par',status='unknown')
   write(18,1999)
   open(20,file='tmp.par')

c
c... Read fracture data file
c Rev MAC 4/13/98
   read (12,*)
   i = 0
10  i = i + 1
c   rev MAC 6/29/98 - Don't read in height
c   read(12,*,end=99)dist(i),strike(i),dip(i),atrace(i),
c   &   btrace(i),height(i)
   read(12,*,end=99)dist(i),strike(i),dip(i),atrace(i),
c   &   btrace(i)
   go to 10
99  ns = i - 1
   dist(ns+1)=99999.9
   close(12)

c
c Added MAC 6/25/98
c   initialize combine
   do j=1,npar
     do i=1,nlayers
       combine(i,j) = 0d0
     end do
   end do

c-----
c Added MAC 4/17/98
c   Loop through model layers, assiging station ranges
c   Define endp1, endp2, ns1, ns2
c
c   DO layer = 1,nlayers
     endp1 = unitsta(layer)
     endp2 = unitend(layer)
     write(*,*)unitname(layer),endp1,endp2
     ns1 = 0
     ns2 = 0
     do i = 1,ns+1
       if (((dist(i).ge.endp1).and.(dist(i-1).lt.endp1))
c   &   .or.(((dist(i).ge.endp1).and.(i.eq.1)))
c   &       ns1 = i
       if ((dist(i).gt.endp2).and.(dist(i-1).le.endp2))
c   &       ns2 = i - 1
     end do
c   MAC V1.1 - changed 0.0 to 0
   if ((ns2-ns1).le.0) go to 999
   write(*,*)'      ',dist(ns1),dist(ns2)

```

```

c      outfile = unitname(layer)
c      outfile = 'dummy'
c      if ((layer.eq.48).or.(layer.eq.27)) then
c          outfile = unitname(layer)
c          write(*,*) 'Tecplot file for',unitname(layer),
c      +          unitsta(layer),unitend(layer)
c      end if
c... Find size distribution for all fractures
c      if(ans2.eq.'y')then
c          fmesf = 0.3d0
c          frint = 0.2d0
c      do i = ns1,ns2
c          trlen = atrace(i) + btrace(i)
c          do k = 1, ni
c              fgrp1 = fmesf + dble(k-1)*frint
c              fgrp2 = fmesf + dble(k)*frint
c              if(trlen.ge.fgrp1.and.trlen.lt.fgrp2)
c      &          nfrint(k)=nfrint(k)+1
c          enddo
c      enddo
c      endif
c
c Added MAC 4/98 find minimum trace length before excluding
c      trcmin = fmax
c      do i = ns1,ns2
c          trcmin = min((atrace(i)+btrace(i)),trcmin)
c      enddo
c... Find fractures that are within range if given
c      n = 0
c      nfr = 0
c      do i = ns1,ns2
c          if(dip(i).ge.dipmin.and.dip(i).le.dipmax.and.atrace(i)+
c      +      btrace(i).ge.fmin.and.atrace(i)+btrace(i).le.fmax)
c      +      then
c          n = n + 1
c          nfr(i) = i
c          nfr = n
c      endif
c      enddo
c      if (nfr.le.1) go to 999
c
c... Calculate proportion of total fractures
c      proptf = dble(nfr)/(dble(ns2-ns1+1))
c
c... Find total trace length
c      do n = 1, nfr
c          nn = nfr(n)
c          trace(n) = atrace(nn) + btrace(nn)
c      enddo
c
c... Find maximum trace length
c      trcmax = -1.d5

```

```

c      outfile = unitname(layer)
c      outfile = 'dummy'
c      if ((layer.eq.48).or.(layer.eq.27)) then
c          outfile = unitname(layer)
c          write(*,*) 'Tecplot file for',unitname(layer),
c +             unitsta(layer),unitend(layer)
c      end if
c... Find size distribution for all fractures
c      if(ans2.eq.'y')then
c          fmesf = 0.3d0
c          frint = 0.2d0
c      do i = ns1,ns2
c          trlen = atrace(i) + btrace(i)
c          do k = 1, ni
c              fgrp1 = fmesf + dble(k-1)*frint
c              fgrp2 = fmesf + dble(k)*frint
c              if(trlen.ge.fgrp1.and.trlen.lt.fgrp2)
c &                 nfrint(k)=nfrint(k)+1
c          enddo
c      enddo
c      endif
c
c Added MAC 4/98 find minimum trace length before excluding
c      trcmin = fmax
c      do i = ns1,ns2
c          trcmin = min((atrace(i)+btrace(i)),trcmin)
c      enddo
c... Find fractures that are within range if given
c      n = 0
c      nfr = 0
c      do i = ns1,ns2
c          if(dip(i).ge.dipmin.and.dip(i).le.dipmax.and.atrace(i)+
c +         btrace(i).ge.fmin.and.atrace(i)+btrace(i).le.fmax)
c +         then
c             n = n + 1
c             nfr(i) = i
c             nfr = n
c         endif
c      enddo
c      if (nfr.le.1) go to 999
c
c... Calculate proportion of total fractures
c      proptf = dble(nfr)/(dble(ns2-ns1+1))
c
c... Find total trace length
c      do n = 1, nfr
c          nn = nfr(n)
c          trace(n) = atrace(nn) + btrace(nn)
c      enddo
c
c... Find maximum trace length
c      trcmax = -1.d5

```

```

do n = 1, nfr
  trcmax = max(trace(n),trcmax)
enddo

c
c... Length of fracture segment for plotting is 0.15 inch/meter
do n = 1, nfr
  nn = nfrc(n)
  alen(n) = atrace(nn)*0.15d0
  blen(n) = btrace(nn)*0.15d0
enddo

c
c... Calculate blocksize (interval length)
  blksize = endp2 - endp1
  blkht = 6.d0
  blkdp = 6.d0

c
c Rev MAC 4/17/98 - moved perm, frac volume, porosity to after
c parameters

c Rev MAC 4/98 - zero sum parameters
totalht = 0d0
totaltr = 0d0
ssqht = 0d0
ssqtr = 0d0
sspac = 0d0
ssqsp = 0d0
ssqlsp = 0d0
slgsp = 0d0
c
c MAC V1.1
gmlen = 0d0
intarea = 0d0

c Added MAC 5/98
do n = 1, intmax
  intspace(n) = 0d0
  intfreq(n) = 0d0
  intnfr(n) = 0
  intrace(n) = 0d0
end do
intn = 0
intlayer = 0

c
c... Calculate fracture parameters - loop through fractures
do n = 1, nfr
  nn = nfrc(n)
  totaltr = trace(n) + totaltr
  ssqtr = trace(n)**2 + ssqtr

c
c MAC V1.1
gmlen = gmlen + dlog10(trace(n))

  if(n.gt.1)then
    nml = nfrc(n-1)
c rev MAC 4/13/98 - put in if
    spac = dabs(dist(nn)-dist(nml))
    if (spac.eq.0.0) then

```

```

        write(*,*) 'station overlap',dist(nn),nn,nml
    end if
2099 format(1x,a5,3(1x,f9.2))

        sspac = spac + sspac
c correction MAC 4/13/98
c      put in '+ slgsp' in place of '+ sspac'
c      put in dlog10 and if-then
    if (spac.ne.0.0) then
        slgsp = dlog10(spac) + slgsp
c correction MAC 4/98
c      put in '+ ssqlsp' in place of '+ ssqsp'
c      put in dlog10
        ssqlsp = (dlog10(spac))**2 + ssqlsp
    else
c rev MAC 4/98 for zero spacing use 0.005 m which is 1/2
c      of the measurement precision
        slgsp = dlog10(5d-3) + slgsp
        ssqlsp = (dlog10(5d-3))**2 + ssqlsp
    end if

        ssqsp = spac**2 + ssqsp

c added MAC 5/98 - for determining frequency and intensity over interval
c      added MAC 7/98 - if-then statement to prevent from
c      overextending interval boundary
    intn = INT((dist(nn)-endp1)/intlength)+1
    if ( (endp1+(intn*intlength)).le.endp2 ) then
        if (intn.gt.intmax) then
            write(*,*) 'Max number of intervals exceeded -',
+             ' program stopped'
            write(*,*) 'Resize intmax - intmax,intn',intmax,intn
            stop
        end if
        intspace(intn) = intspace(intn) + spac
        intnfr(intn) = intnfr(intn) + 1
        intrtrace(intn) = intrtrace(intn) + trace(n)
        intlayer = intn
    end if
endif
300 continue
enddo

    avgsp = sspac/dble(nfr-1)
    freq = 1.d0/avgsp

c added MAC 5/98 - for determining frequency and intensity over interval
do intn = 1,intlayer
    if (intnfr(intn).gt.1) then
        intspace(intn) = intspace(intn)/dbles(intnfr(intn)-1)
        intfreq(intn) = 1d0/intspace(intn)
    else
        intfreq(intn) = 1d0/intlength
    end if
    intrtrace(intn) = intrtrace(intn)/intlength/blkht

```

```

end do

c MAC 5/98 added if-then for small # of fractures
if (nfr.gt.2) then
c nfr-1 is the number of pairs used to calculate spacing
varsp = (ssqsp - ((sspac**2)/dble(nfr-1)))/dble(nfr-2))
if (varsp.gt.0.0) then
sdspac = sqrt(varsp)
c added comment and put in varsp rather than sdspac**2 by MAC 5/98
c V[f]= V[s]*(-E[s]**-2)**2
sdfreq = sqrt((((-avgsp)**(-2))**2)*varsp)
else
sdspac = 0d0
sdfreq = 0d0
end if
else
varsp = 0d0
sdspac = 0d0
sdfreq = 0d0
end if

frcint = totaltr/blksize/blkht
avglen = totaltr/dble(nfr)
varlen = (ssqtr - ((totaltr**2)/dble(nfr)))/dble(nfr-1)
if (varlen.gt.0.0) then
sdlen = sqrt(varlen)
else
sdlen = 0d0
end if

c Rev MAC 4/17/98 - calculate b (in um) from airk
aperture = 1d6*(12d0*(10**logairk(layer))/freq)**(1.0/3.0)

c... Calculate permeability of each fracture and pass to ktensor
do n = 1, nfr
aper(n) = aperture*1.d-6
kfrc(n) = (aper(n)**3)/12.d0
enddo

c Rev MAC 4/98 - zero sum parameters
frcvol = 0d0
frarea = 0d0
do i = 1,9
ktens(i) = 0d0
end do

c... Calculate fracture volume based on penny-shaped fractures
do n = 1, nfr
frcrad = trace(n)*0.5d0
frcvol = pi*aper(n)*frcrad**2 + frcvol
frarea = aper(n)*frcrad*2.d0 + frarea
c MAC V1.1 - will divide by block volume after combining
intarea = pi*frcrad**2 + intarea

enddo
c... Calculate fracture porosity
frcpor = frcvol/(blksize*blkht*blkdp)

```

```

frcp2d = frarea/(blksiz*blkht)

c Added MAC 4/22/98 - include 1-D porosity
frcpld = freq*aperture*ld-6

c
c... Calculate components associated with each fracture, then sum
radian = pi/180.d0
do n = 1, nfr
nn = nfrc(n)
if (strike(nn) .le. 90.d0) then
stkrad = strike(nn)*radian
diprad = dip(nn)*radian
elseif (strike(nn) .gt. 90.d0 .and. strike(nn) .le. 180.d0) then
stkrad = strike(nn)*radian
diprad = (180.d0-dip(nn))*radian
elseif (strike(nn) .gt. 180.d0 .and. strike(nn) .le. 270.d0) then
stkrad = strike(nn)*radian
diprad = (180.d0-dip(nn))*radian
else
stkrad = strike(nn)*radian
diprad = dip(nn)*radian
endif
sdsq = (dsin(diprad))**2
kxx = 1.d0 - ((dcos(stkrad))**2)*sdsq
kxy = 0.5d0*dsin(2.d0*stkrad)*sdsq
kxz = -0.5d0*dsin(2.d0*diprad)*dcos(stkrad)
kyx = kxy
kyy = 1.d0 - ((dsin(stkrad))**2)*sdsq
kyz = 0.5d0*dsin(2.d0*diprad)*dsin(stkrad)
kzx = kxz
kzy = kyz
kzz = sdsq
kf = kfrc(n)*freq
ktens(1) = kxx*kf + ktens(1)
ktens(2) = kxy*kf + ktens(2)
ktens(3) = kxz*kf + ktens(3)
ktens(4) = kyx*kf + ktens(4)
ktens(5) = kyy*kf + ktens(5)
ktens(6) = kyz*kf + ktens(6)
ktens(7) = kzx*kf + ktens(7)
ktens(8) = kzy*kf + ktens(8)
ktens(9) = kzz*kf + ktens(9)
enddo

c Added MAC 4/21/98
kzzkxx = ktens(9)/ktens(1)
kyykxx = ktens(5)/ktens(1)
kzzkyy = ktens(9)/ktens(5)

c Added MAC 4/21/98
c Calculate alpha (see equation 7)
alpha = aperture*ld-6/2d0/72d-3

c
c Commented out MAC 7/98
c... Open and write permeability components of fracture networks
c open(11,file=outfile//' .prm',status='unknown')
c write(11,*) 'Permeability Tensor for: ',outfile

```

```

c      write(11,450) 'kxx', 'kxy', 'kxz', 'kyx', 'kyy', 'kyz', 'kzx'
c      +   'kzy', 'kzz'
c      write(11,460) ktens(1), ktens(2), ktens(3), ktens(4),
c      +   ktens(5), ktens(6), ktens(7), ktens(8), ktens(9)
c      write(11,*) 'kzz/kxx= ', ktens(9)/ktens(1)
c      write(11,*) 'kyy/kxx= ', ktens(5)/ktens(1)
c      close(11)

c... Calculate orientations and open and write GMT plot file
      open(11,file=outfile//'.plt',status='unknown')
      do n = 1, nfr
        nn = nfr(n)
        if(strike(nn).le.90.d0) then
          adip = dip(nn)
          bdip = dip(nn) + 180.d0
        elseif(strike(nn).gt.90.d0.and.strike(nn).le.270.d0) then
          adip = 180.d0 - dip(nn)
          bdip = 360.d0 - dip(nn)
        else
          adip = dip(nn)
          bdip = dip(nn) + 180.d0
        endif
        write(11,404) dist(nn), adip, alen(n), unitname(layer)
        write(11,404) dist(nn), bdip, blen(n), unitname(layer)
      enddo
      close(11)

c-----
c      Below by MAC 4/98
c      Completely changed output file formatting
c      now 'all1.par' and 'all2.par' which list data for each subunit
c      Deleted E.S. output file writing

      if (endp2.lt.9999.0) then
        write(13,443) unitname(layer), endp1, endp2, trcmin, fmin,
+       trcmax, nfr, avgsp, sdspac, freq, sdfreq, avglen, sdlen, frcint
        write(14,444) unitname(layer), fmin, nfr, freq,
+       aperture, frcpor, frcp2d, frcp1d, alpha, kzzkxx, kyykxx, kzzkyy
        write(13,443) '      ', dist(ns1), dist(ns2)
      else
c       alcove data & ECRB data
c       ECRB is read in as if it is alcove 9 MAC 3-23-99
        if (endp1.lt.90000.0) then
          write(13,2443) unitname(layer), INT(endp1/10000.0), trcmin, fmin,
+         trcmax, nfr, avgsp, sdspac, freq, sdfreq, avglen, sdlen, frcint
          else
            write(13,2445) unitname(layer), trcmin, fmin,
+           trcmax, nfr, avgsp, sdspac, freq, sdfreq, avglen, sdlen, frcint
          end if
          write(14,444) unitname(layer), fmin, nfr, freq,
+         aperture, frcpor, frcp2d, frcp1d, alpha, kzzkxx, kyykxx, kzzkyy
          write(13,2444) (dist(ns2)-dist(ns1))
        end if
441      format(1x, ' Unit', 1x, '<---Station--->', 1x,
+       ' Min-m', 1x, 'MinUse', 1x, ' Max-m', 1x, ' #Frac', 1x,
+       ' Spac-m', 1x, 'SDSpac', 1x, 'Fq-1/m',
+       1x, 'SDFreq', 1x, 'Leng-m', 1x, 'SDLeng', 1x, 'Intens')

```

```

442  format(1x,' Unit',1x,
+     'MinUse',1x,' #Frac',1x,'Fq-1/m'
+     ,1x,'Apr-um',1x,' Por-3D',1x,' Por-2D',1x,' Por-1D'
+     ,1x,' alpha',1x,'kzz/kxx',1x,'kyy/kxx',1x,'kzz/kyy')
443  format(1x,a5,2(1x,f7.2),3(1x,f6.2),1x,i6,7(1x,f6.2))
444  format(1x,a5,1x,f6.2,1x,i6,1x,f6.2,1x,f6.0,4(1x,es9.2),
+     3(1x,f7.2))
2443 format(1x,a5,4x,'Alcove',i2,4x,3(1x,f6.2),1x,i6,7(1x,f6.2))
2444 format(7x,f7.2,1x,'meters')
2445 format(1x,a5,4x,'ECRB ',2x,4x,3(1x,f6.2),1x,i6,7(1x,f6.2))

```

```

c Save results for combined output
c added MAC 4/98

```

```

combine(layer,1)=endp1
combine(layer,2)=endp2
combine(layer,3)=trcmin
combine(layer,4)=trcmax
combine(layer,5)=dble(nfr)
combine(layer,6)=avgsp*dble(nfr-1)
combine(layer,7)=ssqsp
combine(layer,8)=avglen*dble(nfr)
combine(layer,9)=ssqtr
combine(layer,10)=frcpor*blksiz/(aperture*1d-6)
combine(layer,11)=frcp2d*blksiz/(aperture*1d-6)
combine(layer,12)=ktens(1)/freq
combine(layer,13)=ktens(5)/freq
combine(layer,14)=ktens(9)/freq
combine(layer,15)=slgsp
combine(layer,16)=ssqlsp

```

```

c MAC V1.1
combine(layer,17)=intarea
combine(layer,18)=gmlen

```

```

c Added MAC 5/98 - Output interval results to 'interval.par'
do intn=1,intlayer

```

```

write(18,2000)unitname(layer),
+ (endp1+(intn-1)*intlength),
+ (endp1+(intn)*intlength),
+ intnfr(intn),intspace(intn),intfreq(intn),
+ (dble(intnfr(intn))/intlength),intrtrace(intn)
end do

```

```

1999 format(1x,' Unit',2(1x,' Station'),1x,' #Frac',4x,
+ 'Spacing',2x,'Frequency',3x,'#/Length',2x,'Intensity')
2000 format(1x,a5,2(1x,f9.1),1x,i8,4(1x,f10.2))
c-----

```

```

c... Write fracture size distributions

```

```

if(ans2.eq.'y')then
open(12,file=outfile//'.szd',status='unknown')
do k = 1, ni
fgrpl = fmesf + dble(k-1)*frint
fsiz = fgrpl + frint*0.5d0

```

```

c rev MAC 5/12/97 write(12,470)fsiz,dble(nfrint(k))/dble(ns)
write(12,475)fsiz,nfrint(k)
enddo
close(12)
fsum = 0.d0

```

```

c      write cumulative size distributions
open(12,file=outfile//'.csd',status='unknown')
  ftot = 1.d0
  write(12,470) fmesf,ftot
do k = 1, ni
  fgrpl = fmesf + dble(k)*frint
  fsum = dble(nfrint(k))/dble(ns) + fsum
  write(12,470) fgrpl,1.d0 - fsum
enddo
close(12)
endif

```

c

c Added MAC 4/17/98

```

999  continue
      END DO
      close(13)
      close(14)

```

c-----

c Below is all new code added by MAC 4/98

c Combine results for single values for each model layer

c

c Output to files 'comb1.par' & 'comb2.par' - combined results of
 c all1.par & all2.par

c Output to file 'calibrate.par' - data to be used for inversion

c

```

open(13,file='comb1.par',status='unknown')
open(14,file='comb2.par',status='unknown')
open(15,file='calibrate.par',status='unknown')

```

```

write(13,1441)

```

```

write(14,442)

```

```

write(15,2501)

```

```

DO i = 1,ntotal

```

```

  trcmin = 1d6

```

```

  trcmax = 0d0

```

```

  nfr = 0

```

```

  avgsp = 0d0

```

```

  sspac = 0d0

```

```

  sdspac = 0d0

```

```

  ssqsp = 0d0

```

```

  avglen = 0d0

```

```

  sdlen = 0d0

```

```

  ssqtr = 0d0

```

```

  frcpor = 0d0

```

```

  frcp2d = 0d0

```

```

  blksiz = 0d0

```

```

  kxx = 0d0

```

```

  kyy = 0d0

```

```

  kzz = 0d0

```

```

  slgsp = 0d0

```

```

  sslgsp = 0d0

```

c

```

  MAC V1.1

```

```

  intarea = 0d0

```

```

  gmlen = 0d0

```

```

first = modlayer(i)
if (i.ne.ntotal) then
  last = modlayer(i+1) - 1
else
  last = nlayers
end if
n = last - first + 1
DO layer = first,last
  trcmin = min(trcmin,combine(layer,3))
  trcmax = max(trcmax,combine(layer,4))
  nfr = nfr + NINT(combine(layer,5))
  sspac = sspac + combine(layer,6)
  ssqsp = ssqsp + combine(layer,7)
  avglen = avglen + combine(layer,8)
  ssqtr = ssqtr + combine(layer,9)
  frcpor = frcpor + combine(layer,10)
  frcp2d = frcp2d + combine(layer,11)
  blksiz = blksiz + combine(layer,2) - combine(layer,1)
  kxx = kxx + combine(layer,12)
  kyy = kyy + combine(layer,13)
  kzz = kzz + combine(layer,14)
c
  slgsp = slgsp + combine(layer,15)
  ssqlsp = ssqlsp + combine(layer,16)
c
  MAC V1.1
  intarea = intarea + combine(layer,17)
  gmlen = gmlen + combine(layer,18)
  if ((layer.eq.last).and.(nfr.gt.(n+1))) then
    avgsp = sspac/dbl(nfr-n)
    freq = 1.d0/avgsp
c
    nfr-n is the number of pairs used to calculate spacing
    varsp = (ssqsp - ((sspac**2)/dbl(nfr-n)))/(dbl(nfr-n-1))
    if (varsp.gt.0.0) then
      sdspac = dsqrt(varsp)
    else
      sdspac = 0d0
    end if
    varlen = (ssqtr - ((avglen**2)/dbl(nfr-n)))/
      (dbl(nfr-n-1))
  >
    avglen = avglen/dbl(nfr)
    if (varlen.gt.0.0) then
      sdlen = dsqrt(varlen)
    else
      sdlen = 0d0
    end if
    if (sdspac .gt. 0.0) then
      sdfreq = dsqrt(varsp/(avgsp**4))
    else
      sdfreq = 0d0
    end if
    aperture = 1d6*(12d0*(10**logairk(layer))/freq)
  &
      *(1.0/3.0)
    alpha = aperture*1d-6/2d0/72d-3
    frcpor = frcpor*(aperture*1d-6)/blksiz

```

```

frcp2d = frcp2d*(aperture*ld-6)/blksiz
frcp1d = freq*aperture*ld-6
c calculate k ratios (note freq cancels)
kzzkxx = kzz/kxx
kyykxx = kyy/kxx
kzzkyy = kzz/kyy
c calculate fracture intensity
frcint = avglen*dbln(nfr)/blksiz/6e0
c MAC V1.1
gmlen = 10**(gmlen/dbln(nfr))
intarea = intarea/blksiz/(gmlen**2)

write(13,1443)unitname(layer),trcmin,fmin,
+   trcmax,nfr,avgsp,sdspac,freq,sdfreq,avglen,sdlen,frcint
write(14,444)unitname(layer),fmin,nfr,freq,
+   aperture,frcpor,frcp2d,frcp1d,alpha,kzzkxx,kyykxx,kzzkyy

c
ssqlsp = (ssqlsp - slgsp**2/dbln(nfr-n))/dbln(nfr-n-1)
slgsp = slgsp/dbln(nfr-n)
logf = -slgsp
loga = (ld0/3d0)*(dlog10(12d0)+logairk(layer)-logf)
>   - dlog10(2d0*72d-3)
sdalpha = sdfreq*dsqrt(ld0/72d-3) *
>   ( (10**logairk(layer))/18d0/(freq**4) )**(1.0/3.0)
if (ssqlsp.le.0.0) then
write(*,2500)unitname(layer),slgsp,ssqlsp
ssqlsp = 0.0
end if

c MAC V1.1 add new parameters gmlen (gemetric mean length) and
c intarea (fracture area/block volume where block volume is
c block length * gmlen^2). Also changed output for calibrate.par
write(15,2500)unitname(layer),fmin,frcp2d,(aperture*ld-6),freq,
+   intarea,gmlen,alpha,sdalpha,loga,dsqrt(ssqlsp/9d0)
2500 format(1x,a5,5x,f9.2,2(3x,es9.2),3x,f9.2,2(3x,f9.3),
+   2(3x,es9.2),2(3x,f9.2))
2501 format(1x,'Unit',1x,'Min-Fr-Length',1x,'Fr-Porosity',4x,
+   'Aperture',3x,'Frequency',2x,'Inter-Area',3x,'Gm-length',
+   4x,'Fr-Alpha',4x,'SD-Alpha',4x,'LogAlpha',1x,'SD-LogAlpha')
c2500 format(1x,a5,2(1x,f7.2),2(1x,es9.2),3(1x,f7.2),1x,f7.3,1x,f7.2,
c   +   1x,i5,2(1x,f7.2))
c2501 format(1x,'Unit',4x,'Freq',2x,'SDFreq',5x,'alpha',3x,'sdalpha',
c   +   4x,'loga',2x,'logsda',2x,'<loga>',
c   +   1x,'s<loga>',2x,'gmFreq',1x,'#Frac',3x,'Block',3x,'#Freq')

c added else statement - MAC 6/25/98
else
if (layer.eq.last) then
write(13,2500)unitname(layer)
write(14,2500)unitname(layer)
write(15,2500)unitname(layer)
end if

end if
END DO
END DO

```

```
1441 format(1x,' Unit',1x,  
+ ' Min-m',1x,'MinUse',1x,' Max-m',1x,' #Frac',1x,  
+ 'Spac-m',1x,'SDSpac',1x,'Fq-1/m',  
+ 1x,'SDFreq',1x,'Leng-m',1x,'SDLeng',1x,'Intense')  
1443 format(1x,a5,3(1x,f6.2),1x,i6,7(1x,f6.2))  
close(13)  
close(14)
```

stop

```
400 format(a200)  
404 format(f13.2,1x,f8.4,1x,f9.5,1x,a5)  
408 format(a10)  
410 format(i2,1x,f5.2)  
415 format(a21,2(1x,f7.2))  
420 format(a48,2(1x,f7.3),1x,i5,1x,f5.3)  
425 format(a78)  
430 format(f8.4,5(2x,f8.4),2(2x,e10.4))  
440 format(a40)  
450 format(9(4x,a4,3x))  
460 format(9(1x,e10.3))  
470 format(f10.3,1x,f8.4)  
475 format(f10.3,1x,i8)
```

c

stop
end

111-1.2A

File 'datblk11.f'
File with data blocks for
frac_calc Version 1.1

Referenced on p. 13

111-51 JEH 4/7/00


```

+ , 'ptn26', 'ptn26' ! Alcove 4
+ , 'tsw31', 'tsw31', 'tsw31', 'tsw31'
+ , 'tsw32', 'tsw32', 'tsw32', 'tsw32', 'tsw32'
+ , 'tsw33', 'tsw33', 'tsw33', 'tsw33', 'tsw33', 'tsw33'
+ , 'tsw33' ! ECRB
+ , 'tsw34', 'tsw34', 'tsw34', 'tsw34'
+ , 'tsw34', 'tsw34', 'tsw34', 'tsw34', 'tsw34' ! Alcove 5 & 6
+ , 'tsw34' ! ECRB
+ , 'tsw35'
+ , 'tsw35' ! ECRB
+ , 'tsw36' ! ECRB
+ , 'tsw37' ! ECRB
c + , 'burst'
+ /
data modlayer / 1,2,8
+ , 12,15,16,17,20,22
+ , 28,32,37,44,54,56,57
c + , 58
+ /
c station for start and end of unit in meters & log airk (m2)
data unitsta /348.8 !tcw11
+ , 61.7,441.9,6725.5,6769.4,7514.2 !tcw12
+ , 30003.00 !tcw12 alcove 3
+ , 776.5,6718.5,6761.4,7507.8 !tcw13
+ , 793.6,6697.5,7495.4 !ptn21
+ , 0.0 !ptn22
+ , 0.0 !ptn23 - no data
+ , 875.8,6680.7,7481.3 !ptn24
+ , 894.6,7476.3 !ptn25
+ , 1021.0,6637.5,6996.5,7451.9 !ptn26
+ , 40000.0,40029.55 !ptn26 alcove 4
+ , 1075.7,6632.8,6990.3,7440.0 !tsw31
+ , 1191.0,6507.7,6527.4,6885.0,7341.5 !tsw32
+ , 1716.0,6308.0,6327.5,6791.8,7167.5,7290.0 !tsw33
+ , 90000.0 !tsw33 ECRB
+ , 2720.0,5878.3,7057.4,7143.0 !tsw34
+ , 50000.0,51000.0,52000.0,60000.0,61000.0 !tsw34 alc 5 & 6
+ , 91015.0 !tsw34 ECRB
+ , 5729.2 !tsw35
+ , 91444.0 !tsw35 ECRB
+ , 92326.0 !tsw36/37 ECRB
+ , 92326.0 !tsw36/37 ECRB
c + , 4000.0
+ /
data unitend /435.2 !tcw11
+ , 198.6,776.5,6761.4,6787.5,7875.0 !tcw12
+ , 30035.0 !tcw12 alcove 3
+ , 793.6, 6725.5,6769.4,7514.2 !tcw13
+ , 869.3,6718.5,7507.8 !ptn21
+ , 0.0 !ptn22
+ , 0.0 !ptn23 - no data
+ , 894.6,6694.0,7494.0 !ptn24
+ , 1021.0,7481.3 !ptn25
+ , 1075.7,6680.7,7057.4,7476.3 !ptn26
+ , 40022.2,40051.0 !ptn26 alcove 4
+ , 1191.0,6637.5,6996.5,7451.9 !tsw31
+ , 1716.0,6525.2,6632.8,6990.3,7440.0 !tsw32

```

```

+ ,2720.0,6324.2,6507.7,6885.0,7255.0,7341.5 !tsw33
+ ,91015.0 !tsw33 ECRB
+ ,5729.2,6308.0,7100.0,7167.5 !tsw34
+ ,50012.0,51015.0,52140.0,60024.0,61175.0 !tsw34 alc 5 & 6
+ ,91444.0 !tsw34 ECRB
+ ,5878.3 !tsw35
+ ,92326.0 !tsw35 ECRB
+ ,92583.0 !tsw36 ECRB
+ ,92583.0 !tsw37 ECRB
c + ,5200.0
+ /
data logairk /-10.52 !tcw11
+ , -11.28,-11.28,-11.28,-11.28,-11.28 !tcw12
+ , -11.28 !tcw12 alcove 3
+ , -11.34,-11.34,-11.34,-11.34 !tcw13
+ , -11.49,-11.49,-11.49 !ptn21
+ , -12.52 !ptn22
+ , -12.52 !ptn23
+ , -11.53,-11.53,-11.53 !ptn24
+ , -12.78,-12.78 !ptn25
+ , -12.66,-12.66,-12.66,-12.66 !ptn26
+ , -12.66,-12.66 !ptn26 alcove 4
+ , -12.20,-12.20,-12.20,-12.20 !tsw31
+ , -12.15,-12.15,-12.15,-12.15,-12.15 !tsw32
+ , -12.11,-12.11,-12.11,-12.11,-12.11,-12.11 !tsw33
+ , -12.11 !tsw33 ECRB
+ , -12.80,-12.80,-12.80,-12.80 !tsw34
+ , -12.80,-12.80,-12.80,-12.80,-12.80 !tsw34 alc 5 & 6
+ , -12.80 !tsw34 ECRB
+ , -12.04 !tsw35
+ , -12.04 !tsw35 ECRB
+ , -11.87 !tsw36 ECRB
+ , -11.87 !tsw37 ECRB
c + , -12.80
+ /

```


Sample Input & Output for ~~Calc~~ MC 8/10/98 8/10/98

Below are the data for ptn25 in the North Ramp.
 ✓ → indicates that value checks with hand calculations below.

Sample input data from DLS:

LOCATION	STRIKE	DIP	LENGTH A	LENGTH B
879.700	20.000	8.000	2.000	6.000
882.370	184.000	78.000	3.500	1.670
887.300	299.000	78.000	.000	1.110
893.860	20.000	49.000	.100	.330
893.920	22.000	80.000	.680	.620
894.130	20.000	67.000	1.200	1.600

extracted from
 8ta10.txt in
 D:\DLS → DTN: GS 9711
 08314224.005 using
 single user macro
 Read-TDB (see p.
 82-87 in Ymp-LBNL-658-
 MC-1
 MC 3/31/99

Sample output from frac_calc.f (for fractures ≥ 1 meter in length)

all1.par

Unit	Station	Min-m	MinUse	Max-m	#Frac	Spac-m	SDSpac	Fq-1/m	SDFrac	Leng-m	SDLeng	Intens
ptn25	875.80 894.60	.43	1.00	8.00	5	3.61	2.78	.28	.21	3.68	2.91	.16

all2.par

Unit	MinUse	#Frac	Fq-1/m	Apr-um	Por-3D	Por-2D	Por-1D	alpha	kzz/kxx	kyy/kxx	kzz/kyy
ptn25	1.00	5	.28	504.	5.93E-05	8.21E-05	1.40E-04	3.50E-03	1.69	1.81	.93

calibrate.par

Unit	Frac	SDFrac	alpha	salpha	loga	logstda	sigma	sloga	sdFrac	sdFrac	sdFrac
ptn25	.21	.67	3.85E-03	1.23E-04	-2.4	3.91	2.50	.422	.38	5	16.80

Calculations below are by hand (with a calculator)

this portion assumed that there would be two ptn25 sections
 one in the North ramp and one in the South Ramp. see p 106

	length	spacing
1.	879.7	8
2.	882.37	5.17
3.	887.3	1.11
4.	893.86	0.43 ← exclude since ≤ 1
5.	893.92	1.3
6.	894.13	2.8

so # Frac = 5 , average length = 3.676 m, std. dev. length = 2.912

spacing:

2-1	2.67 m
3-2	4.93 m
exclude 4	5 MC 8/10/98 A-3 6.62 m
6-5	MC 8/10/98 0.21 m

average = 3.6075 m sd = 2.784 m

frequency $F = \frac{1}{L} = 0.277 / m$
 $sd = \frac{2.784 m}{(3.6075 m)^2} = 0.214 / m$

MC
 9/23/99

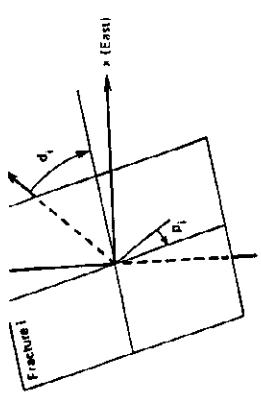


Fig. 4.6. Direction and dip of a fracture in three dimensions.

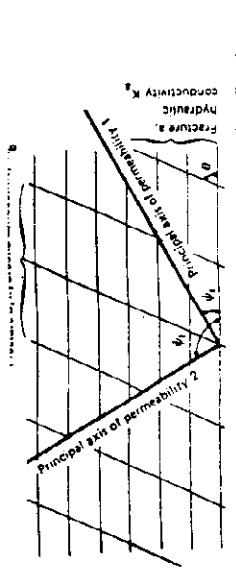


Fig. 4.7. Orientation of the principal axes of anisotropy in a fractured medium in two dimensions. [From Maini and Hocking (1977). Reproduced with permission from the Geological Society of America.]

tology for Engineers,

intensity $I = \frac{\sum \text{trace lengths}}{\text{area}} = \frac{(8+5.17+1.11+1.3+0.21)m}{(894.6-875.8)m(6m)}$

2.8 mc @ 110 MB

$I = 0.163 \text{ m/m}^2$

$\log a =$
 $\log \frac{\sigma}{\sigma_0} =$

Aperture $b = \left(\frac{12k}{f}\right)^{\frac{1}{3}} = \left(\frac{12 \cdot 10^{-11.53} \text{ m}^2}{0.277/m}\right)^{\frac{1}{3}} = 5.0377 \times 10^{-4} \text{ m}$

OR 503.8 μm

$\log f =$
 < 10

$\log k = -11.53$ from databk.f
(p. 96-97 in Ref Notebook YMP-LBNL-65B-MC-1.1A)

Porosity

3D: $\phi_{3D} = \frac{\pi b (\sum t_i^2)}{4} = 5.933 \times 10^{-5}$

5 mc @ 110 MB

gmF

2D: $\phi_{2D} = bI = (5.0377 \times 10^{-4} \text{ m})(0.163 \text{ m/m}^2) = 8.212 \times 10^{-5}$

1D: $\phi_{1D} = bf = (5.0377 \times 10^{-4} \text{ m})(0.277/m) = 1.395 \times 10^{-4}$

$< \log a ?$

Alpha

$\alpha = \frac{b}{2T \cos(0^\circ)} = \frac{5.0377 \times 10^{-4} \text{ m}}{2(0.072 \text{ N/m})} = 0.003498 \text{ Pa}$

see note on p. 105, calibrate.par expects 2 layers for ptrn25 based on databk.f. Made temporary modification to databk.f and reran program to get appropriate calibrate.par

S<

calibrate.par see all 1.par

Unit	Freq	SDFreq	alpha	salpha	loga	logada	<loga>	<loga>	gmFreq	#Frac	Block
ptrn25	.28	.21	3.50E-03	2.41E-04	-2.46	-3.62	-2.54	.344	.48	5	18.80

block - 1

std dev $\alpha = \frac{\sigma_s}{s^2} \left(\frac{k}{18f^2}\right)^{\frac{1}{3}} \frac{1}{T^{\frac{1}{2}}}$

assumed 2 degrees of freedom

$= \frac{2.784 \text{ m}}{(3.6075 \text{ m})^2} \left(\frac{10^{-11.53} \text{ m}^2}{18(0.277/m)^2}\right)^{\frac{1}{3}} \frac{1}{(0.072 \text{ N/m})^{\frac{1}{2}}}$

$= 0.00024165 \text{ /Pa}$

$k_{zz}/k_{xx}, k$
 $k_{zz} =$
 k_{xx}

(see p. 124-125 in YMP-LBNL-MC-1)

2.8 mc 8/10/98

$$\frac{17+1.11+1.3+0.21}{99.6-875.8} \text{ m (6m)}$$

$$\frac{1}{2} \text{ m/m}^2$$

$$\log a = \log(\alpha) = -2.456$$

sda mc 8/10/98

$$\log \frac{1}{2} = \log(\sigma_a) = -3.6168$$

$$\left(\frac{10^{-11.53} \text{ m}^2}{2.277/\text{m}} \right)^{1/3} = 5.0371 \times 10^{-4} \text{ m}$$

OR 503.8 um

log f:

$$\langle \log f \rangle = -\langle \log s \rangle$$

and

$$\langle \log s \rangle = \frac{\log 2.67 + \log 4.93 + \log 6.62 + \log 0.4}{4}$$

$$= 0.3156 \text{ or geometric mean of spacing.}$$

$$\sigma_{\log s} = 0.6823$$

$$\text{gmFreq} = \text{geometric mean } f = 10^{\langle \log f \rangle} = 10^{-\langle \log s \rangle}$$

$$= 10^{-0.3156} = 0.4835 / \text{m}$$

5 mc 8/10/98

$$= 5.933 \times 10^{-4}$$

$$\frac{2.163 \text{ m}}{\text{m}^2} = 8.212 \times 10^{-5}$$

$$\frac{277/\text{m}}{\text{m}^2} = 1.395 \times 10^{-4}$$

$\langle \log a \rangle, s \langle \log a \rangle$ see p124-125 in YMP-LBNL-65B-MC-1

$$\langle \log a \rangle = \frac{1}{3} (\log 12 + \log k - \langle \log f \rangle) - \log 2Z$$

$$= \frac{1}{3} (\log 12 - 11.53 + 0.3156) - \log((2)(0.072 \text{ N/m}))$$

$$= -2.537$$

$$\frac{x \cdot 10^{-4} \text{ m}}{\text{N/m}} = 0.003498$$

cts 2 layers for ptn25
modification to databk.f
to calibrate.par

$$s \langle \log a \rangle = \sigma_{\log a} = \frac{1}{3} \sigma_{\log s} = \frac{1}{3} (0.6823)$$

$$= 0.2274 \leftarrow \text{assumes 3 degrees of freedom}$$

ga	<loga>	gmFreq	#Prac	Block
2.54	.344	.48	5	18.80

assumes 2 degrees of freedom

block - length of block in ESE - station to station that represents stratigraphic unit

$$894.6 \text{ m} - 875.8 \text{ m} = 18.8 \text{ m}$$

$$\left(\frac{\text{m}^2}{77/\text{m}} \right)^{1/3} \frac{1}{(0.072 \text{ N/m})^{1/2}}$$

$$= 4165 / \text{Pa}$$

-MC-1)

~~$$\frac{k_{zz}}{k_{xx}} = \sin \left(\frac{\text{mc}}{8/10/98} \right)$$~~

go to next page

strike	dip	true dip	in degrees
20°	8°	8°	
104	78	8°	102
299	78	78	
22	80	80	
20	67	67	

Compiler I

The program

$$\sum \sin^2(\text{dip}) = 3.75$$

$$\sum (1 - \sin^2(\text{strike}) \sin^2(\text{dip})) = \frac{5 \cdot \text{MC } 8/10/98 \cdot 0.974}{\text{MC } 8/10/98} - 7.92875 = \frac{\text{MC } 8/10/98 \cdot 4.026}{\text{MC } 8/10/98} - 7.92875 = 3.09725$$

$$\sum (1 - \cos^2(\text{strike}) \sin^2(\text{dip})) = \frac{5 \cdot \text{MC } 8/10/98}{\text{MC } 8/10} - 2.776 = \frac{2.224}{\text{MC } 8/10} = 2.224$$

$$\frac{k_{zz}}{k_{xx}} = \frac{3.75 \cdot \text{MC } 8/10/98}{\frac{2.224}{\text{MC } 8/10/98}} = \frac{3.75}{2.224} = 1.686$$

$$\frac{k_{yy}}{k_{xx}} = \frac{\frac{4.026 \cdot \text{MC } 8/10/98}{3.09725}}{\frac{2.224}{\text{MC } 8/10/98}} = \frac{1.381}{\text{MC } 8/10/98} = 1.81$$

$$\frac{k_{zz}}{k_{yy}} = \frac{3.75}{4.026} = 0.931$$

All calculations in frac-calc.f check.

(SIGNATURE REMOVED) 8/10/98

111-60 886 4/7/00

Mark 6

Compiler Information for Frac_Calc.f

8/25/98

The program Frac_Calc.f was compiled using

Fortran Powerstation 4.0
Microsoft 1994-1995

Product ID: 36785-411-0083773-30563

(part of Microsoft Developer Studio)

74 mc 8/10/98 4.026
75 = 2.07425 3.07425
8

76 = ~~1.224~~ 2.224
mc 8/10

1.686

1.81

check.

1/98

(SIGNATURE REMOVED) 8/25/98

111-61 8/24/98

Version 1.0
MC 7/21/99

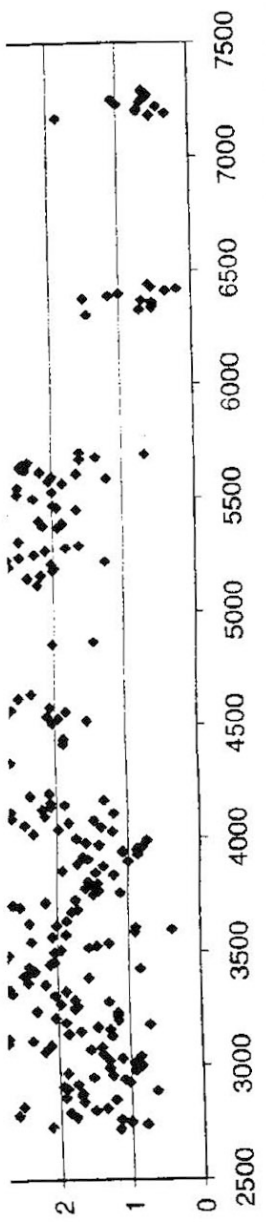
8/10/98

Frac-Calc & ESF Fracture Data

can be seen a
40+00 and 52+00.
other interval
Notebook

The code frac-calc is listed in Reference Notebook
YMP-LBNL-GSB-MC-1.1A pages 88-97.
The development of the code was discussed previously on
pages 60-69, 124-125, 137 YMP-LBNL-GSB-MC-1
The code was previously listed on p 40-46 in this notebook.
Results are used throughout both notebooks. The most
recent code addition is discussed on p. 98 of this
notebook.

Also see
p 102-103
this notebook
7/10/98
8/10/98



Using d:\salcove.dat (see p. 54-56, this notebook), fracture
properties were calculated for the model layers (see p. 64,
this notebook). ^{YMP} More detailed output is given in
Reference Notebook YMP-LBNL-GSB-MC-1.1A p. 98-106.
This gives

- all1.par & all2.par → properties ^{MC} for individual sections of each layer
- comb1.par & comb2.par → properties for each model layer (combined above)
- calibrate.par → additional properties for each model layer.

see
p. 114
this notebook
for MC
8/29/98

Frac-calc is defined as a "Multi-User" Macro.
A Form M was completed and submitted to
qualify the code as a "macro"

The code is in d:\code\calc_frac\frac-calc-f
and includes databk.f

(SIGNATURE REMOVED)

8/10/98

111-67 05H 4/100

Fracture Permeability Components Calculations

8/10/98

from a

from Sonnenthal et.al. (1997) ref. on p. 60 in SM-MC-1

↑ page 7-21

YMP-LBNL-GSR

MC
9/3/99

The large-scale saturated fracture permeability is dependent on the fracture connectivity and the permeability of individual fractures. Although the connectivity of the fractures is difficult to ascertain, over a large scale the ratios of the permeability components can give some indication as to the preferred flow directions. Assuming an array of infinite fractures in three dimensions, the permeability tensor for a fracture network modified from the conductivity tensor in de Marsily (1986) is given by:

$$\bar{k}_f = \begin{bmatrix} k_{xx} & k_{xy} & k_{xz} \\ k_{yx} & k_{yy} & k_{yz} \\ k_{zx} & k_{zy} & k_{zz} \end{bmatrix} = \sum_{i=1}^N k_{f,i} \bar{R}_i \quad (16)$$

The permeability of each fracture is given by the cubic law (Equation (5)), assuming uniform apertures. The tensor \bar{R}_i relates the strike (d_i) and dip (p_i) of each fracture to the components of the permeability tensor, as follows:

$$\bar{R}_i = \begin{bmatrix} 1 - \cos^2 d_i \sin^2 p_i & \frac{1}{2} \sin 2d_i \sin^2 p_i & -\frac{1}{2} \sin 2p_i \cos d_i \\ \frac{1}{2} \sin 2d_i \sin^2 p_i & 1 - \sin^2 d_i \sin^2 p_i & \frac{1}{2} \sin 2p_i \sin d_i \\ -\frac{1}{2} \sin 2p_i \cos d_i & \frac{1}{2} \sin 2p_i \sin d_i & \sin^2 p_i \end{bmatrix} \quad (17)$$

The permeabilities in the principal directions would have to be derived from this matrix; however as the UZ model does not at this time incorporate the off-diagonal terms, and because our fracture permeabilities are based on air-injection measurements, this is not necessary at present.

The code ~~calc~~^{MC} frac calc.f includes these calculations. parts 3 & 4

The first portion converts the angle from degrees to radians and gives the dip angle in terms of the "true" dip rather than the "apparent" dip. The second part computes the components of the matrix shown in equation 17 above. The third part then multiplies each component by the fracture permeability (k_{frc}) and the frequency (f) (see eqn 16 above). The 4th part sums these for all the fractures in the layer. The 5th and last part (added by myself on 4/21/98) calculates the ratios k_{zz}/k_{xx} , k_{yy}/k_{xx} , & k_{zz}/k_{yy} . Note that the ratios are independent of k and f .

The parts 1-4 were written by Eric Sonnenthal.

The code (excerpt is shown on the next page).

Reference for de Marsily given on p104 (with excerpt)

K. MC
8/10

c... Cal
re
dc

part 1

part 2

part 5

e.
c Added
k
k
k

from d:\code\calc_frac\frac_calc.f

lations 8/10/98

YMP-LBNL-658

on p. 60 in SN-MC-1

MC
9/3/99

connectivity and the permeability tensor for a fracture given by:

198

(16)

part 1

assuming uniform apertures. components of the permeability tensor

$\sin^2 p \cos d$
 $\sin^2 p \sin d$
 $\sin^2 p$

(17)

part 2

in this matrix; however as the use our fracture permeabilities

these calculations.

parts 3 & 4

n degrees to s of the "true" second part

is shown in m multiplies permeability (kfrc) here). The 4th

part 5

s in the layer. self (m 9/21/98) k_{xx}/k_{yy} , & k_{zz}/k_{yy} out of k and f.

invariant.

t page).

(with excerpt)

```

c... Calculate components associated with each fracture, then sum
radian = pi/180.d0
do n = 1, nfr
  nn = nfrc(n)
  if (strike(nn) .le. 90.d0) then
    stkrad = strike(nn)*radian
    diprad = dip(nn)*radian
  elseif (strike(nn) .gt. 90.d0 .and. strike(nn) .le. 180.d0) then
    stkrad = strike(nn)*radian
    diprad = (180.d0-dip(nn))*radian
  elseif (strike(nn) .gt. 180.d0 .and. strike(nn) .le. 270.d0) then
    stkrad = strike(nn)*radian
    diprad = (180.d0-dip(nn))*radian
  else
    stkrad = strike(nn)*radian
    diprad = dip(nn)*radian
  endif
  sdsq = (dsin(diprad))**2
  kxx = 1.d0 - ((dcos(stkrad))**2)*sdsq
  kxy = 0.5d0*dsin(2.d0*stkrad)*sdsq
  kxz = -0.5d0*dsin(2.d0*diprad)*dcos(stkrad)
  kyx = kxy
  kyy = 1.d0 - ((dsin(stkrad))**2)*sdsq
  kyz = 0.5d0*dsin(2.d0*diprad)*dsin(stkrad)
  kzx = kxz
  kzy = kyz
  kzz = sdsq
  kf = kfrc(n)*frc
  ktens(1) = kxx*kf + ktens(1)
  ktens(2) = kxy*kf + ktens(2)
  ktens(3) = kxz*kf + ktens(3)
  ktens(4) = kyx*kf + ktens(4)
  ktens(5) = kyy*kf + ktens(5)
  ktens(6) = kyz*kf + ktens(6)
  ktens(7) = kzx*kf + ktens(7)
  ktens(8) = kzy*kf + ktens(8)
  ktens(9) = kzz*kf + ktens(9)
enddo

```

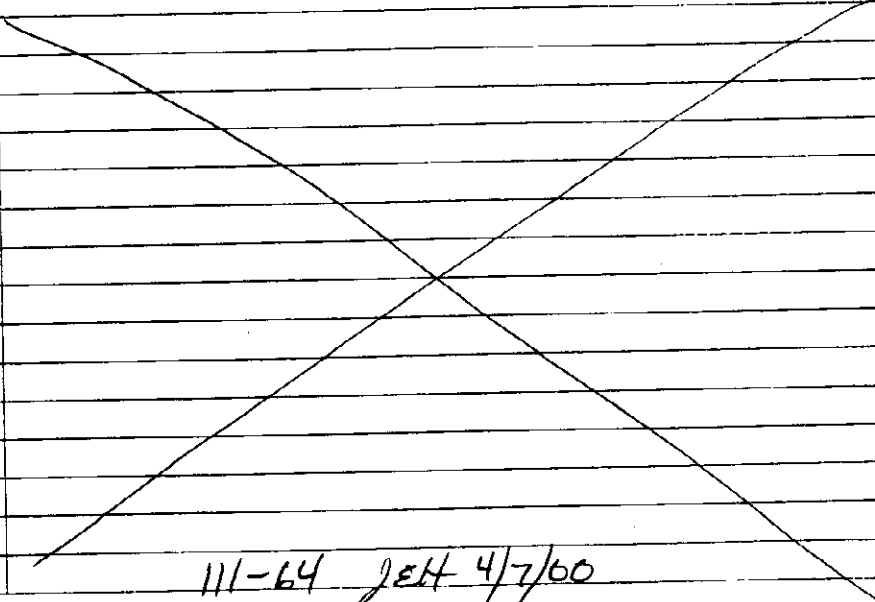
oper MC 8/24/98

but does not effect ratios since it cancels out
Mark A. Conway
8/24/98

```

c Added MAC 4/21/98
kzzkxx = ktens(9)/ktens(1)
kyykxx = ktens(5)/ktens(1)
kzzkyy = ktens(9)/ktens(5)

```



111-64 JEH 4/7/00

number of fractures in the block of side l , e_i the aperture of each individual fracture, and k_i the hydraulic conductivity of each individual fracture

$$R_i = \begin{bmatrix} 1 - \cos^2 d_i \sin^2 p_i & \frac{1}{2} \sin 2d_i \sin^2 p_i & -\frac{1}{2} \sin 2p_i \cos d_i \\ \frac{1}{2} \sin 2d_i \sin^2 p_i & 1 - \sin^2 d_i \sin^2 p_i & \frac{1}{2} \sin 2p_i \sin d_i \\ -\frac{1}{2} \sin 2p_i \cos d_i & \frac{1}{2} \sin 2p_i \sin d_i & \sin^2 p_i \end{bmatrix}$$

In the matrix R_i , the direction d_i and the dip p_i of each fracture are defined as in Fig. 4.8.

Once the tensor K has been determined, the principal axes of anisotropy and the diagonal components of K in these directions can be determined by calculating the eigenvalues and the eigenvectors of the matrix K .

This method of the continuous medium approximation is valid for a certain scale of observation: the flow velocities or the hydraulic heads in each fracture are not described with precision, but a mean value of these magnitudes is taken over all the fractures.

The definition of the hydraulic conductivities of each family of fractures may be approached in two ways: either (1) by measuring (or estimating) the mean geometric properties of the fractures (aperture, distance from each other, roughness, etc.) and using the expressions given above, or (2) through *in situ* tests by injecting water and measuring the hydraulic conductivities K_i of the elementary fractures directly.

The drawback of both methods is that they assume the fractures to be infinite and to have the same properties everywhere. Their results must be taken with caution. The directions of the principal axes of the conductivity tensor are probably more accurate than the value of the conductivities; these

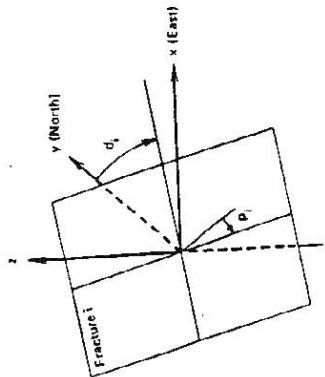


Fig. 4.8. Direction and dip of a fracture in three dimensions.

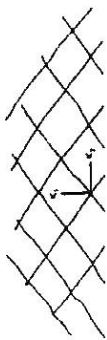


Fig. 4.6. Principal axes of anisotropy of a fractured medium.

For example, in two dimensions, two fracture systems with the same directional conductivity give the principal axes of anisotropy shown in Fig. 4.6. Maini and Hocking (1977) give the following expressions for calculating the directions of anisotropy and the principal hydraulic conductivities of the equivalent medium:

$$\psi = \frac{1}{2} \arctan \left(\frac{\sin 2\theta}{\cos 2\theta K_a / K_b} \right)$$

$$K_1 = \frac{K_a K_b \sin^2 \theta}{K_a \sin^2 \psi + K_b \sin(\theta - \psi)}$$

where K_a and K_b are the equivalent directional hydraulic conductivities of the fracture networks a and b , as shown in Fig. 4.7.

In three dimensions, Feuga (1981) gives the following expressions for determining the hydraulic conductivity tensor of a fractured medium with several fracture directions:

$$K = \sum_{i=1}^N e_i k_i R_i$$

where l is the arbitrary dimension of the side of a square block of the fractured medium, large enough to statistically sample all the families of fractures, N the

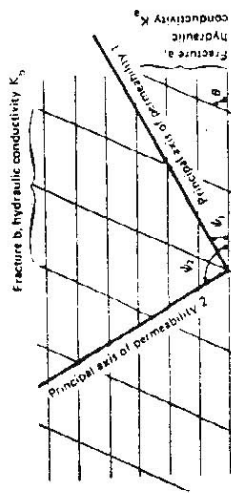


Fig. 4.7. Orientation of the principal axes of anisotropy in a fractured medium in two dimensions. [From Maini and Hocking (1977). Reproduced with permission from the Geological Society of America.]

de Marsily, G. 1986. Quantitative Hydrogeology, Groundwater Hydrology for Engineers, Orlando, Florida: Academic Press. NNA.19910207.0116.

(SIGNATURE REMOVED)

8/10/98

111-65 JEM 4/7/00

Sample

Below are

✓ → indica

Sample input data :

LOCATION	STRIKE
879.700	20.000
882.370	184.000
887.300	299.000
893.860	20.000
893.920	22.000
894.130	20.000

Sample output from

all1.par
Unit ← Station → X: ptn25 875.80 894.60

all2.par see above
Unit MinUse #Frac Eq: ptn25 1.00 5

calibrate.par
Unit Freq SDFreq ptn25 21 07 3.6

Calculations below

1. 879.7
2. 882.37
3. 887.3
4. 893.86
5. 893.92
6. 894.13

SO #1

Spacing

exclude 4

Frequen

this pattern assumed that there would be two ptn25 sections one in the north ramp and one in the south ramp. see p 106

TDB - fracture properties

4/17/98

Began analyzing fracture data. The first step was to recreate and verify the calculations in Chapter 7 of the Site-Scale Unsaturated Zone Model of Yucca Mountain.

I started with the code from E. Sonnenthal. It is located on hydra.lbl.gov in the directory

`/m/ultra2/u/esonn/ymp/`
 \uparrow ~~dir~~ `/src` MAC 8/25/98

The name of the code is `cnvfr2.f`

The original data analyzed (which only is up to station 90+00) was in the file

those data were only used for testing code results and were not used for VMP Q-work
 MC 4/29/98

`~ /ymp/fractures/ESF/frcpar.dat`
 and
`~ /ymp/fractures/esf/station.dat`

All changes to the code are indicated with my initials (MAC) and dated. The new filename for the code is: `calc_frac.f`

and it is located on `NWD-cushey` in `d:/code/calc_frac/`

This code differs in that it processes all of the DLS data at once. Station numbers are assigned to model layers in data statements.

The following calculations are performed:

$$\text{avg. spacing} = \frac{1}{nf-1} \sum_{i=2}^{nf} (D_i - D_{i-1})$$

where nf - the number of fractures
 D_i - is the location of fracture i

$$\text{fracture frequency} = \frac{1}{\text{avg. spacing}} = \frac{1}{\bar{s}}$$

\bar{s} - average spacing

ret
 MC
 4/11/98

SIGNATURE _____

READ AND UNDERSTOOD _____

DATE _____

DATE _____

19

19

111-66 J&H 4/1/00

Sonnenthal, E.L.; Ahlers, C.F.; and Bodvarsson, G.S. 1997. "Fracture and Fault Properties for the UZ Site-Scale Flow Model." Chapter 7 of *The Site-scale Unsaturated Zone Model of Yucca Mountain, Nevada, for the Viability Assessment*, edited by G.S. Bodvarsson, T.M. Bandurraga, and Y.S. Wu. Yucca Mountain Site Characterization Yucca Mountain Project Level 4 Milestone SP24UFM4; Report LBNL-40376. Berkeley, California: Lawrence Berkeley National Laboratory. LB970601233129.001 (Q).

$$b = \left(\frac{12 k}{f} \right)^{\frac{1}{3}}$$

where b - aperture
 k - air permeability (frac. perm.)
 f - frequency

$$\alpha = \frac{b}{2\tau \cos\theta}$$

where α - van Genuchten α for fractures
 b - aperture
 τ - surface tension of pure water at 20°C (0.072 N/m)
 θ - contact angle (assumed to be 0)
 This calculation was not previously in the code

porosities:

$$\phi_{1D} = F b$$

$$\phi_{2D} = \frac{b \sum_{i=1}^{nf} t_i}{\text{area}} = \frac{b \sum_{i=1}^{nf} t_i}{(6m) \text{ block length}}$$

$$\phi_{3D} = \frac{\pi b \sum_{i=1}^{nf} r_i^2}{\text{volume}} = \frac{\pi b \sum_{i=1}^{nf} r_i^2}{(6m)(6m) \text{ block length}}$$

t_i - trace length of fracture i
 block length - length along DLS corresponding to model layer (full length)
 r_i - one-half the trace length
 $r_i = t_i / 2$

For the above calculations, the fractures are assumed to be circular disks.

SIGNATURE _____

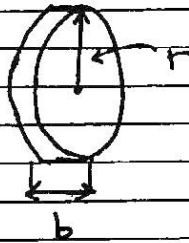
READ AND UNDERSTOOD _____

DATE _____

DATE _____

19 _____

19 _____



$$\text{volume in 3D} = b \pi r^2$$

The probability that the tunnel cut intersects these disks offcenter is not accounted for.

The area about the DLS centerline is assumed to include a 3 meter band on each side.

The ^{MC 9/17/98} ϕ_{3D} may underestimate porosity since it assumes fracture traces represent fracture diameters.

The ϕ_{1D} may overestimate porosity since it assumes infinitely long fractures.

ratios of permeability components:

ratios k_{zz}/k_{xx} , k_{yy}/k_{xx} , and k_{zz}/k_{yy} were calculated as defined in eqns 16 & 17 in Chapter 7.

For spacing, fractures located at the same station were assumed to be at a separation distance of 0.

The minimum measurement precision was 0.01 m for the DLS (Altman, 1997)

ref Altman, S.J. Determining reasonable ranges for van Genuchten fracture α for use in unsaturated flow modeling Sandia National Laboratory

DTN SNT05091597001.003

T.D.I.E 306502

November 25, 1997.

SIGNATURE (SIGNATURE REMOVED)
READ AND UNDERSTOOD

DATE 4/17 19 98
DATE 19

111-68 JEH 4/7/00

TDB - fracture properties - verification of code

4/24/98

To verify the code, the original dataset was used and compared to Chapter 7 results.

Data from /m/ultra1/u/esonn/ymp/Fractures/ esf stored on NWD-Cushey as dlsall in d:/code/

This data was transformed to a readable (numeric) format (convert station numbers to lengths) and stored in ericdls.dat in d:/code/calc=frac.

The code was run and results were compared to those in Chapter 7.

To combine disconnected segments the following formulations were used. This is different from the method used original by E. Sennertthalas noted in the comparison (typically averages of the segments). The below procedure combines all sublayers into one continuous layer (the pairing of fractures for spacing are limited to the sublayers). This is similar to the method used by (Altman, 1997)

see nomenclature on p. 60-61

$$\bar{S}_{comb} = \frac{\sum_{j=1}^{ns} \left[\sum_{i=2}^{nf_j} D_{i,j} - D_{i-1,j} \right]}{\sum_{j=1}^{ns} nf_j - j}$$

ns - # of segments
subscript j → segment j
comb - combined

The denominator is the number of pairs of fractures used to calculate the \bar{S}_{comb} .

SIGNATURE _____
READ AND UNDERSTOOD _____

DATE _____ 19____
DATE _____ 19____

111-69 g&H 4/7/00

$$\bar{f}_{comb} = \frac{1}{S_{comb}}$$

$$b_{comb} = \left(\frac{12k}{\bar{f}_{comb}} \right)^{\frac{1}{3}}$$

$$\phi_{30} = \frac{\pi b_{comb} \sum_{j=1}^{ns} \sum_{i=1}^{nf_j} r_{i,j}^2}{(6m)(6m) \sum_{j=1}^{ns} \text{blocklength}_j}$$

$$\phi_{20} = \frac{b_{comb} \sum_{j=1}^{ns} \sum_{i=1}^{nf_j} t_{i,j}}{(6m) \sum_{j=1}^{ns} \text{blocklength}_j}$$

$$\phi_{10} = b_{comb} f_{comb}$$

The alternative would be to calculate ^{A198} each parameter for each sublayer and then ~~compute~~ computed a weighted average based on the segment length

$$X = \frac{\sum_{j=1}^{ns} x_j \text{blocklength}_j}{\sum_{j=1}^{ns} \text{blocklength}_j}$$

for any parameter X

The first (continuous layer) method was used since the break-up of layers is arbitrary due to the location of the tunneling. On the other hand, the second method might better capture local phenomena which are averaged out by the averaging over longer

SIGNATURE _____
READ AND UNDERSTOOD _____

DATE _____ 19____
DATE _____ 19____

lengths. Considering though that these parameters are to represent the entire layer over the site, the first (continuous) method is deemed appropriate at this time.

An additional note is that the spacing calculation is along the DLS centerline and is not the "true" spacing. The calculation of "true" spacing will be considered at a later time. (see Geology of the Exploratory Studies Facility Topopah Spring Loop Attachment I

BAB 0 01717-0200-0002

REV 1.)

For the following verification - first the individual sublayers and then the overall layers are compared. Only fractures ≥ 1 m are included

SIGNATURE _____
READ AND UNDERSTOOD _____

DATE _____ 19 ____
DATE _____ 19 ____

111-71 JEH 4/7/00

YMP-LBNL DOCUMENT REVIEW/COMMENT RESOLUTION (DRCR) FORM

Document No. and Title: Frac-Calc Version 1.1 Page 1 of 1
 Date of Document / revision no. (as applicable): Version 1.1 Author: Mark Cushey
 Are Scientific Notebooks or other background documents/data included in the scope of this review? Yes No (If yes, identify on Attachment 3)
 Specific Review Criteria or Governing Procedure: YMP-LBNL-QIP-6.1 & AP-SI-1Q
 General Review Criteria: (Identify relevant criteria on Attachment 4): 5-7 to 5-10 in YMP-LBNL-QIP-6.1 & Section 5.1 of AP-SI-1Q
 Checker Technical Reviewer EA Reviewer OQA Reviewer
 Name: Johnny Hu Signature: _____ Date: 7/2/99
 (SIGNATURE REMOVED)

COMMENT NO MANDATORY (M) NON- MANDATORY (NM)	SECT. AND PAGE NO.	COMMENTS	AUTHOR'S RESPONSE			Reviewer Disposition for Mandatory Comments	
			ACCEPT Initial/Date	REJECT Initial/Date	Response required for all technical mandatory and non-mandatory comments	ACCEPT Initial/Date	REJECT Initial/Date
1 (NM)	16	(the application file is free-uh-ll-1 the program source code file is free-uh-ll-1)			Added to p.16 and p.67 in reference binder <u>in</u> <u>YMP-LBNL-MC-1.2</u> <u>MC 9/23/99</u>		
2 (NM)	67 68 69 70	check the source code file, there should have more codes to be printed out following p. 67 cross-out = 3.75			source code continues onto pp. 83-87		
3 (NM)	108	check the file contents & contents of file itself, cross-out for the file at following p. 67			Crossed-out 3.75 & initials added the inclusion of code itself on p.65 to not include note only		

May be on separate sheets to be attached, in which case the comments shall be numbered and this form will be used to track the comments and their resolution according to such numbers.
 Resolution of Disputed Comments
free-calc-f MC 4460 MC 1/100
 Office of Quality Assurance _____ Date _____ Project Manager _____
 YMP-LBNL Management Approval (Project Manager or Designee) _____ Date _____
 (SIGNATURE REMOVED) for G.S. Bodvarsson 9/23/99

III-72 284 4/2/00

TBgas3D v.1.0
Routine/Macro Documentation Form

Page 1 of 1

The following information can be included in the scientific notebook. Attach and reference notebook pages and diskettes with files as needed when submitting routine/macro to records.

1. Name of routine/macro with version/OS/hardware environment:
TBgas3D v.1.0 (routine) / UNIX SUNOS Solaris 5.5.1/Sun workstation

2. Name of commercial software with version/OS/hardware used to develop routine/macro:
FORTRAN 77/UNIX SUNOS Solaris 5.5.1/Sun workstation

3. **Test Plan.**
 - Explain whether this is a routine or macro and describe what it does:
This routine is used to prepare the input file (timvsp.dat) for the gas calibration from an EOS3 input file. timvsp.dat is the file specifying top gas pressure boundary condition for gas calibration.

 - Source code: (including equations or algorithms from software setup (LabView, Excel, etc.):
p. 61 S/N YMP-LBNL-GSB-LHH-2 (annotated with a description of what each step does)

 - Description of test(s) to be performed (be specific):
During the test, the routine reads in top boundary element names and gas pressures from input file fort.101 (EOS3 output only containing top boundary elements), read in pressure values from file fort.100 containing needed gas pressure fluctuations, and calculate gas pressures for each top boundary element. To facilitate verification by the hand calculation method, the number of iterations the code operates will be limited as explained on p. 62 (bullet 2a). The resulting output are compared and verified using hand calculation.

 - Specify the range of input values to be used and why the range is valid:
In the input file, a single top boundary element was used for simplicity. Because the routine does the same simple calculation repeatedly for each top boundary element, the use of one element is adequate for the test purpose.

4. **Test Results.**
 - Output from test (explain difference between input range used and possible input):
The output from the test is given on pp. 62-63 of S/N YMP-LBNL-GSB-LHH-2. The specific test case input range is deemed valid because the routine's simple arithmetic changes can be inspected using only a small sampling of lines from the very large output file.

 - Description of how the testing shows that the results are correct for the specified input:
The output results are the same as those by hand calculation.

 - List limitations or assumptions to this test case and code in general:
The format of input file fort.101 should be the same as an EOS3 output file, and fort.101 only contains top boundary elements. The input values must be between 0 and ∞ .

 - Electronic files identified by name and location (include disc if necessary):
The routine and test files are printed on pp.61-63, S/N YMP-LBNL-GSB-LHH-2.

111-74 JEH 4/7/00

TBgas3D v.1.0
Routine/Macro Documentation Form

Page 2 of 1

5. **Supporting Information.** Include background information, such as revision to a previous routine or macro, or explanation of the steps performed to run the software. Include listings of all electronic files and codes used. Attach Scientific Notebook pages with appropriate information annotated:

See attached pages for technical review forms, referenced scientific notebook pages and other supporting documentation

Note: All relevant scientific notebook (SN) pages are included in this package. In some instances, the included SN pages cross-reference other pages that are not included here because these were not essential to the documentation of this routine.

MAINTAIN PAGES IN THIS ORDER:

- 1) This 2-page Routine Documentation Form
- 2) pp. 61-63 for S/N YMP-LBNL-GSB-LHH-2
- 3) Review Forms

111-75 JEH 4/7/00

Test of TBgas 2D of a single user manual
 nrg 8-17-00
 section 4.1
 macros
 routine 8-17-00

① Description of the code (Ver 1.0)
 Fortran 77 (2011)

8-2-99

This code is used to determine an input file for the gas calibration from a EoS3 output. The detailed function of this code can be found from steps A through D given on pages 61 & 62.

```

real*8 p(3000),pp(2000)
character*8 Name(3000)
c n -- # of TP blocks
n=29 (n = # of TP blocks)
nn=324 (nn+1 = total lines for each element in file fort.100)
c
c do i=1,n
99 read(101,99)Name(i)
format(A5)
read(101,*)p(i),x1,x2,x3,x4
write(102,*)Name(i),p(i)
enddo
c
c do i=1,nn
ii=i-1
read(100,*)pp(ii),pp(ii+1),pp(ii+2),pp(ii+3)
enddo
read(100,*)pp(1297)
c
c sum=0.0
do i=1,1297
sum=sum+pp(i)
enddo
c
c sum=sum/real(1297)
write(*,*)sum
c
c do i=1,1297
pp(i)=pp(i)-sum
enddo
c
c do i=1,29
write(300,10)Name(i)
format(A5)
c
c do j=1,324
ii=(j-1)*4+1
write(300,20)pp(ii)+p(i),pp(ii+1)+p(i),
pp(ii+2)+p(i),pp(ii+3)+p(i)
enddo
c
c write(300,20)p(i)+pp(1297)
enddo
20 format(7x,f7.1,7x,f7.1,7x,f7.1,7x,f7.1)

stop
end
  
```

Top Boundary

Fort.101 Contains EoS3 output for TP blocks

Fort.100 Contains a file with correct pressure fluctuation in TP elements

1297 = nn * 4 + 1 for nn = 324

h h e
 Remain 8-2-99
 Remove mean from fort.100

n = 29

nn = 324

The code needs to do the following:

A: Read correct element names and gas pressures from fort.101, which contains EoS3 outputs.

B: Read pressure values from file fort.100, which contains needed gas pressure fluctuations.

hsc
8-2-99

C Remove mean for pressures ~~code~~ code reads from a file

D: For each element the code reads from fort.101, add the pressure ^{or mean} ~~pressure~~ pressure value from fort.101 to those calculated in step C. The output file is fort.300

(2) plan of testing

- (a) Fort testing with a small number of data, in the code change "n=27" and "nn=324" to "n=1" and "nn=1"; change "1297" to "5"; (= $nn \times d + 1$) change "27" to "1"; (= n) change "324" to "1"; (= nn)

(b) input file

Fort.101

TPa 1

0.8553300847658E+05 0.1080000001054E+02 0.2500000000000E+02 0.1999999894600E+00 0.1999999894600E+00 → a single line

Fort.100

87351.7
87307.0

87351.7

87223.4

87264.1

(c) hand calculation results (following steps A, B, C, D)

PP. 61-62

TPa 1

85585.1

85585.1

85456.9

85497.5

85540.4

③ Testing results

output from the code fort. 300

TPa 1				
	85585.1	85585.1	85456.8	85497.5
	85540.4			

④ Acceptance criteria:

The differences between the simulated results and ones calculated by hand are less than 1%.

The code is acceptable.

⑤ Valid input range:

No limitation as long as the input format and n, n_n and other values are consistent with the code. (see plan of test (a)).

$\frac{h \cdot n \cdot L}{8 \cdot 2 \cdot 19}$

**YMP-LBNL
 REVIEW RECORD**

1. QA: L
 2. Page 1 of 1

3. Originator: Hui Hai Liu

4. Document Title: Documentation for Routine Tbgas3D V1.0 (Option 1 per AP-SI.1Q/Rev. 2/ICN4, Sec. 5.1)

5. Document Number: N/A 6. Revision/Mod.: N/A 7. Draft: N/A

8. Governing Procedure Number: AP-SI.1Q 9. Revision/Mod: 2/4

REVIEW CRITERIA

10. Standard Review Criteria (One time use Option 1)

(Taken from Attachment 5)

11. Specific Review Criteria:

AP-SI.1Q/Rev. 2/ICN4, Sec. 5.1.1 (One time use routine)

12. Comment Documentation:

Comment Sheets

Review Copy Mark-up

13. YMP-LBNL Project Manager (PM): Gudmundur S. Bodvarsson

14. Reviewer: Randall Hedegaard

Org./Discipline: LBNL/Hydrogeologist

Reviewer

Org./Discipline

Review Criteria

COMMENTS DUE:

15. Due Date: 1 MAR 2000

16. Originator/Review Coordinator: Hui Hai Liu

Print Name

REVIEW BY:

17. Randall F. Hedegaard

Print Name

18. (SIGNATURE REMOVED) (MAR 00)

Signature

Date

19. Mandatory Comments: Yes No

ORIGINATOR/REVIEW COORDINATOR (After response completed):

(SIGNATURE REMOVED) 3-1-00

Print Name/Signature

Date

CONCURRENCE:

21. Document Draft No. NA

Date: NA

22. Review (SIGNATURE REMOVED) (MAR 00)

Signature

Date

23. PM: (SIGNATURE REMOVED) 2/2/00

Signature

Date

DISPUTE RESOLUTION: (if applicable)

24. PM:

Signature

Date

111-79 GEN 4/7/00

YMP-LBNL COMMENT SHEET				OA: L
1. Document Title: Routine Documentation for Tbgas3D V1.0		2. Page 1 of 1		
3. Document No. N/A	4. Revision/ Change/Mod: N/A	5. Draft N/A	6. <input checked="" type="checkbox"/> Q <input type="checkbox"/> NQ	
7. Reviewer: Randall F. Hedegaard				
8. NO. CODE	9. SECT./PARA./P#	10. COMMENT	11. RESPONSE	12. ACCEPT
		<p>--NO COMMENTS-- The documentation for this routine was reviewed and it was found to meet the requirements of AP-SI.1Q/Rev. 2/ICN4. The test case was checked by both hand calculation and by running the code as needed to fully check the test case. The test case fully checks the routine for the input specified and proves that the routine produces acceptable results.</p>		

111-80 JEH 4/7/00

YMP-LBNL
 REVIEW RECORD

1. QA: L
 2. Page 1 of 1

3. Originator: H. H. Liu
 4. Document Title: Routine TBgas3D U.I.O Documentation
 5. Document Number: AP-5I.1A 6. Revision/Mod.: — 7. Draft: —
 8. Governing Procedure Number: AP-5I.1A 9. Revision/Mod.: Reva. ICM4

REVIEW CRITERIA

10. Standard Review Criteria NA 11. Specific Review Criteria: AP-5I.1A/Rev. 2, ICM4
 (Taken from Attachment 5) Sec. 5.1.1 (one time use)
12. Comment Documentation:
 Comment Sheets Attached:
 Review Copy Mark-up Scientific notebook/data associated with this review as noted on Attachment 3
13. YMP-LBNL Project Manager (PM): Gudmundur S. Bodvarsson
 14. Reviewer G. Li Org./Discipline LBNL Techn Reviewer — Org./Discipline — Review Criteria —

COMMENTS DUE:

15. Due Date: 2-24-00
 16. Originator/Review Coordinator: H.H. Liu
 Print Name — Date —

17. REVIEW BY: G. Li
 Print Name — Date —
 Signature (SIGNATURE REMOVED) 2-24-00
 18. (SIGNATURE REMOVED) 2-24-00 Date —
 Signature — Date —

19. Mandatory Comments: Yes No
 ORIGINATOR/REVIEW COORDINATOR (After response completed):
 20. (SIGNATURE REMOVED) 2-24-00 Date —
 Print Name/Signature — Date —

CONCURRENCE:
 21. Document Draft No: NA Date: —
 22. Review (SIGNATURE REMOVED) 2/24/00 Signature — Date —
 23. PM: (SIGNATURE REMOVED) 2/3/00 Signature — Date —

DISPUTE RESOLUTION: (if applicable)
 24. PM: — Signature — Date —

111-82 JGH 4/7/00

YMP-LBNL COMMENT SHEET				QA: L
1. Document Title: <i>Routine Tgas3D v1.0</i>		2. Page <u>1</u> of <u>1</u>		
3. Document No. <i>NA</i>	4. Revision/Change/Mod: <i>NA</i>	5. Draft <i>NA</i>	6. <input checked="" type="checkbox"/> Q <input type="checkbox"/> O <input type="checkbox"/> NQ	
7. Reviewer: <i>G. Li</i>				
8. NO. CODE	9. SECT./PARA./P#	10. COMMENT	11. RESPONSE	12. ACCEPT
		<p>The previous comments were given on the corresponding pages on the Scientific Notebook. No error is found during this review. The documentation for this routine was reviewed and it was found to meet the requirement of AP-SI.1Q/Rev.2/ICM4. The test case fully checks the routine for all input specified.</p>		

STANDARD REVIEW CRITERIA

Page 1 of 1			
<u>Routine/Macro Review Criteria, Option 1</u>			
NOTE: Where a checklist item does not apply to the software product, check "N/A".			
	Yes	No	N/A
R/M-1	x		
R/M-2	x		
R/M-3	x		
R/M-4	x		
R/M-5	x		